GEOLOGICA ULTRAIECTINA

Mededelingen van de
Faculteit Aardwetenschappen der
Rijksuniversiteit te Utrecht

No. 102

Deformation Processes in Mantle Peridotites

With emphasis on the Ronda peridotite of SW Spain

DIRK VAN DER WAL

GEOLOGICA ULTRAIECTINA

Mededelingen van de
Faculteit Aardwetenschappen der
Rijksuniversiteit te Utrecht

No. 102

Deformation Processes in Mantle Peridotites

With emphasis on the Ronda peridotite of SW Spain

Deformation Processes
in
Mantle Peridotites

With emphasis on the Ronda peridotite of SW Spain.

Deformatie processen in mantel peridotieten -
met nadruk op de Ronda peridotiet in ZW Spanje.

(met een samenvatting in het Nederlands)

PROEFSCHRIFT

TER VERKRIJGING VAN DE GRAAD VAN DOCTOR
AAN DE RIJKSUNIVERSITEIT TE UTRECHT,
OP GEZAG VAN DE RECTOR MAGNIFICUS PROF. DR. J.A. VAN GINKEL,
INGEVOLGE HET BESLUIT VAN HET COLLEGE VAN DEKANEN
IN HET OPENBAAR TE VERDEDIGEN OP
MAANDAG 1 MAART 1993 DES NAMIDDAGS TE 14.30 UUR

DOOR

DIRK VAN DER WAL

GEBOREN OP 9 MAART 1966 TE ORANJEWOUD

PROMOTOR: PROF. DR. S.H. WHITE
CO-PROMOTOR: DR. R.L.M. VISSERS

CIP-GEGEVENS KONINKLIJKE BIBLIOTHEEK, DEN HAAG
Wal, Dirk van der
Deformation Processes in Mantle Peridotites : with emphasis on the Ronda peridotite of SW Spain / Dirk van der Wal. - Utrecht : Faculteit Aardwetenschappen der Rijksuniversiteit Utrecht. - (Geologica Ultratraiectina, ISSN 0072 - 1026; no. 102)
Proefschrift Rijksuniversiteit Utrecht. - Met lit. opg. - Met samenvating in het Nederlands.
ISBN 90-71577-55-4
Trefw.: aardmantel / Ronda peridotiet / Zuidwest-Spanje ; geologie.

In dankbare herinnering aan mijn vader

Contents

Dankbetuiging (Acknowledgements)

Hierbij wil ik iedereen bedanken die bijgedragen hebben tot het ontstaan van dit proefschrift. Mijn bijzondere dank gaat in de eerste plaats uit naar mijn ouders en naar Erna, voor hun onvoorwaardelijke en volledige steun gedurende mijn studiejaren in Utrecht.

Natuurlijk gaat evenzoveel dank uit naar mijn promotiebegeleider Reinoud Vissers. In zijn inzet en interesse in het Ronda project heb ik de afgelopen 4 jaar geen plafond kunnen ontdekken. The support and time of my promotor Prof. Dr. S.H. White is greatly acknowledged. I owe a great deal to Martyn Drury for his interest in the project, and for providing the opportunity to visit the RSES in Canberra to perform part of my Ph.D. research. Eilard Hoogerduijn Strating heeft veel bijgedragen tot mijn bewustwording van de problematiek rond structureel-gericht onderzoek in mantel peridotieten. Eilard, heel veel dank.

Ik dank iedereen werkzaam bij de Faculteit Aardwetenschappen voor hulp en collegialiteit. Met name noem ik hier Timon Fliervoet en Rian Visser, en ook Coen ten Brink, met wie ik veel inhoudelijke discussies heb gevoerd die zeer nutig zijn geweest. Wim Spakman dank ik hartelijk voor het beschikbaar stellen van Fig. 7.1. Verder dank ik Magda Mathot-Martens voor haar hulp.

Tilly Bouten en René Poorter hebben geassisteerd bij het calibreren van de microprobe. Ing. J. Pieters, Brad Smith en ook John FitzGerald hebben me electronen mikroskopie geleerd. Het enthousiasme voor de electronen mikroskoop dat zo zichtbaar is bij Joop Pieters is op mij overgeslagen, waarvoor ik hem heel hartelijk wil bedanken. Het personeel van AV dienst en slijpkamer stonden altijd voor mij klaar.

My gratitude goes to Martyn, Gill and Anna-Joy Drury, John and Leslie FitzGerald, Prame Chopra, Sally Rigden and Robert Hill, Rob Scott, and to everyone in the Petrofysics-group of the RSES for their hospitality during my stay in Australia.

The contents of this thesis have been greatly improved through discussions with the following people. Special thanks go to Jean-Louis Bodinier, as well as to Carlos Garrido, Malika Remaïdi, Fernando Gervilla, Martin Menzies and Elaine McPherson for their kind cooperation in the Ronda project. Herman van Roermund, John Platt, George Gibson, M. Obata, F. Frey, D.A. Carswell, Prof. A. Nicolas, Bill McDonough and Prof. D.H. Green provided valuable comments to various parts of the manuscript. The Department of Geology and Geochemistry of the University of Montpellier II is thanked for hospitality during several stays in 1992.

Mijn dank voor financiële ondersteuning gaat uit naar de Nederlandse Organisatie voor Wetenschappelijk Onderzoek (NWO, SIR 14-210/380) en Koninklijke Shell Nederland. A grant from the Australian National University is greatly acknowledged.

Tot slot wil ik alle andere personenen bedanken die direct of indirect een bijdrage hebben geleverd aan mijn onderzoek en de voltooiing van dit proefschrift.

Samenvatting (summary in Dutch)

Experimenteel werk gedurende de laatste decennia wijst erop dat boven-mantel gesteenten in vergelijking tot korst-gesteenten relatief sterk zijn (bijv. Carter en Tsenn 1987). Deze sterkte van de boven-mantel heeft belangrijke implicaties voor het mechanisch gedrag van de lithosfeer tijdens orogenese en bekken-ontwikkeling, en rechtvaardigt geologische onderzoek naar de *geometrie en kinematiek* van de deformatie zowel als naar de *thermische respons* en *rheologisch gedrag* van boven-mantel gesteenten tijdens orogenese. Dit proefschrift getiteld "Deformatie processen in mantel peridotieten" betreft een in principe veldgerichte studie naar zulke gegevens toegespitst op de ultramafische gesteenten van het westelijke Middellandse zee gebied en de betekenis van de gesteenten in de context van de recente geologische geschiedenis van het gebied. Als rode draad door dit proefschift fungeren de resultaten van een gedetailleerde structurele en microstructurele analyse van het westelijke Ronda massief in de westelijke Betische Cordilleren van zuid-west Spanje.

In vergelijking met korst-gesteenten zijn er betrekkelijk weinig technieken beschikbaar om de kinematiek van ductiele deformatie in boven-mantel gesteenten te onderzoeken. In hoofstuk 2 worden twee nieuwe technieken onderzocht, te weten een microstructurele techniek gebaseerd op olivijn *vorm-voorkeursmaaksels* en een veldtechniek welke voortbouwt op het structurele concept van *vergenties* in een gelaagd gesteentepakket. Het olivijn vorm-voorkeursmaaksel is een karakteristieke olivijn microstructuur welke ontwikkeld is onder een hoek met de dominante foliatie in peridotieten van de Erro-Tobbio peridotiet (Ligurische Alpen, NW Italië). Aangetoond wordt dat de monocliene symmetrie van deze microstructuur gebruikt kan worden om de bewegingszin tijdens de deformatie te bepalen. Het vergentie-concept gebruikt de asymmetrie van een samenstellingsgelaagdheid, ten opzichte van de zich vormende foliatie, om onder een aantal gespecificeerde voorwaarden uitspraken te kunnen doen over de beweginszin.

Deels met behulp van de technieken ontwikkeld in Hoofstuk 2 wordt in Hoofdstuk 3 de structuur van de Ronda peridotiet bestudeerd. Het massief blijkt een drietal kilometer-schaal structurele domeinen te bevatten welke ontwikkelden gedurende verschillende, in de tijd gescheiden stadia van het orogene proces. In volgorde van afnemende relatieve ouderdom worden deze domeinen gekarakteriseerd door intens vervormde granaat-houdende peridotieten in het noord-westelijke deel van het massief, granulaire spinel peridotieten in het centrale deel van het massief, en vervormde plagioclaas-houdende peridotieten in het oostelijke en zuid-oostelijke deel. De granaat-houdende peridotieten bestaan voornamelijk uit spinel tektonieten, relatief homogeen ontwikkeld op de schaal

van het domein, welke doorsneden worden door sterk vervormde granaat-spinel myloniten ontwikkeld op 100 m schaal. Deze structurele overgang weerspiegelt een toenemende graad van gelokaliseerde vervorming onder metamorfe condities welke geleidelijk veranderden van de Ariégietfacies (d.i. het diepere deel van de spinel-peridotiet facies, O'Hara 1967) naar de granaat-peridotiet facies. De granulaire peridotieten ontwikkelden ten koste van de eerder gevormde granaat-houdende peridotieten tijdens een latere fase van statische rekristallisatie in het Seiland veld van de spinel-peridotiet facies, derhalve onder beduidend lagere drukken dan de granaat-houdende peridotieten. Dit stadium van rekristallisatie leidde tot een zo goed als volledig uitwissen van de structuren en mikrostructuren gerelateerd aan de granaat-houdende peridotieten. Het rekristallisatie front is bewaard gebleven en vertegenwoordigt een abrupte structurele en petrologische, en mogelijk ook een geochemische discontinuïteit in de Ronda peridotiet. De plagioclaas peridotieten, in het verleden beschreven als een relatief homogeen vervormd domein (Darot 1973, Obata 1980), beslaan in werkelijkheid twee verschillende schuifzone structuren met een tegenovergesteld bewegingszin. De jongste structuur is geassocieerd met tektonische lenzen afkomstig uit de midden-korst, hetgeen aangeeft dat de jongste structuur in de plagioclaas peridotieten gerelateerd is aan het schuiven van het Ronda boven-mantel fragment in de Betische korst.

De relatieve ouderdomsrelaties van de drie structurele en metamorfe domeinen in het Ronda massief vormen de basis voor een thermisch gerichte studie in hoofstuk 4. Hierbij wordt gebruik gemaakt van pyroxeen thermometrie om de heersende temperaturen tijdens de ontwikkeling van de hierboven geschreven domeinen te bepalen. De pyroxeen-thermometrie gegevens wijzen op een thermische geschiedenis van de Ronda peridotiet gekarakteriseerd door hoge temperaturen (>1000°) gedurende een groot deel van de opheffingsgeschiedenis (Tubia en Cuevas 1986), doch onderbroken door een belangrijke fase van afkoeling (≤850°C) tijdens de ontwikkeling van de granaat-houdende peridotieten.

Bestaande microstructuur studies naar de mechanische eigenschappen van mantel gesteenten baseren zich veelal op empirische relatie tussen experimenteel gerekristalliseerde olivijn korrelgrootte en differentiele spanning (piezometrie). Recent is echter gebleken dat er grote onzekerheden bestaan in de gemeten spanningen in zgn. solid-medium deformatie apparaten van het Griggs-type (Green en Borch 1990). Dit maakt de toepassing van de in de literatuur gepubliceerde empirische relaties hoogst twijfelachtig. Met het oog op deze onzekerheden worden in Hoofstuk 5 een tweetal nieuwe empirische relaties afgeleid op basis van een eerdere experimentele studie van Chopra en Paterson (1981, 1984) waarbij natuurlijke peridotieten werden gedeformeerd in een zgn. gas-medium deformatie apparaat van het Paterson-type (Paterson 1970). In tegenstelling tot de eerdere solid-

medium experimenten vertonen deze experimenten, door de aard van de experimentele opstelling, verwaarloosbare onzekerheden in de gemeten spanningen. Aan de hand van een microstructureel georienteerde studie van het experimenteel gedeformeerde materiaal worden nieuwe piezometers gecalibreerd, welke toepasbaar zijn op natuurlijke gehydrateerde peridotieten. Hierbij wordt uitgebreid aandacht besteed aan mogelijke beperkingen op de toepasbaarheid van deze piezometers ten gevolge van factoren als de aanwezigheid van water in het gesteente, temperatuur en de deformatie geschiedenis. De verkregen resultaten worden gebruikt in Hoofdstuk 6 om de rheologische betekenis van de deformatie structuren in de Ronda peridotiet te bestuderen. Op basis van de mikrostructurele gegevens wordt geconcludeerd, dat met name de structurele overgang van spinel-tektoniet naar granaat-spinel myloniet, op dieptes waar de boven-mantel als erg sterk verondersteld wordt, tot een belangrijke verzwakking van de mantel geleid kan hebben.

Bovenstaande gegevens worden in Hoofdstuk 7 gebruikt om bestaande werkhypothesen voor het ontstaan van het huidige W Middellandse zee gebied en de ontsluiting van mantel peridotieten in de regio te evalueren. Dit leidt tot een tektonisch scenario, consistent met zowel de interne karakteristieken van de Ronda peridotiet als met andere geologische en geofysische gegevens waarbij de granaat-houdende peridotieten worden geassocieerd met het bovenblok van een zone van significante onderschuiving en mogelijk subductie. Het afbreken van koude en daardoor gravitatief onstabiele lithosfeer (Platt en Vissers 1989, Blanco en Spakman 1993) heeft mogelijk geleid tot convectief opwellen van heet asthenosferisch materiaal tot op de plaats van de eerder gevormde zone van verdikte lithosfeer. Dit kan een verklaring vormen voor het statisch rekristalliseren en ontwikkelen van granulair peridotieten in de overblijvende lithosferische boven-mantel gesteenten in het bovenblok, voor het ontstaan van een lage-druk / hoge-temperatuur metamorfe serie in de crustale eenheden naast en onder de Ronda peridotiet (Loomis 1972a), voor de recentelijke magmatische activiteit (Torres Roldán et al. 1986, Remaïdi et al. 1991), alsmede voor het thermisch gedreven omhoogkomen (England en Houseman 1986) van mantel gesteenten door het Seilandveld tot in de plagioclaas peridotiet facies. Vanuit deze, structureel hoge, positie konden fragmenten van de boven-mantel, nu ontsloten in de ultramafische massieven van het W Middellandse zee gebied, verplaatst worden langs subhorizontale plagioclaas-houdende ductiele breuk-zones tijdens gravitatief gedreven tectonische denudatie van de Betische lithosfeer in een stadium voorafgaand aan het ontstaan van de Alboran zee door thermische daling.

CHAPTER 1

Introduction and summary.

1.1 Aims and backgrounds of this study

Since the introduction of plate tectonics it has become clear that tectonic activity is closely associated with plate boundary processes, in response to the movement of relatively rigid lithospheric plates. This implies that tectonic processes are at least in part controlled by the mechanical properties of the lithosphere. The composition of the lithosphere is strongly heterogeneous. The upper part, i.e., the crust, is dominated by quartzite and feldspathic compositions. The mechanical behaviour of the crust is therefore reasonably approximated by quartz and feldspar dominated rheologies. The upper mantle is mainly made up of peridotite, such that its mechanical behaviour can be approximated by that of poly-crystalline olivine. Experimental rock deformation studies performed over the last two decades indicate that for common continental geotherms the strength of the lithosphere is concentrated in the peridotitic upper mantle (e.g. Goetze and Evans 1979, Kirby 1985, Carter and Tsenn 1987). A typical strength profile across the lithosphere is shown in Fig. 1.1b.

The study of mountain building and basin development thus requires accurate knowledge of deformation processes operating in the lithospheric upper mantle. This motivates geological studies concerned with the geometry and kinematics of upper mantle deformation and with the thermal evolution of the upper mantle in orogenic areas. In addition, as any understanding of tectonic processes necessarily requires consideration of the forces responsible for tectonic activity, there is need for detailed

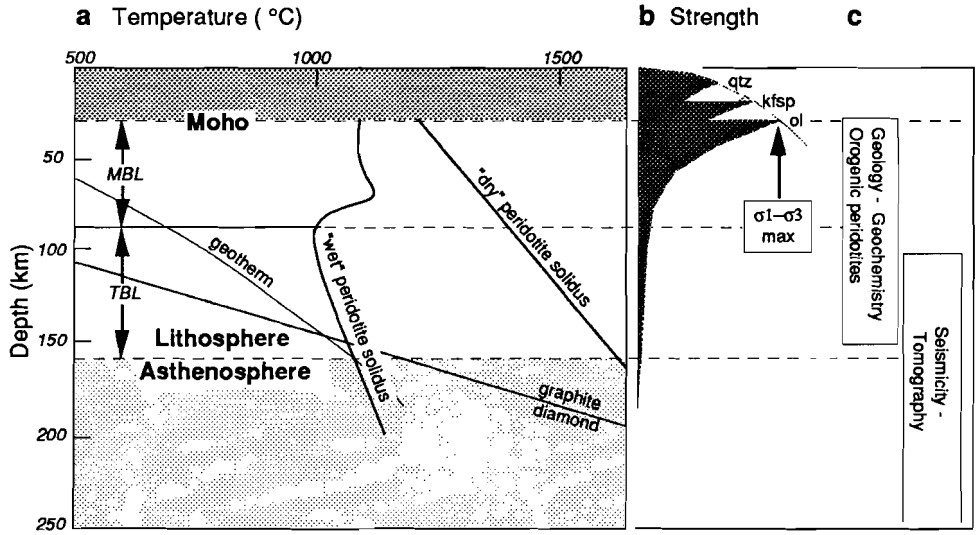

Fig. 1.1: The mechanically (MBL) or thermally (MBL+TBL) defined lithosphere in relation to (a): the "dry" and "wet" solidus, an average shield geotherm and the graphite-diamond transition, (b) a typical strength profile of the lithosphere and (c) the depth range from which lithospheric mantle rocks may be sampled by geological and geophysical techniques.

rheological information, hence for geological techniques to extract this information from naturally deformed upper mantle rocks, in order to constrain the rheological properties of the mantle sections involved.

Direct studies of upper mantle processes are necessarily confined to the limited exposure of upper mantle rocks in peridotite massifs and upper mantle xenoliths sampled by volcanic vents (Fig. 1.1c). Most orogenic belts include ultramafic massifs of variable sizes composed of metamorphic lherzolites and/or harzburgites. It is reasonable to suppose that tectonic activity may lead to significant structural and chemical heterogeneity in the upper mantle. Ultramafic massifs are therefore main sources of direct information on the behaviour of the upper mantle during orogeny, and on the nature and scale at which mantle heterogeneities develop underneath orogenic regions. Many peridotite massifs indeed show a complicated heterogeneous structure (Nicolas 1984, 1986, Drury et al. 1991), regionally variable metamorphic assemblages (e.g. Obata 1980), and a heterogeneous trace element and isotope geochemistry (McDonough and Frey 1989, Menzies and Dupuy 1991 and refs. therein). Geological studies aiming to understand upper mantle processes allied with orogenic activity should therefore focus on such

heterogeneous peridotite massifs.

This thesis aims to study upper mantle deformation processes in a case study of the Ronda peridotite in the Alpine Betic Cordilleras of SW Spain. The choice for this massif is motivated by its following characteristics: (i) pioneering geochemical and geological studies have shown that the W Mediterranean peridotites are among the most heterogeneous mantle fragments exposed at the Earth's surface (e.g. Kornprobst 1969, Dickey 1970, Obata 1980, Zindler et al. 1983, Frey et al. 1985, Suen and Frey 1987, Saddiqi et al. 1988, Pearson et al. 1989, Reisberg et al. 1991). This heterogeneity is particularly evident in the Ronda massif of Southern Spain. Obata (1980) was the first to show that the Ronda peridotite has preserved all three peridotite facies, i.e. garnet-, spinel- and plagioclase-lherzolite facies, in an essentially coherent outcrop of some 300 km^2. (ii) The isotopic (e.g. Reisberg and Zindler 1986/7) and elemental (Frey et al. 1985, Suen and Frey 1987) heterogeneity of the Ronda peridotite suggests a *lithospheric origin* for the Ronda peridotite (Menzies and Dupuy 1991) as opposed to an asthenospheric origin. In addition, the recent recovery of graphite pseudomorphs after diamond documented from the Beni Bousera peridotite in N Morocco (Pearson et al, 1989, Tabit et al. 1990) as well as from Ronda (G.R. Davies, pers. comm.) point to an origin at deep lithospheric or asthenospheric levels. In any case, it follows that the Ronda and other W Mediterranean peridotites have preserved imprints of successive stages in their history of uplift and eventual emplacement in the crust. (iii) A third reason motivating the present choice for the Ronda peridotite is its geologically young emplacement age (~22 Ma; Priem et al. 1979, Zindler et al. 1983). Marked gravity highs underneath the W Mediterranean (Bonini et al. 1973) indicate that tectonic processes in the region are still active. The onshore peridotite exposures can thus be expected to contain (micro)structures and metamorphic assemblages related to a still active geodynamic setting that can also be studied independently by geophysical observation such as to provide tests for geology-based working hypotheses and vice versa.

This study aims to obtain detailed information on the geometry and kinematics of upper mantle deformation preserved in the Ronda peridotite, on the thermal history of the peridotite body and on the rheological significance of the various structures observed, and to evaluate these data in the context of an orogenic process in a still active tectonic environment.

1.2 Historical background

The inferred active role of ultramafics in lithosphere dynamics dates from the days of Steinmann (1906) at the beginning of this century. Many uncertainties, however, surrounded the possible mechanisms involved in the uplift and emplacement of mantle peridotites. Among a large number of mechanisms proposed to explain the nature and emplacement of ultramafic rocks, two major mechanisms have prevailed throughout the years: emplacement in a partly molten state (diapirism; e.g. Hess 1938) and emplacement in the predominantly solid state (e.g. De Roever 1957).

Den Tex (1969) was the first to introduce a structural and microstructural approach (often referred to as structural petrology) to unravel the structural, metamorphic and igneous history of mantle peridotites. This approach involved correlation between structural and metamorphic assemblages in the peridotites with those in the surrounding crustal rocks, to yield information on the relative ages of the structures and assemblages from which the nature of peridotite emplacement could be deduced (Den Tex 1969). Under Den Tex' supervision, several structurally oriented case-studies of orogenic peridotites and peridotite xenolith suites were initiatated (e.g. Collée 1963, Avé Lallement 1967, Möckel 1969, Buiskool Toxopeus 1976). Work of broadly similar nature has been continued until recently under the supervision of A. Nicolas (e.g. Darot 1973, Boudier 1976, Coisy and Nicolas 1978, Nicolas et al. 1987, 1988).

This study of upper mantle deformation processes is principally based on a structural and microstructural analysis of upper mantle rocks, with emphasis on the Ronda peridotite. Other data presented below are from the Erro-Tobbio peridotite (Ligurian Alps, NW Italy) and from experimentally deformed peridotites from Anita Bay (New Zealand) and Åheim (Norway). As compared with earlier work in natural mantle peridotites, this study benefits from advances made since the early seventies in mechanically and chemically oriented experimental studies in the Earth- and material sciences (e.g. Carter and Avé Lallemant 1970, Raleigh and Kirby 1970, Boyd 1973). Such experimental studies strongly facilitate research in natural rocks aiming to assess the geometry and kinematics of deformation, ambient temperature conditions (thermometry) or differential stress conditions (piezometry). Despite the advances made in recent years, there is still need for further improvement of basic methods and techniques with regard to both kinematic and rheological aspects. An important part of this thesis therefore concerns further development of such techniques.

1.3 Summary

The limited number of criteria available to assess the kinematics of ductile flow in upper mantle peridotites motivates the search for additional kinematic indicators in these rocks. Two such kinematic criteria are developed in Chapter 2. The first is an *oblique grain shape fabric* similar to type II S-C fabrics well documented from quartz and calcite dominated shear fabrics (e.g. Lister and Snoke 1984). In olivine-dominated rocks, its formation involves syn-kinematic rotation recrystallization followed by deformation-induced grain boundary migration leading to a characteristic microstructure, oblique with respect to the flow plane of the deformation. The second tool involves the use of the *vergence concept*, where the sense of asymmetry of a pre-existing layering with respect to the shear-induced foliation is applied to study the kinematics of upper mantle flow. These techniques are used where possible to analyse the kinematics allied with some of the deformational structures preserved in the Ronda peridotite.

The *structures and microstructures* of the Ronda peridotite form the topic of Chapter 3. Structural analysis shows that the Ronda massif consists of three different, km-scale structural and metamorphic domains (in order of descending relative age): strongly deformed garnet-bearing peridotites, granular spinel peridotites, and deformed plagioclase peridotites. The garnet-bearing peridotites in the NW Ronda massif are dominated by spinel-tectonites developed at the scale of the domain, which are transected by 100 m scale garnet-spinel mylonite zones. This structural transition reflects increasingly localized deformation at ambient conditions changing from the Ariégite-subfacies to the spinel-garnet peridotite transition. The granular peridotites in the central part of the massif developed at the expense of intensely deformed garnet-bearing peridotites during pervasive annealing recrystallization at Seiland subfacies conditions. Annealing progressively removed most of the pre-existing fabric elements. The deformed plagioclase peridotites include two shear zone generations with different senses of movement. The youngest of these shear zones include tectonic lenses of crustal rocks, indicating that the plagioclase peridotites developed during the early ductile stages of emplacement of the massif.

The relative age relations of the different structural and metamorphic domains form the basis to study the thermal and tectonic history of the Ronda massif, as each domain can be related to events recorded at specific upper mantle, and eventually, lower crustal levels. Microstructurally controlled pyroxene geothermometry is used in Chapter 4 to quantify ambient temperatures. Uplift of the Ronda massif essentially occurred at high temperatures, however, a stage of significant cooling of at least 250°C in the upper mantle

preceeded further high-temperature uplift towards crustal levels.

Existing inaccuracies in flow stresses measured in solid-medium deformation experiments (Green and Borch 1990) have motivated a study of the flow-stress dependence of *olivine recrystallized grain size and subgrain size* in experimentally deformed Anita Bay and Åheim dunites (Chopra and Paterson 1981, 1984). These latter experiments employed a gas-medium deformation apparatus free of such uncertainties in flow stress values. On the basis of this experimentally deformed material, new recrystallized grain size and subgrain size piezometers are developed in Chapter 5, and factors such as water-content and deformation history affecting these piezometers are identified and quantified. The results are used in Chapter 6 to investigate the rheological significance of the various deformation structures preserved in the Ronda peridotite.

Finally, all of the above data are used in Chapter 7 to test current hypotheses on the tectonic setting and mode of uplift and emplacement of the W Mediterranean peridotites, to arrive at a tectonic scenario consistent with their internal features as well as with other geological and geophysical data from the region as a whole. The garnet-bearing peridotites of the Ronda massif are interpreted to reflect progressive ductile deformation in the hanging wall of a major zone of underthrusting (subduction). Subsequent detachment of cool, gravitationally unstable lithosphere (Platt and Vissers 1989, Blanco and Spakman 1993) presumably induced convective counterflow of hot asthenospheric mantle replacing the detached lithosphere. Such ascent of asthenospheric mantle accounts for thermally induced annealing recrystallization in the upper mantle hanging wall reflected by the granular fabrics at Ronda, for the development of LP facies series in crustal sequences adjacent to the peridotites, and probably contributed to uplift of the peridotites through Seiland subfacies conditions into the plagioclase stability field. It is inferred that, once uplifted to depths of around 30 km, fragments of the upper mantle now represented by the western Mediterranean peridotites became exhumed along low-pressure, plagioclase-tectonite shear zones, i.e., major upper mantle extensional faults accommodating gravity-driven tectonic denudation. Upon final emplacement, these ductile zones evolved into cataclastic fault zones.

CHAPTER 2

Kinematic studies in mantle peridotites.*

2.1 Introduction

Structural studies in middle and lower crustal rocks have shown that the bulk deformation imposed on these rocks is often localized within ductile shear zones (e.g. Ramsay and Graham 1970, White et al. 1980). This has motivated structural research into the kinematics of ductile flow in such zones and, more specifically, into practical ways by which various small-scale to meso-scale structures in shear zones can be used to infer details of the kinematics of the deformation. These studies have resulted in the recognition of a growing number of *monoclinic fabric elements* which may serve as kinematic or shear sense indicators (e.g. Nicolas and Poirier 1976, Lister and Williams 1979, Platt and Vissers 1980, White et al. 1982, Simpson and Schmid 1983, Passchier and Simpson 1986) and include both microstructural properties such as grain size and shape and textural properties of crystal aggregates (lattice preferred orientation or LPO patterns).

Mainly as a result of their km-scale compositional and structural homogeneity, there is less evidence for strain localization in peridotite massifs. To resolve the kinematics of mantle deformation, olivine LPO patterns have traditionally received disproportionate attention as compared with other criteria (see e.g., Collée 1963, Den Tex 1969, Darot 1973,

*Parts of this chapter have been published as: Van der Wal, D., Vissers, R.L.M., Drury, M.R., and Hoogerduijn Strating, E.H. 1992. Oblique fabrics in porphyroclastic Alpine-type peridotites: a shear-sense indicator for upper mantle flow. J. Struct. Geol. 14: 839-846.

Boudier 1978, Tubia and Cuevas 1986). There are, however, two important limitations of LPO patterns in the kinematic interpretation of upper mantle structures: (i) the technique is time-consuming and cannot be applied directly in the field, it is therefore unsuitable to recognize deformational heterogeneities developed at the km-scale of structural domains, (ii) there is growing awareness that LPO patterns may not be particularly reliable kinematic indicators (Wenk and Christie 1991). The principal assumptions underlying the application of LPO patterns in kinematic studies are as follows: (i) in axial compression the slip-plane normal is expected to orient itself parallel to the compression direction, whilst (ii) in simple shear deformation, the "easiest" slip direction is thought to rotate towards parallelism with the macroscopic shear direction with the "easiest" slip-plane, i.e. the slip-plane with the lowest value of the critical resolved shear stress orienting itself parallel to the macroscopic shear plane (the "easy slip principle"; e.g. Law 1990). Recent modelling of fabric development in polycrystalline olivine aggregates (Ribe and Yu 1991, Wenk et al. 1991) on the basis of long established principles of LPO development such as strain compatibility (Taylor 1938) and stress equilibrium (Schmid 1928) have shown that the above assumptions should be looked at more critically and that they may not apply in many natural cases (Wenk and Christie 1991). An additional complication involved in the interpretation of LPO patterns of natural rocks is the largely unknown and poorly constrained role of static or dynamic recrystallization during fabric development (e.g. Karato 1988, Bussod and Christie 1991). It follows that kinematic interpretations of LPO patterns are surrounded by hitherto underexplored limitations and uncertainties.

There is clearly a strong need for additional tools that can be used in mantle peridotites to reliably assess the kinematics of mantle flow. In this chapter I will present two such tools: (i) olivine *oblique grain shape fabrics* as a shear sense indicator for upper mantle flow and (ii) an application of the *vergence concept* in the analysis of sheared compositional banding and pyroxenites, to assess deformational heterogeneities and kinematic framework at the scale of the domain.

2.2 Oblique fabrics in orogenic peridotites

A well-known monoclinic fabric element in deformed crustal rocks is a grain-shape fabric of elongate recrystallized grains, oriented oblique to the dominant mylonitic foliation. These structures are currently referred to as oblique fabrics (e.g. Law et al. 1984), and form the S component of type II S-C mylonites (Lister and Snoke 1984). Oblique fabrics have

been described from shear zones in many different rock types including quartzites (e.g. Lister and Snoke 1984, Law et al. 1984, Platt and Behrmann 1986, Burg 1986, Dell'Angelo and Tullis 1989) and carbonate rocks (Simpson and Schmid 1983, Schmid et al. 1987, De Bresser 1989), as well as from experimentally deformed analogue materials such as ice (Bouchez and Duval 1982, Burg et al. 1986) and octochloropropane (Jessell 1986). A microstructure similar to the oblique fabrics reported from crustal shear zone rocks occurs in a kilometer-scale high-temperature shear zone developed in the Erro-Tobbio peridotites of the Voltri massif (Ligurian Alps, NW Italy). Below, this oblique microstructure and its development are examined in order to investigate its potential as a shear sense indicator for high-temperature non-coaxial flow in the upper mantle.

Geological setting

The Voltri Massif in the Ligurian Alps includes the largest exposure of ultramafic rocks in the Alpine suture zone (inset Fig. 2.1). The massif is located at the southernmost extremity of the Alpine arc, immediately NW of Genova, and is separated from the Apennines to the east by the Sestri-Voltaggio zone. Previous work (Chiesa et al. 1975, Piccardo et al. 1977) has shown that the large-scale structure of the massif is dominated by a number of sub-horizontal thrust sheets, dismembered by younger N-S trending faults. The uppermost thrust sheet is made up of a subcontinental to transitional, lherzolite-dominated peridotite body, the Erro-Tobbio peridotite.

The microstructure concerned occurs in lherzolites exposed in the eastern part of the Voltri massif, in the area around Mt. Tobbio (Fig. 2.1). The main thrust contact between the Erro-Tobbio peridotite and underlying serpentinites is strongly dissected by dextral and sinistral oblique slip faults, but coherent outcrop of the Erro-Tobbio peridotite occurs around Mt. Tobbio in the eastern part of the map area as well as further west in the Gorzente river section and around Mt. Tugello. In these exposures, which are less affected by later movement zones, a gradual transition occurs over a distance of several hundreds of meters between granular, virtually undeformed peridotites in the north and intensely foliated, porphyroclastic peridotite tectonites to the south (Drury et al. 1990, Vissers et al. 1991). The transition is marked by a gradually increasing intensity of the tectonite foliation and a decreasing angle between foliation and pyroxenite layers, suggesting an increasing strain from the granular peridotites towards the strongly foliated tectonites. In the more intensely deformed rocks, elongate and locally asymmetric pyroxene porphyroclast systems (Passchier and Simpson 1986) define a stretching lineation, which runs sub-horizontal in the Gorzente River section, but is more steeply oriented around Mt. Tobbio, presumably as a result of rigid body rotations related to alpine imbricate stacking.

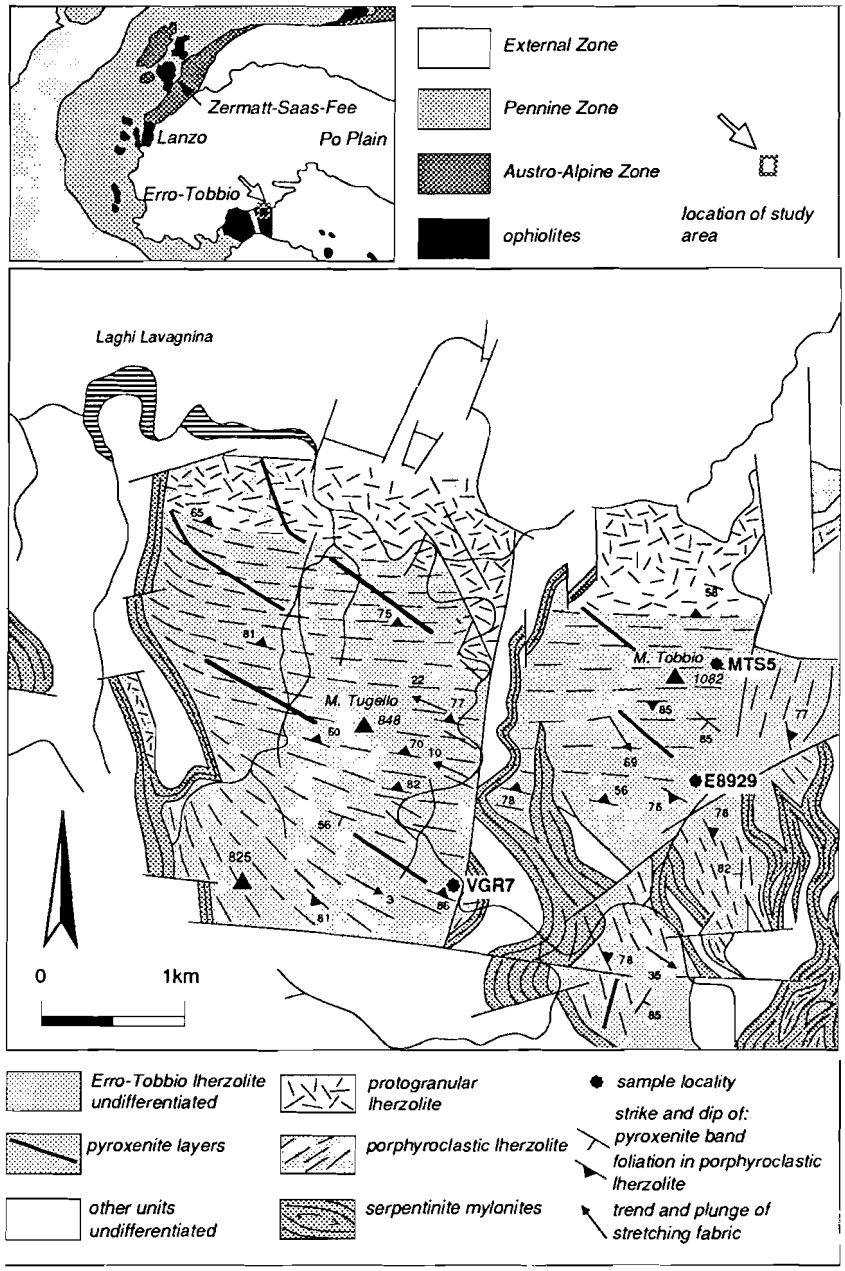

Fig. 2.1 Structural map of the Erro-Tobbio peridotite in the M. Tobbio area, with sample locations. Inset: geological sketch map of the W Alps, with location of study area in NE Voltri massif.

From the map pattern (Fig. 2.1) it is evident that the tectonites occur in a km-scale zone of localized deformation. Minor but systematic changes in the orientation of the tectonite foliation over distances of the order of 50 meters associated with small variations in the angle between pyroxenite layers and the foliation probably reflect variations in strain magnitude. However, apart from such variations, the structures are remarkably homogeneous at outcrop to 50 meter scale. This suggests that the oblique microstructures described below are unrelated to local heterogeneities of the flow field.

Thermobarometry by Hoogerduijn Strating (1991) indicates that deformation in the tectonite shear zone occurred at temperatures > 950°C in the spinel lherzolite stability field, which implies that the tectonites formed in the upper mantle and that they are unrelated to the later stages of deformation associated with emplacement. The tectonites and adjacent granular peridotites are interpreted as a relict of a km-scale shear zone system, formed during localized non-coaxial flow in the upper mantle at the onset of lithosphere extension and continental breakup, prior to the development of the Piemonte Ligurian ocean (Vissers et al. 1991).

Microstructures

The microstructure of the tectonites is dominated by aligned elongate and tabular olivine grains, parallel to the long dimensions of stretched orthopyroxenes and partly recrystallized clinopyroxene aggregates (e.g. Boullier and Nicolas 1975, Drury et al. 1990). However, several samples from the Erro-Tobbio tectonites (labelled MTS5, E8929 and VGR7, sample localities shown in Fig. 2.1) show a microstructure characterized by elongate olivines oriented at angles of 25° to 40° to the tectonite foliation (Fig. 2.2a) similar to the S-component of a type II S-C mylonite as defined by Lister and Snoke (1984). Unfortunately, late serpentinization and weathering completely conceal the oblique microstructure in outcrop, such that its extent is as yet poorly documented. Line drawings on the basis of photomicrographs (Fig. 2.2b) show the details of the deformation and recrystallization microstructures which, at first inspection, are not immediately obvious due to a strong lattice preferred orientation and a variable degree of serpentinization. Serpentinization, in particular, often obscures the oblique microstructure, however, in some cases it strongly accentuates a grain boundary alignment.

The microstructure shown in Fig. 2.2 is oriented such that the tectonite foliation defined by stretched pyroxenes and elongate spinel aggregates is horizontal (shown at bottom of Fig. 2.2a). Oblique to this foliation, a grain shape fabric is defined by slightly inequant to highly elongate olivine grains. The elongate grains commonly dominate the microstructure (~70%), they show aspect ratios of up to 5:1 and have smoothly curved to serrate grain

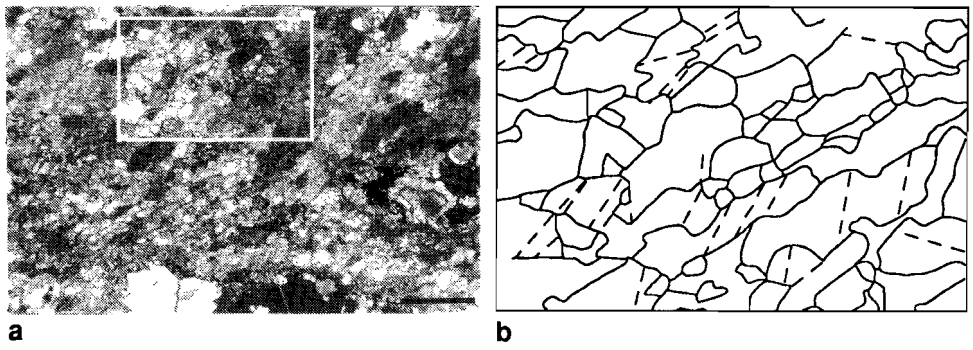

Fig. 2.2 a) Photomicrograph of oblique fabric, sample MTS 5. Oriented clinopyroxene aggregates at bottom of micrograph define tectonite foliation shown horizontal. Scale bar 2 mm. b) Line drawing of the oblique microstructure within inset shown in (a)

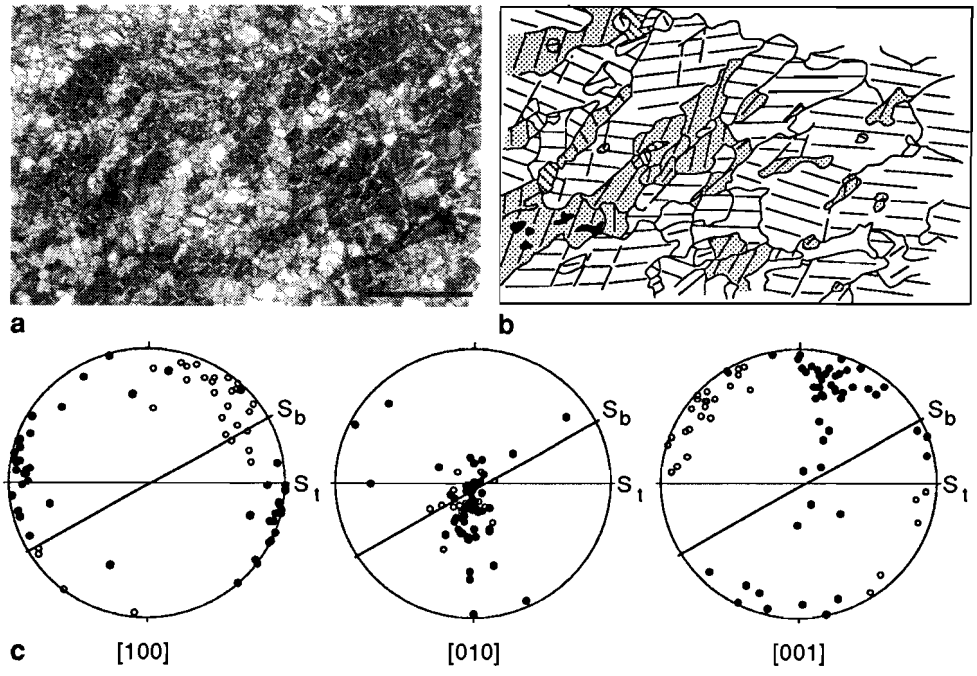

Fig. 2.3 (a) Photomicrograph, (b) AVA-diagram and (c) corresponding LPO diagram of oblique fabric, sample E 8929. Scale bar 1 mm. Black dots in fabric diagrams correspond to non-shaded grains, open circles to shaded grains. For further explanation see text.

boundaries. The grain size of the olivines ranges between 0.2 and 2 mm, with average values of 0.5 mm. Kink-type subgrain boundaries are < 10° to (100), and are mostly

oriented at somewhat larger angles (70-80°) to the tectonite foliation than the oblique grain shape fabric. It appears that at least some grain boundaries are high-angle kink-type boundaries.

Lattice preferred orientation patterns

The lattice preferred orientation (LPO) patterns of the tectonites in general, determined optically in thin sections oriented parallel to the stretching lineation and perpendicular to the foliation, are dominated by point maxima of olivine [100] and (partial) girdles of olivine [010] and [001] (Hoogerduijn Strating et al. 1990, Hoogerduijn Strating 1991). LPO patterns in domains with the oblique fabric show slightly different characteristics, i.e., a *double* point maximum distribution of olivine [100] and [001] (Fig. 2.3c). The dominant [100] concentration is oriented close to the tectonite lineation, while a second concentration is oriented at a large angle (70°) to this dominant maximum and at a small angle to the trace of the oblique fabric. Olivine [010] is concentrated in a point maximum within the plane of the foliation and perpendicular to the stretching lineation. Olivine [001] also shows a double maximum pattern, with the dominant concentration sub-perpendicular to the foliation and a second maximum close to the lineation. A bimodal LPO pattern in association with an oblique grain shape fabric has also been reported from experimentally deformed polycrystalline ice (Bouchez and Duval 1982).

AVA analysis

In order to investigate the topology of the bimodal olivine [100] and [001] distributions, I applied an AVA analysis (Achsen-Verteilungs-Analyse, Sander 1950) of a sample with the oblique fabric and associated bimodal lattice preferred orientation patterns (Fig. 2.3). This analysis shows, that the two point maxima of olivine [100] and [001] are related to two classes of grains, with the dominant olivine [100] and [001] point maxima corresponding to the non-shaded grains in Fig. 2.3b, whilst the secondary point maxima are related to the shaded grains.

These two groups of grains will now be considered in some detail. From careful inspection of Fig. 2.3b it follows, that some microstructural differences exist between both grain groups. The non-shaded grains are often relatively large, they show the highest aspect ratios and commonly host the (100) tilt walls. Instead, the shaded grains are much smaller and show lower aspect ratios. They tend to occur in elongate clusters, with dimensions similar to those of the large, non-shaded grains. They also occur as narrow elongate grains, located at the grain boundaries of the non-shaded grains. Note also that

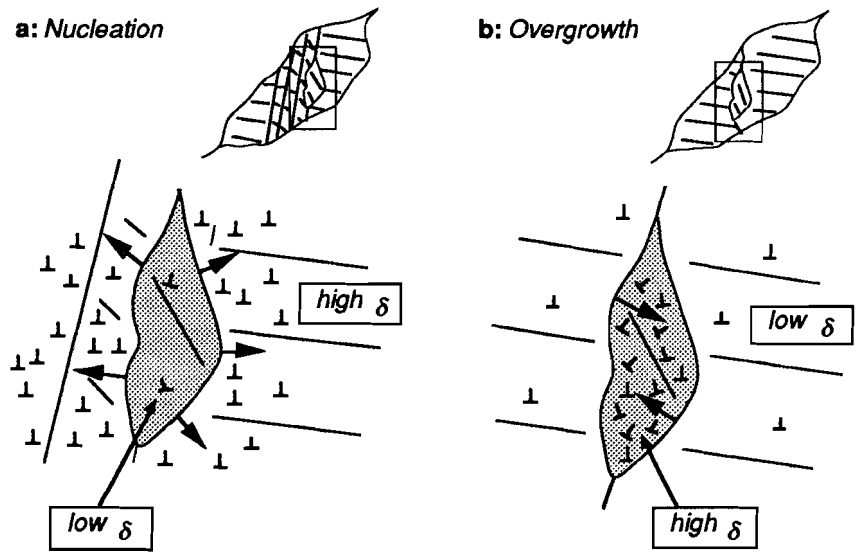

Fig. 2.4 Diagram showing expected effect of (a) nucleation recrystallization versus (b) progressive overgrowth, on dislocation density distribution. The newly recrystallized phase (shaded: unfavourably oriented grains in the nucleation case and favourably oriented grains in the overgrowth case) will have the lowest dislocation density. Arrows indicate direction of grain boundary migration.

tilt walls sub-parallel to (100) are distinctly less common in the shaded grain group.

The traces shown in the individual grains have been drawn parallel to the trace of the olivine (001) plane, which is known as a high temperature olivine slip plane (Carter and Avé Lallemant 1970). As all high-temperature slip systems of olivine are of the form {0kl} (Carter and Avé Lallemant 1970, Phakey et al. 1972), it follows that the non-shaded grain group is oriented *favourably* for intracrystalline slip on the high-temperature olivine slip systems, and that the shaded grain group is *unfavourably* oriented for slip on these systems, both with respect to feasible orientations of the kinematic framework during development of the foliation in the tectonite shear zone (oriented horizontal in Fig. 2.3).

Dislocation substructure

Two different recrystallization mechanisms can account for the microstructure of the unfavourably oriented grains located at the grain boundaries of large, favourably oriented grains: (i) nucleation recrystallization, i.e. the unfavourably oriented grains may have nucleated at high-angle kink-type boundaries during deformation, and (ii) progressive overgrowth of unfavourably oriented grains by favourably oriented grains (Bouchez and

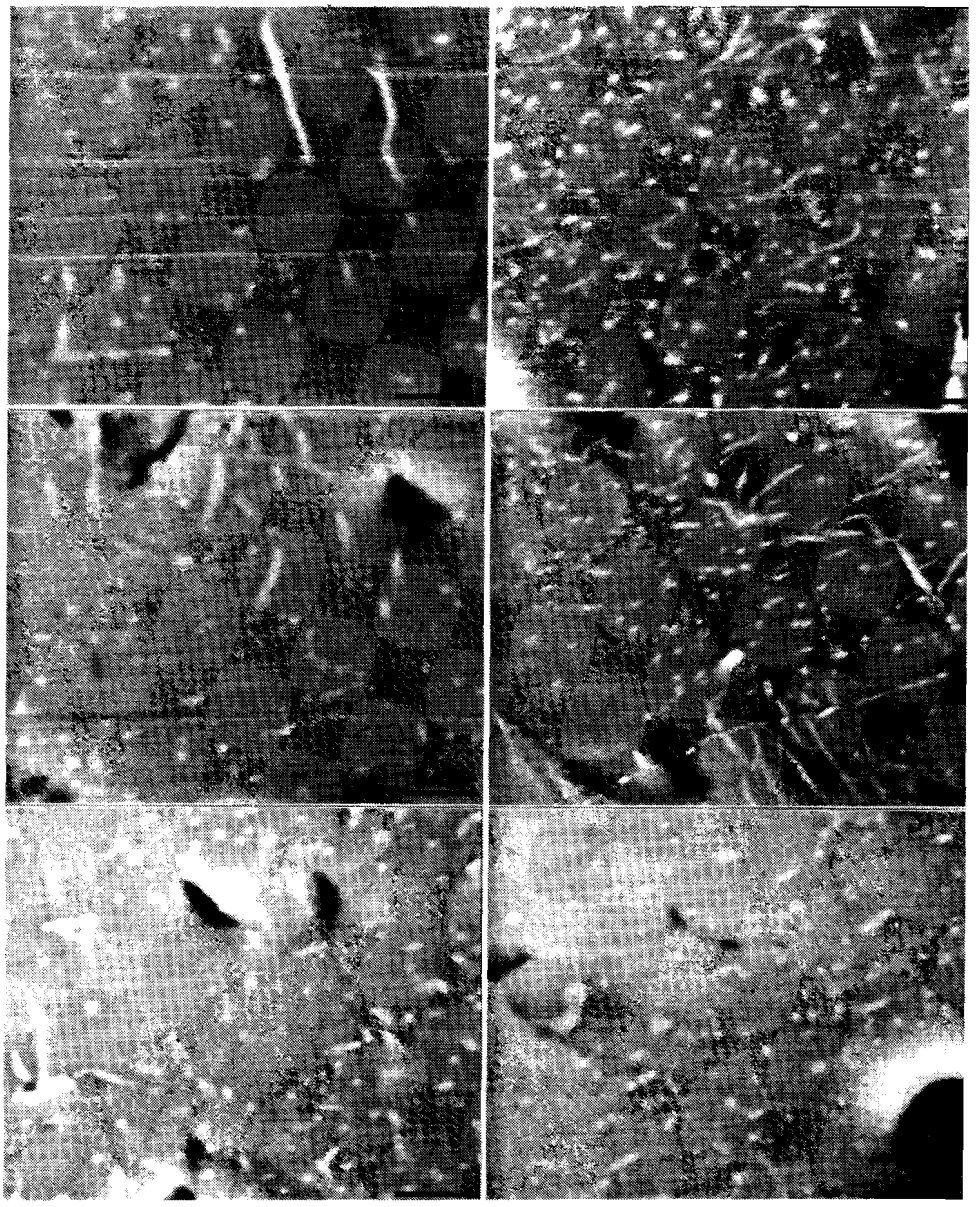

Fig. 2.5 Backscattered electron micrographs of dislocation substructures in olivine grains with oblique micro-structure (sample MTS 5). Left column shows dislocation densities of favourably oriented grains, right column shows dislocation densities of unfavourably oriented grains. Scale bar in all micrographs 2 μm.

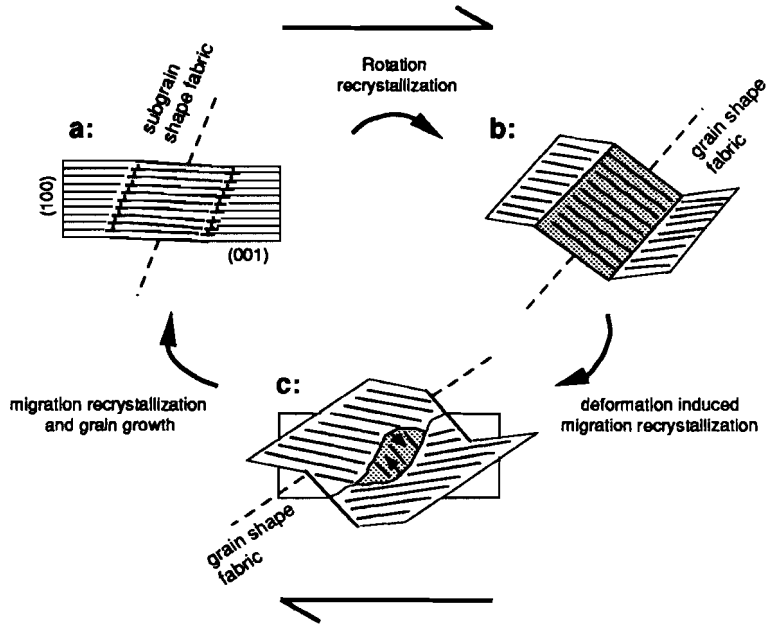

Fig. 2.6 Synoptic diagram illustrating the inferred evolution of the oblique grain shape fabric during progressive dextral shear. The shaded grain becomes unfavourably oriented for high temperature flow due to rotation recrystallization, such that slip on the easy slip systems becomes difficult. Other slip systems are activated instead, leading to tangling of dislocations and an increase of the dislocation density, which drives deformation induced grain boundary migration.

Duval 1982, Urai et al. 1986, Drury and Urai 1990). These two alternatives are illustrated in Fig. 2.4a and b, respectively. In each case the newly recrystallized phase would be expected to show the lowest dislocation density, so the two different options may be discriminated by investigating the dislocation substructure of both grain types. In order to do this, the dislocations in the samples have been decorated at 900°C for a time span of 20 minutes according to the decoration technique described by Kohlstedt et al. (1976) and extended by Karato (1987). This method allows a first order approximation to the dislocation densities in the two grain types. Fig. 2.5 shows the dislocation substructure of favourably oriented grains (left column) vs. unfavourably oriented grains (right column). With the number of decorated dislocations per unit area as a measure of the dislocation density, it follows that the dislocation density of the unfavourably oriented grains ranges from about the same to approximately twice the dislocation density of the favourably oriented grains. This can possibly be explained by tangling of dislocations in unfavourably oriented grains, during slip on *non-easy* slip planes, resulting in a high dislocation density.

The dislocation densities suggest that the unfavourably oriented grains are remnants with high dislocation densities rather than newly nucleated grains with low dislocation densities, and that migration recrystallization during deformation led to progressive overgrowth of the unfavourably oriented grains by favourably oriented ones.

Discussion

Based on the above microstructural observations the following deformation and recrystallization mechanism is suggested to explain the development of oblique fabrics in the high-temperature tectonites of the Erro Tobbio lherzolite. A dominantly simple shear deformation will cause intracrystalline slip on the olivine high-temperature slip systems (Fig. 2.6a). With progressive strain, (100) tilt walls develop and a subgrain boundary alignment initiates an oblique fabric. With progressive shear, shown dextral in Fig. 2.6, the tilt walls rotate into high-angle grain boundaries or kinks (Fig. 2.6b), and some of the favourably oriented grains rotate away from their favourable orientation (subgrain rotation), which eventually results in a bimodal LPO pattern. The grain shape fabric, characteristic for dextral shear, is now well developed. With ongoing deformation, a heterogeneous dislocation density between favourably and unfavourably oriented grains is introduced and deformation-induced grain boundary migration leads to progressive overgrowth of the unfavourably oriented grains (Fig. 2.6c)

The above mechanism accounts for the oblique microstructure as well as for the lattice fabric, by explaining these as the result of progressive subgrain rotation and deformation-induced migration recrystallization. From the geometry of the process it follows that the sense of shear inferred from the oblique fabric should be consistent with that inferred on the basis of an oblique orientation of the associated lattice fabrics. In the Erro-Tobbio tectonites the sense of shear derived from the oblique fabrics is entirely consistent with the sense of shear inferred from all other shear sense indicators. The microstructure is effectively reset when all unfavourably oriented grains are completely consumed and (100) tilt walls may form again. This allows a steady-state microstructure to develop during ongoing flow in the shear zone.

It may be expected that oblique grain shape fabrics of the type described here also occur in some lherzolite xenoliths sampled by volcanic vents. In small xenoliths, which do not include a coarsely developed tectonite fabric defined by stretched pyroxenes, oblique grain shape fabrics may be confused with tabular microstructures of the type described by Mercier and Nicolas (1975). These tabular shape fabrics, however, are almost parallel to a distinct unimodal [100] axis lattice fabric, which is readily recognized in these samples by a large angle between kink-type tilt walls and the shape fabric, as opposed to the

distinctly smaller angles observed in the oblique microstructure (e.g. Fig. 2.2b).

Comparison with oblique fabrics in quartzites and polycrystalline ice

Although some similarities exist between the oblique fabrics described from mylonitic quartzites or experimentally deformed polycrystalline ice (often used as an analoque for quartz) and the olivine microstructures documented here from deformed lherzolites, they are quite different in many respects.

Firstly, many of the oblique grain shape fabrics in quartzose tectonites and mylonites show much more equant grain shapes, with lattice fabrics dominated by an oblique girdle rather than a bimodal LPO pattern. This may be largely due to differences in crystallography between the two minerals and inherent differences in the relative contribution of potential slip systems during flow. Lister and Snoke (1984) ascribe the inequant grain shapes to a number of effects, the most important of which is the progressive deformation of small quartz grains formed by rotation recrystallization and counterbalanced by migration of the grain boundaries tending to reset the inequant shapes. Such progressive deformation of the obliquely oriented grains is less marked in the olivine microstructures dominated by a kink-type glide polygonization process. However, the olivine grain shape fabric is strongly reminiscent of some quartz microstructures dominated by prismatic subgrain boundaries primarily controlled by slip on the quartz basal plane (e.g. Lister and Snoke, 1984, their Fig. 10c).

A second apparent inconsistency between the olivine oblique grain shape fabrics studied here and oblique grain shape fabrics developed in experimentally deformed polycrystalline ice is the inferred origin of the unfavourably oriented grains. In the latter experiments, the unfavourable oriented grains are thought to originate from initially unfavourably oriented grains that survive and partly increase their abundance during the initial stages of the development of the oblique grain shape fabric (Bouchez and Duval 1982). At high shear strains, however, they are progressively removed and, as a consequence, the bimodal LPO pattern disappears. The olivine oblique fabrics described here developed from granular peridotites and possibly the lowest-strain tectonites. Both structures show a strong preferred orientation of olivine [100] (Van der Wal, unpubl. results), which implies that there is no significant population of unfavourably oriented grains in the initial microstructure. Therefore, the process involved in the development of the oblique fabric must account for the syn-kinematic formation of such unfavourably oriented grains, by subgrain rotation along olivine (100) kink-type boundaries as discussed above.

Conclusions

The oblique olivine grain shape fabrics observed in the Erro Tobbio tectonites developed as the result of intracrystalline slip, subgrain rotation and concomitant deformation-induced grain boundary migration. These processes resulted in a monoclinic fabric element with a consistent orientation relative to the sense of shear. The oblique fabric can thus be used as a reliable kinematic indicator for high-temperature flow in orogenic peridotites.

2.3 Application of the vergence concept in the analysis of layered materials deformed in non-coaxial flow

The absolute or "finite" state of deformation of a material can only be assessed if the material contains markers capable to reflect shape changes. The most common amongst such markers is bedding in sedimentary rocks deformed into structures such as folds due to heterogeneity of the deformation at the scale of observation. Vergence, traditionally defined as "the systematic variation in the asymmetry between folds and their axial plane" (Hobbs et al. 1976, p. 167), is a concept commonly used in structural analysis of folded rocks with clearly developed axial plane foliations. At a scale smaller than that of the individual folds, this systematic variation allows to readily infer the position of a given exposure relative to adjacent antiforms and synforms (Fig. 2.9a). Vergence in this sense commonly refers to the geographical direction towards the next antiform and coincides with the sense of asymmetry of an earlier layering with respect to the foliation. The

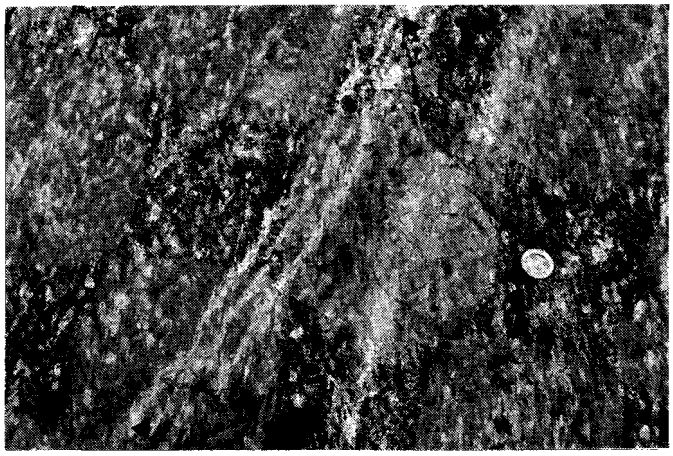

Fig. 2.7 Layering in mantle peridotites: compositional banding (indicated by black triangles). Shear foliation indicated by open triangles. Note the obliquity of layering and shear foliation, denoting a dextral vergence. Diameter of coin 2 cm.

vergence concept represents a geometrical property successfully used in structural analyses over almost a century.

In case of complicated shear zone structures developed at a regional scale, a tool similar to the vergence concept in folded rocks can be extremely useful. A layered medium affected by localized deformation in shear zones will reflect its deformed state in that it will show contortions of the primary layering in these zones. The principle aim of this section, therefore, is to introduce the vergence concept to the kinematic analysis of sheared layered materials, with special reference to mantle peridotites. Below I wish to focus principally on the *theoretical background* underlying application of the vergence principle to layered materials deformed during non-coaxial flow, and on limitations and practical aspects of the technique. The method will be applied in Chapter 3 in a study of some of the shear zones developed in the Ronda peridotite of SW Spain.

Layering in mantle peridotites

Mantle peridotites exposed in ultramafic massifs comprise two major classes of layering: (i) compositional banding and (ii) pyroxenite layers. Compositional banding constitute layers up to several cm thickness which are enriched or depleted in pyroxenes relative to the host peridotite but still contain several tens of volume percent of olivine (Fig. 2.7). Any mechanical contrast between such layers and the lherzolitic or harzburgitic matrix must, therefore, be very low. A second class of layering in mantle peridotites comprises pyroxenite layers (e.g., see Fig. 3.2a). These layers consist mainly of clinopyroxene and orthopyroxene, and may contain an Al-rich phase such as garnet, spinel or plagioclase. Their composition suggests that a substantial mechanical contrast could exist with the lherzolite/harzburgite matrix (see also Nicolas and Boudier 1975).

In view of the relative compositional homogeneity of mantle peridotites at the scale of the massif but the frequent occurrence of compositional banding and pyroxenite layering, it may be expected that application of the vergence concept could be particularly useful to unravel the kinematics of upper mantle flow. Layering in the Lanzo peridotite of NW Italy has been used previously to infer the flow pattern during intrusion of a mantle diapir (Nicolas and Boudier 1975). The vergence concept as outlined below elaborates on this early work, although it is emphasized that it principally applies not only to mantle peridotites but to all layered materials deformed in non-coaxial flow.

Definition of vergence

Any obliquity of the layering with respect to the deformation induced foliation may be

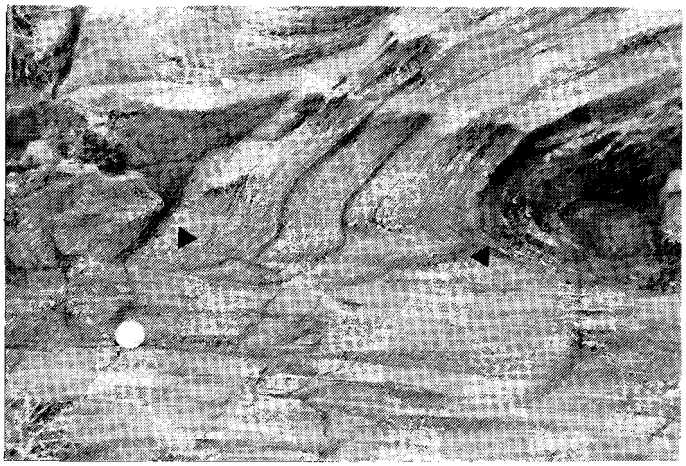

Fig. 2.8 Contortion and folding of sedimentary layering allied to strain localization in a shear zone margin. Cap de Creus, NE Spain. Note folding of the layering due to locally imposed bulk shortening in the shear zone margin (indicated by black triangles).

expressed in terms of vergence of the layering on the foliation. To be largely consistent with the definition of vergence in folded and cleaved rocks, vergence is defined here as the sense of the acute angle measured *from* the shear foliation to the layering (Fig. 2.9b). The vergence may be expressed as sinistral or dextral or, when the shear sense is known, as opposite or parallel to the shear sense. Clearly, vergence can also be expressed in horizontal (map) sections as being directed towards a particular geographical direction. Obviously, vergence in this sense can be determined in any section of the strain ellipsoid, however, it may become conclusive to the kinematics of the flow *only* in sections parallel to the stretching lineation, i.e., in the XZ plane of the finite strain ellipsoid. The orientation of the XZ plane is known once stretching lineations develop in the foliation plane. If these conditions can be ascertained, then a 2-D analysis such as outlined below is sufficient to reveal the kinematics of the flow.

Contortions versus folds

Local variations in vergence as defined here may occur as a result of heterogeneous deformation on the scale of the shear zone, but also as a result of bulk shortening at a scale much smaller than the shear zone. Analogous to the analysis of rocks folded at mesoscopic scales, the important information to be extracted concerns systematic changes of vergence related to strain variations at a larger scale. To illustrate this, an example is shown in Fig. 2.8 from a crustal shear zone developed in metapelites at Cap de Creus, NE Spain, in which a sedimentary layering at a distinct angle to the shear zone rotates into parallelism with the foliation in the shear zone. At a scale comprising shear zone and host rock, the layering is "folded" due to the progressive rotation of the layering into the shear

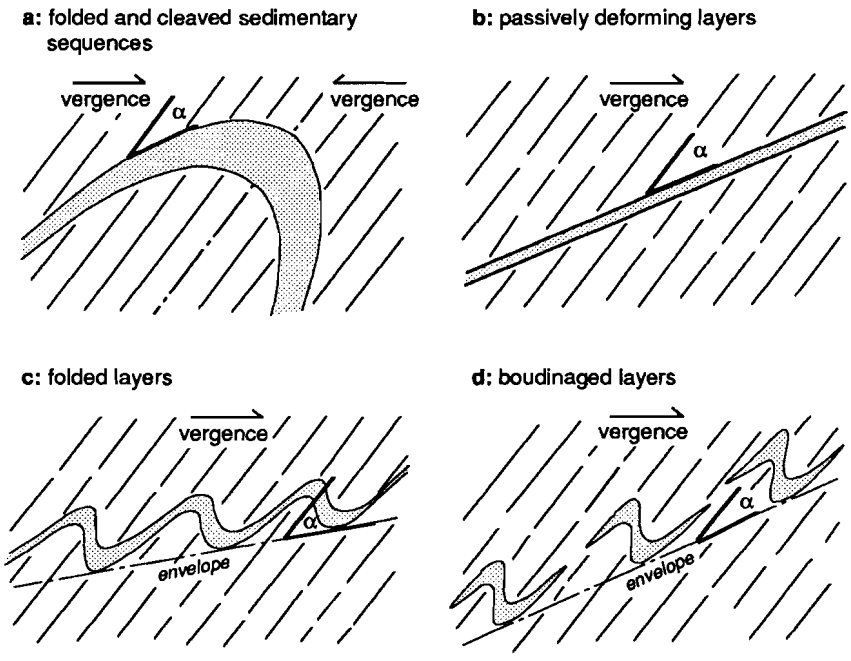

Fig. 2.9 Vergence relations defined for [a] folded and cleaved sedimentary rocks, (b) Passively deforming layers in a sheared medium, (c) Folded layers in a sheared medium, and (d) Boudinaged layers in a sheared medium.

zone (hereafter referred to as contorted). This structure reflects the cumulative effect of the entire strain history. In the shear zone margin (indicated by the black triangles in Fig. 2.8), however, the layering is also folded at a much smaller scale. These folds are most likely due to locally imposed bulk shortening at an early stage of deformation and development of the shear zone when the layering temporarily resided in the shortening field of the strain ellipsoid (Ramsay 1967). Rather than the entire strain history, these folds represent a relatively short stage of the deformation history. The contortion of the layering due to localization of the deformation obviously provides more information on the kinematics of the deformation (e.g. shear strain, shear sense) than the folds presumably developed as buckling instabilities in response to a transient stage of bulk shortening in the shear zone margin. It follows that before interpreting vergence changes allied to heterogeneous deformation across a shear zone, vergence changes arising from such transient stages of shortening need to be identified.

This can be done by considering the following: under the assumption of bulk homogeneous flow, the most important variables controlling the fold morphology of a

layer are: (i) the mechanical (viscosity) contrast between layer and matrix, (ii) the thickness of the layer, (iii) the degree of non-coaxiality in the shear zone, and (iv) the amount of strain accommodated (e.g. Hobbs et al. 1976, Ramsay and Huber 1987). In the deformed state the layer can be either planar, folded or boudinaged (Ramsay and Huber 1987). Analogue deformation experiments with layered materials have shown that layers with a low mechanical contrast with the surrounding matrix, when subject to shortening, do not fold but shorten homogeneously ("passive" behaviour). In this case, folding of the kind exemplified by the minor folds in Fig. 2.8 will not develop and, for appropriate initial orientations, contortions of the layering related to the localization of strain are the only features to be expected. Any change of the vergence in such cases reflects the kinematics of the shear zone. Instead, buckling of layers may be expected when a distinct mechanical contrast exists between layers and matrix, and the wavelength and amplitude of the folds will be controlled by this mechanical contrast and by the thickness of the folded layers (Ramberg 1960, Biot 1961). For most layered geological materials, the wavelength of the folds can be expected to fall within one to two orders of magnitude of the thickness of the fold if the imposed strain is distributed homogeneously over the total rock volume. The only kinematic information that can be obtained from the fold symmetry is that the layer resided in the shortening field of the incremental strain ellipsoid. When contortions of a layering due to shear localization are used to infer the kinematics of the deformation, it is clearly needed to identify any buckle folds related to transient shortening and, where they develop, to use the enveloping surface of the folded layering. The overall vergence in such cases is the polarity of the acute angle measured from foliation to the *enveloping surface* of the folded layer (Fig. 2.9c). Similarly, in case a mechanically strong layer is stretched such as to form boudins, the enveloping surface to boudins derived from *one single layer* can be used to assess the vergence (Fig. 2.9d).

A clear example of cm to m scale folded vs. km-scale contorted layering has been documented by Nicolas and Boudier (1975) in mantle peridotites of the Lanzo massif (see their Figs. 2 and 4, respectively). Note also from that study that the contortions of the layerering, shown by the enveloping surface of the individual folds drawn in their Fig. 4, are used to infer the heterogeneity of ductile flow in a rising mantle diapir.

The Mohr diagram for stretch

The orientation of a layer (or its enveloping surface) deformed by a crosscutting shear zone principally depends on the initial orientation of the layer with respect to the flow plane and on the deformation path in the shear zone. This deformation path varies with the degree of non-coaxiality of the deformation in the shear zone, and with the magnitude

Fixed parameters:			**tensors:**
Xi:	external reference axes		L: velocity gradient tensor
APi:	flow apophyses	i=1,2	F: position gradient tensor (Langrangian)
ISAi:	instantaneous stretching axes		Fi: incremental position gradient tensor
			H: positions gradient tensor (Eulerian)
tensor components:			**deformation parameters:**
X, Z:	long and short axis of finite strain ellipse with suffix 0 refers to undeformed state		S: stretch; 1+ex/z , where footnotes refer to the long and short axis of strain ellipse.
LNFLS:	lines of no finite longitudinal stretch		e: elongation; (l-lo/)lo
			Rf: measure of the flattening of the finite strain ellipse (X/Z)
			Wk: Truesdell's (1954) kinematic vorticity number

Table 2.1 Abbreviations and symbols used in the text.

of the accumulated finite strain. A powerful tool to investigate the geometry of progressive deformation is the use of tensors to describe the velocity field of individual deforming markers. It is convenient to represent these tensors in Mohr diagrams (e.g. DePaor and Means 1984). Below I will use Mohr diagrams to investigate the vergence relationships in sheared layered materials with progressive deformation. A comprehensive review of the use of Mohr diagrams in kinematic analysis has recently been given by Means (1990). Throughout the rest of this Chapter I will use abbreviations and symbols as listed in Table 2.1.

The deformation of a volume of material at any instant of time is completely described by its (vector) velocity field, hence by the velocity gradient tensor L_{ij} (e.g. Means 1990):

$$\frac{dx_i}{dt} = L_{ij} x_j \tag{2.1}$$

where x_i and x_j describe the position of a material point in 2-D space.
Integration of L_{ij} yields the cumulative or finite deformation of the material described by the material (Langrangian) position gradient tensor F or the spacial (Eulerian) position gradient tensor H (Passchier 1988a):

$$x_i^0 = F_{ij} X_j \tag{2.2}$$

and

$$X_i = H_{ij} x_j^0 \tag{2.3}$$

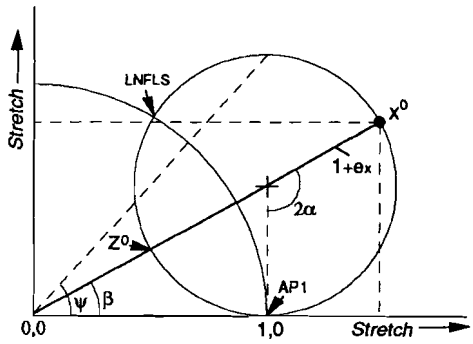

Fig. 2.10 Illustration of some F-Mohr diagram properties (after Passchier 1988a). See text for explanation.

where x_I^0 and x_J^0 refer to the position of a marker in the undeformed state.
H is very useful in geological applications using data on finite deformation to reconstruct the initial or undeformed state, but F better illustrates the way in which flow parameters influence the finite deformation fabric. In order to investigate vergence relationships with progressive deformation, F is obviously the more convenient tensor.

Tensor F describes the finite degree of coaxiality of the deformation and the total amount of strain accommodated. Its properties can be illustrated by Mohr circles (Means 1982). Means (1982, 1983) has shown that, although tensor components are plotted and read as Cartesian coordinates in Mohr space, polar coordinates of any point on the F-Mohr circle represent the *stretches* (s) and *rotations* (β) of material lines in true space resulting from deformation with respect to an external reference frame in true space. The Mohr diagram, however, bears many other noteworthy properties (Passchier 1988a) as follows (see Fig. 2.10).

- the *initial* angle between two material lines (i.e. in the undeformed state) is read as a double angle 2α in Mohr space.
- Material lines parallel to the finite strain axes X and Z, i.e. those lines which show maximum shortening and extension after deformation, plot as X^0 with stretch $1+e_x$ and Z^0 with stretch $1+e_z$ along the line from the origin through the centre of the Mohr circle. The double angle 2α represents the initial orientation of the material line X^0, eventually parallel to X, with respect to the external reference frame.
- The initial orientations of lines of no finite longitudinal stretching (LNFLS) plot on a circle with radius 1 around the origin of Mohr space. They are useful in distinguishing stretched and shortened layers.
- Material lines in stable non-rotational orientations coincide with the flow plane and/or flow apophyses (AP1, AP2) of the deformation and plot on the horizontal axis of the Mohr

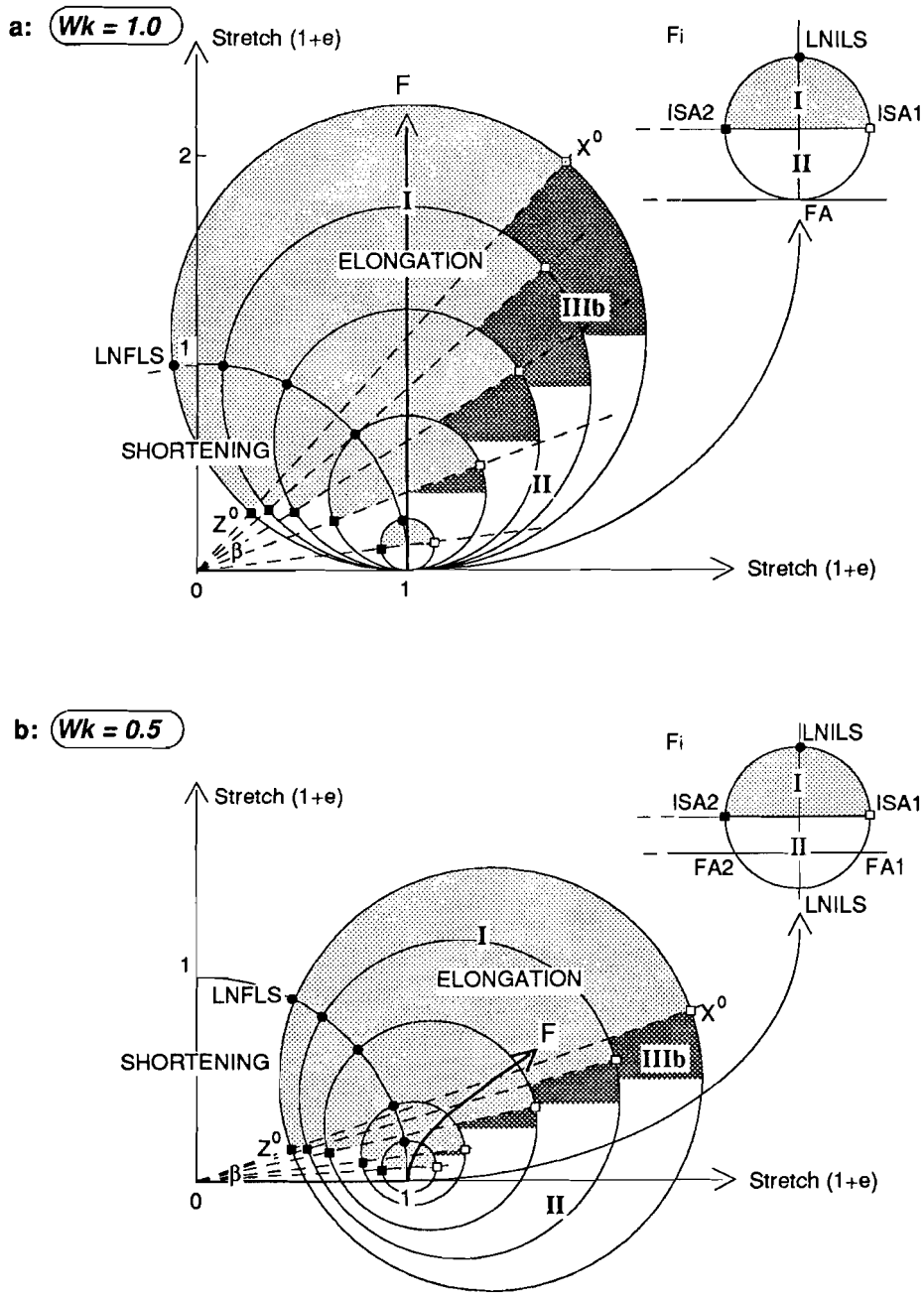

Fig. 2.11 Progressive deformation illustrated in a Mohr diagram, (a) for simple shear, (b) as (a) for sub-simple shear (Wk=0.5). For further explanation see text.

space. All material lines rotate towards parallelism with the flow apophyses (e.g. Passchier 1988a). The flow apophyses are useful as internal reference frame because their orientation is stable with respect to the incremental stretching axes provided that the flow is constant through time in its parameters

- The rotation of a material line during deformation can be read from an F-Mohr diagram as the angle ψ. As initial orientations of material lines can also be read from the Mohr circle, finite orientations with respect to the flow plane are easily calculated.
- The finite strain is quantified as the ratio $R_f = (1+e_x/1+e_z)$. Any shear strain may be calculated from the angle of rotation γ of a material line *initially perpendicular* to the flow plane as $\tan(\psi)$.
- The vorticity number w_k (Truesdell 1954, Passchier 1987) describing the degree of non-coaxiality or vortical component of the flow is graphically represented by the location of the Mohr circle centre in stretch space, and is quantified as the distance of the centre of the circle from the horizontal axis divided by the radius of the circle.

As a consequence of the above properties of the F-Mohr circle representation, the complete stretch and rotation history of layers in a two-dimensional progressive deformation can be illustrated in Mohr space by plotting Mohr circles for successive steps of the deformation. This can be done in one diagram as a series of circles of increasing diameter which shift from (1,0) on the horizontal axis of the Mohr diagram (Passchier 1988b). For a flow constant in its parameters and ISA fixed in the external reference frame during progressive deformation, a point on the circle at a certain angle from the horizontal always represents the same material line. It is therefore possible to follow individual material lines (in our case layers of different initial orientation) with progressive deformation and to determine their geometrical relationships, hence their vergence, with respect to the *shear-induced foliation* during progressive deformation. Below I will discuss two cases to investigate vergence relationships of layers with initial orientations between 0° and 180° to the flow plane. Flow in the first case is progressive simple shear deformation ($w_k = 1$), whilst in the second case progressive shear deformation has a strong coaxial component (referred to as sub-simple shear, $w_k = 0.5$).

Vergence relations during progressive simple shear

Fig. 2.11a illustrates the progressive deformation of a volume of material under progressive simple shear. Consider the deformation after a first increment represented by the smallest circle close to (1,0). From the properties of this Mohr circle (F_i; outlined in Fig. 2.11a) it follows that shear-related foliations will initially develop parallel to material lines of maximum instantaneous stretch, i.e., at an angle of 45° to the flow plane (ISA1). Material

lines with an initial angle of 135° (parallel to ISA2) will be perpendicular to the shear foliation. Thus, any layer with an initial orientation ISA1< α <ISA2 with respect to the flow plane will *initially* have a vergence on the foliation opposite to the movement sense. These material lines are represented by their double angles 2α in segment I of the Mohr circle of Fig. 2.11a. Layers at angles α < ISA1 and α >ISA2 (segment II) will *initially* have a vergence on the shear foliation parallel to the shear sense.

Next, consider progressive simple shear as illustrated by the series of Mohr circles for F (Fig. 2.11a). From inspection of the diagram it is clear that with progressive deformation the finite strain axes are not fixed with respect to ISA1 and ISA2. Instead, *the initial angles, with respect to the flow plane, of material lines eventually parallel to X and Z increase with increasing finite strain* (Fig. 2.11a). It follows that with progressive deformation the upper and lower bounds of segments I and II enclosing material lines with, respectively, a vergence opposite and parallel to the shear sense track the long and short axes of the finite strain ellipse. This implies that the vergence relationships for material lines initially oriented at ISA2< α <Z^0 (segment IIIa) and ISA1< α <X^0 (segment IIIb) *reverse* with progressive deformation. Layers in segment IIIa initially have a vergence on the shear-induced foliation parallel to the shear sense, but with progressive simple shear the vergence reverses. Similarly, layers of segment IIIb initially show a vergence opposite to the shear sense but with progressive deformation the vergence becomes parallel to the shear sense. On the other hand, layers in segment I will always show a vergence opposite to the shear sense irrespective of the magnitude of accumulated finite strain, whilst layers in segment II will always show a vergence parallel to the shear sense.

Deviations from simple shear

Ideal simple shear is probably rare in nature, and descriptions of natural shear deformations by simple shear models can be expected to only approximate flow in real rocks. Some natural deformations are much better described by flow with a vorticity number considerably less then 1 (e.g. Platt and Behrmann 1986; Vissers 1989). Fig. 2.11b illustrates, in Mohr space, the progressive deformation of a volume of material in a flow regime with simultaneous pure and simple shear components ($W_k = 0.5$). Again, vergence relations set after a first increment of deformation can be read from the incremental Mohr circle (F_1; outlined in Fig. 2.11b). Shear-related foliations will initially develop parallel to ISA1, at an angle of 15° to the flow plane (FA1). Therefore, any layer with an initial orientation, relative to FA1, of ISA1< α <ISA2 (segment I) will *initially* have a vergence on the shear-induced foliation opposite to the shear sense, whilst layers at angles α <ISA1 and α >ISA2 (segment II) will *initially* have a vergence parallel to the shear sense. Now consider

progressive deformation in this flow regime characterized by $w_k = 0.5$, illustrated by the series of Mohr circles for F shown in Fig. 2.11b. Similar to the previous case of ideal simple shear, lines of maximum and minimum stretch, i.e. the finite strain axes X^0 and Z^0, are represented in Mohr space by material lines with stretches $1+e_x$ and $1+e_z$. Because X^0 and Z^0 are not fixed with respect to the external reference frame, all layers with initial angles $ISA2 < \alpha < Z^0$ (segment IIIa) and $ISA1 < \alpha < X^0$ (segment IIIb) reverse their vergence on the foliation with progressive deformation. Layers in segment I always have a vergence opposite to the shear sense, whilst layers in segment II will always show a vergence parallel to the shear sense irrespective of the accumulated finite strain. For the above material lines no principal differences exist with the case of ideal simple shear.

The principal difference with ideal simple shear is the existence of a second flow apophyse FA2 which, for flow with a vorticity number of 0.5, lies at 120° with respect to FA1 (Fig. 2.11b). Layers initially at angles $\alpha > FA2$ (segment IV) also rotate towards the flow plane of deformation (FA1) but in a sense opposite to the material lines in segments I-III. This implies that all layers of segment IV have a consistent vergence on the shear-induced foliation parallel to the shear sense irrespective of the total strain accumulated with progressive deformation.

Practical aspects and limitations at high shear strains

Up to this point, much of our attention has focussed on the initial or undeformed state of the layered material. Most natural shear zones, however, cannot be expected to contain much information on the *deformation path* followed by the individual markers and just reflect the finite state of the deformation. As outlined above, Mohr circles for F also contain information on this finite state. Fig. 2.12 shows the orientation of the *finite strain axes* X and Z and the orientation of material lines with different initial orientation with respect to the flow plane, as a function of the shear strain for a deformation history with a kinematic vorticity number of 1. From this figure, the vergence of any layer with a particular initial orientation can be read for different values of finite shear strain. Some practical aspects and limitations of applying the vergence principle to natural sheared terrains can be read from this diagram as follows.

1: The diagram shows that the vergence relations strongly depend on the initial orientation of the layering. The application of the vergence concept to the kinematic analysis of sheared terrains, therefore, is possible *only* when the pre-deformed geometry of the layering is known. This requirement will be sufficiently fulfilled if it can be ascertained that the layering in question was virtually planar, hence that its orientation

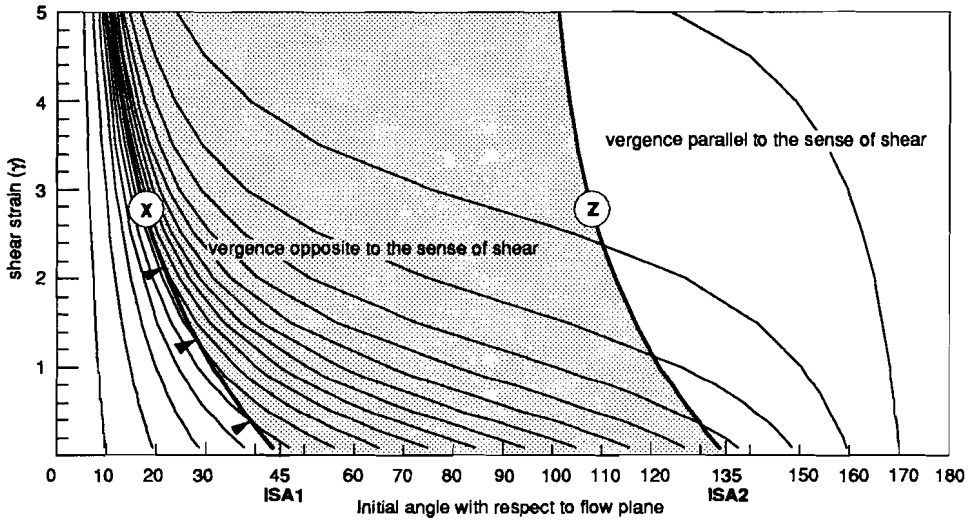

Fig. 2.12 Plot of shear strain versus finite orientation of the shear foliation (X parallel to shear foliation, Z perpendicular to shear foliation) and material lines with different initial orientation. Shaded area corresponds to orientations of layers with a vergence opposite to the sense of shear. Arrows denote reversals of vergence.

was constant throughout a given domain before deformation. From Fig. 2.12 it follows, that if this condition cannot be ascertained, variations in the vergence of the shear foliation may be simply due to different initial orientations.

2: Layers with initial orientations $\alpha < X^0$ have a vergence on the shear foliation parallel to the shear sense, whilst some of these layers (initial orientation $ISA1 < \alpha < X^0$) may have reversed their vergence during deformation. In most natural cases, however, no record of this vergence-reversal needs to be preserved. At moderate to high strains, the shear-induced foliation, supposed for present purposes to be parallel to X, rotates towards parallelism with the flow plane. This implies that layers with initial orientation $\alpha < X^0$ accumulate in orientations between X and FA1. Consequently, angular relationships between layering and foliation will become very small and thus sensitive to errors. As a consequence, like in analyses of folded sequences, the method may become difficult to apply and therefore unreliable at very high strains.

3: With increasing shear strain, layers with a range of initial orientations $\alpha > Z^0$ maintain their vergence on the shear foliation parallel to the shear sense. A noteworthy feature to be read from the diagram, however, is that this range becomes increasingly narrowed towards high initial angles at high strains (e.g., $\alpha > 160°$ at $\gamma = 2.4$, $\alpha > 170°$ at $\gamma > 5$).

4: A full kinematic interpretation of the vergence relations is only possible when a strain gradient is preserved in the area under investigation. If no strain gradient allied to progressive non-coaxial flow has been preserved, vergence relations cannot be used to infer the kinematics of the deformation unless the initial orientation of the layering in the host to the shear zone is known. A change of vergence allied to strain localization in the shear zone, however, may be preserved in the shear zone margin. Layers at initial angles ISA1$<\alpha<X^{o}$ and ISA2$<\alpha<Z^{o}$ will show a change of the vergence associated with the strong deflection of the marker into the shear zone. Shear zone margins, therefore, may contain valuable kinematic information to be inferred either from changing vergence relations or from contortions of the layering (see also Ramsay and Graham 1967). Thus, where constant vergence relations over large terrains are difficult to interpret in terms of shear sense, *changing vergence relations* related to strain localization in the margins of shear zones may render conclusive information not only on the shear sense but, provided that sufficient data are available, also to determine the finite strain and possibly even the vorticity-number of the deformation.

The vergence concept as outlined above is used in Chapter 3 to unravel the kinematics of some of the km-scale shear zones developed in the Ronda peridotite of SW Spain.

CHAPTER 3

Structure and microstructure of the Ronda Peridotite, Betic Cordilleras, SW Spain.*

3.1 Regional setting of the Ronda peridotite

The Betic Cordilleras of southern Spain form the northern and northwestern part of an arc- shaped mountain belt surrounding the western end of the Mediterranean or Alboran Sea (Fig. 3.1). The belt represents the westernmost termination of the Alpine orogenic system of southern Europe. It developed in response to Late Mesozoic to Tertiary convergence between Africa and Iberia. The Betic Cordilleras are commonly divided into an External and an Internal Zone. The External Zone consists of non-metamorphic Mesozoic and Tertiary sediments preserved in the Pre- and Subbetic units and represents the deformed remnants of the Iberian margin faulted and thrusted during the Early Miocene. The Internal or Betic Zone is made up of intensely deformed and metamorphosed Paleozoic and Mesozoic rocks, exposed in elongate ranges approximately parallel to the trend of the belt. The Betic rocks constitute a large number of tectonic units commonly grouped in three tectonic complexes (e.g., Torres Roldán 1979). These are, in ascending order, (1) the Nevado-Filabride complex, (2) the Alpujarride complex and (3) the Malaguide complex. Only the Malaguide complex consists of essentially unmetamorphosed sediments, the other units experienced pluri-facial metamorphism (see e.g. Bakker et al.

* Parts of this chapter have been published as: Van der Wal, D., and Vissers, R.L.M. 1991. Deformation processes in mantle peridotites: the Ronda peridotite record. Abstracts Geol. Soc. Australia, SGTSG conference, Margaret River, WA, September 30 - October 4, p. 72-73.

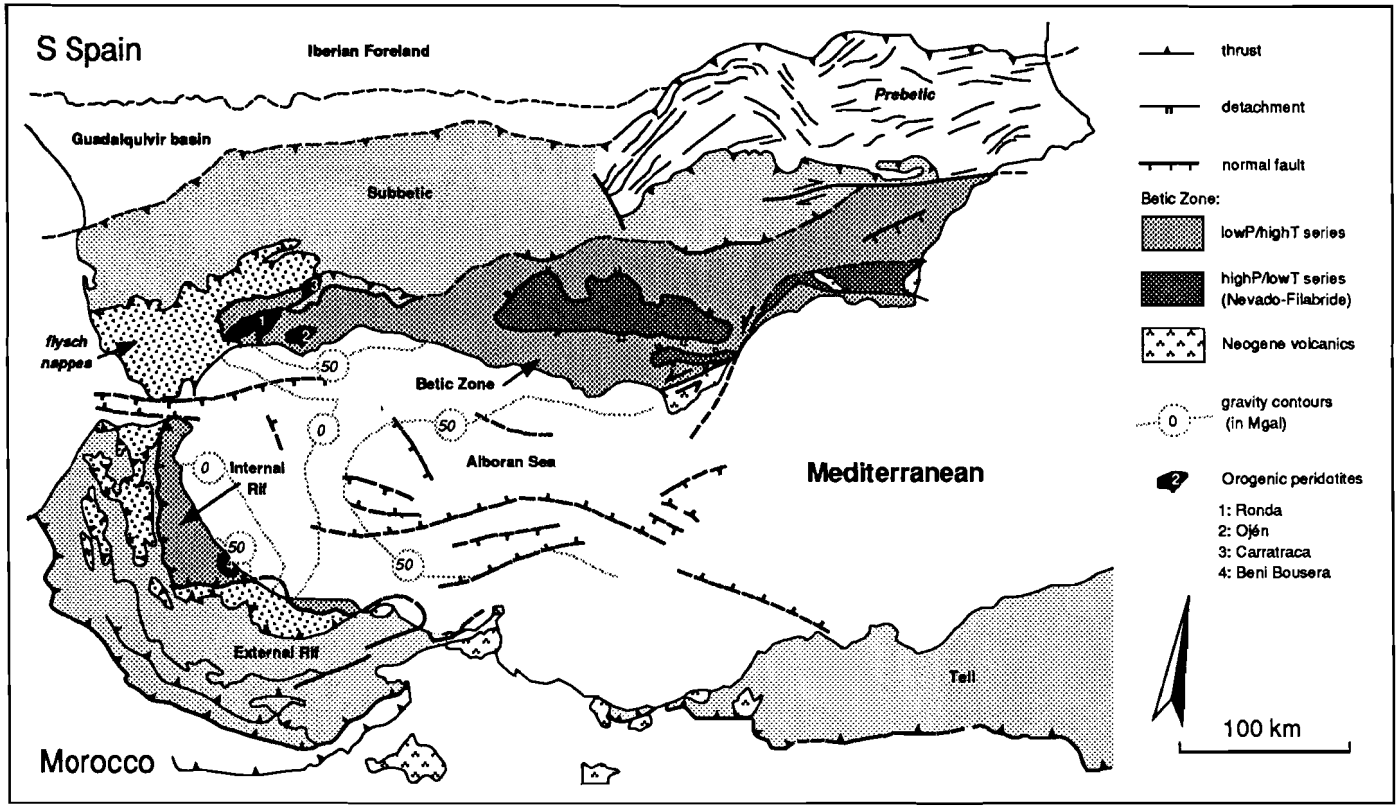
S Spain
Iberian Foreland
Prebetic
Guadalquivir basin
Subbetic
flysch nappes
Betic Zone
Alboran Sea
Mediterranean
Internal Rif
External Rif
Tell
Morocco
thrust
detachment
normal fault
Betic Zone:
lowP/highT series
highP/lowT series (Nevado-Filabride)
Neogene volcanics
gravity contours (in Mgal)
Orogenic peridotites
1: Ronda
2: Ojén
3: Carratraca
4: Beni Bousera
100 km

1989, and references therein). The Betic ranges are separated by in part fault-bounded intra-montaneous basins with a highly variable record of continental and marine sediments of Neogene and Quaternary age.

In the western part of the Betic Zone and in the Rif and Tell ranges of Morocco and Algeria, ultramafic massifs with Neogene emplacement ages (Priem et al. 1979) occur thrusted amidst metamorphic rocks of clearly crustal origin. These massifs include the peridotite bodies of Ronda, Ojén and Carratraca in SW Spain, of Beni Bousera in Morocco, and of Collo in Algeria (Fig. 3.1). The present study focusses entirely on the Ronda peridotite, located at the westernmost termination of the Internal or Betic Zone NW of the Alboran Sea. This peridotite forms a 1.5 km thick thrust sheet which overlies high-grade gneisses and marbles of the Blanca Unit (Lundeen 1978) commonly assigned to the Alpujarride complex. To the NW and W, the peridotite body is bound by a thin, 100 m scale high-grade metamorphic sequence of relict granulites (kinzingites), overprinted by a LP/HT facies series grading towards sillimanite-facies schists close to the peridotite contact (Torres Roldán 1981, Hollerbach 1985). These rocks are known as the Ronda aureole rocks of the Casares Unit (Loomis 1972a). The Ronda peridotite has preserved all three peridotite facies, i.e., garnet-, spinel- and plagioclase-lherzolite facies in an essentially coherent outcrop of some 300 km² (Obata 1980). The recent recovery, in the Beni Bousera peridotite in N Morocco (Pearson et al. 1989, Tabit et al. 1990) as well as in Ronda (G.R. Davies, pers. comm. 1992), of graphite pseudomorphs after diamond point to an origin from deep-lithospheric or asthenospheric levels. It follows that the Ronda and other W Mediterranean peridotites have preserved the imprints of successive stages in their history of uplift and eventual emplacement in the crust. The structural and metamorphic history of the peridotites and the significance of the ultramafics for the geodynamic evolution of the W Mediterranean region has hitherto been subject of debate, reflected by diverging interpretations of the structures and assemblages observed in the peridotites (see, e.g., Obata 1980, Tubia and Cuevas 1986, Saddiqi et al. 1988, Chapter 7 this thesis). For coherency, these and other previous and current studies are summarized in Chapter 7 where the structural and thermal data obtained in this study are used to evaluate the various views on the tectonic significance of the W Mediterranean peridotites.

◁ Fig. 3.1 (previous page): Simplified tectonic map of the Western Mediterranean (after Platt and Vissers 1989), showing the tectonic stratification of the Betic-Rif orogenic belt, onshore exposures of ultramafic massifs, spatially associated positive gravity anomalies underneath the Alboran basin (Bonini et al. 1973) and the major localities of Neogene volcanics. Ultramafics exposed at Collo are situated further east.

3.2 Contact relations and main characteristics of the Ronda massif

The western Ronda massif is entirely bound by brittle faults. A brittle fault gouge of up to 10 m wide separates the garnet-spinel mylonites in the NW part of the massif from high-grade metamorphic rocks of the Casares unit. Likewise, the southern or lower peridotite contact is faulted and marked by extensive brecciation. At several localities at the southern contact the peridotite is bound by high-angle normal faults affecting the low-angle brittle thrust fault separating the Ronda peridotite from the underlying Blanca unit (Lundeen 1978). In view of the ubiquitous evidence for extensive brittle deformation associated with final emplacement of the peridotite, and the large rigid block rotations of up to 60° documented in several nearby rocks of the Betic zone (e.g., Platzman 1992) it is emphasized that all ductile kinematic data presented in this Chapter refer to present-day geographical coordinates, and that kinematic interpretation of these data to a W Mediterranean tectonic framework is surrounded by uncertainties on unconstrained but conceivable rigid body rotations during brittle thrusting.

Form-surface mapping in the Ronda massif reveals that the internal structure of the peridotite is dominated by three SW-NE trending structural and metamorphic domains (App. A3). These domains are:
1: porphyroclastic spinel peridotites and mylonitic garnet-spinel peridotites in the NW part of the Ronda peridotite, hereafter referred to as garnet-bearing peridotites,
2: granular spinel peridotites in the central part of the mapped area, and
3: porphyroclastic plagioclase peridotites in the southern and eastern part of the Ronda peridotite.

All peridotites show a moderate to strong imprint of late serpentinization, which will not be considered in detail. The massif is transected by sinistral strike-slip faults with estimated displacements of up to several hundreds of meters. In the NE part of the map area a prominent "graben" structure has been identified, bound by extensional brittle faults. Towards the east, the map area is bound by a major sinistral strike slip fault with a displacement of at least 10 km. E of this fault the massif consists mainly of plagioclase peridotites (see also Obata 1980). This part of the massif has not been mapped in detail. All of the structural and metamorphic domains are cut by up to 10 m thick aplitic dikes.

In this chapter I investigate the structures and assemblages of the Ronda peridotite by means of a detailed structural and microstructural analysis, with the aim to assess the geometry and kinematics of the deformation and the relationship of the deformational

structures with the various metamorphic assemblages. The *relative ages* of the different domains as inferred from the structural and metamorphic overprinting relationships are carefully constrained, and provide the basis to study the thermal evolution of the peridotites in Chapter 4 and the mechanical evolution of the peridotites in Chapter 6.

3.3 Garnet-bearing peridotites: the earliest structures preserved

Structure and microstructure of spinel tectonites

The earliest structure preserved in the Ronda peridotite occupies the NW part of the Ronda massif and is dominated by porphyroclastic spinel peridotites, hereafter referred to as spinel tectonites (App. A3). Their maximum dimension is ~10 km measured perpendicular to the foliation. They are bound by granular peridotites to the S and SE, and by a 500 m thick garnet-spinel mylonite to the NW.

The spinel tectonites are dominantly lherzolites with minor (<5%) garnet pyroxenites. The porphyroclastic structure of the spinel tectonites is accentuated by elongated pyroxenes in an olivine-dominated matrix (Fig. 3.2a). The intensity of the foliation is fairly homogeneous throughout the domain, but locally there are 100m-scale discontinuous lensoid domains in which the rocks are less deformed and display a coarse-grained granular structure. Such heterogeneities provide evidence for km-scale strain localisation. The main foliation in the spinel tectonites dips steep to the NW and SE (App. A3). Stretching lineations in the plane of the tectonite foliation are dominantly subhorizontal but, locally, also subvertical. Pyroxenite layers are generally straight and always oriented parallel to the spinel tectonite foliation. Only in the most intensely foliated spinel tectonites, pyroxenite layers may be isoclinally folded or boudinaged.

The spinel tectonite microstructure is dominated by large elongate olivines (1-2 mm) surrounded by small olivine neoblasts (200-400 μm). The grain boundaries are straight to curved. Deformation induced undulatory extinction and deformation bands (sub)parallel to olivine (100) are common. Elongate orthopyroxenes clasts (enstatite) with clinopyroxene exsolution lamellae (Fig. 3.2b) are surrounded by polygonal orthopyroxene and clinopyroxene (diopside) neoblasts, suggesting deformation-induced dynamic recrystallization of the pyroxenes (Urai et al. 1986). Orthopyroxene also occurs as small exsolution-free grains amidst olivine. Clinopyroxene clasts (diopside) are mostly replaced by polygonal shaped neoblasts delineating elongate clusters, aligned parallel to the

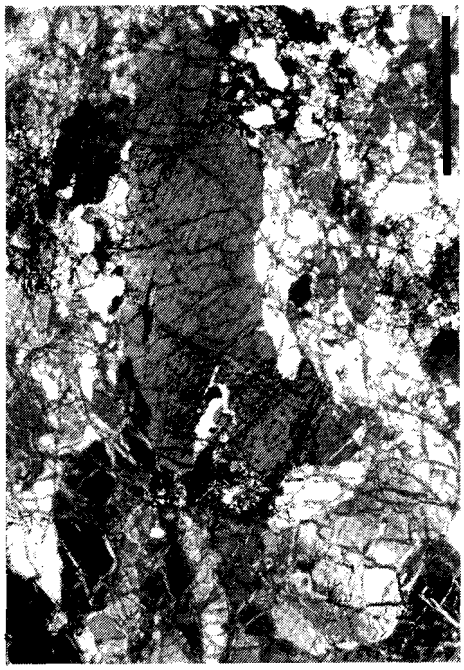

b

d

a

c

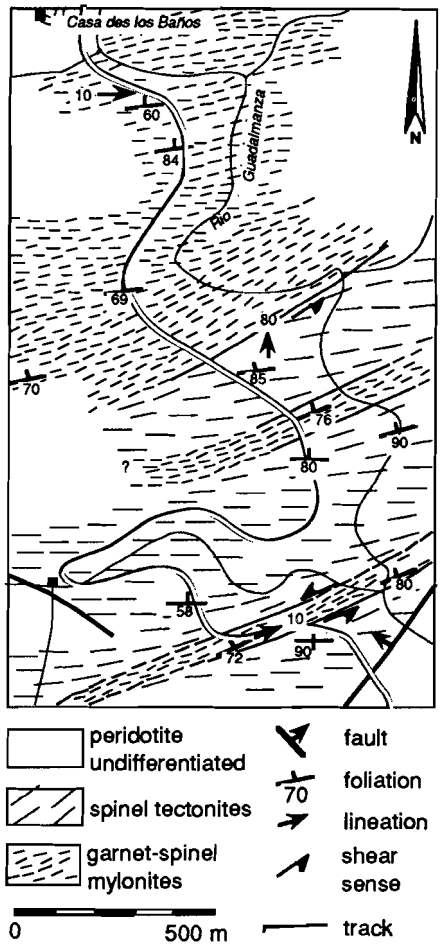

Fig. 3.3: Detailed structural map of the upstream part of River Guadalmanza (locality shown as inset in App. A2), showing localization of the deformation in garnet-spinel mylonite zones within a wall rock of spinel tectonites.

◁ Fig. 3.2 (previous page): Structures and microstructures in spinel tectonites and garnet-spinel mylonites. (a) Field aspect of the spinel tectonite foliation with a garnet pyroxenite layer parallel to the foliation. Diameter of coin 2 cm. (b) Photomicrograph of a spinel tectonite microstructure. Scale bar 2 mm. (c) Field aspect of garnet-spinel mylonites with strongly boudinaged garnet pyroxenite bands. Diameter of coin 2 cm. (d) Photomicrograph of a garnet-spinel mylonite microstructure, showing a spinel rimmed by a symplectitic assemblage. Scale bar 2 mm. (e) this page: Microstructure of a garnet-spinel mylonite showing extremely stretched orthopyroxene. Scale bar 2 mm.

foliation. Spinel shows a holly-leaf (Mercier and Nicolas 1975) microstructure, and occurs in trails of several grains aligned parallel to the foliation. The spinel tectonite microstructure is broadly similar to the porphyroclastic microstructures commonly observed in mantle xenoliths (Mercier and Nicolas 1975). Small amounts of amphibole (pargasite) replaced pyroxene on grain boundaries and triple junction contacts, possibly indicating the presence of hydrous fluids during deformation.

Olivine lattice preferred orientation (LPO) patterns in the spinel tectonites are shown in Fig. 3.4a. Olivine [100] axes are concentrated in a point maximum at small angles (<5°) to the foliation and subparallel to the lineation. A second maximum occurs perpendicular to the lineation at small angles to the foliation plane. Olivine [010] is mainly concentrated in a point maximum perpendicular to the foliation, whilst fewer [010] axes define a small partial girdle running perpendicular to the foliation. Olivine [001] shows a dominant maximum at large angles to the lineation in the foliation plane, with a partial girdle running towards the periphery of the stereonet. Following Bouchez et al. (1983), this fabric pattern suggests crystal-plastic deformation accommodated by intracrystalline slip on the olivine [100]{0kl} slip systems, with a strong contribution of [100](010). These slip systems are well known from olivines experimentally deformed under mantle conditions (Avé Lallemant and Carter 1970).

Structure and microstructure of garnet-spinel mylonites

In a 500m wide zone along the NW periphery of the massif, but also in narrow zones within the massif, the spinel tectonite fabric gradually passes into a mylonitic fabric. This is particularly evident in the upstream part of river Guadalmanza in the eastern part of the mapped area, where the spinel tectonite foliation consistently rotates, within a distance of less than 10 meters, into parallelism with the mylonitic foliation of these zones (Fig. 3.3). This relationship provides conclusive evidence that the mylonites *postdate* the spinel tectonites. The sense of rotation of the spinel-tectonite foliation into the mylonite zones can be used as a shear sense indicator (Ramsay and Graham 1970) and indicates a sinistral sense of shear in the mylonites with respect to present-day geographical coordinates. This movement sense is consistent with previous kinematic interpretations of olivine LPO patterns by Darot (1973).

The mylonites are mainly lherzolites with minor harzburgites and dunites. The mylonitic foliation dips steeply to the W and NW, with mineral stretching lineations which are dominantly subhorizontal. Locally, the mylonites contain up to 50 volume% of pyroxenite layers. These layers are either straight or boudinaged, and are always parallel to the foliation (Fig. 3.2c). Extreme boudinage of these pyroxenite layers led in some cases to

complete dismembering, to the extent that single crystals occur as isolated microboudins dispersed in the mylonitic matrix. In addition, dismembered pyroxenite layers are often isoclinally folded. These structures suggest that the pyroxenite layers deformed mainly by semi-brittle mechanisms.

The mylonite microstructure is characterized by elongate olivines aligned parallel to the foliation. The olivine grain size is heterogeneous, with few relict large grains (0.5-1.0 mm) in a matrix of smaller recrystallized grains (25-200 μm). The olivine grain boundaries are commonly slightly curved. An AVA analysis (Sander 1950) of this microstructure reveals that the orientation of the small recrystallized olivine grains does not follow that of the neighbouring larger grain, suggesting that the smaller grains principally result from a migration recrystallization mechanism (Poirier and Guillopé 1979). Orthopyroxene clasts (enstatite) are stretched by slip on (100) to aspect ratios exceeding 1:10 (Fig. 3.2e), but some enstatite also occurs dispersed in the olivine matrix as small exsolution-free neoblasts with similar grain sizes as the olivines. Clinopyroxene (diopside) occurs as slightly elongate clusters of several recrystallized grains embedded in the olivine matrix, and as isolated

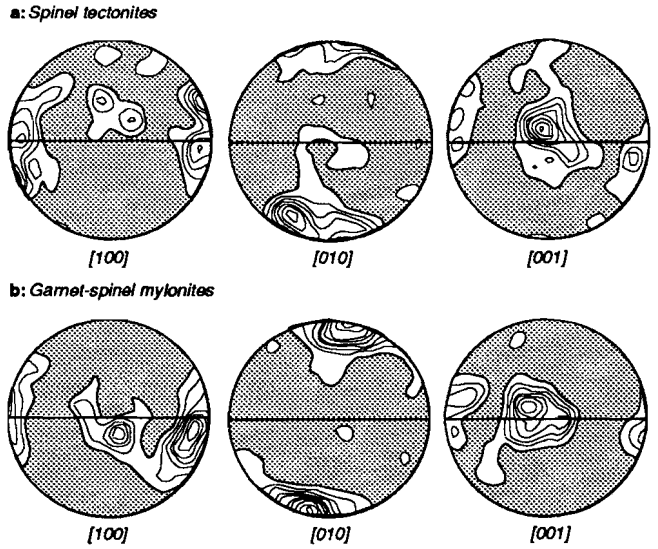

Fig. 3.4: (a) LPO pattern of recrystallized olivine in a spinel tectonite (DR89.10). Note strong point maxima distribution of crystallographic axes. The spinel tectonite foliation is shown horizontally. 100 measurements contoured at 1% intervals. (b) LPO pattern of recrystallized olivine in a garnet-spinel mylonite (DR89.3). Note strong point maxima distribution of all crystallographic axes. 116 measurements contoured at 1% intervals.

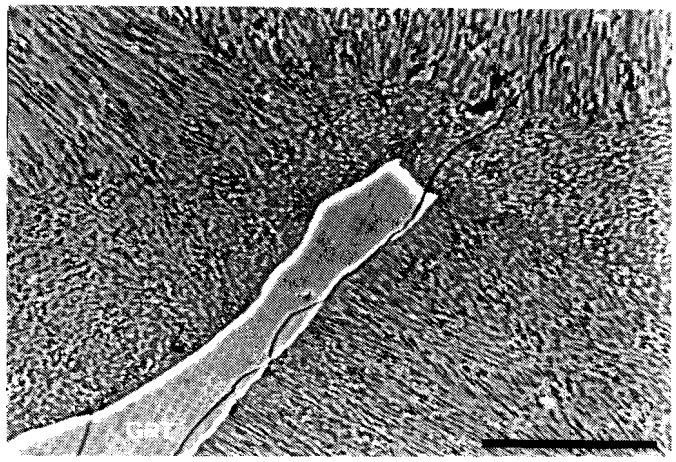

Fig. 3.5: (a) Backscattered electron photomicrograph of kelyphitic rims around garnet from a garnet pyroxenite layer, scale bar = 25 μm.

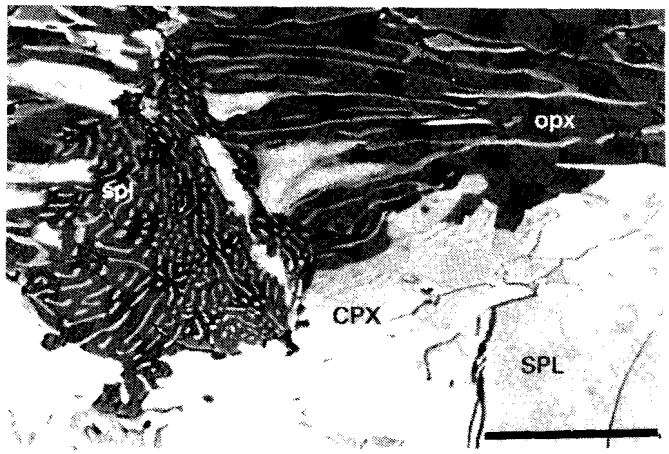

(b) Backscattered electron photomicrograph of symplectitic rims around spinel in a garnet-spinel mylonite. Note the undeformed microstructure. Scale bar = 25 μm.

grains. Spinel grains are elongate with their long axes parallel to the mylonitic foliation. Only the larger spinels have preserved their holly-leaf shapes, the smaller ones show rounded shapes and occur isolated in the olivine matrix. Spinel is often rimmed by a fine-grained symplectitic assemblage (Fig. 3.2d) considered in detail below. The characteristics of the mylonite microstructure are intermediate between those of the porphyroclastic and tabular equigranular microstructures defined by Mercier and Nicolas (1975).

Olivine LPO patterns in the garnet-spinel mylonites are shown in Fig. 3.4b. Olivine [100] is concentrated in a point maximum at small angles to the lineation, with a partial girdle running subparallel to the foliation plane. Olivine [010] shows a strong point maximum sub-perpendicular to the foliation. Olivine [100] shows two maxima: a dominant

maximum sub-perpendicular to the lineation in the foliation plane, and a second one at small angles to the foliation. This fabric suggests that slip occurred dominantly on the olivine [100](010) slip system (e.g. Mercier 1985).

Mafic layers

The dominant type of mafic layer enclosed in the garnet-bearing peridotites are up to 3 m thick garnet pyroxenites. They show a foliated microstructure characterized by elongate clinopyroxene and garnet, with minor orthopyroxene, olivine, spinel and amphibole. Occasionally, garnet pyroxenites contain significant amounts (~40%) of plagioclase. Clinopyroxene shows characteristic core-and-mantle microstructures of slightly elongate grains with serrate grain boundaries, surrounded by fine-grained clino- and orthopyroxene, ±plagioclase and amphibole. Both clinopyroxene and plagioclase show some lattice preferred orientation. These observations suggest that most garnet pyroxenite layers recrystallized dynamically, such that their earlier magmatic and/or metamorphic textures and assemblages became largely obliterated.

Garnets are rimmed by fine-grained symplectitic assemblages, made up of radial lamellae of orthopyroxene and plagioclase, with dispersed ultra-fine grained spinel (<1μm) (Fig. 3.5a). This assemblage is clearly undeformed and shows a pronounced outward coarsening. Similar symplectitic rims around garnets are common in many other ultramafic rocks and rocks of basic composition (e.g. Carswell 1986) and are known as kelyphite. They are believed to have grown after garnet during decompression (e.g. Mukhopadhyay 1991).

Spinel rimmed by kelyphite

In the garnet-spinel mylonites from the NW margin, apparently stable spinel grains occur together with spinels surrounded by fine-grained symplectitic rims (Fig. 3.2d). These latter spinels are common and bear no obvious relationship with the isolated microboudins dispersed in the mylonitic matrix described above. Mm-scale elongate symplectite assemblages scattered in the olivine matrix are also common and contain small angular spinels embedded in the fine-grained symplectite matrix. These small angular spinels probably developed from former larger spinels by micro-boudinage. The necks of the microboudins, as well as the rims of spinel clusters consist of a fine-grained intergrowth of pyroxenes and spinel, with grain sizes up to a few μm. It is emphasized that the assemblage is clearly undeformed (Fig. 3.5b). The amount of plagioclase in this assemblage is variable and always occurs associated with spinel, suggesting that plagioclase crystal-

	SPL-1	KEL	OPX	CPX	SPL-2	PLAG
SIO2	0	40.13	55.56	52.04	0	49.07
TIO2	.05	.07	.16	.52	.01	0
AL2O3	59.44	19.77	3.39	7.57	62.12	29.16
CR2O3	9.67	1.43	.21	.36	6.37	.39
CAO	.07	8.79	.33	20.99	.23	12.06
MGO	19.78	19.36	32.87	13.72	20.20	1.22
FEO	11.38	7.74	7.06	2.68	10.12	.37
MNO	.15	.42	.16	0	.07	.04
NA2O	.01	.64	0	2.03	0	4.50
K2O	0	0	0	0	.09	0
P2O5	0	0	0	0	0	0
CL	0	.04	0	0	0	.03
TOTAL	100.54	98.40	99.73	99.91	99.20	96.85
SI	0	2.959	1.928	1.882	0	2.315
TI	.001	.004	.004	.014	0	0
AL	1.798	1.717	.138	.323	1.874	1.620
CR	.196	.083	.005	.011	.129	.015
CA	.002	.694	.013	.814	.006	.609
MG	.757	2.127	1.700	.740	.770	.086
FE	.244	.477	.205	.081	.216	.014
MN	.003	.026	.005	0	.002	.002
NA	0	.093	0	.143	0	.411
K	0	0	0	0	.003	0
P	0	0	0	0	0	.03
CL	0	.040	0	0	0	0
		~Py64Gr21Al14				~An60

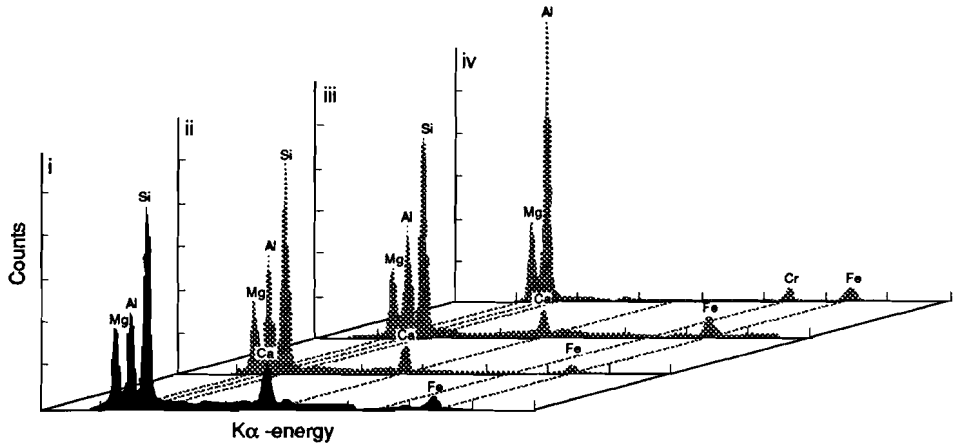

Table 3.1: Mineral compositions and bulk compositions of symplectitic rims around spinel. SPL-1: "Left-over" spinel from core of symplectitic assemblage, KEL: broad-beam analysis of symplectitic assemblage, SPL-2: fine-grained spinel of symplectitic assemblage. Shown are X-ray spectra of (i) symplectitic assemblage around spinel, (ii) kelyphite around garnet , (iii) a garnet from a garnet pyroxenite layer, and (iv) a spinel with symplectitic reaction rims.

lized at the expense of a precursor spinel at a stage later than, and unrelated to the development of the kelyphitic assemblage.

The composition of the following phases in the symplectitic assemblage, as shown in Fig. 3.5b, are given in Table 3.1: relict spinel (Spl1), the bulk composition of the kelyphitic assemblage (Kel), which is made up of fine-grained orthopyroxene (Opx), clinopyroxene (Cpx), spinel (Spl2) and, occasionally, plagioclase (Plag). Also shown are broad-beam (ø 15 μm) X-ray spectra of: (i) the above symplectitic assemblage, (ii) kelyphite around garnet from a pyroxenite layer, shown in Fig. 3.5a, (iii) garnet from a garnet pyroxenite layer, and (iv) a spinel, respectively. From these compositional data it is concluded that the symplectites around spinel represent a precursor pyrope-rich garnet. The field data and microstructures suggest that the transformation of early spinel into a pyrope-rich garnet occurred during mylonitization. Instead, the undeformed nature of the symplectitic rims suggests that the transformation of garnet into kelyphite postdates the mylonitic deformation, hence that this transformation is unrelated to mylonitization and associated ambient conditions. Symplectitic reaction rims broadly similar to those documented here have been reported from deformed domains of the Horoman peridotite in Japan (Niida 1984).

Discussion

The significance of the garnet-bearing peridotites as regards the ambient pressure-temperature conditions during their development is subject to considerable debate. This arises from the fact that there are at least three principally different ways in which garnet can be produced within a peridotite assemblage: (1) as primary minerals formed at appropriate pressures and temperatures within the mantle, (2) by tectonic dispersion of garnet pyroxenite layers, and (3) as secondary minerals formed during metamorphism of spinel-peridotite or serpentinite possibly assisted by enrichment of the spinel-peridotite protolith in mafic components (Menzies and Dupuy 1991).

The present study confirms that mechanical isolation of garnets due to extreme boudinage of garnet pyroxenite layers at very high strains, hence tectonic dispersion, has been an important mechanism. Similar observations have restrained many workers from classifying the garnet-bearing mylonites in the NW Ronda peridotite as "true" garnet peridotites (e.g. Schubert 1982, Pearson et al. 1989, Kornprobst et al. 1990). On the other hand, in view of the presence of clearly stable garnet-olivine contacts, Obata (1980) has argued that these mechanically introduced garnets remained stable, and therefore equally reflect garnet-peridotite facies conditions. A similar conclusion was put forward by Saddiqi et al. (1988) for the garnet-peridotites in the Beni Bousera peridotite. Obata's

reasoning was heavily criticized (Schubert 1982) and till date it has remained unestablished whether the Ronda peridotite actually equilibrated in the garnet peridotite stability field.

This study shows that many spinels in the garnet-spinel mylonites are rimmed by kelyphitic aggregates of ultra-fine grained pyroxenes and spinel. Such kelyphite rims around spinel have not been observed in the spinel tectonites. The present recovery of symplectitic reaction rims around spinel with bulk compositions of a pyrope-rich garnet suggests that the mylonites indeed represent true garnet peridotites, developed during metamorphism of a spinel peridotite. It is emphasised that there are also stable spinels in the mylonites. This can either be due to slow reaction kinetics with respect to possibly high strain-rate deformation in the mylonites, or indicate that garnet and spinel occurred together in a peridotitic assemblage equilibrating near the garnet- to spinel peridotite transition (~2000 MPa, see App. A1). The width of this transition can be considerable as a result of variations in Cr-content of the spinels (Caroll Webb and Wood 1986). Whether destabilization of spinel was primarily related to mixing of mafic components from pyroxenite layers with the host lherzolite, or to slightly changing PT conditions towards the garnet-peridotite facies, is difficult to assess. In any case, the occurrence of the kelyphitic symplectites in the mylonites seems unrelated to intensely stretched pyroxenite layers, which lends support to secondary formation of garnet.

In view of the complete lack of microstructural evidence for destabilization of spinel in the spinel tectonites, the transition from spinel tectonites to garnet-spinel mylonites is inferred to reflect a change in ambient PT conditions, i.e., from Ariégite subfacies conditions to conditions around the spinel-peridotite to garnet-peridotite transition.

Provenance of the peridotite

Graphite pseudomorphs after diamond in pyroxenites from the studied part of the Ronda peridotite (G.R. Davies, pers. comm. 1992) suggest that the spinel tectonites went through a complicated uplift history starting at base-of-lithosphere or asthenospheric levels. Scattered pyroxene-spinel clusters, often used in mantle xenolith suites to infer a garnet peridotite protolith (e.g. Mercier and Nicolas 1975), have not been observed in the Ronda peridotite, presumably because of the intense deformation. Virtually complete equilibration in the Ariégite subfacies thus probably obliterated most of the structural and metamorphic imprints related to this early uplift history.

Conclusions

Detailed structural analysis shows that the garnet-bearing peridotites consist mainly of

spinel tectonites, locally transected by garnet-spinel mylonite zones. Apart from significant strain localization, there is a change in ambient conditions allied to this structural transition, i.e., from Ariégite subfacies conditions preserved in the spinel tectonites towards the spinel-peridotite to garnet-peridotite transition in the mylonites. The fault gouge at the NW peridotite contact suggests that all of the above internal features of the garnet-bearing peridotites may be unrelated to the features seen in the surrounding crustal units.

3.4 Granular peridotites: annealing recrystallization

Coarse-grained, virtually undeformed granular peridotites define a second structural domain dominating the central part of the massif. The granular peridotites are bound by spinel tectonites to the N and NW and porphyroclastic plagioclase peridotites to the S and SE (App. A3). The granular peridotites are characterized by equigranular pyroxenes, floating in a homogeneous olivine matrix (Fig. 3.6a). The average pyroxene grain size is remarkably heterogeneous throughout the domain, and varies from coarse (>1 cm) to relative fine grained (<0.2 cm).

The peridotites are mainly harzburgites with minor lherzolites. Small to m-sized indigenous dunitic bands occur in the granular domain and their abundance and sizes increase towards the S. At several localities, the granular peridotites include cm- to 100m-scale layered sequences of harzburgite and dunite (Fig. 3.6b). Similar harzburgite-dunite associations have been interpreted as layered magmatic structures arising from a percolating silicate melt (Quick 1981, Keleman 1990, Remaïdi et al. 1991, Takahashi 1992, Takazawa et al. 1992).

The NW boundary of the granular domain shows some typical characteristics that may be used to infer the relative age relation with the garnet-bearing peridotites NW and N of the granular peridotites. These characteristics are as follows:

1: The high relief in the NW part of the Ronda massif allows to estimate the three-dimensional shape of the boundary. Field mapping suggests that this boundary is curved, delineating parts of a km-scale dome.

2: Several well-exposed localities at the transition from garnet-bearing peridotites to granular peridotites show that this transition coincides with a change from lherzolitic to harzburgitic compositions.

3: At the scale of the map, the domain boundary associated with the transition from

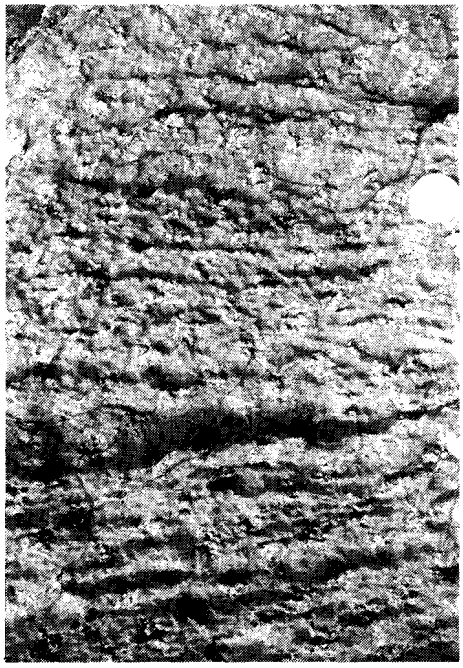

b

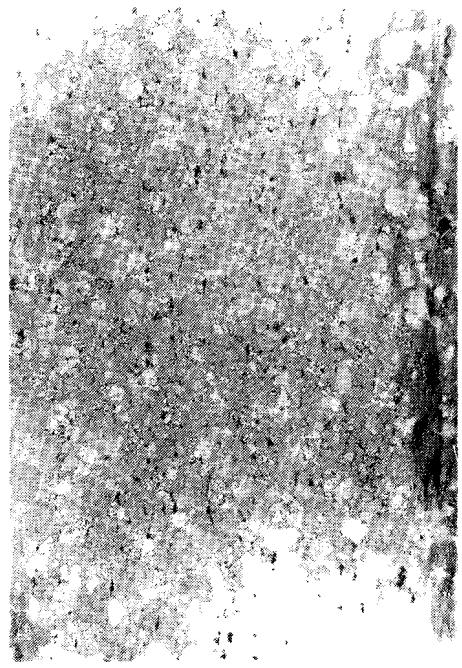

d

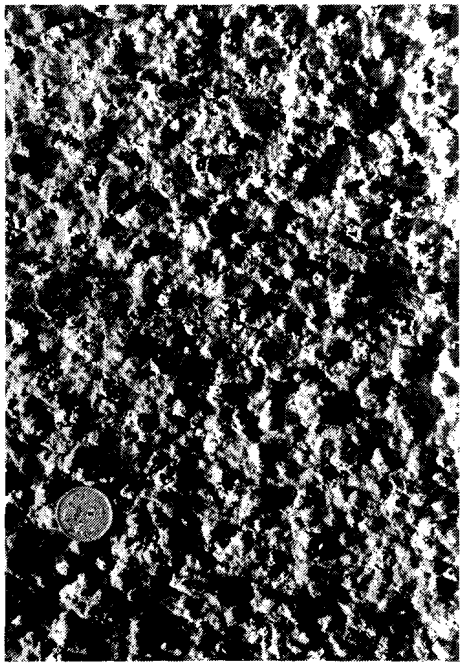

a

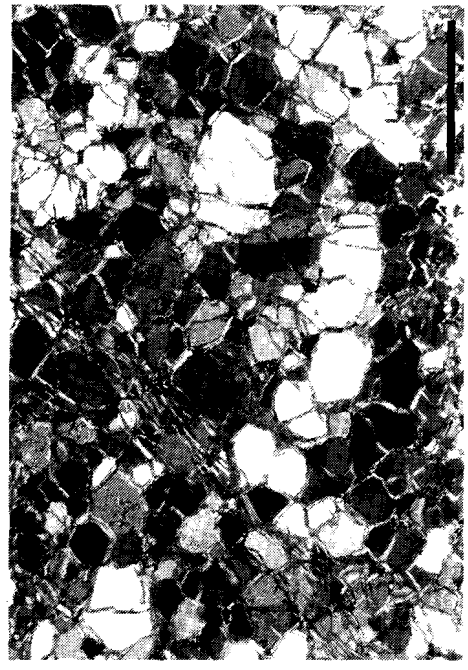

c

garnet-bearing peridotites to granular peridotites is markedly oblique to the structural trend of the spinel tectonites (App. A3).
4: The layering, i.e. compositional layering and pyroxenite dikes, is essentially continuous across the transition, and the orientation of the layering in the spinel tectonites is virtually parallel to that in the granular domain.
5: The transition from "typical" spinel tectonites to "typical" granular peridotites is not abrupt, but occurs within a narrow zone of 200 meters at the most. The transition is marked by the gradual disappearance, towards the south, of fabric elements such as the foliation and elongate pyroxenes, in that olivine and pyroxene gradually loose their shape-preferred orientation and evolve towards an equigranular microstructure.
6: The alignment of spinel grains, in trails parallel to the foliation of the spinel tectonites, is also observed in the NW part of the granular domain and, across the transition, remains constant in orientation and parallel to the layering.
All of these features suggest that the domain boundary between the spinel tectonites and granular peridotites is not the result of later juxtaposition along faults such as the en-echelon arranged sinistral strike slip faults affecting the Ronda peridotite in other parts of the area. The nature of the boundary between the granular peridotites and the plagioclase peridotites to the south and southeast will be discussed in paragraph 3.5.

Microstructures of the granular peridotites
The microstructure of the granular peridotites varies considerably as a function of their distance from the transition zone with the garnet-bearing peridotites. In the central and southern part of the domain, the microstructure is characterized by large olivine grains (2-10 mm) with curvi-linear grain boundaries and triple junction contacts. Subgrain walls, dominantly parallel to olivine (100), are common. Orthopyroxene (enstatite) and clinopyroxene (diopside) occur as often isolated, coarse and equigranular crystals embedded in the olivine matrix. Spinel grain shapes vary from idiomorphic, via holly-leaf, to small rounded grains scattered in the olivine matrix. No obvious pyroxene-spinel clusters as described by Mercier and Nicolas (1975) have been observed. The microstructures are therefore largely analogous to those documented as secondary protogranular (Mercier and Nicolas 1975) or secondary recrystallized (Downes 1987) microstructures. Amphibole

◁ Fig. 3.6 previous page: (a) Field aspect of granular peridotite. Diameter of coin 2 cm. (b) Small-scale dunite/harzburgite associations in the granular peridotites inferred to reflect melting processes. Diameter of coin 2 cm. (c) Typical annealed olivine microstructure from the transition zone between sheared spinel tectonites and granular peridotites. Scale bar 2 mm. (d) Photomicrograph of granular peridotite with typical spinel fabric. Vertical dimension 8 cm.

(pargasite) is a common constituent within less than 2 km of the transition zone with the spinel tectonites. Further away from the transition zone, no amphiboles have been observed.

In the transition zone towards the spinel tectonites, the granular peridotite microstructures are typically intermediate between the porphyroclastic microstructure of the spinel tectonites and the granular microstructures described above. At one locality in this transition zone, a conspicuous planar zone of several m width shows a microstructure characterized by the joint occurrence of stretched orthoyroxenes with high aspect ratios (>1:10) as well as rounded orthopyroxenes, both embedded in a fine-grained matrix of strain-free equigranular olivines. Many of the olivine grain boundaries are pinned at tiny spinel grains. The microstructure strongly suggests annealing recrystallization accompanied by grain growth (Fig. 3.6c, cf. Karato 1989). It is inferred that the planar zone with these microstructures represents a former high-strain garnet-spinel mylonite of which the microstructure was modified by annealing recrystallization. This annealing, however, mainly affected the olivine and some of the orthopyroxenes, whereas spinel and most pyroxenes largely retained their earlier grain shape. The wall-rock of this planar zone largely resembles that of a non-annealed spinel tectonite, with the exception of abundant triple junctions and some largely strain-free olivines. The extent of annealing recrystallization and grain growth in the wall-rock as compared to the planar zone is limited. The reason for this could be the coarser grain size in the wall-rock of the planar zone, limiting the surface stored strain energy driving grain boundary migration (e.g. Poirier 1985).

A more evolved granular microstructure from the transition zone is illustrated in Fig. 3.6d. This microstructure is characterized by coarse-grained equigranular olivines which enclose coarse equigranular pyroxenes and holly-leaf shaped spinels. The spinel grains show a distinct shape preferred orientation, oriented parallel to the long side of Fig. 3.6d, and are aligned in trails. Similar spinel trails can be traced in the field across the transition into the spinel tectonite domain where they are parallel to the spinel tectonite foliation. These trails are therefore inferred to reflect the earlier deformation history.

The microstructures from the transition zone suggest that they represent an intermediate stage in the development of the granular peridotites by annealing recrystallization and grain growth affecting a *deformed* protolith. It is noted in this context that the processes and mechanisms leading to obliteration of the pyroxene shape fabrics during progressive annealing are not well understood.

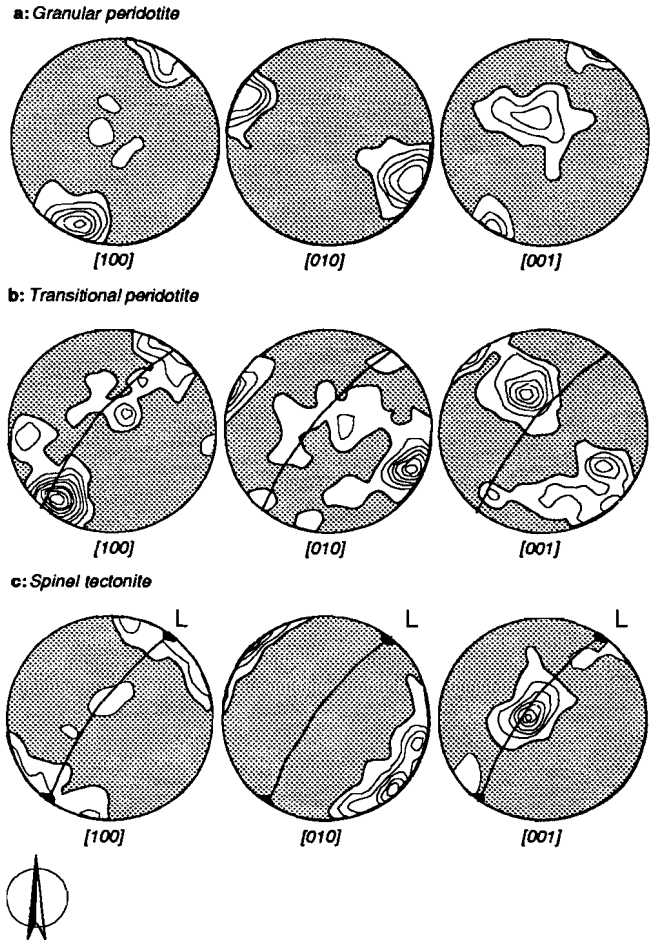

Fig. 3.7: Olivine LPO patterns across the transition zone from porphyroclastic spinel peridotites to granular peridotites, represented relative to geographical coordinates. (a) LPO of typical granular peridotite (DR89.91), 87 measurements contoured at 1% intervals. (b) Peridotite from the transition zone between spinel tectonites and granular peridotites (DR90.22), 133 measurements contoured at 1% intervals. Foliation indicated. (c) Spinel tectonite (DR89.65), 100 measurements contoured at 1% intervals. Foliation and pyroxene stretching lineation indicated. Note annealing recrystallization and grain growth has not significantly affected the olivine LPO patterns.

Lattice preferred orientation patterns

In order to further investigate the nature of the transition between the two domains, olivine LPO patterns have been measured in peridotites with a variable degree of annealing recrystallization. The presumption underlying this exercise is that annealing

recrystallization and grain growth cannot be expected to completely remove a pre-existing LPO pattern (Green 1967, Hobbs 1968). The results are shown in the stereograms of Fig. 3.7, where the orientation data are plotted with respect to present-day geographical coordinates. This approach bears the advantage that it allows to examine possible changes, across the transition, in the geometry of the LPO patterns, as well as in the orientations of the finite fabric (i.e. the spinel trails) and the flow plane (inferred to be parallel to the dominant olivine slip plane). From inspection of Fig 3.7 it is clear that the preferred orientation of olivine [010]) in the granular peridotites, transitional peridotites and spinel tectonites are essentially parallel. The 1% contour is somewhat variable, but this is probably due to a variable number of measurements and to slight variations among the LPO patterns in the garnet-bearing peridotites (Fig. 3.4). The olivine LPO patterns seem thus consistent with the hypothesis that the granular peridotites developed due to annealing recrystallization and grain growth affecting the spinel tectonites and garnet-spinel mylonites, hence that they progressively developed at the expense of a previously deformed protolith. At this stage it is noted, however, that the largely annealed microstructures and their olivine LPO patterns are as such also consistent with high temperature, low-stress defromation dominated by migration recrystallization. This alternative interpretation is further discussed below.

Mafic layers

The transition from spinel tectonites to granular peridotites is accompanied by a change in mineral composition of the mafic layers from garnet pyroxenites to spinel pyroxenites (App. A3). Notably, garnet pyroxenites from the transition zone often show symmetrical rims of spinel pyroxenite. In addition, some spinel pyroxenites from the transition zone show typical pyroxene-spinel aggregates or clusters with a diameter < 1 cm, commonly believed to represent precursor garnets (e.g. Smith 1977, Green and Burnley 1988). These observations suggest that at least part of the spinel pyroxenites from the granular domain represent the transformed and recrystallized equivalents of former garnet pyroxenites.

Further south in the granular domain, spinel pyroxenites consist of coarse-grained ortho- and clinopyroxenes, coarse greenish spinels and, occasionally, a significant amount of pargasitic amphibole. Irregular pyroxenite layers are rimmed by cm-scale depletion zones, consistent with subordinate melting in the granular domain (Remaïdi et al. 1991).

Chromium-pyroxenites

Bright-green pyroxenite layers, composed mainly of clinopyroxene with minor orthopyroxene, olivine, spinel and phlogopite, are an important constituent of the Ronda peridotite. They have been documented as Cr-pyroxenites by Obata (1980). Cr-pyroxenites occur in all different structural domains, however, over 90% of all Cr-pyroxenites are found in the granular peridotites where they occur in two different types of layers. Tiny, 1-5 cm wide "replacive" layers occur parallel to the primary banding and often contain relics of a replaced mineral assemblage, e.g. spinel. Up to 10 m thick, "intrusive" dikes have sharp, well-defined boundaries and cut across the primary banding of the peridotite wall-rock.

Though extremely uncommon, Cr-pyroxenites do occur in the garnet-spinel mylonites as undeformed "intrusive" dikes, several cm thick, which cut across the mylonitic foliation. Cr-pyroxenites are slightly more common in the spinel tectonites where they are undeformed and again discordant with respect to the layering. Cr-pyroxenites in the spinel tectonites are generally associated with garnet-pyroxenites. In the plagioclase tectonites, at one locality, a strongly deformed Cr-pyroxenite has been observed with a foliation parallel to the plagioclase tectonite foliation, indicating that the Cr-pyroxenites predate the development of the plagioclase tectonite structure.

Remaïdi et al. (1991) suggest that the Cr-pyroxenites crystallized from low-Ti and High Cr- melts which were probably boninitic (i.e. Si-rich) in composition. The Cr-pyroxenites thus provide evidence that the development of the granular peridotite was accompanied by infiltration of possibly asthenospheric melts. The structural data suggest that such infiltration occurred during or after annealing recrystallization in the granular domain but prior to the development of the plagioclase peridotites.

Discussion

Peridotites with a granular microstructure are common in many ultramafic massifs and have been documented in e.g. the Lanzo peridotite (Boudier 1978), the Erro-Tobbio peridotite (Drury et al. 1990, Vissers et al. 1991), the Josephine peridotite (Norell and Harper 1988), the Zagarbad peridotite in the Red Sea (Bonatti et al. 1981) and Lherz/ Fontête Rouge in the French Pyrenees (Conguéré 1978). Granular microstructures are also common in mantle xenolith suites, e.g. Massif Central, France (Coisy and Nicolas 1978), South Africa (Boullier and Nicolas 1975), Hawaii (Jackson 1968), Victoria, Australia (Frey and Green 1974). These observations suggest that large portions of the upper mantle underneath orogenic and volcanic belts consist of granular peridotites.

Many views exist on the development and significance of granular peridotites. There

seems to be common agreement, however, on the notion that the granular microstructures observed in mantle massifs and mantle xenolith populations reflect an *early stage* of the peridotite history prior to the development of other structures and microstructures (e.g. Green and Gueguen 1974, Boyd and Nixon 1975, Mercier and Nicolas 1975, Drury et al. 1990). The present study, however, indicates that the granular peridotites of the Ronda massif form an exception to this rule. The structures and microstructures observed across the transition zone clearly show that the granular microstructures *postdate* the spinel tectonites and garnet-spinel mylonites. This relative chronological relationship is opposite to that traditionally inferred for mantle rocks underneath kimberlite pipes (Boyd and Nixon 1975), xenoliths from alkali-basalts (Mercier and Nicolas 1975), mantle diapyrs (Green and Gueguen 1974, Coisy and Nicolas 1978) and some peridotite massifs (e.g. Drury et al. 1990).

The structures and microstructures of the granular peridotites suggest that annealing recrystallization and grain growth have been important. However, from the nature of the microstructures alone it cannot be immediately decided whether they represent entirely static annealing, or dynamic recrystallization in response to low stress-high temperature deformation. In the latter case, grain sizes will tend to adjust to the newly achieved (lower) flow stresses, facilitated by olivine grain growth (e.g., Ross et al. 1980, see also Chapter 5 below). Furthermore, annealing recrystallization and grain growth cannot be expected to completely remove older deformation microstructures when the total strain achieved during the low stress deformation is low (e.g. Knipe 1989). However, as pointed out previously, the granular domain is dome-shaped at the scale of several km. Therefore, it seems highly unlikely that this boundary represents the boundary to a zone of localized low-stress deformation dominated by migration recrystallization and grain growth, developed in a deformed and fine-grained wall-rock. Furthermore, the olivine LPO patterns traced across the transition provide no evidence for any rotation of the flow plane or finite fabric, expected across any shear zone boundary (e.g., Ramsay and Graham 1970). It is thus concluded that the granular peridotites in the Ronda massif must have developed as the result of static annealing recrystallization and grain growth rather than low stress-high temperature deformation.

During this annealing recrystallization event, garnet pyroxenites progressively transformed to spinel pyroxenites indicating significantly lower pressures (Seiland subfacies conditions, ~800-1400 MPa at 1100°C, App. A1) than those associated with progressive deformation in the garnet-bearing peridotites. In follows that significant uplift of the massif, equivalent to about 1000 MPa confining pressure, must have occurred in a stage between the development of the garnet-bearing peridotites and the granular spinel peridotites. There are no structures associated with this stage of uplift.

Conclusions

The structures and microstructures indicate that the granular peridotites developed as a result of annealing recrystallization and grain growth, accompanied by minor magmatic processes. This annealing recrystallization event occurred at Seiland subfacies conditions, and affected a deformed protolith composed of spinel tectonites and garnet-spinel mylonites. The granular spinel peridotites thus *postdate* the foliated garnet-bearing peridotites. The preservation of the transition zone, i.e., the annealing recrystallization front, seems a rather unique feature of the Ronda peridotite. This transition zone represents a major structural, metamorphic and possibly also geochemical boundary in the Ronda massif.

3.5 Plagioclase peridotites: shear localization and ductile emplacement

Structures and microstructures of the plagioclase tectonites

Porphyroclastic plagioclase peridotites make up a third structural and metamorphic domain in the southern and eastern part of the Ronda massif (App. A3). This domain is characterized by the occurrence of plagioclase as the Al-bearing metamorphic phase both in the host peridotite and in enclosed mafic layers. The plagioclase peridotites comprise both lherzolites and harzburgites, and they enclose indigenous dunites.

At the southern margin of the granular domain, peridotites with a clearly granular microstructure gradually pass into plagioclase-bearing porphyroclastic peridotites, hereafter referred to as plagioclase tectonites. This transition towards the plagioclase-bearing rocks is reflected by an increasing intensity of the foliation towards the south, a grain-size reduction of all the mineral phases, an increasing elongation of pyroxenes towards a porphyroclastic structure (Fig. 3.8a), the sudden occurrence of plagioclase as elongate rims around spinel and, with increasing intensity of the foliation, a decreasing angle between this foliation and the compositional banding and pyroxenite layers hereafter referred to as layering. Close to the transition zone with the granular peridotites, few 10-100 m scale lenses occur of granular peridotite completely surrounded by foliated plagioclase peridotites. Dunitic layers are tightly folded, with the plagioclase tectonite foliation parallel to the axial planes of the folds. These relationships conclusively demonstrate that the plagioclase tectonites developed at the expense of, hence later than, the granular microstructures and assemblages.

Although the plagioclase tectonites are fairly uniform in their foliation development,

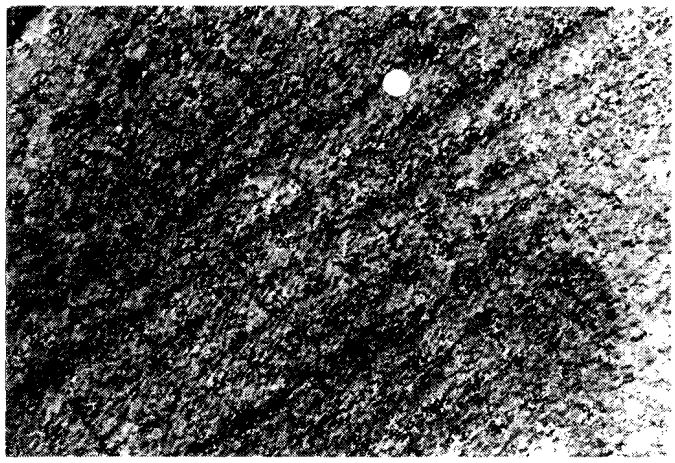

Fig. 3.8: (a) Field aspect of plagioclase tectonites. Note distinct angle between compositional banding and plagioclase tectonite foliation. Diameter of coin 2 cm.

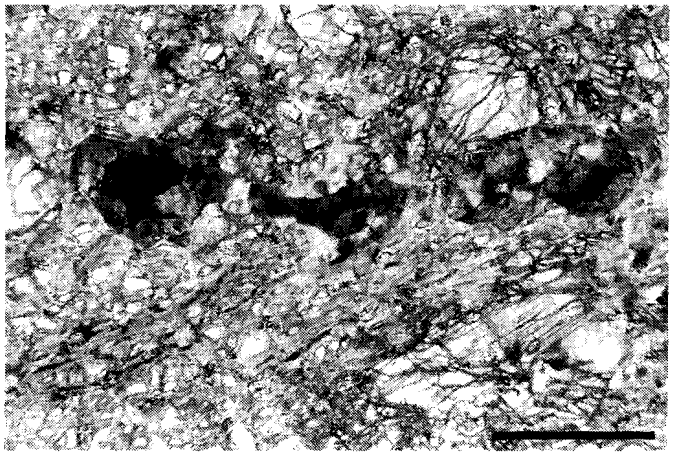

(b) Photomicrograph of the plagioclase tectonite microstructure. Note saussurite around spinel, replacing plagioclase. Scale bar 2 mm.

there are two different km-scale domains with opposite vergence (Chapter 2) of the layering on the tectonite foliation. A first and dominant domain of plagioclase tectonites is characterized by a S-ward vergence relative to present-day geographical coordinates (App. A3). Foliations in this domain dip dominantly to the N, and show mainly NS trending pyroxene stretching lineations. The minimum width of this domain is several km. Within these S-vergent plagioclase tectonites, planar zones occur of up to 1 km width with a vergence to the N and E (Fig. 3.9, App. A3). Foliations in these planar zones dip NNE

Fig. 3.9 (next page): N-S section parallel to the Cerro del Duende ridge (locality outlined in App. A3), ▷ showing vergence changes inferred to relate to late-stage shear localization in N/E vergent plagioclase tectonites overprinting S vergent plagioclase tectonites.

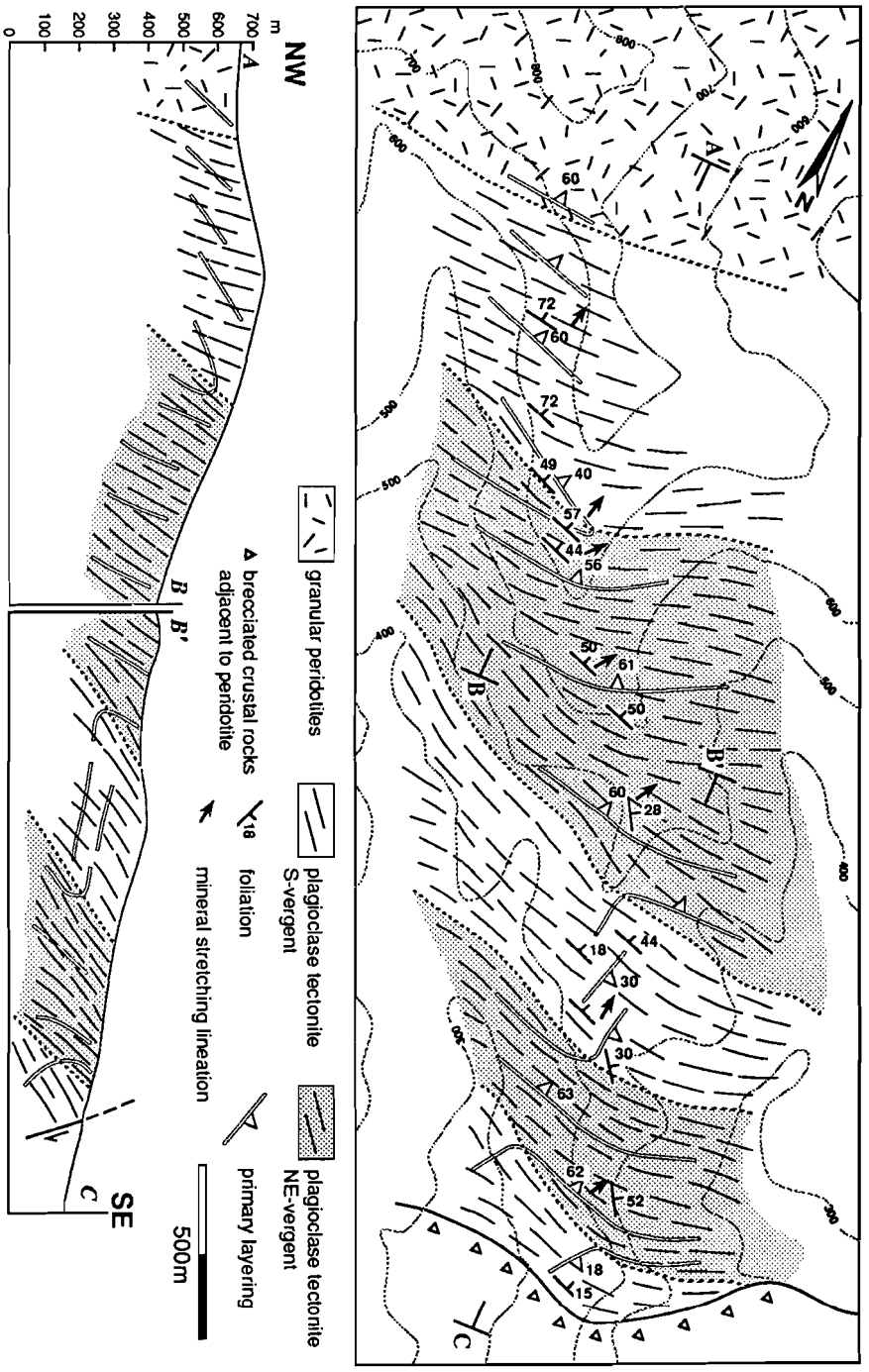
NW
SE
m
700
600
500
400
300
200
100
0
A
B
B'
C
granular peridotites
plagioclase tectonite S-vergent
plagioclase tectonite NE-vergent
breccia adjacent to peridotite
foliation
mineral streching lineation
primary layering
500m

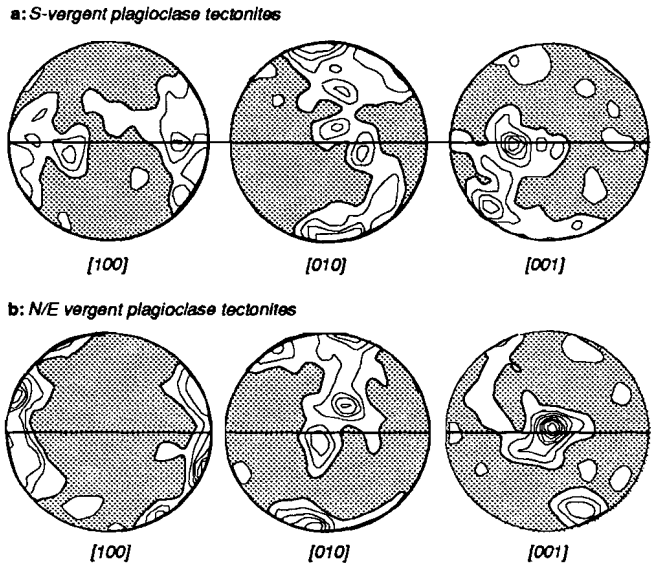

Fig. 3.10: LPO patterns of recrystallized olivine from (a) a S-vergent plagioclase tectonite (DR89.42) and (b) a N/E vergent plagioclase tectonite (DR91.32), 100 measurements contoured at 1% intervals.

to E, with mostly steep stretching lineations plunging towards 040-090. Meter-scale folds of the layering with shallow ENE dipping fold axes occur in transition zones between adjacent vergence domains. The significance of the vergence changes as regards the kinematics of the plagioclase tectonites will be discussed below.

The microstructure of the plagioclase tectonites is characterized by elongate olivine with grain sizes in the range 0.5-1 mm. Strain-free neoblasts with abundant polygonal grain shapes in some samples from S-vergent zones suggest that the microstructure has been partly annealed after deformation. Orthopyroxene (enstatite) occurs as elongate clasts occasionally rimmed by a neoblast assemblage of two-pyroxenes and some minor pargasitic amphibole. Clinopyroxene (diopside) does not show a clear shape preferred orientation. Spinel is rimmed by "dusty" aggregates with low refractive indices known as saussurite (Fig. 3.8b). In this assemblage, relict plagioclase indicates that the tectonites developed in the plagioclase peridotite facies (<700 MPa). Unfortunately, most of the details of the plagioclase tectonite microstructure have been obliterated by intense serpentinization affecting these rocks much more pervasively than those of the other structural domains. Systematic microstructural differences, if any, between the microstructures of both vergence domains are therefore difficult to assess, and have not been

observed in this study.

Both vergence domains in the plagioclase tectonites show essentially similar olivine LPO patterns, and examples are shown in Fig. 3.10. Olivine [100] is concentrated in a point maximum at small angles to the mineral stretching lineation, olivine [010] is distributed along a partial girdle perpendicular to the foliation and lineation, with a point maximum sub-perpendicular to the foliation. Olivine [001] is also distributed along a partial girdle, with a point maximum in the foliation plane. Such fabrics are consistent with crystal plastic slip on the olivine [100]{0kl} slip system ("pencil glide", Avé Lallemant and Carter 1970) during dominantly non-coaxial flow.

Mafic layers: olivine gabbros

Mafic layers composed of greenish spinel, plagioclase, orthopyroxene, clinopyroxene, olivine and amphibole, referred to as olivine gabbros by Obata (1980), are confined to the plagioclase tectonites and the southernmost 500 meters of granular peridotites. Clinopyroxene and plagioclase show a weak shape preferred orientation and some LPO. Olivine and plagioclase occur in elongate rims around spinel parallel to the tectonite foliation, suggesting syn-kinematic breakdown of spinel to plagioclase and olivine. This breakdown of spinel is consistent with the breakdown of spinel in the lherzolitic and harzburgitic assemblages. Coarse-grained clinopyroxene shows exsolution of plagioclase, facilitating the breakdown of pyroxene into a new assemblage of clinopyroxene and plagioclase (Schubert 1977). Occasionally, strong shearing in olivine gabbros has led to fine-grained (10 μm) mylonitic microstructures. The observed microstructures and assemblages of the olivine gabbros and their exclusive occurrence in the southernmost granular peridotites and plagioclase tectonites indicate that they represent deformed and recrystallized equivalents of former spinel pyroxenites.

Crustal lenses

Lens-shaped bodies of high-grade crustal gneisses and migmatites occur strictly associated with N/E-vergent plagioclase tectonites. The maximum observed dimension of such lenses is 15 m. The mineral assemblages in these lenses strongly resemble those of the high-grade gneisses and migmatites underlying the Ronda peridotite (Lundeen 1978). *The foliations and lineations developed in mylonitic rims of the lenses are parallel to those in the peridotite wall rock*, suggesting that such lenses deformed synchronous with shear deformation in the peridotite. Felsic crustal lenses may show irregular patches of granitic composition, and small granitic dikes similar to the aplitic dikes described by Obata (1980)

are observed to root in such lenses. These observations indicate that tectonic interleaving of the crustal rocks and peridotites was accompanied by minor melting of the crustal rocks. Cooling ages of granitic dikes transecting all peridotite assemblages indicate a Miocene age for their final emplacement (~22 Ma, Priem et al. 1979, Zindler et al. 1983).

Kinematic interpretation of the plagioclase peridotites

In Chapter 2 it has been shown that vergence relations may be used as a kinematic indicator, provided that the initial orientation of the layering is virtually planar. The map pattern shown in App. A3 indicates that the layering in the granular peridotites, i.e. the host of the plagioclase peridotites, sufficiently fulfills this requirement.

Folding of the primary layering occurs at a scale of several hundreds of meters (Fig. 3.9). Ramberg (1960) and Biot (1961) have shown that the wavelength of buckle folds depends on the thickness of the folded layers and the viscosity contrast between folded layer and host rock (see also review by Ramsay and Huber 1987, p. 383). An explanation of the observed fold-wavelength by buckling mechanisms thus requires viscosity contrasts at a scale of the wavelength of the folds. As the thickness of compositional banding and pyroxenite layers in an elsewhere uniform peridotite matrix is several m at the most, mechanical contrasts associated with the layering at 100 m scale must have been negligible such that folding due to mechanically controlled buckling mechanisms can be ruled out. It follows that the contortions of the layering such as those shown in Fig. 3.9 in a cross section parallel to the stretching lineation may be used to infer the kinematics of the plagioclase peridotites.

Despite the distinct strain localization reflected by the microstructures across the transition from granular peridotites to plagioclase tectonites, this transition is not accompanied by a major contortion of the layering. Following the principles of vergence relations outlined in Chapter 2 this may be explained by an initial orientation of the pre-existing layering at small angles to the flow plane of the developing shear zone, i.e., in a dominantly non-rotational orientation provided that the sense of movement in the shear zone is "top to the north". The asymmetry of the olivine LPO patterns in the south-vergent plagioclase tectonites is consistent with a "top to the north" sense of shear, indicating that the south-vergent plagioclase tectonites indeed developed in a non-coaxial flow regime with a "top to the north" sense of movement.

Major contortions of the layering are associated with the transitions from S-vergent to N/E- vergent zones (Fig. 3.9). Following Chapter 2 these contortions can be interpreted to result from strain gradients preserved in shear zone margins, where the layering mainly resided in a rotating orientation with respect to the flow plane. The sense of contortion

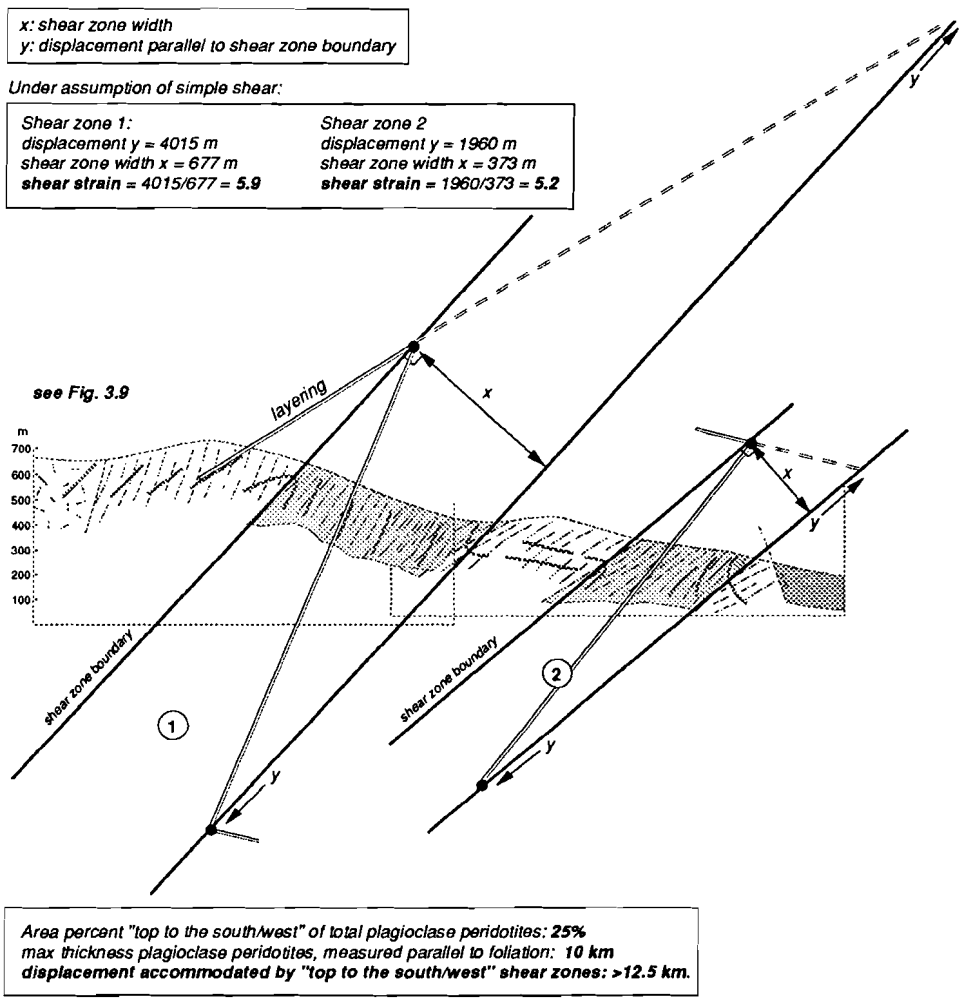

Fig. 3.11: Geometrical calculation of shear strain allied with the development of N/E vergent plagioclase tectonites. The total thickness of the plagioclase peridotites, measured perpendicular to the foliation in the eastern part of the massif is 15 km. From the map (App. A2) it can be reconstructed that ~25% of this column consists of "top to south/west" plagioclase tectonites.

of the layering into the N/E-vergent plagioclase tectonites suggests a "top to the south/west" sense of shear, consistent with the asymmetry of olivine LPO patterns in the N/E-vergent plagioclase tectonites.

Based on the observed contortions of the layering in the plagioclase peridotite allied with systematic vergence changes it is inferred that the plagioclase peridotites comprise

two shear zone generations with opposite senses of shear. The earliest S-vergent plagioclase tectonites developed during rather homogeneous, non-coaxial flow with "top to the north" senses of movement occurring in a zone at least as wide as the entire plagioclase peridotite domain. The second generation plagioclase tectonites are characterized by "top to the south/west" movements in much more localized but still km-scale shear zones.

The crustal lenses described above are exclusively associated with the N/E-vergent plagioclase tectonite shear zones, indicating that these shear zones developed during ductile emplacement of the peridotites into the crust. The contortions of the layering into these zones can be used to infer shear strains achieved during "top to the south/west" shearing. As outlined in Fig. 3.11, shear strains of $\gamma>5$ are obtained geometrically and the minimum *cumulative* displacement obtained for the "top to the south/west" tectonites is inferred to be around 12.5 km, a value throughout reasonable for shear zone structures associated with emplacement. The low angles between the layering and the inferred flow plane in the "top to the north" plagioclase peridotites preclude to reliably calculate shear strains and displacements build up during this phase of deformation.

Comparison with the Ojén massif

A similar reversal in shear sense in plagioclase peridotites can be inferred from the structural map of the Ojén massif E of the Ronda massif (Tubia and Cuevas 1986, 1987). The youngest generation of shear zones with dominantly SW-NE stretching lineations in the NW margin of the massif clearly developed synchronous with adjacent crustal units and are, therefore, also emplacement-related. In addition, Tubia and Cuevas (1986) report olivine LPO patterns from these plagioclase peridotites developed during olivine [c]-slip. Such olivine [c]-fabrics are known to result from crystal-plastic deformation accommodated by low-temperature slip systems (Mercier 1985), consistent with an interpretation of the "top to the south/west" plagioclase tectonites as being related to ductile emplacement of the peridotites into the crust.

Conclusions

The internal structure of the plagioclase peridotites is more heterogeneous than previously assumed (see e.g. Darot 1973, Obata 1980). They developed at the expense of the granular peridotites primarily as a result of pervasive shear deformation. Two shear zone generations have been recognized with an opposite kinematic framework. The youngest and more sharply localized shear zones are related to emplacement of the massif into the crust.

CHAPTER 4

Thermal history of the Ronda peridotite.

4.1 Introduction

Two main objectives in this study of mantle deformation processes motivate a detailed thermal analysis of the Ronda peridotite. First, the kinetics of the various deformation mechanisms operative in deforming crystalline aggregates is principally a function of ambient temperature. Therefore, any quantitative analysis of the deformation processes recorded in the Ronda peridotites requires temperature estimates as accurate as possible for each of the structures identified. Second, the thermal evolution of a metamorphic terrain is of crucial importance in any interpretation of structural and metamorphic processes in terms of lithosphere dynamics (Oxburgh and Turcotte 1974, England and Thompson 1984, Spear 1989). The PT evolution of the Ronda peridotites can thus be expected to embrace critical information on the geodynamic evolution of the W Mediterranean mantle discussed in Chapter 7.

The structural and microstructural study of the Ronda peridotite presented in the preceding chapter reveals the progressive development of three different structural and metamorphic domains. The relative ages of the stable mineral assemblages preserved in these domains clearly indicate a multistage uplift history with a well-defined pressure-path. Unfortunately, the metamorphic assemblages contain less information on the *thermal* evolution of the massif, as most of these assemblages are principally pressure dependent (App. A1).

The main analytical technique employed below to elucidate the temperature evolution

of the Ronda massif is *microstructurally controlled* pyroxene thermometry. However, several of the features discussed in the preceding Chapter place some qualitative constraints on the thermal history of the Ronda peridotite and these features will be summarized first. I then proceed to discuss a number of problems common to geothermobarometry and their consequences for an analytical strategy, before summarizing the analytical techniques and calculated temperatures. The results of the analyses are evaluated against further problems involved in the interpretation of the analytical temperatures in terms of ambient conditions. Finally, with some constraints on timing, the structural (Chapter 3) and thermal data (this Chapter) are compiled in a P-T-(t) trajectory for the Ronda peridotite.

4.2 Geological constraints

Though accompanied with uncertainties, several of the field and microstructural observations in the Ronda peridotite body permit a qualitative assessment of its thermal history as follows.

1: The garnet-bearing peridotites have preserved a transition, from essentially homogeneous deformation at the scale of the domain (spinel tectonites), to highly localized deformation in relatively narrow mylonitic shear zones (garnet-spinel mylonites) developed towards the NW periphery of the massif. In a recent paper by Drury et al. (1991) such localization of the deformation in progressively narrower shear zones is ascribed to decreasing temperatures, where mechanisms like grain-size-sensitive creep and brittle deformation, responsible for shear localization, become increasingly important. It is noted, however, that an order of magnitude increase of the imposed strain rate could have a similar effect.
2: An increasingly semi-brittle behaviour of the pyroxenite layers towards the NW periphery of the massif, reflected in progressive boudinage down to the level of individual constituent grains, seems consistent with progressively lower temperatures, although progressive boudinage may also be related to an increase in strain rate.
3: The facies boundary between garnet- and spinel-peridotite has a distinct, positive slope ($dP/dT \sim 0.9$ MPa/K). This implies that the transition allied with the development of the garnet-spinel mylonites, from Ariégite subfacies to garnet-peridotite facies assemblages, is consistent not only with pressurization but also with decreasing temperatures, or with

a combination of pressurization and temperature decrease (App. A1).
4: Local discordant dunite-harzburgite bodies exclusively occur in the granular peridotites (Paragraph 3.4, see also Remaïdi et al. 1991). Similar dunite-harzburgite bodies have been documented from the Trinity peridotite (Quick 1981), and are believed to be related to infiltration of silicious melts leading to the development of local percolation systems and concomitant reactions between melt and host lherzolite (Kelemen 1990, Takahashi 1992, Takazawa et al. 1992). For such super-solidus processes to occur, temperatures exceeding 1100°C are needed in a hydrous mantle (App. A1, Wallace and Green 1991). In addition, recent experimental work (Ingrin et al. 1991) has shown that melting of dry single crystals of clinopyroxene (implied in the formation of harzburgite or dunite by partial fusion of a lherzolite host) may occur at temperatures as low as 1130°C at atmospheric pressures. The discordant dunite-harzburgite bodies in the granular peridotites would thus indicate peak temperatures of over 1100°C during annealing recrystallization and development of the granular peridotites, whilst the mineral assemblages in the spinel pyroxenite layers indicate Seiland subfacies conditions.
5: The mere preservation of an annealing recrystallization front in those parts of the upper mantle now exposed in the Ronda massif suggests a thermal gradient, during annealing recrystallization, between the granular domain and the garnet-bearing peridotites as follows. Toriumi (1982) and Karato (1989) have shown that the grain-growth kinetics of olivine are strongly temperature dependent. Ingress of hydrous fluids could also produce a similar recrystallization front, even during a T-decrease well below 1000°C, because the presence of the fluids strongly promotes diffusional processes at the grain boundaries. The movement of a possible fluid front would be expected to be monitored behind the recrystallization front by a significant change in rock composition (e.g., crystallization of amphiboles). Minor amounts of hydrous phases, however, occur at both sides of the annealing recrystallization front (Chapter 3), hence their abundance is not spatially related to this front. It thus seems unwarranted to relate the annealing recrystallization to infiltration of a hydrous fluid. Therefore, annealing recrystallization is expected to be thermally-driven, and equilibrium temperatures behind the annealing front can be expected to be higher than, or equal to, those ahead of the annealing front such that the activation energy for grain growth (Urai et al. 1986) is provided or preserved, respectively. As a consequence, ambient temperatures in the spinel tectonites and garnet-spinel mylonites at the onset of annealing recrystallization should not have exceeded temperature values recorded in the granular peridotites.

The above summary of field and microstructural features suggests that a "thermal"

discontinuity may have existed in the Ronda peridotite body which coincides with the annealing recrystallization front characterizing the boundary between the garnet-bearing and granular peridotites. Field and microstructure observations NW of this boundary suggest progressively decreasing temperatures, whilst SE and S of the annealing front there is evidence for high temperature processes. In the absence of temperature-sensitive mineral assemblages it will be clear that mineral-chemistry based thermometry is needed to substantiate this interpretation.

4.3 Pyroxene thermometry

Thermometry refers to a technique where the temperature dependence of the equilibrium constant between coexisting phases is used to infer metamorphic temperatures (Boyd 1973). The equilibrium constant can be determined by measurement of the compositions of coexisting minerals in natural or simplified chemical systems. Below I will apply pyroxene thermometry to further constrain the thermal evolution of the Ronda peridotite. It will be shown that the temperature evolution derived from pyroxene thermometry is entirely consistent with the above geological data, and that taken together the data demonstrate a complicated thermal evolution of the Ronda peridotite, involving significant cooling at depth, followed by a stage of renewed heating prior to emplacement at crustal levels.

Throughout this Chapter I will use the following abbreviations of mineral names: OL: olivine; OPX: orthopyroxene; En: enstatite; CPX: clinopyroxene; SPL: spinel; GRT: garnet; AMPH: amphibole.

Thermometers available for ultramafic systems

A large number of thermometric formulations have been proposed for ultramafic systems (reviews in Finnerty and Boyd 1984, 1987, Carswell and Gibb 1987). They are based on a variety of slightly different concepts, which can be summarized as follows (after Spear 1989):

- *Exchange thermometers* based on cation exchange reactions, for example between garnet and pyroxene (e.g. Ellis and Green 1979, Harley 1984, Lee and Ganguly 1984).
- *Solvus thermometers* based on the distribution of Ca and Mg and other elements between

coexisting CPX and OPX. A further distinction between solvus thermometers can be made:
- two-pyroxene thermometers (e.g. Wood and Banno 1973, Wells 1977, Kretz 1982, Lindsley 1983, Gasparik 1984, Bertrand and Mercier 1985, Brey and Köhler 1990), or
- single-pyroxene thermometers (e.g. Mercier 1980, Sachtleben and Seck 1981, Brey and Köhler 1990, Witt-Eikschen and Seck 1991).

In general, two-pyroxene thermometers are to be preferred over single-pyroxene thermometers, because their calibration is independent of whole-rock chemistry, whilst single-pyroxene thermometers depend on whole-rock chemistry to an unknown extent. Moreover, experimentally calibrated thermometers are to be preferred over empirically calibrated ones because the P-T conditions of the experiments are accurately controlled. A serious drawback of the experimentally calibrated thermometers, however, is that the experimental phase chemistry is ideal, whereas empirical calibrations incorporate the non-ideality of the phases.

Thermometers used in this study

From the large population of pyroxene thermometers available, five different and representative thermometers have been selected. These are:

I: The Wells (1977) formulation of a two-pyroxene thermometer. Below I will refer to this thermometer as W2px:

$$T_{W2px} = \frac{7341}{3.355 + 2.44X_{Fe}^{opx} - \ln K} \qquad (4.1)$$

where K is the equilibrium constant for coexisting OPX and CPX written as a function of the activity of the enstatite component in OPX and CPX (see Wood and Banno 1973). This thermometer is well-known and widely used, and therefore bears the advantage that its results are directly comparable with other studies using this thermometer in other lherzolite massifs and in lower crustal rocks.

II: The Bertrand and Mercier (1985) formulation of a two-pyroxene thermometer (hereafter referred to as BM2px) which is based on one of the most comprehensive studies of natural system experiments:

$$T_{BM\,2px} = \frac{36273 + 399P}{19.31 - R\ln(K^*) - 12.15(Ca^*_{cpx})^2} \qquad (4.2)$$

where K* is the equilibrium constant for the En(cpx) - En(opx) transfer reaction expressed as a function of Ca- and Na-concentrations and Mg-number of CPX. This thermometer tends to slightly underestimate temperatures in experiments on natural systems (Brey et al. 1990).

III and VI: The Brey and Köhler (1990) formulations of a two-pyroxene thermometer (BK2px) and a single-pyroxene thermometer (Ca-in-OPX, BK1px), derived from the most recent experiments in natural four-phase lherzolites for conditions in the range of 1000 to 6000 MPa and 900-1400°C (Brey et al. 1990):

$$T_{BK\,2px} = \frac{23644 + (24.9 + 126.3X_{Fe}^{cpx})P}{13.38 + (\ln K_D^*)^2 + 11.59X_{Fe}^{opx}} \qquad (4.3)$$

where K_D^* is defined as in Bertrand and Mercier (1985), and:

$$T_{BK\,1px} = \frac{6425 + 26.4P}{-\ln Ca^{opx} + 1.843} \qquad (4.4)$$

with P in Kbar. The Ca-in-OPX single-pyroxene thermometer bears the advantage that it can also be used for harzburgitic compositions, but suffers from the unknown influence of whole-rock chemistry on Ca-concentrations in OPX, the low abundances of Ca in OPX, and the inferred rapid diffusion of Ca with respect to Mg, Al and Si (Sautter and Fabriès 1990) possibly making Ca-concentrations in OPX extremely sensitive to re-equilibration during cooling. It is as yet unclear if the single pyroxene thermometer can be used in mafic (pyroxenite) assemblages.

V: The Witt-Eikschen and Seck (1991) Al-in-OPX thermometer (hereafter referred to as WS1px):

$$T_{WS1px} = 636.54 + 2088.21X_{Al}^{M1} + 14527.32X_{Cr}^{M1} \qquad (4.5)$$

This recently published and hitherto rather unknown thermometer has been empirically derived for peridotite xenoliths from the Eifel-region, Germany, from systematic variations of Al/Cr-concentrations in OPX with temperature as estimated with the Brey and

	T-site		M1-site						M2-site				
	Si	Al	Al	Ti	Cr	Mg	Fe	Mn	Ca	Na	Mn	Fe	Mg
BM2px						●	●		●	●			
W2px			●	●	●	●	●		●	●	●	●	●
BK2px						●	●		●	●			
BK1px									●				
WS1px			●	●	●					●			

Fig. 4.1: Diagram showing elements involved in the geothermometers employed in this study.

Köhler Ca-in-OPX thermometer. A major advantage of this thermometer is that diffusion of Al in OPX is inferred to be the slowest of all elements (Sautter and Fabriès 1990) such that OPX retains its Al-content through subsequent cooling. It is noted that the calibration of the Witt-Eikschen and Seck (1991) thermometer is valid for four-phase *spinel-bearing* peridotites only, whilst the effect of whole-rock chemistry on the calibration is unknown. It cannot be applied to garnet peridotite or pyroxenite assemblages.

The elemental chemistry for which the above thermometers are calibrated is graphically shown in Fig. 4.1. Note that the calculated temperatures will be sensitive only to analytical and other errors incorporated in the concentrations of those elements that are used in the calculation, i.e., for example the Witt Eikschen and Seck thermometer is insensitive to late stage Fe and Mg re-equilibration as long as Al and Cr concentrations remain unchanged.

Problems and limitations

Any interpretation of the temperatures calculated with the above thermometers is surrounded with a number of problems. Chief among these, bearing directly influence on the analytical procedure, are possible microstructural (e.g., Pike and Schwartzman 1977) or chemical *disequilibrium coexistence* of the analysed phases, and the effect of metamorphic reactions (*net transfer mechanisms*, Spear 1989). Disequilibrium coexistence limits the application of two-pyroxene thermometers, whilst e.g. the notable absence, in the garnet spinel lherzolites, of equilibrium garnets transformed into a symplectitic assemblage inhibit the application of garnet-pyroxene exchange thermometers.

A further complication as regards the significance of the analytical temperatures concerns the effects of re-equilibration upon (slow) cooling during uplift. This will be further discussed below. For convenience, I will refer to temperatures calculated with the various thermometers as analytical temperatures (T_a), to temperatures representing re-equilibration upon (slow) cooling during uplift and closure of the system as closure

Fig. 4.2: (a) Photomicrograph of the neoblast assemblage in the spinel tectonites and garnet-spinel mylonites (assemblages 2 and 3) amidst orthopyroxene porphyroclasts (assemblage 1). Scale bar = 200 μm

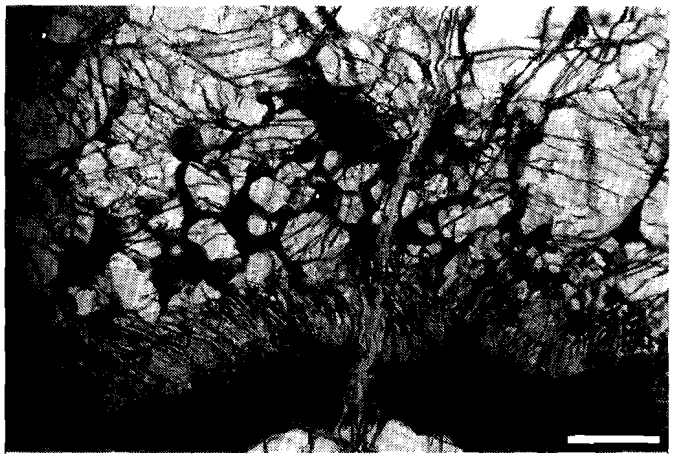

(b) Photomicrograph of the spinel pyroxenite assemblage 4. Note kelyphitic rim around garnet at top of graph, progressively coarsening to the spinel pyroxenite of assemblage 4. Scale bar = 200 μm.

	N	median grain diameter (μm)	sectioning correction factor	**grain size (μm)**
assemblage 1	17	3500	1.2	**4200**
assemblage 2	33	275	1.2	**330**
assemblage 3	32	175	1.2	**210**
width zonations	11	40	unknown,<1	**<40**
assemblage 5	8	3500	1.2	**4200**

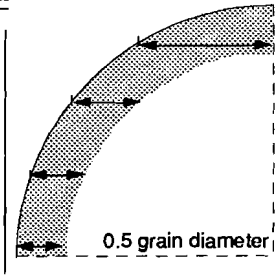

temperatures (T_c), and to temperatures prevailing during the development of the different structural and metamorphic domains as equilibrium temperatures (T_e).

4.4 Sample selection and analytical techniques

Equilibrium assemblages

The structural and microstructural analysis of the Ronda peridotite presented in Chapter 3 reveals a sequential development of microstructures and metamorphic assemblages in different structural and metamorphic domains. It is emphasized again that the overprinting relationships documented at map-, outcrop- and specimen-scale leave no doubts as to the relative ages of the assemblages. It can be expected that the mineral chemistry of these assemblages potentially reflects ambient conditions during the development of the allied microstructures.

The garnet- and spinel pyroxenite layers in the Ronda peridotite often preserve assemblages in notable disequilibrium with the host spinel lherzolites or harzburgites, such as graphitized diamonds (Davies et al. 1992), corundum (Kornprobst et al. 1990) and quartz (Obata 1980, Davies et al. 1992). The mere existence of such ultra-high pressure assemblages locally preserved in pyroxenites implies that pyroxenite equilibration during deformation and metamorphism must have been incomplete in many cases. For this reason, attention is focused on the host lherzolites and harzburgites only, except for spinel-pyroxenites at the annealing recrystallization front, developed at the expense of an earlier garnet-pyroxenite assemblage. Plagioclase peridotites and olivine gabbros have been excluded from the analysis because ample geological data exist to reconstruct the thermal history of the plagioclase peridotites (paragraph 4.7).

The following mineral assemblages, listed and summarized in order of decreasing relative age, have been selected for detailed X-ray analysis.

1: Pyroxene porphyroclasts (OPX, CPX) in the garnet-bearing peridotites (Fig. 4.2a), referred to as the "primary assemblage" by Obata (1980). The recovery of graphite pseudomorphs after diamond in the Ronda massif (Davies et al. 1992) clearly indicates

◁ Table 4.1 (previous page): Pyroxene grain size data. The correction factor 1.2 is frequently applied in the geological literature (e.g. Karato 1982). The sketch of a zoned crystal shows that the sectioning correction factor for the measured width of the rims must be smaller than 1.

that this assemblage cannot be the earliest in a strict sense, although, it represents the earliest mineral assemblage preserved on a regional scale, i.e. the scale of the massif.
2: A syntectonic neoblast assemblage (OPX, CPX, OL, SPL, ±AMPH) developed at the expense of the "primary assemblage" during development of the spinel tectonites (Fig. 4.2a).
3: A syntectonic neoblast assemblage (OPX, CPX, OL, SPL, GRT, ±AMPH) developed at the expense of the spinel tectonite assemblage during development of the garnet-spinel mylonites.
4: A spinel-pyroxenite assemblage (OPX, CPX, SPL, ±AMPH), sampled at the annealing recrystallization front bounding the granular domain, and developed at the expense of the garnet-pyroxenites enclosed in the spinel tectonites (Fig. 4.2b).
5: An equilibrium mineral assemblage in the granular domain (OPX, OL, SPL) developed during pervasive annealing recrystallization and grain growth at the expense of the mineral assemblages preserved in the garnet-bearing peridotites.

Setting and microstructural aspects of selected samples
The cores of the pyroxene porphyroclasts in the spinel tectonites and garnet-spinel mylonites (assemblage 1) have been measured in three spinel tectonites (DR89.10, 26 and 65; for location of the samples analyzed see App. A2). The microstructure of the pyroxene porphyroclasts strongly suggests disequilibrium. OPX occurs as slightly elongated clasts, deformed by slip on (100) without any optically detectable recrystallization. On the other hand, CPX often occurs in clusters of several grains recrystallized during deformation. This observation indicates that two-pyroxene thermometers can be expected to yield unreliable results. Exsolution features in the pyroxene porphyroclasts are common. In view of the grain-size dependence of elemental blocking temperatures, average grain sizes have been calculated in each of the analyzed samples (Table 4.1). This involved calculation of an *average maximum grain diameter* and multiplication of the result by a factor 1.2, as commonly applied in the geological and metallurgical literature to correct for section effects. The average grain size of the pyroxene porphyroclasts in the spinel tectonites is ~ 4.2 mm.

The lherzolitic neoblast assemblage in the spinel tectonites (assemblage 2) has been analyzed in two samples from the spinel tectonites, such as to cover variability in deformation intensity, with one sample showing a low intensity of the foliation (DR89.26), whereas the intensity of the foliation in the other sample was very high (DR89.65). The pyroxene neoblasts do not show chemical zoning or exsolution on the scale of resolution of the back-scattered electron images (~1 μm). The average recrystallized

(neoblast) grain size in the spinel tectonites is ~330 μm. It is noted that the grains of the neoblast assemblage appear essentially strain-free.

The lherzolitic neoblast assemblage in the garnet-spinel mylonites (assemblage 3) has been analyzed in three samples selected on the basis of homogeneity in terms of composition, microstructure and intensity of the deformation (DR89.3, 5A, and 49). The three mylonite samples are from the 500 m wide mylonite zone at the NW periphery of the Ronda massif. Again, pyroxene neoblasts do not show any chemical zoning or exsolution on the scale of resolution of the back-scattered electron images (~1 μm), the average pyroxene grain size is ~210 μm (Table 4.1), and the grains appear essentially strain-free.

As mentioned previously, the only pyroxenites analyzed in this study are poly-metamorphic garnet-spinel pyroxenites from the annealing recrystallization front. Two garnet-pyroxenites with spinel pyroxenite rims have been selected (DR90.5 and 7). These pyroxenites are essentially garnet-pyroxenites with *newly recrystallized* spinel pyroxenite margins (Fig. 4.2b), which implies that the mineral chemistry of the precursor garnet-pyroxenite has been reset during recrystallization to form a newly recrystallized spinel pyroxenite assemblage (assemblage 4). The analyses only involved small exsolution-free pyroxene grains developed amidst newly recrystallized spinel. The choice of these samples for thermometry was motivated by the possibility that mineral chemistry data from this assemblage, developed at the annealing recrystallization front, might reveal ambient temperatures at the onset of annealing recrystallization.

The coarse-grained lherzolitic to harzburgitic assemblage in the granular peridotites (assemblage 5) has been analyzed in four samples selected from the granular domain, i.e., two samples with a characteristic coarse-grained granular microstructure and a harzburgitic composition (DR91.18, DR90.10), and two samples (DR90.22, DR91.4) showing typically intermediate microstructures such as aligned trails of spinel as described in Chapter 3. The orthopyroxenes in the coarse-grained granular samples are markedly well-rounded, with an average grain size of 4.2 mm (Table 4.1). Many OPX-OL contacts have a pronounced concave shape facing OPX. Relative to OPX, the remaining CPX in the harzburgitic samples is much finer-grained.

Analytical details

The analyses have been performed by combined wavelength- (WDS) and electron-dispersive spectrometry (EDS) using the Jeol JXA Superprobe at the Institute of Earth Sciences, Utrecht. The instrument operated at an acceleration voltage of 15 kV, a beam current of 10 nA, and a counting time (on peak) of 40 s. The analyses have been performed

assemblage 1:
Pyroxene cores - Spinel tectonites, (DR89.10, DR89.26, DR89.65)

	OPX	CPX	OL	SPL	AMPH
SIO2	54.08±.56	51.55±51	not	not	not
TIO2	.12±.04	.51±.09	preserved	preserved	preserved
AL2O3	5.60±.39	6.94±.52			
CR2O3	.65±.18	1.06±.23			
CAO	.69±.39	20.91±.93			
MGO	32.64±.60	14.54±1.04			
FEO	6.13±.31	2.44±.33			
MNO	.11±.07	.06±.05			
NA2O	.07±.05	1.79±.20			
TOTAL	100.09	99.80			
oxygen	6	6			
SI	1.867	1.871			
TI	.003	.014			
AL	.228	.297			
CR	.018	.030			
CA	.026	.813			
MG	1.680	.787			
FE	.177	.074			
MN	.003	.002			
NA	.005	.126			

Assemblage 2:
Neoblasts - Spinel tectonites, (DR89.26, DR89.65)

OPX	CPX	OL	SPL	AMPH
58.18±.71	51.86±.58	41.07±.36	0	42.98±.54
.05±.03	.43±.13	.01±.02	0	1.95±.22
2.86±.74	5.79±.85	.04±.08	56.54±2.44	14.90±.32
.37±.17	.89±.15	0	12.39±2.59	1.17±.10
.41±.10	21.82±.59	0	0	11.72±.38
33.74±.48	15.01±.45	49.57±.44	19.86±.37	17.52±.53
6.24±.32	2.31±.26	9.64±.44	10.94±.54	3.56±.21
.15±.05	.08±.03	.13±.05	.12±.02	.04±.02
.02±.01	1.58±.23	.01±.01	0	3.89±.04
100.02	99.77	100.50	99.96	97.73
6	6	4	4	23
1.936	1.886	.999	.001	6.098
.001	.012	0	0	.21
.116	.248	.001	1.734	2.491
.010	.026	0	.255	.131
.015	.850	.001	.001	1.782
1.733	.814	1.798	.770	3.705
.180	.070	.196	.238	.422
.004	.003	.003	.003	.005
.001	.111	.001	0	1.070

Assemblage 3:
Neoblasts - Grt-Spl mylonites, (DR89.3, DR89.5A, DR89.49)

OPX	CPX	OL	SPL	AMPH
55.85±.52	52.18±.49	40.77±.32	unstable	45.64±.18
.09±.03	.62±.09	.01±.01		.55±.02
2.96±.50	5.77±.28	0		13.16±.46
.23±.13	.84±.23	.01±.03		1.25±.30
.37±.11	20.68±.53	.03±.04		12.24±.01
33.29±.39	14.80±.25	49.11±.32		18.31±.06
6.98±.85	2.64±.32	10.09±.37		2.86±.00
.14±.05	.06±.05	.14±.07		.09±.04
.03±.02	1.79±.20	0		3.28±.06
99.94	99.38	100.17		97.38
6	6	4		23
1.933	1.900	.998		6.439
.002	.017	0		.058
.121	.248	0		2.188
.006	.024	0		.139
.014	.801	.001		1.850
1.717	.803	1.792		3.851
.202	.080	.207		.337
.004	.002	.003		.011
.002	.126	.001		.897

Assemblage 4:
Spinel pyroxenites, (DR90.5, DR90.7)

	OPX	CPX	OL	SPL	AMPH
SIO2	54.58±.63	50.81±.60		0	not
TIO2	.09±.04	.55±.18		.04±.03	analyzed
AL2O3	4.89±.69	7.35±.92		62.92±1.54	
CR2O3	.17±.14	.31±.20		3.75±1.62	
CAO	.53±.16	21.63±.97		0	
MGO	32.36±.55	14.51±.63		20.94±.49	
FEO	7.27±.51	2.87±.31		11.07±.51	
MNO	.18±.04	.08±.05		.10±.06	
NA2O	0	1.28±.33		0	
TOTAL	100.15	99.47		98.98	
oxygen	6	6		4	
SI	1.890	1.854		.002	
TI	.003	.015		.001	
AL	.200	.316		1.895	
CR	.005	.009		.076	
CA	.020	.846		.001	
MG	1.670	.790		.798	
FE	.211	.088		.237	
MN	.005	.003		.002	
NA	.002	.091		0	

Assemblage 5:
Granular peridotites, (DR91.18, DR90.10)

OPX	CPX	OL	SPL	AMPH
54.96±.50	51.85±.45	41.58±.08	0	not
.06±.02	.19±.03	0	0	observed
4.43±.45	5.99±.41	0	50.54±1.18	
.72±.16	1.44±.21	.07±.04	18.08±1.27	
.81±.57	21.99±.40	0	0	
33.33±.57	14.96±.33	49.97±.17	19.03±.33	
5.81±.24	2.30±.21	8.96±.17	11.83±.42	
.12±.05	.08±.05	0	.11±.05	
.04±.04	1.38±.12	0	0	
100.28	100.18	100.58	99.67	
6	6	4	4	
1.892	1.878	1.007	.001	
.002	.005	0	.001	
.180	.256	0	1.596	
.012	.041	.001	.383	
.030	.854	0	.001	
1.711	.808	1.803	.760	
.167	.070	.181	.265	
.004	.003	0	.003	
.003	.097	0	0	

on thin sections in the XZ plane of deformation, in order to maintain microstructural control. All pyroxene analyses were performed such as to carefully avoid regions around exsolution lamellae. Neighbouring ortho- and clinopyroxenes, often separated by olivine, have been regarded as "pairs" in the calculation of two-pyroxene thermometers. Per thin section, about 15-20 pyroxene pairs have been analyzed. Pyroxene zoning patterns have been determined "manually", again to avoid regions around exsolution lamellae which imposes a limit to the number of measurements defining the zoning pattern. A spreadsheet program has been used to perform mineral- and temperature calculations. Pressures values required for the BM2px, BK2px and BK1px thermometers have been set at 2000 MPa for assemblages 1-3, and 1000 MPa for assemblages 4-5.

4.5 Results - analytical temperatures

The average mineral compositions of the assemblages analyzed are shown in Table 4.2. Analytical temperatures for these assemblages, calculated on the basis of the five thermometers choosen, are listed in Table 4.3 and shown graphically in Fig. 4.3.

Assemblage 1

The cores of the pyroxene porphyroclasts in the spinel tectonites have preserved analytical temperatures ranging from 977°C (BK1px) to 1110°C (WS1px). Note the large range in analytical temperature and the large standard deviation of the mean analytical temperature given by the Brey and Köhler single pyroxene thermometer, which could be due to exsolution. As noted above, textural disequilibrium between OPX and CPX porphyroclasts precludes temperature estimates from two-pyroxene thermometers. This textural disequilibrium is complementary to a marked chemical disequilibrium, as OPX porphyroclasts are chemically zoned, whereas CPX porphyroclasts are homogeneous in composition (Obata 1980). Analytical temperatures of 1110°C calculated with the Witt-Eikschen and Seck (WS1px) thermometer agree well with the "primary conditions" of 1100-1200°C at 2000-2500 MPa reported by Obata (1980).

Assemblages 2 and 3

The rim compositions of the neoblasts do not significantly deviate from the core

◁ Table 4.2 (previous page): Mineral chemistry of the microstructurally defined assemblages 1-5 outlined in text.

	W2px	BM2px	BK2px	BK1px	WS1px
assemblage 1	no textural eq.	no textural eq.	no textural eq.	977±95	1110±65
assemblage 2	853±49	811±74	851±84	880±55	896±90
assemblage 3	845±34	828±29	881±57	865±60	not applicable
assemblage 4	836±56	768±77	808±89	878±63	not applicable
assemblage 5	harzburgites	harzburgites	harzburgites	960±112	1087±69

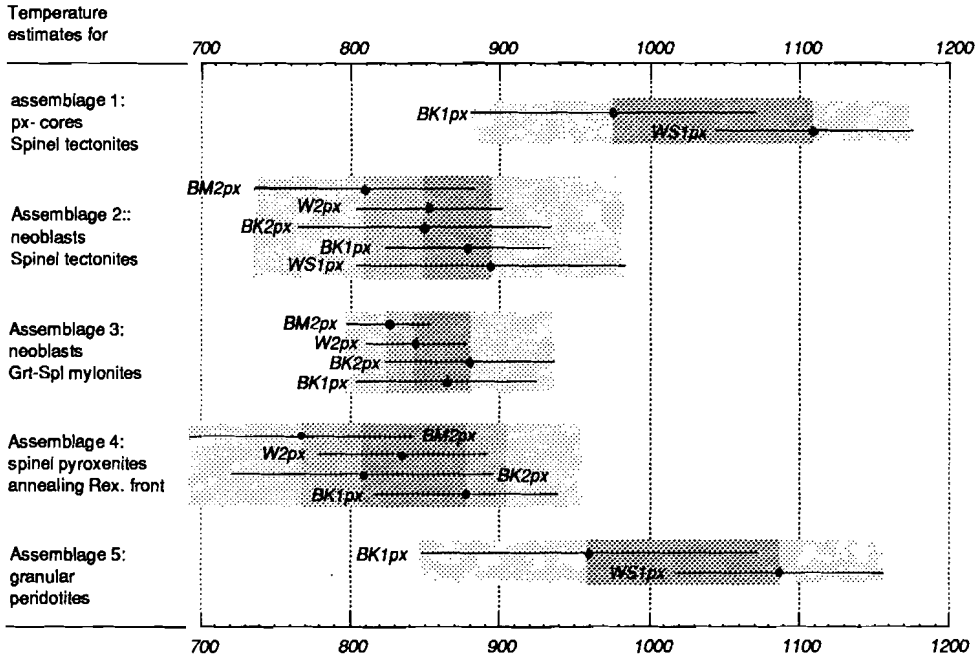

W2px	Wells 1977	BK1px	Brey and Köhler 1990-2
BM2px	Bertrand and Mercier 1985	WS1px	Witt-Eikschen and Seck 1991
BK2px	Brey and Köhler 1990-1		

Δ

Table 4.3 (top of page): Temperatures calculated for the assemblages 1-5. Number of measurements: Two-pyroxene thermo-meters: >20. Single pyroxene thermometers: ~80.

Fig. 4.3: Diagram showing analytical temperatures obtained for the assemblages distinguished.

compositions which indicates that the neoblasts are compositionally homogeneous. The neoblast assemblage in the spinel tectonites has preserved analytical temperatures ranging from 811°C (BM2px) to 896°C (WS1px). The neoblast assemblage in the garnet-spinel mylonites has preserved similar analytical temperatures: 828°C (BM2px) to 881°C (BK1px). This range decreases considerably if the systematically low analytical temperatures obtained with the Bertrand and Mercier thermometer (Brey and Köhler 1990) are discarded. Omission of the BM2px results leads to mean analytical temperatures for the spinel tectonite neoblast assemblage in the range 851-896°C, and for the garnet-spinel mylonite neoblast assemblage in the range 845-881°C (Fig. 4.3) It is noted again that the Witt-Eikschen and Seck thermometer (WS1px) is not calibrated for the garnet-bearing 5-phase system of the garnet-spinel mylonites.

Assemblage 4

The spinel-pyroxenite assemblage from the annealing recrystallization front has preserved analytical temperatures ranging from 768°C (BM2px) to 878°C (BK1px). There is no systematic variation in analytical temperature between core and rim of the crystals. Note that the Bertrand and Mercier (BM2px) thermometer again yields the lowest analytical temperatures. Note also that the validity of the Brey and Köhler single-pyroxene thermometer (BK1px) for mafic assemblages is doubtful. Omission of the analytical temperatures calculated with the BM2px and BK1px thermometers results in a range of 808°C (BK2px) to 833°C (W2px).

Assemblage 5

The large variety in microstructure in the granular peridotites allied to a variable degree of annealing recrystallization induces a number of problems when trying to assess significant analytical temperatures for the coarse-grained granular assemblages. In the following, these problems are discussed in some detail.

Obata (1980) was among the first to demonstrate plateaus of a particular chemical composition in OPX porphyroclasts from orogenic peridotites. He showed that OPX from the garnet-, Ariégite- and some Seiland-facies peridotites in Ronda preserved plateaus of ~6 wt% Al2O3, with rapidly decreasing Al-concentrations towards the rims (~2 wt%, Obata 1980, his Fig. 6). Average compositions obtained in this study for pyroxene cores from the spinel tectonites are around 5.60 wt% Al2O3 (Table 4.2). These values compare well with Obata's data. OPX from plagioclase peridotites in the Ronda massif does not preserve compositional plateaus, which was explained by Obata (1980) to result from

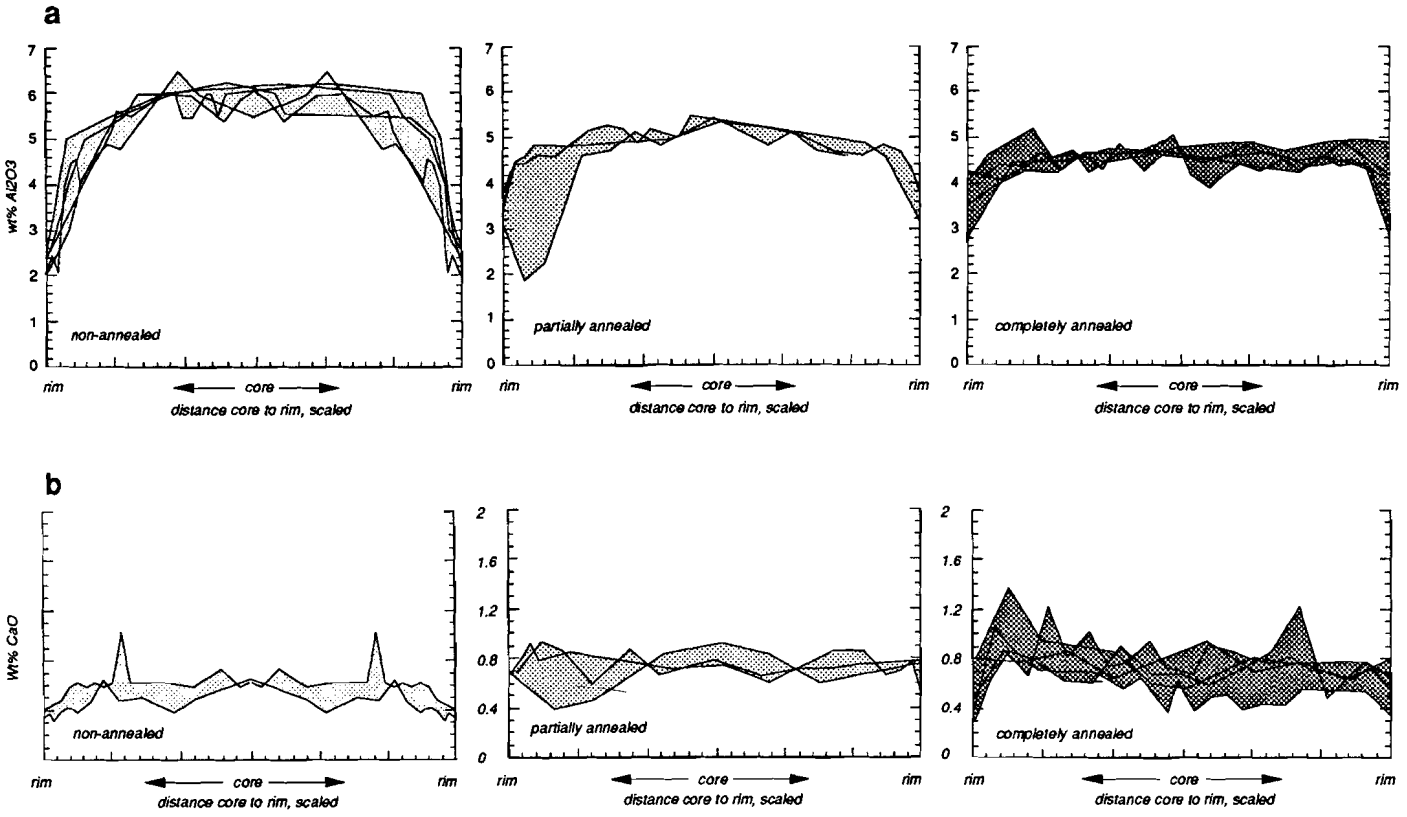

Fig. 4.4: (a) & (b): Al- and Ca-concentration profiles across OPX from non-annealed-, partially-, and completely annealed peridotites. Each line represents a traverse across one grain. In all cases the bounding phase is olivine. Note that the horizontal axes are scaled, hence that the slope of decreasing concentrations bears no quantitative meaning. Note systematic variation of Al-concentration pattern with degree of annealing recrystallization whilst Ca-concentration profiles show no systematic variation.

pervasive recrystallization and re-equilibration in the plagioclase-peridotite stability field.

Upon recognition of an annealing recrystallization stage affecting the spinel tectonites and garnet-spinel mylonites prior to development of the plagioclase tectonites, the question arose if and how annealing recrystallization and grain growth would affect existing zoning patterns in OPX, and how this zoning pattern relates to the thermal history during annealing recrystallization and development of the granular rocks. In other words, in order to assess peak conditions during annealing recrystallization in the granular domain, the relationship between mineral chemistry and the annealing recrystallization process needs to be understood first.

Probe-traverses have been made across orthopyroxenes in (i) non-annealed spinel tectonites (ii) partially annealed granular peridotites with a spinel fabric from the annealing front, and (iii) in completely annealed granular peridotites sampled several km away from the annealing front. Some additional traverses across OPX porphyroclasts from *non-annealed peridotites* are taken from Obata (1980). In order to avoid complications arising from different concentration gradients across grain boundaries with different neighbouring phases, only OPX adjacent to olivine has been studied. Al- and Ca-concentration gradients in OPX are shown in Fig. 4.4.

The Al-concentration profiles across OPX in non-annealed peridotites (Fig. 4.4a) are characterized by a high-Al plateau (~6 wt% Al2O3), which rapidly decreases towards the rims (<3 wt% Al2O3). The rim composition correlates well with the average composition of the OPX-neoblasts in the spinel tectonites and garnet-spinel mylonites (2.86 and 2.96 wt% Al2O3 respectively, Table 4.1). OPX from partially annealed granular peridotites also show significant chemical zoning, from ~5 wt% Al2O3 in the core, down to ~3 wt% Al2O3 towards the rims (Fig. 4.4a). There is still a plateau preserved, but the Al-concentrations of the plateau are lower, while those in the rims show slightly higher values as compared with the traverses in the non-annealed rocks. The average width of the rims, in orthopyroxene porphyroclasts, with a chemical composition significantly different to that of the plateaus (i.e. <4 wt% Al2O3) is <40 μm (Table 4.1). Note the obvious "well" in one of the profiles for the partially annealed samples. Unfortunately, such an "inverted" zonation profile has as yet been observed in one grain only. OPX from completely annealed peridotites show remarkably homogeneous compositions, with Al-concentrations in core and rim around 4 wt% Al2O3 (Fig. 4.4a). These values are preserved within very small distances of at most a few microns from the OPX grain boundaries.

An increasing degree of annealing recrystallization is thus allied to a *flattening of the Al-concentration profiles* (or chemical homogenization) such that with increasing degree of annealing recrystallization, the cores of the porphyroclasts decrease in Al-concentration,

whilst Al-concentrations in the rims of the porphyroclast increase. This systematic relationship suggests that Al-concentrations have preserved an annealing imprint.

Ca-concentration profiles do not show a systematic trend with the degree of annealing recrystallization (Fig. 4.4b). The Ca-concentration profiles are flat with Ca-concentrations around the same level (~0.4-0.8 wt%) for non-annealed, partially and completely annealed granular peridotites. On the basis of these data it cannot be decided whether the Ca-concentration profiles reflect (rapid) chemical adjustment to changing P-T conditions at the onset of annealing recrystallization or, alternatively, re-equilibration and closure of the system upon cooling during emplacement of the Ronda body.

From the above data it follows that peak analytical temperatures for the granular peridotites should at least be based on probe-traverses across OPX from completely annealed granular peridotites, i.e. those OPX crystals with a flat concentration profile. Many of the granular peridotites, including the granular peridotite analyzed, are harzburgites whose origin is inferred to be related to the development of the annealing recrystallization front. This implies that the subordinate CPX in these rocks most probably represents a meta-stable phase which either reacted out of the system or recrystallized, presumably in the presence of a melt. As thermometry is based on solid-state diffusional processes, it follows that any two-pyroxene thermometer will yield unreliable results. Analytical temperatures based on the single-pyroxene thermometers lie in the range 960°C (BK1px) to 1087°C (WS1px). Note the large range and standard deviation of the analytical temperatures calculated with the Brey and Köhler (BK1px) thermometer, which could again be due to exsolution.

4.6 Discussion - equilibrium temperatures

Many complications surround the assessment of *equilibrium* temperatures on the basis of geothermometry (Spear 1989). Therefore, the above analytical temperatures derived for the different structural and metamorphic assemblages do not necessarily reflect the (in part syntectonic) equilibration conditions for the mineral assemblage investigated. Below, the significance of the analytical temperatures to the equilibrium conditions under investigation will be evaluated.

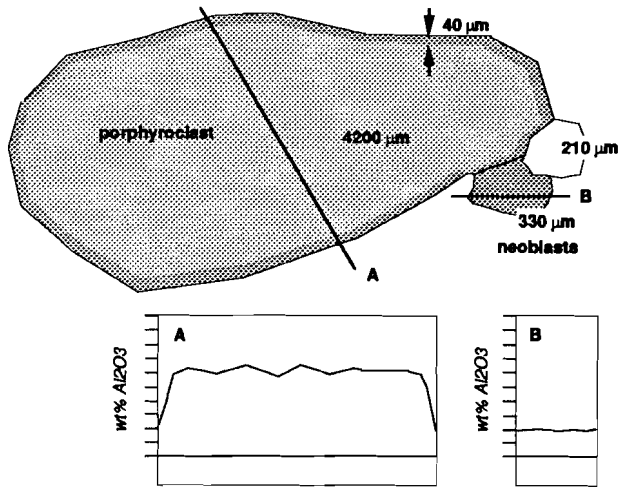

Fig. 4.5: Graph showing the discrepancy between the zoning profiles in porphyroclasts and neoblasts and the size of porphyroclasts and neoblasts. The size of the rim in the porphyroclasts is too small to be correlated with the flat profiles in the neoblasts, hence they result from different processes, i.e. "leaking" upon cooling in the porphyroclasts, and dynamic recrystallization at low temperatures in the neoblasts.

Cooling effects on the spinel tectonite and garnet-spinel mylonite neoblast assemblages

The most important problem to overcome when trying to assess equilibrium temperatures is a possible re-equilibration of the mineral chemistry during uplift-related cooling. This stems from the fact that slow cooling may result in diffusion of elements through the crystal lattice structure, in response to changing P-T conditions. Such re-equilibration processes potentially obliterate the chemical compositions attained during earlier equilibrium conditions. As diffusion-kinetics are relatively slow, these effects are likely to be more important in phases with a small grain size (Dodson 1973). In the case of the Ronda massif, the lowest analytical temperatures are obtained from the small-grained neoblasts of the spinel tectonites and garnet-spinel mylonites (assemblages 2 and 3). In the context of potential re-equilibration effects, this observation clearly necessitates a careful evaluation of the analytical results. The following observations and considerations suggest that the analytical temperatures for these neoblast assemblages indeed do reflect syntectonic equilibrium temperatures :

1: There is a distinct difference between the size of the unzoned pyroxene neoblasts, in the spinel tectonites and the garnet-spinel mylonites (330 and 210 µm respectively), and the true width of the zoned rims (<40 µm) in the orthopyroxene porphyroclasts (Fig. 4.5). This discrepancy is difficult to explain by re-equilibration upon slow cooling, unless porphyroclasts are being resorbed in operation of transfer reactions for which there is no microstructural evidence. If these zoned rims and the mineral chemistry of the neoblasts were due to re-equilibration, and assuming that diffusion-kinetics in the neoblasts and the

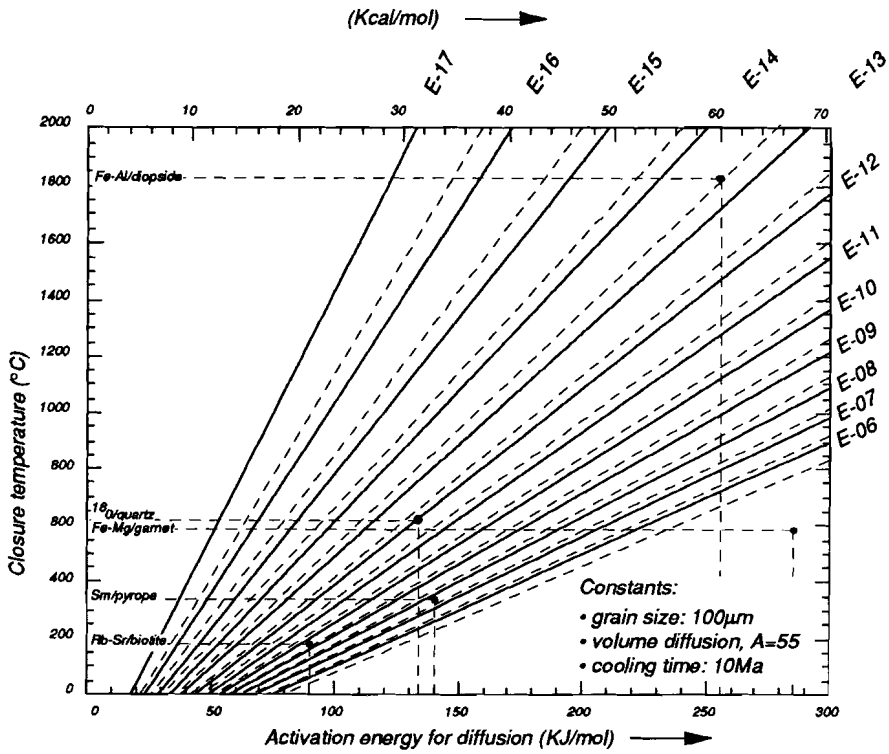

Fig. 4.6: Plot of closure temperature vs. activation energy for diffusion, for a range of pre-exponential diffusion constants in the range E-06 - E-17 (cf. Dodson 1973). Other parameters fixed as indicated. Also shown are calculated closure temperatures for a number of well-known geological systems.

porphyroclasts are roughly the same, one would expect the much larger neoblasts to preserve cores with higher analytical temperatures. Likewise, if the analytical temperatures obtained from the unzoned neoblasts were due to re-equilibration, it is difficult to explain why the zoned rims of the porphyroclasts are much narrower than half the mean neoblast grain size. This discrepancy is even more difficult to explain by re-equilibration when taking into account that diffusion kinetics in the much more strained porphyroclasts may have been faster than in the neoblasts, due to the inferred higher dislocation densities in these porphyroclasts. Dislocations are known to increase diffusion kinetics (e.g. Kramer and Seifert 1991) leading to an increase of the diffusion path. As a consequence, one would expect the zoned rims in the porphyroclasts to be relatively wide as compared with the sizes of the relatively unstrained neoblasts, whilst these rims in the porphyroclasts are much narrower than in the "flat profile" neoblasts.

2: As re-equilibration, in response to uplift-related cooling, is likely to induce exsolution, the lack of exsolution in the spinel-tectonite and garnet-spinel mylonite neoblast assemblages suggests that no significant re-equilibration occurred at any stage following the development of the neoblast assemblage. The presence of exsolution lamellae at submicroscopic level, however, cannot be ruled out.
3: Dodson (1973) proposed a theoretical relation for the cooling temperature T_c of a phase surrounded by an infinite fast diffusing reservoir as a function of diffusion kinetics of the slowest diffusing phase, cooling rate and grain size:

$$T_c = \frac{E/R}{\ln\left\{\frac{ART_c^2 D_0/a^2}{E(dT/dt)}\right\}} \qquad (4.6)$$

where Tc is a function of the activation energy E for diffusion, D_0 the pre-exponential diffusion coefficient, dT/dt the cooling rate, A a geometric factor (A=55 for volume diffusion), a the diffusion distance and R the gas constant.

This relationship was principally developed to explain cooling-related results in geochronology and isotope geochemistry (e.g. Elphick et al. 1988) and successfully reproduces inferred closure temperatures for fast-diffusing elements such as, for example, Rb/Sr in biotite (Dodson 1976), Fe/Mg in garnet (Spear 1989) and ^{18}O in quartz. As Dodson's model essentially describes solid-state diffusional processes, it applies equally to pyroxene thermometry. Fig. 4.6 shows Dodson's theoretical relationship showing closure temperature Tc as a function of activation energy for diffusion, for different values of the pre-exponential factor D_0 for 100 μm size grains, and assuming spherical geometry and a cooling rate of 100°C Ma^{-1}. This latter value seems reasonable for most of the Betic Zone and for the western Betics in particular (Zeck et al. 1992). Diffusion data for major elements in the pyroxenes are scarce, but generally show that pyroxene diffusion kinetics are extremely slow (Freer et al. 1982, Brady and McCallister 1983, Sautter and Harte 1988, Sautter et al. 1988, Sautter and Fabriès 1990). The significance of these data regarding thermometry is widely acknowledged in the above papers, however, there are only few applications documented of Dodson's theoretical relationship to pyroxene thermometry (e.g. Jamtveit et al. 1991). The "null experiment" diffusion data for CPX (diopside) of Freer et al. (1982) are shown in Fig. 4.6. It is evident that temperatures distinctly higher than any ultramafic solidus are required to affect the Al/Fe and Ca/Mg concentrations in the cores of 100 mm grains by *inter-diffusion* (see Freer 1981 for terminology) accommodated

re-equilibration upon cooling. There are no diffusion rate estimates available for OPX but, based on diffusion profiles in natural pyroxenites, Sautter and Fabriès (1990) suggest that diffusion of for example Al in OPX may be even slower than in CPX. It follows from Dodson's quantitative approach that Al concentrations will not re-equilibrate at all, and that analytical temperatures based on such thermometers will always reflect initial equilibration conditions.

4: In contrast to Al, it seems perfectly feasible that Ca-concentrations in OPX re-equilibrate upon slow cooling due to *self-diffusion*. In many natural cases where Al concentrations are heterogeneous across grains, Ca concentrations show flat profiles, suggesting that the diffusion kinetics of Ca are much faster than those of Al (e.g. Sautter and Fabriès 1990, Smith and Barron 1991). This is possibly due to the effect of hydrogen on intracrystalline diffusivity similar to the observed effect of hydrogen on the diffusivity of oxygen in framework silicates (Graham and Elphick 1991). Re-equilibration during uplift-related cooling should thus become evident from diverging analytical temperatures for Ca- and Al-based thermometers. This is certainly not the case for the neoblast assemblages in the spinel tectonites and garnet-spinel mylonites where analytical temperatures are internally consistent and span a narrow temperature range (Fig. 4.3).

On the basis of these considerations it is concluded that the low analytical temperatures obtained in the neoblast assemblages of spinel tectonites and garnet-spinel mylonites (assemblages 2 and 3) do not reflect later re-equilibration, but that they represent syntectonic equilibration temperatures in the range 850-900°C, with the slightly lower equilibrium temperatures for the garnet-spinel mylonites. This result seems entirely consistent with the qualitative geological constraints mentioned previously.

Onset of annealing recrystallization

Ambient conditions at the onset of annealing recrystallization and development of the granular domain overprinting the garnet bearing peridotites can be inferred from the spinel pyroxenite assemblage at the annealing front. Analytical temperatures derived from this assemblage (assemblage 4) lie in the range 808-878°C. The temperatures preserved in the pyroxene rims do not significantly deviate from those preserved in the cores, exsolution is not abundant and the Ca-dominated thermometers (BM2px, BK1px) show the highest analytical temperatures. These data at least suggest that the analytical temperatures closely approximate the equilibration temperatures prevailing during the onset of Seiland-subfacies metamorphism.

Thermal history of the granular peridotites inferred from zoning profiles

The Ca-concentration profiles across OPX in the granular peridotites show no systematic correlation with the degree of annealing recrystallization (Fig. 4.4b). Every Ca-based pyroxene thermometer, therefore, cannot be expected to reveal the temperature evolution during the annealing recrystallization event. According to the Ca-in-OPX thermometer, the cores of OPX from non-annealed ánd completely annealed granular peridotites have preserved temperatures around 950°C. Towards the rims, these values decrease to around 880°C. Similar flat Ca-concentration profiles in natural pyroxenites are currently inferred to result from re-equilibration upon slow cooling (Sautter and Fabriès 1990). The analytical temperatures obtained with the Ca-in-OPX thermometer thus presumably represent closure of Ca during emplacement of the massif, whereas peak equilibrium temperatures for the granular domain can be expected to exceed those values.

In marked contrast to Ca, the variation in Al-concentration profiles in OPX of granular peridotites is related to the degree of annealing recrystallization (Fig. 4.4a). This systematic variation is interpreted to represent the imprint of annealing recrystallization on the pyroxene mineral chemistry. As the Al-isopleths for spinel peridotites are essentially pressure-independent (e.g. Gasparik 1984), the Al-concentration profiles can be translated directly into a temperature evolution during annealing recrystallization.

Based on the Witt Eikschen and Seck (WS1px) thermometer, the following thermal history allied with the annealing recrystallization process can be inferred from the preserved Al-concentrations. The rims of OPX porphyroclasts from non-annealed peridotites have preserved temperatures similar to those in the neoblast assemblages in the spinel tectonites and garnet-spinel mylonites, and could be related to the shearing process. With increasing degree of annealing recrystallization, Al-concentrations in the rims of the grains increase, and preserve progressively increasing temperatures towards ~1100°C. The cores of the porphyroclasts (assemblage 1), however, have not been affected by low temperature shearing preceding annealing recrystallization, but preserve earlier pre-shearing, hence pre-annealing conditions reflected by high analytical temperatures around 1110°C. Equilibration temperatures of over 1110°C are inferred for this assemblage, consistent with the "primary recrystallization conditions" defined by Obata (1980).

At the onset of annealing recrystallization, the above assemblage re-equilibrated, beginning at 1040°C. With progressive annealing, temperatures increased to around 1100°C, analogous to the temperature evolution during annealing recrystallization as reflected by the rims. The data, therefore, indicate that annealing recrystallization and development of the granular peridotites was thermally driven. As the kinetics of Al-diffusion probably lack behind the kinetics of heating, analytical temperatures of 1087°C

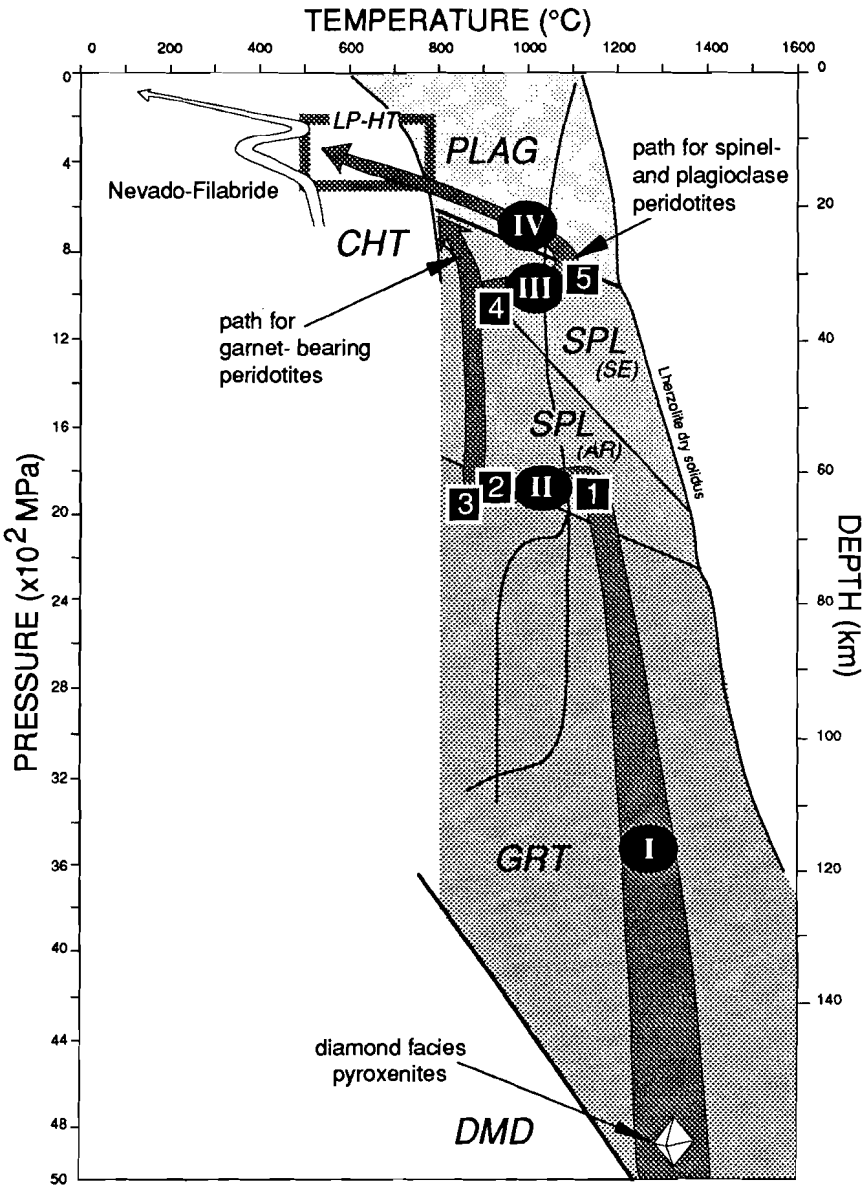

Fig. 4.7: Synoptic PT path for the Ronda peridotite. 1-5 shows PT conditions for the assemblages defined in the text. I-IV refer to different stages in the PT evolution of the Ronda peridotite discussed in paragraph 4.6. Also shown temperature anomaly in the Nevado-Filabride and Alpujarride PT-trajectories, after De Jong (1991), and LP-HT metamorphic conditions of crustal units adjacent to the Ronda massif. Petrogenetic grid layout see App. A1

from the Witt-Eikschen and Seck thermometer should probably be taken as a minimum to peak equilibrium temperatures of over 1100°C as suggested by the local occurrence of discordant harzburgites and dunites.

4.7 The P-T-t evolution of the Ronda peridotite

The sequence of deformational structures (Chapter 3) and allied temperature and pressure estimates recorded by the syntectonic mineral assemblages 1-5 and mineral chemistry data (Fig. 4.7) allow four distinct stages (labelled I-IV) to be identified in the PT history of the Ronda peridotite. These stages, with some possible age-constraints from the literature, are summarized below.

Stage I: Uplift from the diamond field; primary conditions

The earliest mineral assemblage identified in the Ronda peridotite is the assemblage garnet ± quartz ± clinopyroxene ± graphitized diamond in pyroxenite layers (Davies et al. 1992). This high-pressure assemblage is only locally preserved, and indicates an origin of the Ronda peridotite at deep lithospheric or asthenospheric levels (>4500 MPa). Subsequent to uplift from the diamond field (stage I, Fig. 4.7), most of this ultra-high pressure assemblage recrystallized at "primary conditions" (Obata 1980) of high temperatures (≥ 1110°C) in the Ariégite subfacies. The only widespread remnants of this latter assemblage are the OPX cores in the spinel tectonites and garnet-spinel mylonites (assemblage 1).

The age of equilibration in the diamond stability field is the subject of considerable debate. The lack of oxygen isotope equilibration in graphite-bearing pyroxenite layers from Beni Bousera suggest that the pyroxenite layers cannot have resided in the hot, convecting mantle for more then 100 Ma (Pearson et al. in press). This does not preclude a much longer history in relatively cool, non-convecting continental lithosphere, especially because high $^{187}Os/^{186}Os$ ratios for pyroxenite layers from the Ronda massif suggest that they are ancient features of possibly 1.3 Ga (Reisberg et al. 1991). Pb-Nd isotope systematics of the pyroxenites, however, suggest an age within the last 200 Ma for the development of the diamond facies pyroxenites (Pearson et al. in press).

Stage II: High Pressure - Low Temperature deformation

In a second stage, the "primary assemblage" deformed and recrystallized to form assemblages 2 and 3 at temperatures as low as ~ 850°C (Fig. 4.7, stage II). A similar P-T

evolution, involving cooling at depth, for the garnet-bearing peridotites of the Beni Bousera massif (Morocco) has been proposed by Saddiqi (1988). During progressive deformation, metamorphic grade changed from the Ariégite subfacies to the garnet-peridotite facies. It is unclear whether this cooling occurred isobarically or if it was allied to conditions of increasing pressure. The mineral assemblages preserved do not allow the application of barometers to resolve more detail of the pressure history. The present uncertainty as to the magnitude and extent of pressurization is therefore only constrained by the pressure range of the Ariégite subfacies field around 1100°C (~500 MPa). The inferred conditions during progressive deformation and development of the garnet-spinel mylonites clearly reflect a relatively cold geotherm. Such a cold, high-pressure history is also documented in crustal rocks of the Betic Zone, in particular in the Mulhacen complex where HP-LT metamorphism is inferred to be well advanced around 81 Ma (De Jong 1991).

Stage III: Thermally driven annealing recrystallization

A third stage in the PT evolution is characterized by renewed high temperatures, during annealing recrystallization and development of the granular peridotites, of over 1100°C at Seiland subfacies conditions in those parts of the Ronda body now represented by the granular peridotites (assemblage 5) and possibly some plagioclase peridotites (Fig. 4.7, Stage III). The fact that most of the Ariégite subfacies and garnet peridotite facies have been preserved suggests that these preserved assemblages did not experience the high temperatures related to annealing recrystallization, and that they followed a different, low-temperature PT path indicated by the low-temperature trajectory in Fig. 4.7. The obtained equilibrium temperatures for the newly recrystallized spinel pyroxenite assemblage (assemblage 4) indicate that the transformation of the garnet-bearing assemblages to Seiland subfacies assemblages initiated at temperatures as low as 900°C. The preservation of garnet-bearing, low-temperature assemblages NW of the annealing recrystallization front (equilibrium temperatures <900°C) at only 3.5 km from discordant harzburgites/dunites (equilibrium temperatures ≥1100°C) therefore suggests high thermal gradients (~60°C/km) during migration of the annealing recrystallization front .

There are no direct age-constraints available for the annealing recrystallization event, however, the positive temperature anomaly in the Ronda uplift path correlates well with similar temperature anomalies in the Nevado-Filabride and Alpujarride PT trajectories estimated at 25 Ma (de Jong 1991, Fig. 4.7) suggesting a similar or possibly slightly older (Late Oligocene) age for the annealing recrystallization stage in the Ronda peridotite.

Stage IV: Emplacement

It is inferred that the plagioclase tectonites developed at initially high temperatures (~1100°C, see also Tubia and Cuevas 1987), but substantial evidence exists that they cooled rapidly with ongoing uplift and emplacement. Firstly, significantly decreasing temperature conditions are suggested by the transition from high-temperature olivine [a] fabrics in the Ronda massif (Chapter 3) to low-temperature olivine [c] fabrics developed in late plagioclase mylonites from the Ojén massif (Tubia and Cuevas 1986), which is consistent with the increased localization of the deformation (Drury et al. 1991) from "top to the north" tectonites to "top to the south/west" tectonites observed in the W Ronda massif. Secondly, the plagioclase peridotites of the Ronda massif are underlain by high-grade cordierite gneisses (Lundeen 1978) and migmatites, whilst rocks of very similar composition occur as m-scale lenses with tectonized rims enclosed in plagioclase tectonites (see Chapter 3 for detailed field relations). These metamorphic gneisses have experienced two phases of metamorphism: a "hot" stage of HT-HP metamorphism and a "cold" stage of HT-LP metamorphism (Kornprobst 1974). To be consistent with the pressure conditions for the development of plagioclase peridotites (<700 MPa), this last phase of HT-LP metamorphism must be related to ductile emplacement of the peridotite into the crust. Similar conclusions have been drawn by Lundeen (1978), Westerhof (1977), and Torres Roldán (1981). The low degree of partial melting in the gneissic lenses indicates that during tectonic interleaving of these gneisses along "top to the south/west" shear zones ambient temperatures had decreased to values around the melting temperature for felsic systems. Possible PT conditions for emplacement of the peridotite, based on metamorphic criteria in the gneisses, are shown in Fig. 4.7. It is tentatively suggested that the annealing front became effectively "frozen" during this progressive development of plagioclase peridotites allied with ductile emplacement (Fig. 4.7, stage IV). There is good agreement as to an emplacement age of the peridotite of 20-22 Ma (e.g. Loomis 1975, Priem et al. 1979, Zindler et al. 1983).

Previous uplift paths for the W Mediterranean peridotites have been published by Obata (1980) and Davies et al. (1992) for the Ronda peridotite, and Saddiqi (1988) and Kornprobst et al. (1990) for the Beni Bousera peridotite. There are no large discrepancies between those studies and the present structural and petrological approach as regards the ambient conditions allied with the development of the different peridotite facies. However, the relative timing of the various assemblages in the various metamorphic domains allows considerable re-interpretation in terms of a PT uplift trajectory. This re-interpretation and its tectonic implications will be further discussed in Chapter 7.

CHAPTER 5

Recrystallized grain size and subgrain size in experimentally deformed natural peridotites.*

5.1 Introduction

The prominent role of the peridotitic upper mantle in lithosphere dynamics has motivated investigations into the strength of the Earth's ductile upper mantle in the form of numerous experimental studies on the flow behaviour of olivine (e.g. Avé Lallemant and Carter 1970, Post 1977, Chopra and Paterson 1981, 1984, Hitchings et al. 1989). Many of these deformation experiments have shown a flow stress-dependence on microstructural parameters such as dislocation density (Kohlstedt and Goetze 1974), subgrain size (Raleigh and Kirby 1970, Green and Radcliffe 1972) and recrystallized grain size (Post 1977, Mercier et al. 1977, Karato et al. 1980, Ross et al. 1980). Empirical relationships between differential flow stress and the above microstructural parameters have been formulated in palaeopiezometric relationships (e.g. Twiss 1977), which have provided stress estimates for lithospheric rocks covering the range from the brittle-ductile transition zone (~10 km) down to approximately 250 km depth underneath cratonic regions (e.g. Avé Lallemant et al. 1980, Carter and Tsenn 1987). These palaeo-stress estimates complement previously available stress estimates based on principally different techniques (see Hanks and Raleigh 1980) such as mechanical force-balance modelling (e.g. Solomon et al. 1980) and isostasy considerations (e.g. Lambeck 1980, Nakada 1983).

In Chapter 6 I will use palaeopiezometry to investigate the *rheological significance* of the

* Parts of this Chapter have been submitted to Geoph. Res. Lett. as: Van der Wal, D., Chopra, P.N. Drury, M.R., and Fitz Gerald, J.D. Relationships between dynamic recrystallized grain size and deformation conditions in experimentally deformed olivine-rocks.

deformational structures identified in the Ronda peridotite. However, for a number of reasons outlined below indicating that many of the existing palaeopiezometers cannot be applied reliably, it is necessary to derive new piezometric relationships. This chapter, therefore, concerns the formulation of new recrystallized grain size and subgrain size piezometers which apply to natural hydrous peridotites.

Problems surrounding existing palaeopiezometers

Laboratory investigations into the flow behaviour of olivine have included deformation and recovery experiments on polycrystalline dunites and peridotites at high pressures and temperatures (e.g. Carter and Avé Lallemant 1970, Blacic 1972, Ross et al. 1980, Chopra and Paterson 1981, 1984, Karato et al. 1986, Karato 1989), and on single crystals of olivine at both high pressures (Phakey et al. 1972, Karato et al. 1980) and atmospheric pressures (e.g. Kohlstedt and Goetze 1974, Durham et al. 1977, Gueguen and Darot 1980).

Unfortunately, there are a number of limitations to these laboratory deformation experiments. First, many of them have been performed in a solid-medium deformation apparatus (Griggs 1967). Large errors in stress measurements have been suspected for a long time (Tullis and Horowitz 1980), but only recently, Green and Borch (1990) have demonstrated that stress estimates obtained from earlier solid-medium deformation apparatus can be in error by a factor 3-7 due to friction of the solid confining medium. Dead load experiments on olivine single crystals (e.g. Karato et al. 1980) are free of the above limitations, but uncertainties remain to how single crystal mechanical and microstructural data relate to polycrystalline aggregates. For example, many of the single-crystal experiments have been performed at temperatures as high as 1650°C, raising questions about how far the derived palaeopiezometers are applicable to natural upper mantle environments in the temperature range 800-1300°C. In addition, experiments on *synthetic* dunites and olivine single crystals do not incorporate the effect that secondary phases and impurities will have on grain boundary migration and grain growth (Poirier 1985 p. 71-73), hence on the development of a dynamically stable recrystallized grain size (Karato 1989).

A more fundamental problem is the unknown role of water and temperature on the recrystallized grain size and subgrain size. The most recent experimental (Ross et. al. 1980) and theoretical insights (Derby and Ashby 1987, Drury 1992) suggest that water and temperature may strongly influence recrystallized grain size at a given stress, although earlier obtained experimental results have not been able to demonstrate such a dependency (e.g. Post 1977, Mercier et al. 1977). It should be emphasized though that the "solid-medium apparatus" deformation tests remain extremely valuable in showing the qualitative

	Åheim dunite	Anita Bay dunite
chemistry:		
Fo - Py - Chr:	96 - 2 - <1	94 - 5 - 1
Mg/(Mg+Fe):	92.8	93.0
vol. content H2O	0.55±0.04	0.18±0.02
grain size (μm)	900	100
flow properties:		
Q (KJ/mol)	498±38	444±24
n	4.48±0.31	3.35±0.17
10log(A)	2.62±0.18	3.98±0.17

Table 5.1: Main material and rheological properties of Anita Bay and Åheim dunite.

relationships between microstructures and deformation conditions.

In this chapter, I will derive new palaeopiezometric relationships from natural peridotite deformation experiments largely free of the above limitations. Chopra and Paterson (1981, 1984) performed over a hundred deformation experiments on natural "wet" and "dry" dunites in a gas-medium deformation apparatus at 300 MPa confining pressure. These experiments bear the advantage that the stresses during deformation in a gas-medium deformation apparatus are accurately known because load is measured internally and is not influenced by friction. Chopra and Paterson (1981, 1984) presented brief microstructural descriptions of the deformed materials, but their main concern was the creep properties of the mantle materials. Below I present a re-investigation of the microstructures developed in these deformation experiments, with special emphasis on olivine recrystallized grain size and subgrain size. The influence of temperature, water content and starting material properties on the microstructures developed will be evaluated, as well as the relative stability of the microstructures during strain-rate step and stress-relaxation experiments.

5.2 Starting material properties and experimental techniques

Two natural peridotites have been studied, namely Åheim dunite from Norway and Anita Bay dunite from New Zealand. Both are natural peridotites with an inferred mantle origin. Åheim dunite consists dominantly of equant olivine grains with a mean size of 900 μm, although one specimen (label 6147) consists of olivine neoblasts with a mean grain size of 300-600 μm. The grains are essentially undeformed, some of the grains show subgrains

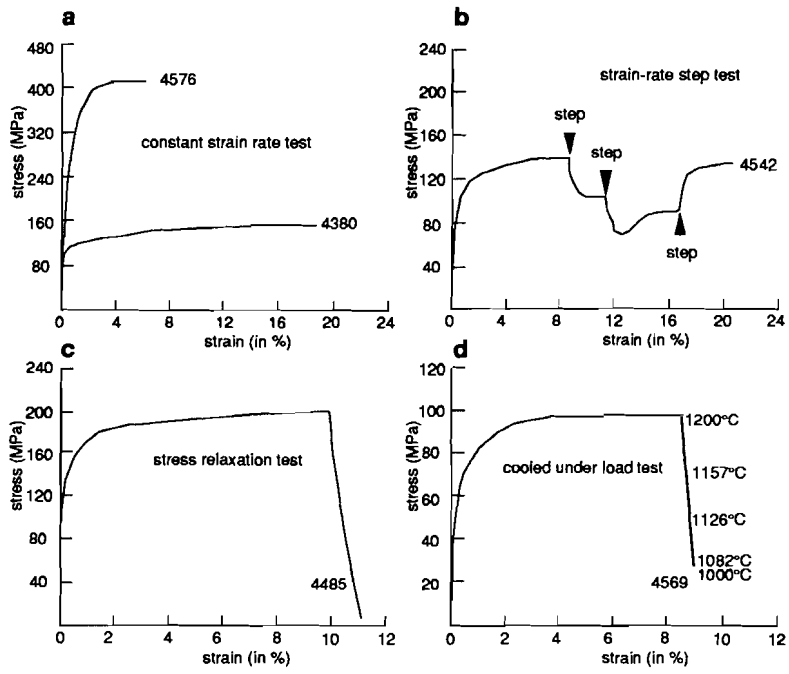

Fig. 5.1: Stress-strain curves for some deformation experiments with (a) a constant strain-rate history, (b) a strain-rate stepping deformation history, (c) a stress relaxation history, and (d) a constant strain-rate test with a "cooled under load" history.

with a 1-2° misorientation. Enstatite occupies up to 7% of the total rock volume, whilst spinel occurs as the accessory Al-phase. Various hydrated phases are present, including clinochlore, phlogopite, talc and tremolite.

Anita Bay dunite consists mainly of olivine neoblasts with a mean grain size of 100 *m*m. Occasionally, larger olivine palaeoblasts can be observed. A small fraction of the olivines contains low misorientation subgrain walls. The grain boundaries are slightly curved. Pyroxene-rich layers may constitute up to 50% of the total rock volume, and these layers have been disregarded in the microstructural analysis of the deformed specimen. Elongate spinels are commonly aligned parallel to the foliation. Hydrous minerals are also present in the Anita Bay dunites, and include clinochlore, tremolite and talc. Total water-contents stored in the crystalline lattices of the hydrous phases may reach 0.6 wt% (Chopra and Paterson 1984), which greatly exceeds the amount of water assumed to be present at upper mantle conditions (e.g. Thompson 1992 and refs. therein). A differential diagnosis of Anita Bay versus Åheim dunite is shown in Table 5.1.

Details on the deformation experiments can be found in Chopra and Paterson (1981, 1984), the most important of them are outlined below. The experiments were conducted in a Paterson gas apparatus (Paterson 1970) at confining pressures of 300 MPa and a differential stress range 10-450 MPa. As mentioned before, errors in stress measurements are believed to be very low due to the absence of friction and finite strength of the confining pressure medium. Temperatures achieved during deformation were 1100°-1400°C at strain-rates between 10^{-4}-10^{-6} s^{-1}. "Wet" experiments were performed on the starting material, "dry" experiments were conducted after pre-drying the sample at 1200°C at an oxygen fugacity of 10^{-5} Pa. During "wet" tests only, leakage of water through the thermocouple holes in the deformation-assembly suggests that the deformed material was water-saturated during the experiment.

The experimental runs reported in this study include a number of "wet" and "dry" Åheim and Anita Bay samples with: i) a constant strain-rate deformation history, ii) a multiple strain-rate "step" deformation history, iii) a stress-relaxation history following the deformation experiment, iv) a "cooled under load" history following a constant strain-rate deformation experiment in order to assess the effect of static recovery and recrystallization on the deformation microstructures, and v) an annealing recrystallization history following a constant strain-rate deformation experiment, in order to assess the kinetics of grain growth. Some typical stress-strain curves illustrating the different deformation histories in stress-strain space are shown in Fig 5.1.

5.3 Sample preparation and methods

The experimentally produced microstructures have been studied mainly by transmitted and reflected light microscopy on single- and double-polished, ultra-thin sections. In order to obtain some additional information on the mechanisms and processes of recrystallization, ion-beam thinned and carbon-coated discs have been studied in a 300 KV Philips 430 Transmission Electron Microscope (TEM) with attached EDAX-microanalysis equipment at the Research School of Earth Sciences in Canberra.

Recrystallized grain sizes have been measured from line-drawings made from a number of projected photographs of recrystallized areas taken at six different flat stage orientations with respect to the polarisation directions of the light microscope. A measurement grid was superimposed on the drawing with the grid spacing larger than the grain size and with the grid lines parallel and perpendicular to the compression axis. The mean linear

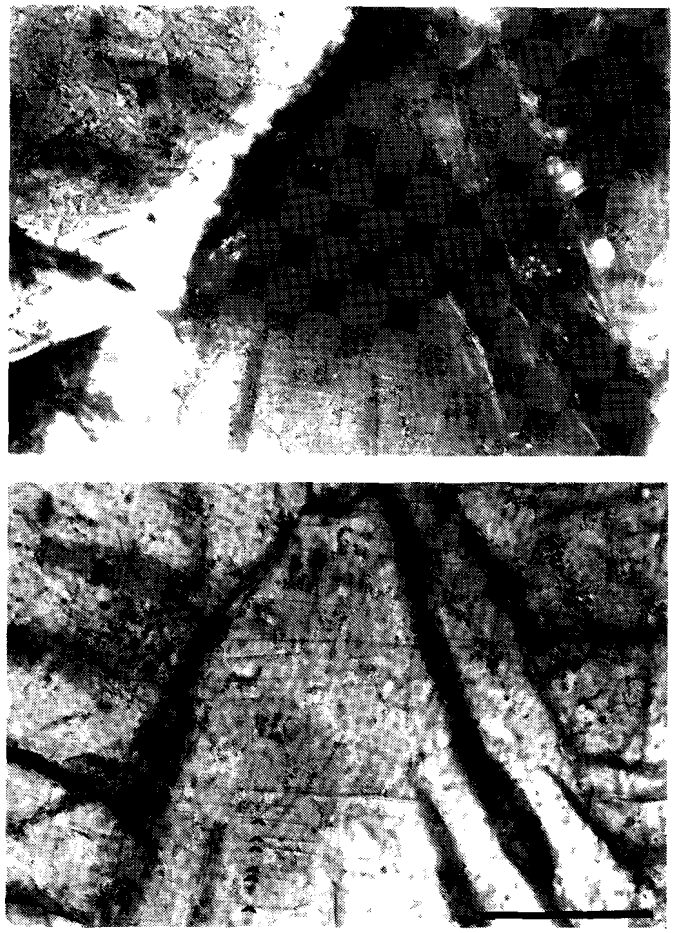

Fig. 5.2: Photomicrographs of a decorated specimen seen with (a) crossed polarizers and (b) parallel polarizers illustrating the improved resolution of low angle subgrain boundaries due to decoration. Arrows denote the decorated subgrain walls. Scale bar = 200 mm.

intercept was calculated from the number of intersecting grain boundaries, divided by the length of the sample line. Average grain diameters were calculated by multiplying the mean linear intercept with a factor of 1.75, which roughly applies to equi-axed polygonal shaped grains (Pickering 1972).

Previous work on deformed polycrystalline aggregates has shown that the measured subgrain dimension depends on the technique employed (e.g. White 1979a, b). TEM studies reveal improved resolution of subgrain spacings towards low values, but this technique is time-consuming and not generally available. On the other hand, the resolution of subgrain spacings in standard light microscopy is limited to misorientations >1-2°. Therefore, the Kohlstedt et al. (1976) decoration technique has been applied to a

selection of specimen, in order to obtain a subgrain resolution intermediate between TEM and conventional light microscopy (Fig. 5.2). Polished samples were decorated for ~10 minutes at 900°C, leading to a penetration depth of decoration up to ~10 μm. Although a decoration time of 1 hour is recommended (Kohlstedt et al. 1976), practise showed that decoration for several minutes is sufficient to reveal all the subgrain walls, whilst the risk of damage to the sample surface such as cracking of the polished surface presumably induced by dehydration of the hydrous phases is limited. Projected colour-slides of the subgrains were used to measure the spacing between the olivine (100) subgrains.

The low degree of recrystallization in the deformed samples limits the number of data. Additionally, in order to preserve as much as possible of the experimentally deformed dunite material, a compromise had to be made as to the amount of decorated samples. Therefore, the qualitative aspects of this study are emphasized, although the quantitative aspects will be addressed as well.

5.4 Qualitative aspects of microstructure development

Both dunites show ubiquitous evidence for deformation of the olivines during the experiments. This is primarily reflected by the variation in optical extinction across subgrain walls (Fig. 5.3c,d). The majority of the subgrains are parallel to [100], with minor subgrains developed parallel to [001]. The subgrains are generally straight.

In both dunites, the olivine grains are recrystallized and show serrated grain boundaries and subgrain boundaries (Fig. 5.3), in particular in wet samples deformed at high temperatures. The volume fraction of recrystallized grains is small, never exceeds 20% and is obviously related to the total amount of strain accommodated. Only few "dry samples" show recrystallization, and where they do, the total volume fraction of recrystallized material is very low. The recrystallized grains are equi-axed to slightly elongate (axial ratios 1.04-1.41) perpendicular to the compression axis. Undulatory extinction is common in the recrystallized fraction. The recrystallized grain size is always less than the initial grain size, and both subgrain size and recrystallized grain size (Fig. 5.3) decrease with increasing differential stress.

Growth of olivine is evident in the relaxed and annealed specimen. Equi-granular polygonal grains, with grain diameters up to 100 μm, have developed from highly recrystallized zones. These grains are notably undeformed and are much larger than newly recrystallized grains in similar but un-relaxed samples.

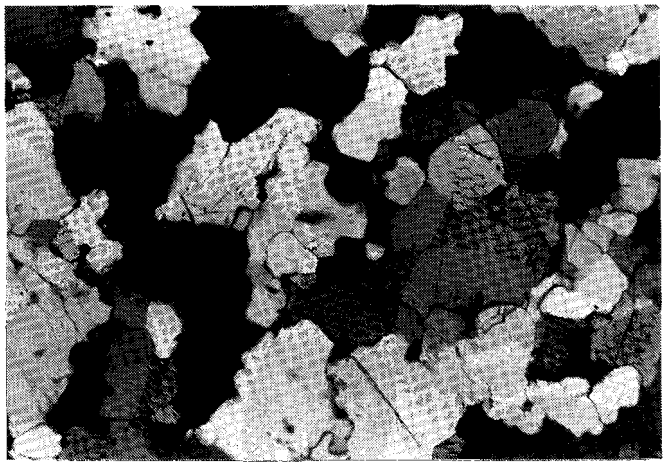

a: *4272 (AB), 63 MPa, Dg = 52 µm.*

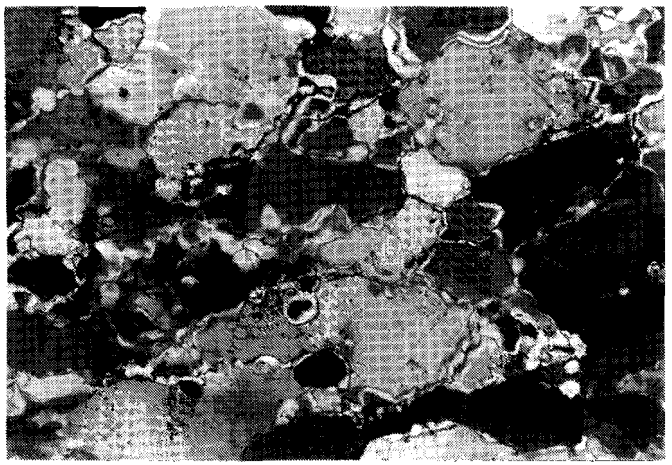

b: *4306 (AB), 113 MPa, Dg = 47 µm.*

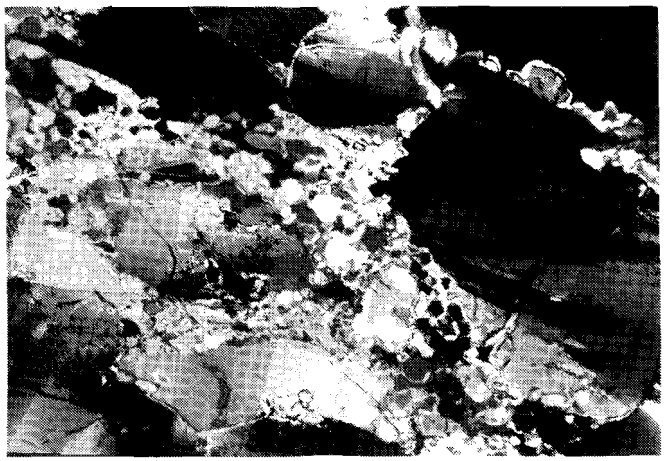

c: *4380 (ÅH), 146 MPa, Dg = 21 µm.*

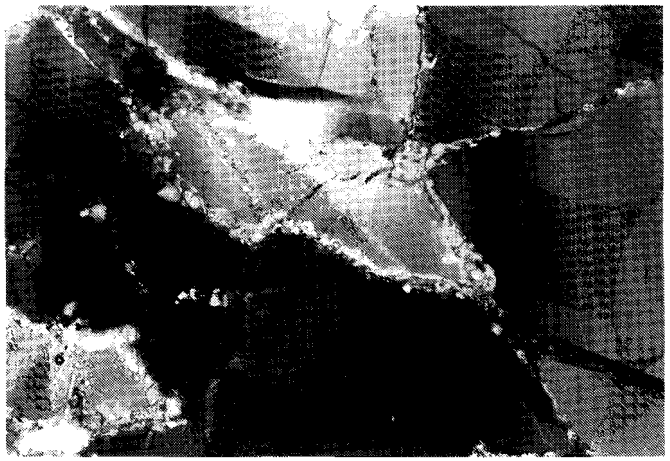

d: *4468 (ÅH), 212 MPa, Dg = 14 µm.*

Fig. 5.4: TEM micrograph showing bulging of a grain boundary. Note low dislocation density at A in the newly recrystallized grain and a subgrain wall in the bulging grain at B, suggesting dynamic recrystallization by a bulging recrystallization mechanism. Also note high dislocation densities at C in the overgrown grain, high subgrain densities at D in the host of the bulging grain possibly providing the energy driving migration of the bulging grain boundary, and small pyroxenes at E possibly responsible for the high subgrain density at D. Scale bar = 2 μm.

◁ Fig. 5.3 (previous page): Photomicrographs showing systematic decrease in olivine recrystallized grain size with increasing differential flow stress. Note subgrains in large grains in 4380 and 4468.

a

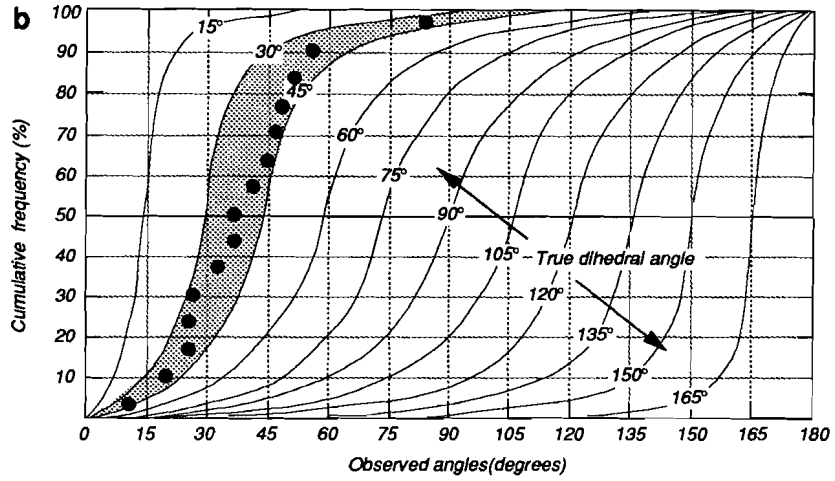

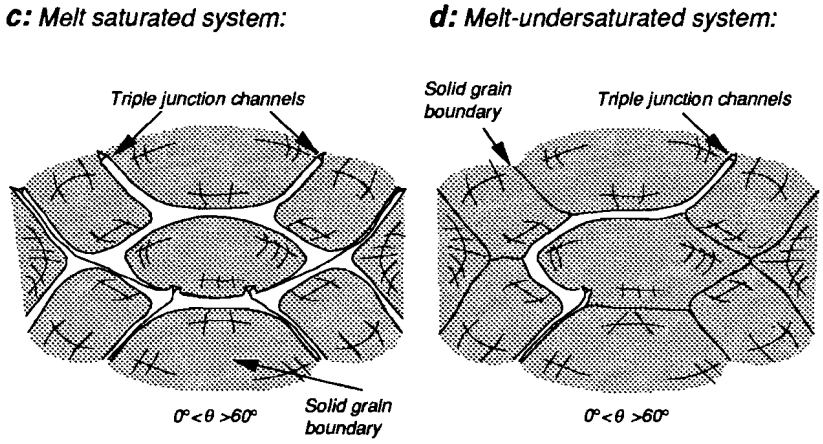

△

◁ Fig. 5.5 (a) previous page: Melt topology in newly recrystallized areas, note beam damage in upper left melt pocket, (b) this page: cumulative apparent dihedral angle plot, suggesting a median dihedral angle of ~40°, (c) melt distribution in melt saturated systems, (d) inferred melt distribution in newly recrystallized areas. θ denotes range of dihedral angles. Scale bars = 0.5 μm.

Recrystallization mechanisms

Preliminary TEM on newly recrystallized areas reveals small newly recrystallized olivine grains with sizes comparable to those measured with the light microscope. They show a low dislocation density relative to the overgrown grains, bulging from intensely deformed grains with a high subgrain and dislocation density (Fig. 5.4). The crystallographic

orientation of the bulging neoblasts is not much different from the orientation of their host. Although subgrain walls are common, no consistent misorientation has been observed along them. Dislocations walls or subgrain boundaries are generally straight, but also curved subgrain boundaries have been observed suggesting that some subgrain boundary mobility occurred during the experiments. These TEM observations suggest that combined subgrain rotation and local grain boundary bulging play an important role in the recrystallization mechanism (e.g. Poirier and Guilopé 1979). It seems feasible, therefore, that the size of the recrystallized grains is primarily controlled by a grain boundary bulging type of mechanism, assisted by subgrain rotation recrystallization (e.g. Urai 1986, Drury and Urai 1990).

Melt topology

Light microscopy shows that all samples contain a small fraction of melt products, hereafter referred to as "melt". It is mostly present as triple point pockets and, occasionally, as grain boundary films or wider openings up to 50 μm width. Melt rich pools commonly occur near the ends of dehydrated chlorites, indicating that the hydrous phases rather than the olivines became unstable at the prevailing experimental temperatures. Generally, newly grown idiomorphic olivine dominates the melt products. It can be seen that some melt has migrated from source regions to inter- and intragranular cracks. The melt content varies considerably between and within samples. Only traces of melt are present in most dry samples, whereas melt contents of several percent may be locally present in wet samples deformed at 1200-1300°C and dry samples deformed at 1400°C. The melt fraction present is usually very low, though.

TEM indicates that in newly recrystallized areas a silica-rich glass occurs only at few triple point junctions. Most grain-boundaries appear to be essentially solid-solid boundaries between adjoining crystals. The structural width of these boundaries observed in TEM (the zone of structural distortion along the interface) is less than about 1-2 nm. No evidence has been found for the presence of wide (10-50 nm width) melt films along grain boundaries, although the presence of much narrower (0.5-1.0 nm width) melt films can not be ruled out.

The geometry of some melt pockets in newly recrystallized areas is shown in Fig. 5.5a. Following Riegger and Van Vlack (1960), the true dihedral angle obtained from the cumulative projected dihedral angles of the solid-glass contact lies in the range 30-47° (Fig. 5.5b) which concurs with the median dihedral angle for olivine-basalt systems (Waff and Bulau 1979, 1982). Such values of the dihedral angle suggest an equilibrium melt morphology where the liquid phase is confined to an interconnected network along grain

triple junctions, schematically shown in Fig. 5.5c (e.g. Kingery et al. 1976, p. 214). TEM, however, shows that only a small fraction of the triple junctions contains a glass phase, thus the true melt morphology in the newly recrystallized areas could resemble that shown in Fig. 5.5d, where only few grain boundary triple junctions contain a wide melt channel. It is therefore inferred that most of the grain contacts are essentially solid-solid contacts and that the recrystallized grain size is only marginally influenced by the presence of a melt channel along some grain boundaries.

Areas of high melt content were excluded from the microstructural analysis, except for sample 4380 in which the recrystallized grain size was measured in areas with a range of melt contents (1-10%) avoiding obvious melt pools. The mean recrystallized grain size was found to be 20 μm, whilst the recrystallized grain size in melt-free areas yielded a mean grain size of 21 μm (Table 5.2). These data show that within measurement error the recrystallized grain size appears independent of local melt content.

5.5 Quantitative aspects of microstructure development

Recrystallized grain size

The recrystallized grain sizes in 31 experimentally deformed specimen are listed in Table 5.2. The recrystallized grain size in "wet" Anita Bay and Åheim dunite, developed in constant strain-rate and strain-rate step deformation experiments show a well defined relationship with *final flow stress,* i.e. the steady state flow stress achieved after the last strain-rate step (Fig. 5.6a). This relationship can be described by the following empirical equation:

$$D_g = 0.0044^{+0.0008}_{-0.0006}(\sigma)^{-1.10\pm.10} \qquad R=0.96 \qquad (5.1)$$

with the recrystallized grain size (D_g) in metres and the differential flow stress (σ) in MPa. R denotes the correlation coefficient.

This relationship does not hold for strain-rate step test 4585. In this case the final flow stress was 37 MPa, and the final grain size was smaller than expected from the stress-grain size relationship (eqn. 5.1). With final flow stresses > 50 MPa the grain size did adjust to the new stress after only 1.5 - 3% strain. This may be explained as follow. For the grain size to adjust to the new stress, grain growth is required presumably driven by the stored strain

specimen	test	Rheological data: ε (%)	T (°C)	final σ1-σ3 (MPa)	max σ1-σ3	$\dot{\varepsilon}$ (s-1)		relax time (hr)	Recrystallized grain size Dg (μm)	calculated error	N	Subgrain size ds (mean)	2σ	ds (median)	2σ	Skewness	Kurtosis	N
Åheim dunite:																		
4380	1	16	1210	146		1E-05			21	1.68	81							
4267	1	20	1200	174		1E-05			18	1.09	139							
4468	1	10	1300	212		1E-04			14	.96	107	5.99	3.76	5.00	1.97	-0.35	-0.51	109
4535	2	13	1300	58	126	1E-06	↓		57	2.87	194	7.92	5.51	6.50	1.92	-0.15	0.30	112
4396	2	16	1190	119	415	1E-06	↓		29	1.76	130							
4509	2	16	1200	284	385	5E-05	↓		8.2		11	8.10	7.40	5.50	2.14	0.27	-0.15	95
4485	3	10	1300	10	196	1E-04		2.83	65	4.39	108	6.32	4.65	5.00	1.94	0.08	-0.19	104
4370	3	10	1200	49	298	1E-04		1.94	20	1.32	108	6.43	4.69	5.00	2.09	-0.07	-0.74	161
4576	1*	6	1300	420		1E-04			<3									
4506	1*	16	1300	350		1E-04			6.3		12							
4581	2*	12	1300	350	360	1.5E-05	↑		7.0		20							
4666	2*	11	1210	280	471	3E-06	↓					7.73	5.28	6.50	2.16	-0.38	-0.59	91
4572	4	22	1200-1300	260		creep			36	2.35	118	5.04	3.61	4.00	1.97	0.05	-0.55	157
6147	4	15	1200	218				0.53	16	1.05	120							
Anita Bay dunite:																		
4272	1	12	1200	63		1E-06			52	2.57	202	8.32	7.04	5.88	2.13	0.17	-0.38	106
4463	1	6	1200	85		5E-06			28	2.03	93	6.44	4.54	5.00	1.97	0.09	-0.91	110
4265	1	9	1200	88		1E-05			30	2.37	76							
4486	1	15	1300	90		1E-05			30		20	5.71	4.49	4.50	1.93	0.32	-0.07	116
4417	1	15	1200	127		5E-05			17	1.29	90	5.73	5.22	3.53	2.34	0.19	-0.78	163
4271	1	9	1100	146		1E-06			16	1.28	80							
4519	1	12	1200	188		5E-05			14	.95	103	5.30	4.29	4.00	2.04	0.17	-0.35	154
4585	2	15	1300	37	84	3E-06	↓		34	3.46	48	6.18	4.80	5.00	1.98	0.18	-0.34	99
4469	2	13	1300	120	400	1E-06	↓		18		20							
4542	2	21	1300	132	132	1E-04.5	↑		19	1.26	106							
4306	3	15	1300	7	113	1E-04		1.38	47	3.14	111	5.81	3.70	4.50	1.87	0.03	-0.85	103
4371	3	11	1200	17	208	1E-04		1.55	20	1.38	106	3.78	5.33	2.35	2.11	0.52	0.89	211
4580	3*	12	1400	96	195	1E-06	↓		24	1.51	122							
4668	2*	4	1200	252	343	1E-06	↓		18	1.54	63	6.27	4.57	5.50	1.75	0.29	1.10	43
4667	2*	12	1210	315	580	3E-06	↓		4.8		10							
4569	5	9	1200	102		1.4E-05			21	1.48	100							
4520	5	12	1200	150		5E-05			17	1.11	120							
4489	5	9	1300	266		1E-04			15	1.17	80							

Key to tests. 1: constant strain-rate tests, 2: strain-rate step tests, arrows denote final down- or up-step, 3: Stress relaxation tests, 4: Annealing recrystallization tests, 5: "Cooled under load" constant strain-rate tests. Asterix (*) denotes "dry" tests.

energy in the deformed old grains and surface stored energy in the newly recrystallized aggregates (e.g. Poirier 1985). Both are controlled mainly by the flow stress prior to the final strain-rate step through the dislocation density and grain- and subgrain size. It follows that the driving force for grain size adjustment decreases with decreasing stress. In addition, at lower stresses, an increasing amount of grain growth is required for the adjustment of grain size to the new stress. The data nonetheless show that at sufficiently high flow stresses the dynamic recrystallized grain size can rather rapidly adjust to any change of the flow stress, namely at laboratory time-scales of several hours.

The recrystallized grain size data in three "cooled under load" specimen show no systematic deviation from the grain size expected from the experimental relationship of eqn. 5.1 (Fig. 5.6a), suggesting that there is no significant effect of grain growth during cooling of the specimen at the termination of the experiment.

Influence of strain, strain-rate and temperature

The effect of the various experimental parameters on the recrystallized grain size is illustrated in Fig. 5.7. In this figure the *deviation* of the measured recrystallized grain size from the grain size expected on the basis of the empirical piezometer is expressed as a percentage of the measured grain size or:

$$\Delta = \frac{D_{g(\text{measured})} - D_{g(\text{calculated})}}{D_{g(\text{measured})}} * 100\%$$

where Δ will be referred to as the relative residual of the measured grain size (see e.g. Clark and Hosking 1986, p. 370).

The residuals are plotted against the final flow stress, whilst in each diagram they are labelled to represent different values of the experimental parameter under investigation. This representation of the data allows systematic deviations of the data from the equilibrium line (which is the empirical piezometric curve) to be identified. If deviations consistently relate to particular values of the experimental parameter in question, the conclusion seems justified that the grain size - stress relationship or piezometer depends on that parameter.

◁ Table 5.2 (previous page): Experimental data for the experimental deformation of Åheim and Anita Bay dunite. N refers to number of measurements. Skewness is a measure of the excess of data at one particular side (or asymmetry) of a frequency diagram relative to a normal distribution. Kurtosis is a measure of the peakedness of the distribution relative to a normal distribution. Note that if either of both significantly deviates from zero, the data cannot be accurately described by the statistics of a normal distribution.

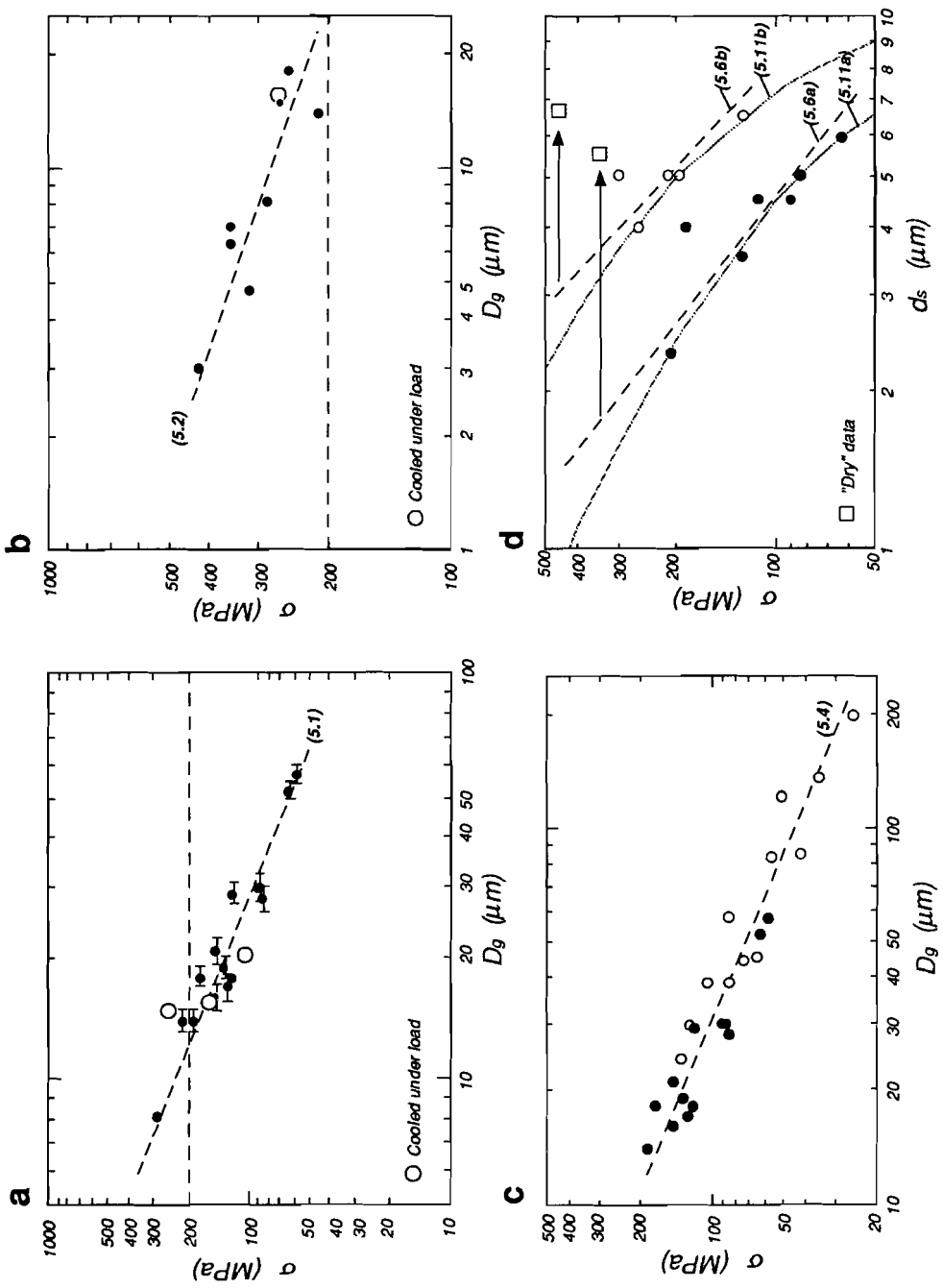
a
b
c
d
σ (MPa)
Dg (μm)
ds (μm)
(5.1)
(5.2)
(5.4)
(5.6a)
(5.6b)
(5.11a)
(5.11b)
Cooled under load
"Dry" data

Before further inspection of Fig. 5.7 it needs to be noted that for strains < 10% there are systematic negative residuals for the measured grain sizes relative to the expected grain sizes calculated with equation 5.1. This probably indicates that only for strains > 10% the recrystallized grain size reaches stable mean values independent of total strain, consistent with the observation that the larger of the newly recrystallized grains show undulatory extinction and are flattened perpendicular to the compression axis suggesting development of a steady-state microstructure. The residuals at low strains are small, however (< 12%), and in view of the limited total number of data the low-strain data have been included in the analysis. Single data cannot be compared and are omitted from this analysis.

The effect of strain-rate on the recrystallized grain size is shown in Fig. 5.7a. The scatter of data for different values of the experimental strain-rate indicates that there is no systematic trend in the residuals of the measured grain size relative to the grain size calculated with eqn. 5.1. Instead, for all strain-rates there are positive and negative residuals suggesting that strain-rate does not affect the recrystallized grain size.

The effect of temperature on the measured recrystallized grain size is shown in Fig. 5.7b. The scatter of residuals of the measured grain size relative to the grain size calculated with eqn. 5.1 for each of the different values of the experimental temperature suggests that the recrystallized grain size is temperature-independent in the range 1100-1300°C. Note however, that the data presented do not preclude a significant effect of temperature on recrystallized grain size at much lower temperatures.

As outlined by White (1979a), the effect of variations in strain-rate may be largely obliterated by temperature variation effects and vice versa. Ideally, the effect of strain-rate and temperature should be evaluated against each other, but the limited amount of data available does not permit that analysis. However, the combined effect of temperature and strain-rate can be evaluated as follows. Laboratory deformation experiments such as those of Chopra and Paterson (1981, 1984) have shown that an increase of temperature leads to a decrease of equivalent viscosity. At conditions of constant flow stress, an increase in temperature will result in an increase of strain-rate equivalent to the decrease in viscosity. A parameter K, defined as temperature over strain-rate, can now be used to study the combined effect of temperature and strain-rate on the recrystallized grain size. Experimental values of logK typically fall in the range 7-9, where low values of logK represent low-

◁ Fig. 5.6 (previous page): Stress - recrystallized grain size relationships for (a) constant strain-rate and strain-rate stepping tests, (b) as (a) for high stress (>200 MPa) data, (c) as (a) but combined with the Karato et al. (1980) data (open circles), (d) stress - subgrain size relations in Anita Bay (black dots) and Åheim dunite (open circles). The fits to the data labelled as in text.

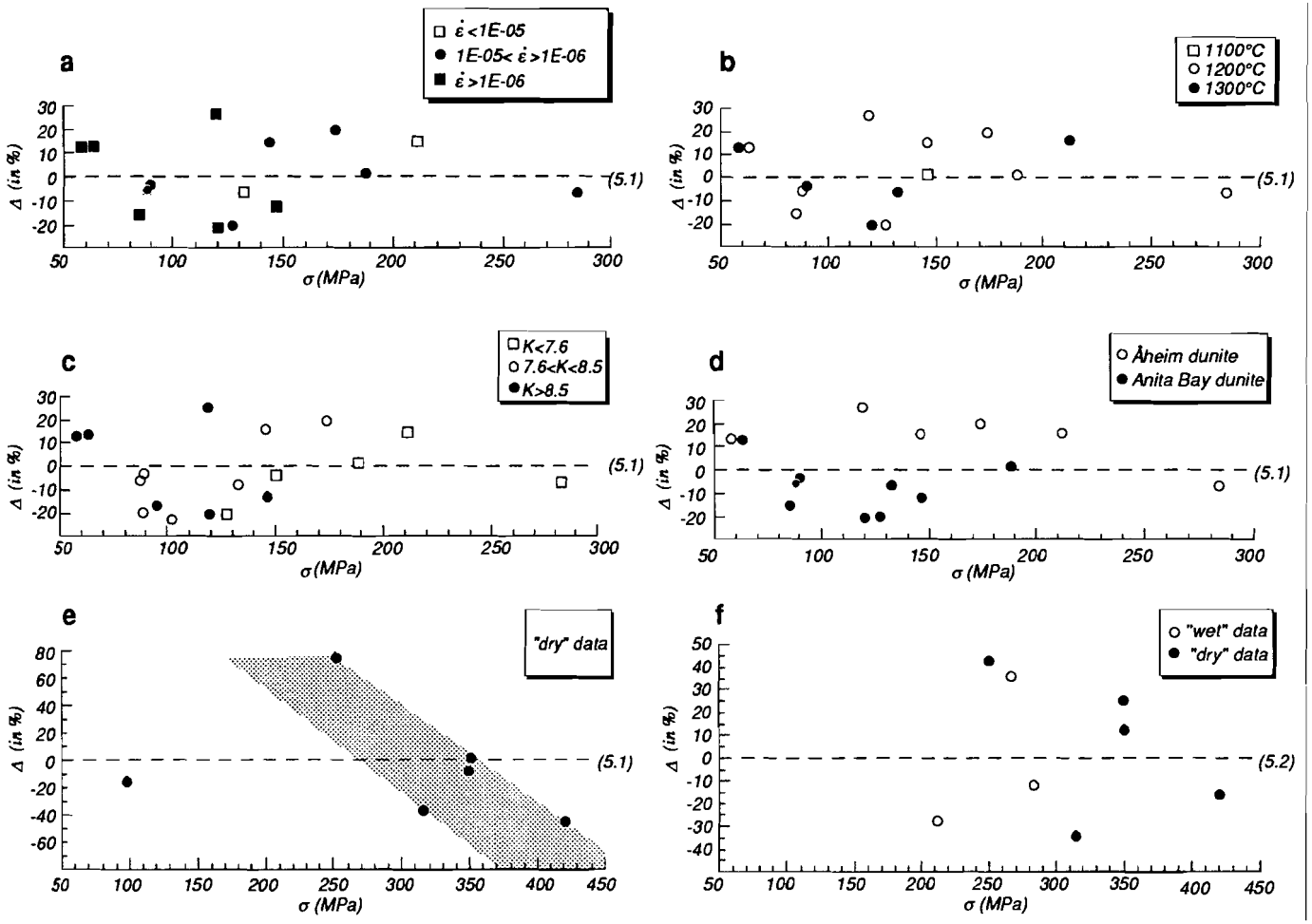
a
□ ε̇<1E-05
● 1E-05< ε̇ >1E-06
■ ε̇>1E-06
Δ (in %)
σ (MPa)
(5.1)
b
□ 1100°C
○ 1200°C
● 1300°C
c
□ K<7.6
○ 7.6<K<8.5
● K>8.5
d
○ Åheim dunite
● Anita Bay dunite
e
"dry" data
f
○ "wet" data
● "dry" data
(5.2)

temperature, high strain-rate conditions whilst high values of logK represent high-temperature, low strain-rate deformation. Fig. 5.7c shows that the residuals of the measured grain size relative to the grain size calculated with eqn. 5.1 do not systematically deviate from the equilibrium line for different values of K. The data therefore suggest that the recrystallized grain size is principally independent of temperature and strain-rate and of coupled variations of these parameters.

Influence of starting material and water content

The effect of starting material (Åheim dunite or Anita Bay dunite) on the recrystallized grain size in both materials is shown in Fig. 5.7d. Note that the residuals of Åheim recrystallized grain sizes systematically plot above the experimental grain size - stress relationship (eqn. 5.1), while residuals of Anita Bay recrystallized grain sizes plot mostly below this line. The data suggest that the recrystallized grain size is slightly dependent on *material properties*, which are for Åheim and Anita Bay dunite in view of their different initial microstructures and different flow properties (Table 5.1; Chopra and Paterson 1981, 1984).

The assessment of the effect of water on recrystallized grain size is difficult because the low degree of recrystallization limits the data for "dry" recrystallized grain sizes. Additionally, the "dry" experiments do not cover the same flow stress range as the "wet" experiments. Nevertheless, an attempt is made to evaluate the existing data. The distribution of the residuals of the measured "dry" recrystallized grain sizes relative to the grain sizes calculated with eqn. 5.1 (Fig. 5.7e) can be described as follows: one data point at low flow stress of 96 MPa plots close to the expected grain size, while the data for flow stresses >200 MPa could plot on a line at a distinct angle to the stress axis (Fig. 5.7e), suggesting a different grain size - stress relationship at high flow stresses. The reason for this could be either some effect arising from high final flow stresses or the effect of the absence of water irrespective of the flow stress. As outlined above, the flow properties of "dry" dunites do not permit flow experiments at low stresses. By consequence it cannot be determined if this new relationship holds for "dry" dunites deformed at flow stresses <200 MPa. To resolve this ambiguity, all the grain size data established in both "wet" and "dry" constant strain-rate and strain-rate stepping tests have been plotted against final flow stresses >200 MPa in Fig. 5.6b. The data are more scattered when compared to Fig. 5.6a, probably due

◁ Fig. 5.7 (previous page): Plots showing the effect of (a) strain-rate, (b) temperature, (c) combined strain-rate and temperature (see text), (d) material properties, and (e & f) water content. Plotted is the residual in % of the calculated grain size with empirical relations (eqn. 5.1) and (eqn. 5.2). For further explanation see text.

to worse statistics on the grain size data, but nevertheless a linear relationship between flow stress and recrystallized grain size can be recognized on a log-log diagram. This relationship is described by the following equation:

$$D_g = 11.89^{+4.46}_{-3.24}(\sigma)^{-2.49\pm.55} \qquad R=0.79 \qquad (5.2)$$

with D_g in meters and σ in MPa. When the residuals of the measured grain sizes relative to the grain sizes calculated with eqn. 5.2, for flow stresses >200 MPa and distinguished on the basis of the presence or absence of water ("wet" or "dry"), are plotted with respect to this experimental grain size - stress relationship (eqn. 5.2), the effect of water can be evaluated (Fig. 5.7f). No systematic distribution of the residuals can be observed, i.e. both the "wet" and "dry" data are equally well described by eqn. 5.2. It follows that the different grain size - stress relationship for high final flow stresses appears not to be a function of water content, but could result from a change in material behaviour at high flow stresses. Chopra and Paterson (1981) report a change in flow behaviour of Anita Bay dunite at around 100 MPa. They ascribe this feature to a change in deformation mechanism when the flow stresses approach or exceed confining pressures of 300 MPa. When other deformation mechanisms such as microfracturing are introduced, additional recrystallization mechanisms like solution-precipitation could accommodate microfracturing to maintain steady-state flow. This could lead to a different recrystallized grain size - stress relationship at high final flow stress. Thus, the experimental relationship (eqn. 5.2) may not bear any significant meaning to upper mantle microstructures, as confining pressures in the mantle greatly exceed 300 MPa.

Consequently, eqn. 5.1 should be re-defined excluding the data for σ >200 MPa as:

$$D_g = 0.0049^{0.0009}_{0.0007}(\sigma)^{-1.12\pm.13} \qquad R=0.96 \qquad (5.3)$$

with D_g in meters and σ in MPa.

Comparison with existing data

Fig. 5.6c shows the Anita Bay and Åheim recrystallized grain size data plotted with the results of Karato et al. (1980) obtained at 1650°C on dry recrystallized single crystals. These single crystal data can be considered the only reliable recrystallized grain size data available, as all the other data are based upon solid-medium deformation experiments. The combined Anita Bay/Åheim data and those of Karato et al. (1980) can be described

by a single recrystallized grain size - stress relationship covering the stress range 25-200 MPa:

$$D_g = 0.015^{0.004}_{0.003}(\sigma)^{-1.33\pm.09} \quad R=0.96 \qquad (5.4)$$

with D_g in meters and σ in MPa. This equation holds for deformation induced recrystallized grain sizes developed at flow stresses lower than the confining pressure (which will always be the case in the ductile mantle) and where both subgrain rotation and grain boundary bulging recrystallization processes can be identified (Karato et al. 1982). The combined data of this study and those of Karato et al. (1980) suggest that the dynamic recrystallized grain size in olivine is controlled mainly by flow stress and is largely independent of water content and temperature in the range 1100°C-1650°C, with some minor dependence on flow properties of the olivine aggregates under investigation.

The grain size - stress relationships measured for Anita Bay and Åheim dunites apply not only to samples with a constant strain-rate history, but also to samples with a more complex multiple strain-rate history. Most of the strain-rate step tests involved a decrease of strain-rate. Similar results were obtained by Ross et al. (1980) for steps with both increasing and decreasing strain-rate. This suggests that in many cases the dynamically recrystallized grain size can rather rapidly adjust to a change of flow stress.

Possible role of fluids

All of the experimentally deformed olivine aggregates (e.g. Zeuch and Green 1984, Chopra and Paterson 1984, Hitchings et al. 1989, Bussod and Christie 1991) including the dry single crystals of Karato et al. (1980) contain a very small to moderate volume fraction of melt. Unfortunately, there are no data available to date on recrystallized grain sizes in melt-free olivine rocks. In consequence, it is possible that grain size - stress relationships in melt-free rocks could be different to those in rocks containing melt. The melt content and also the water content of the polycrystal may be expected to influence this relationship, because the presence and amount of both melt and water will affect the kinetics of the basic processes involved in recrystallization. Recent theoretical models of Derby and Ashby (1987) and Derby (1990) for migration and growth recrystallization and Drury (1992) for rotation and growth recrystallization suggest that the grain size - stress relationship arises because of a dynamic balance between grain size reduction processes and grain growth processes. According to Derby and Ashby (1987), the dynamically recrystallized grain size (D_g) can be described by the following theoretical relationship:

$$D_g = \frac{KEv_{gbm}}{\dot{\varepsilon}} \tag{5.5}$$

where K is a slightly temperature dependent constant, E is a critical strain for nucleation of recrystallization, v_{gbm} is the grain boundary migration rate and $\dot{\varepsilon}$ is the strain-rate. The same equation forms the basis of the analysis of recrystallized grain size in the rotation and growth model of Drury (1992). Models of this type can account for the apparent independence of recrystallized grain size from water content. The influence of water is to increase both the strain-rate and the grain boundary migration rate by roughly similar factors (Karato et al. 1986, Karato 1989). It is clear from eqn. 5.5 that the effects of an increase of v_{gbm} and $\dot{\varepsilon}$ due to the presence of water may cancel each other, or at least that the net effect of water or melt on recrystallized grain size becomes too small to be detected in laboratory experiments.

Subgrain size

The shape of subgrains for a number of different geological materials may vary from roughly equi-dimensional to strongly planar. The size of the subgrains can, therefore, be expressed in many different ways, such as maximum or mean subgrain diameter and average subgrain area. For olivine, subgrain characteristics are generally obtained assuming a normal distribution of an often extensive olivine (100) subgrain spacing data set, and the arithmetic mean forms the basis of many existing olivine subgrain palaeopiezometers (e.g. Ross et al. 1980, Karato et al. 1980). Jin and Green (1989) analyzed olivine (100) and (001) subgrain spacings in decorated samples from eastern China mantle xenoliths and, presumably inspired by earlier work of Ranalli (1984), demonstrated that the frequency distribution of the spacings is distinctly non-normal, putting questionmarks as to the significance of the mean value of such non-normally distributed data. They showed that the frequency distribution of the natural logarithms of the measured (decorated) subgrain spacings much better approximates a normal distribution. Consequently, the median (geometrical mean) of the frequency diagram provides a better description of the subgrain population measured. Note, however, that the characteristic distribution of subgrain dimensions can be expected to depend on the measurement technique employed because the resolution of the different techniques differs significantly (e.g. White 1979a). Therefore, olivine subgrain spacing characteristics as discussed by Jin and Green (1989) may apply only to studies where the decoration technique (Kohlstedt et al. 1976) has been employed.

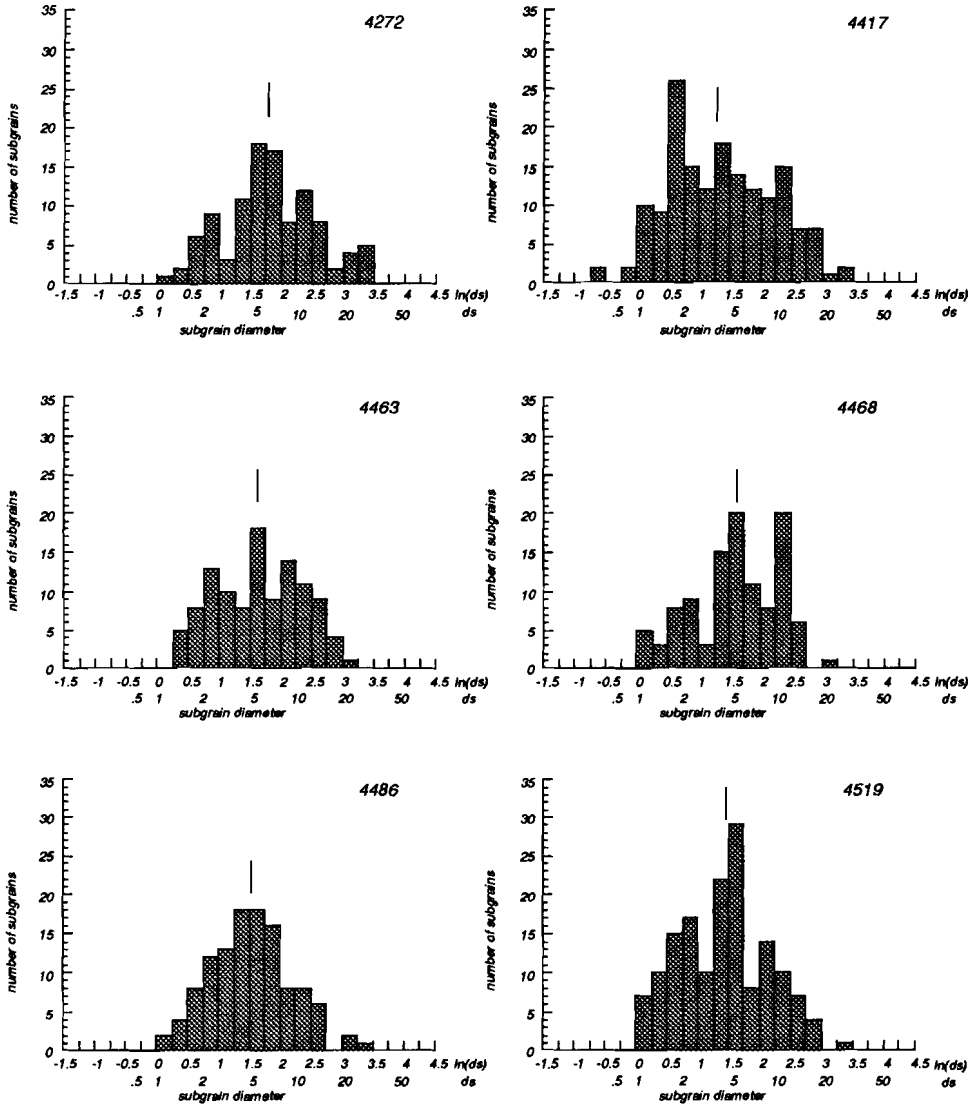

Fig. 5.8: Olivine (100) subgrain wall spacing (ds) frequency histograms for (a) constant strain-rate tests, (b) strain-rate stepping tests, and (c) relaxation tests, showing that the subgrain spacing in all cases closely approximates a log-normal distribution.

The olivine (100) subgrain spacings measured in 16 experimentally deformed Åheim and Anita Bay dunites are listed in Table 5.2. Fig. 5.8 shows the frequency histograms of

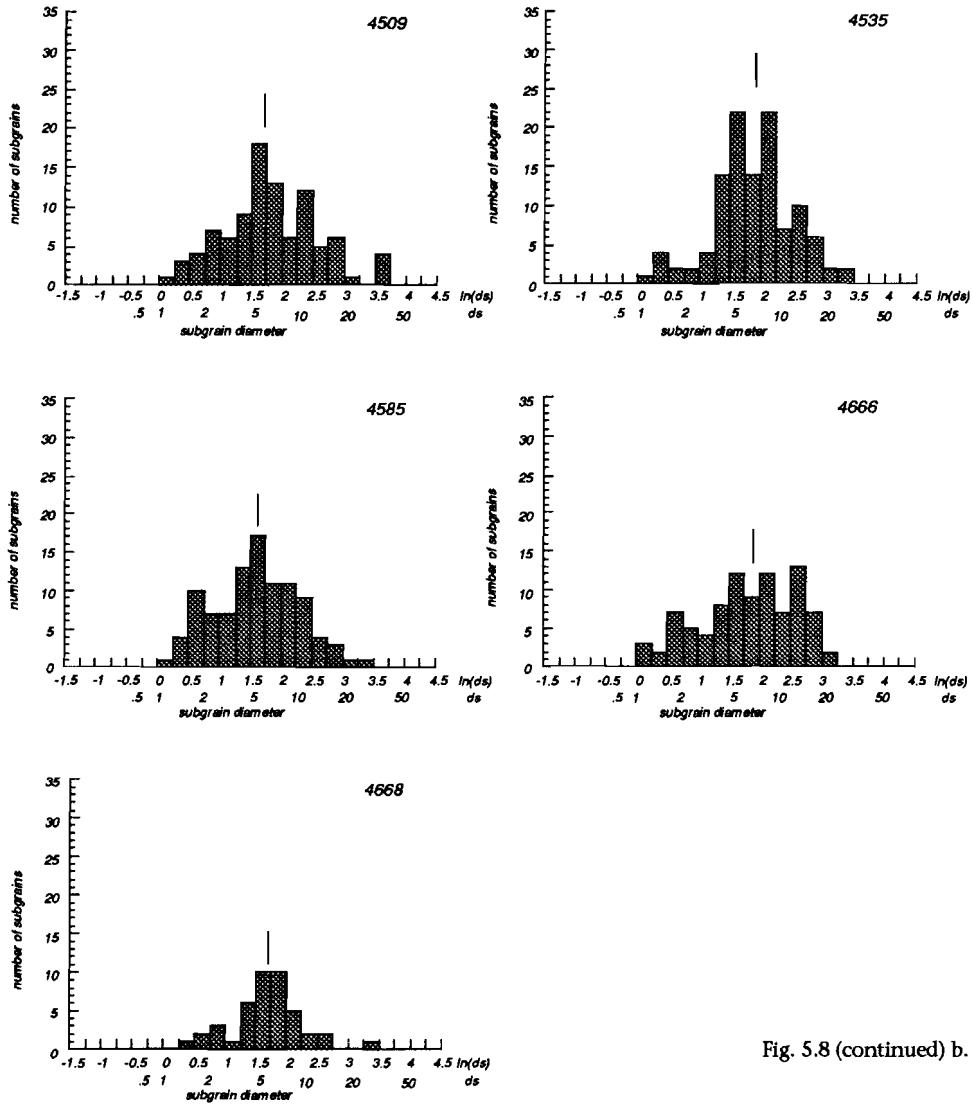

Fig. 5.8 (continued) b.

the natural logarithm of the subgrain spacings in specimen deformed in (a) constant strain-rate experiments, (b) strain-rate stepping experiments and (c) relaxation experiments respectively. The data concur with the data obtained from the Eastern China natural peridotites of Jin and Green (1989) in the sense that the average subgrain spacing shows a lognormal distribution rather than a normal distribution. Consequently, the new

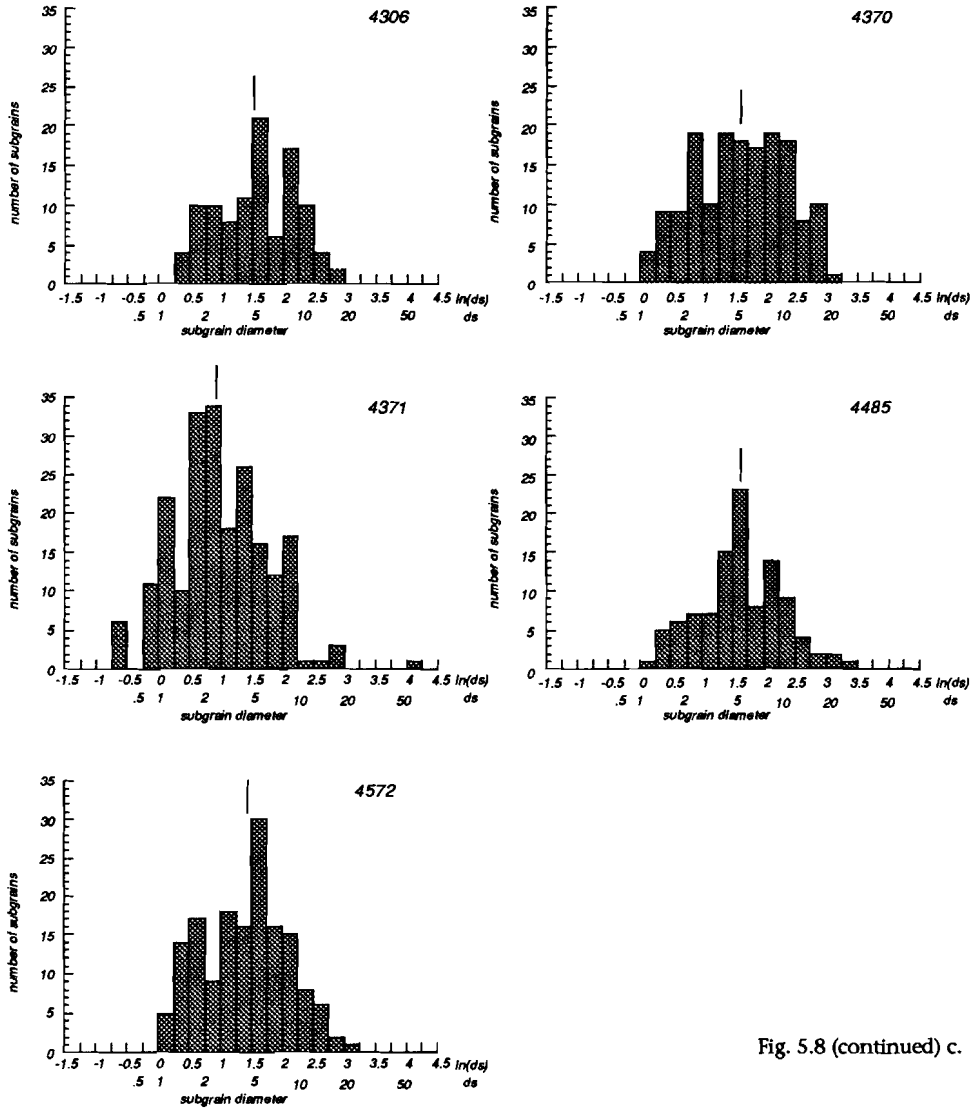

Fig. 5.8 (continued) c.

subgrain size palaeopiezometers derived below for Anita Bay and Åheim dunites will employ the median of the measured subgrain data.

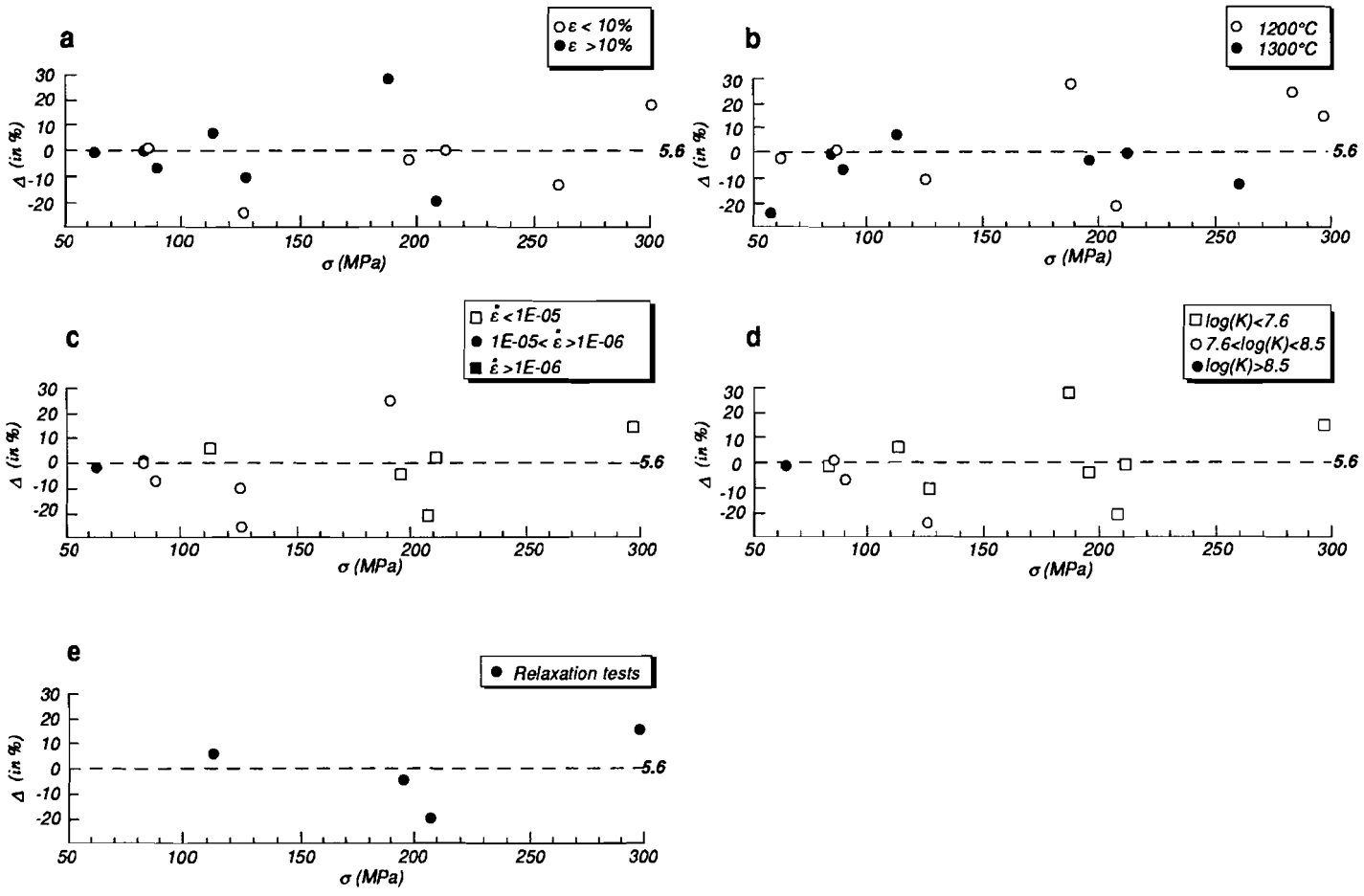
a
○ ε < 10%
● ε > 10%
b
○ 1200°C
● 1300°C
c
□ $\dot{\varepsilon}$ < 1E-05
● 1E-05 < $\dot{\varepsilon}$ > 1E-06
■ $\dot{\varepsilon}$ > 1E-06
d
□ log(K) < 7.6
○ 7.6 < log(K) < 8.5
● log(K) > 8.5
e
● Relaxation tests
Δ (in %)
σ (MPa)
5.6
-5.6

Subgrain size - stress relationships

The average olivine (100) subgrain spacing in "wet" Anita Bay and Åheim dunites deformed at constant strain-rate increases with decreasing flow stress (Fig. 5.6d). In strain-rate step tests, average subgrain sizes obey the same relationship with the *maximum* flow stresses achieved during the deformation experiment. It follows that in cases where the final flow stress is lower than the maximum flow stress, the subgrain spacings are related to the maximum rather than the final flow stresses (see also Ross et al. 1980). The quantitative subgrain size - flow stress relationships differ for Åheim and Anita Bay dunite, which indicates that the piezometers are strongly controlled by initial material properties. Following conventional notation in palaeopiezometry, the relationships between average subgrain spacing and stress for "wet" Anita Bay and Åheim dunite are, respectively:

"wet" Anita Bay: $d_s = 4.72^{+0.59}_{-0.53} * 10^{-05} (\sigma)^{-0.42 \pm .18}$ R=0.91 (5.6a)

"wet" Åheim: $d_s = 6.83^{+1.09}_{-0.94} * 10^{-05} (\sigma)^{-0.59 \pm .13}$ R=0.85 (5.6b)

where d_s is the subgrain size in m and σ the flow stress in MPa.

Effect of strain, strain-rate, temperature and water content

The effect of strain on the measured subgrain spacing is shown in Fig. 5.9a. Analogous to the analysis of recrystallized grain sizes, residuals are shown of the measured spacing relative to the empirically determined subgrain size - stress relationships (eqns. 5.6), labelled for different values of the experimental strain achieved during the pertinent experiment. The diagram clearly shows that there is no systematic distribution of the residuals distinguished on the basis of strain, indicating that the total strain accomplished during deformation does not systematically affect the piezometers.

The residuals of the measured subgrain spacings for different values of the experimental temperature is shown in Fig. 5.9b. The scatter of the residuals around the empirical subgrain size - stress relationship (eqns. 5.6) suggests that this relationship is temperature-independent for the range 1200-1300°C.

Careful inspection of Fig. 5.9c shows that there is no systematic distribution of the residuals of the measured subgrain size for different values of the experimental strain-rate i.e., for all values of strain-rate the data are scattered around the experimental subgrain size

◁ Fig. 5.9 (previous page): Plots showing the effect on the subgrain size piezometers of (a) strain, (b) temperature, (c) strain-rate, (d) the combined effect of temperature and strain-rate (see text), and (e) stress relaxation at the end of the deformation experiment. Data plotted as in Fig. 5.7.

- stress relationship (eqns. 5.6). This again suggests that strain-rate is not a controlling parameter on the sizes of the subgrains.

The combined effect of strain-rate and temperature can be investigated as outlined above for recrystallized *grain* sizes. Again a variable K is defined as temperature over strain-rate, where high values of K indicate that the specimen deformed at high temperatures and low strain-rates, whilst low values of K represent deformation at low temperatures and high strain-rates. Fig. 5.9d shows that the distribution of the residuals of the measured subgrains around the empirical subgrain size - stress relationship (eqns. 5.6) does not provide a basis for a possible combined effect of temperature and strain-rate on the piezometers of equations 5.6.

The average subgrain spacings in the "wet" deformed specimen are much smaller than the subgrain spacings in the two "dry" specimen (Fig. 5.6d), suggesting a major effect of water content on the average subgrain spacing for a given stress. This observation is in marked contrast with the recrystallized grain sizes in "wet" and "dry" material, which seem largely independent of water content. The present study indicates that water does not affect the size of the recrystallized grains, but that it does affect the spacing of the subgrains. This seems consistent with the hypothesis that water-weakening is an *intragranular*, rather than an *intergranular* process (Karato et al. 1986).

An alternative form for the subgrain size - stress relationship

Subgrain size piezometers used in the metallurgical and geological literature are commonly written as:

$$d_s = K\sigma^{-k} \tag{5.7}$$

or

$$\log d_s = \log K - k\log\sigma \tag{5.8}$$

where d_s is the subgrain size, K and k constants and σ the differential flow stress. The subgrain size vs. stress relationship in Anita Bay and Åheim dunites derived in this study (eqns. 5.6a and 5.6b) are presented in this form. The large variety in k and K for many different geological and metallurgical materials (reviews in Takeuchi and Argon 1976, Twiss 1986) have challenged many workers to derive empirical or theoretical subgrain size - stress relationships of a form other than those of eqns. 5.7 or 5.8, that accounts for all of the existing data. Such an alternative relationship can then be used to extrapolate laboratory data to natural conditions (e.g. Holt 1970, Young and Sherby 1973, Twiss 1977, Edward et al. 1982, Twiss 1986). Two of the most promising among these general piezometers will be evaluated below against the data from this study.

Edward et al. (1982) derived a theoretical relationship between subgrain size and stress and found a strong dependency of various material properties upon both k and K, such as the creep stress exponent in k and the creep diffusivity in K. Unfortunately, the temperature interval at which Chopra and Paterson (1981) performed their experiments (1200-1300°C for the specimen reported here) is too small to investigate the latter effect on K with the present subgrain data set. The dependency of k upon the stress creep exponent n as derived by Edward et al. (1982), i.e. $d_s^4 \propto \sigma^n$, is inconsistent with the experimental results found in this study The stress exponent for creep of Anita Bay and Åheim dunite was found to be 3.35 and 4.48 respectively (Chopra and Paterson 1981). Following Edward et al. (1982) the negative slope of the subgrain size - stress relationship in log-log space would thus be expected to be 0.84 and 1.12 for Anita Bay and Åheim dunite, respectively. The experimental values, however, are 0.59 for Anita Bay and 0.42 for Åheim dunite. It follows that the theoretical considerations of Edward et al. (1982) do not provide a particularly good basis to derive a generally applicable form of the subgrain size - stress relationship.

Twiss (1986) re-evaluated an extensive data set from metallurgy and geology relating flow stress and dislocation substructure for a number of metals and minerals, and noted that the sensitivity of dislocation density and subgrain spacing to the flow stress decreased with decreasing stress. He proposed the following empirical subgrain size - stress relationship (eqn. 13 of Twiss (1986)), written here in dimensional form:

$$\log d_s = \log K - k\log(\sigma + \sigma_0') \tag{5.9}$$

In this equation, σ_0' is an empirical constant called the stress constant. In a log-log plot of differential stress vs. subgrain diameter, the stress constant in eqn. 5.9 introduces non-linearity in this relationship. More specifically, the derivative to define the slope yields:

$$\frac{d\log(d_s)}{d\log(\sigma)} = -k(\sigma) / (\sigma + \sigma_0') \tag{5.10}$$

When $\sigma >> \sigma_0'$ the equation 5.9 approaches a linear relationship with a slope of -k and an intercept of logK. In case $\sigma = \sigma_0'$, the slope is -k/2, and assuming a theoretical value of n = 1-2, this yields a slope of 0.5-1 which is commonly observed in the range of experimental flow stresses. For $\sigma << \sigma_0'$ the slope approaches zero and the stress constant places a limit to the subgrain diameter at low stresses, which seems entirely realistic as any maximum subgrain dimension cannot be expected to exceed half the average grain diameter.

From the foregoing it follows that the introduction of a stress constant may explain the range of slopes (range of k) observed for subgrain diameter vs. stress relationships in log-log space. This range runs from ~0.3 to 2 (Twiss 1986, his Fig. 4), although a value of 4 has also been reported (cited in Edward et al. 1982). Additionally, a value of 2 is predicted from theoretical studies (Young and Sherby 1973). Any absolute value of the stress constant, however, will result in a decrease of the absolute value of k. Therefore, in search of a more generalized form of the subgrain size - stress relationship for Anita Bay and Åheim dunite it seems valid to set the value of k to 2. Fitting the present subgrain data, except for those deviating significantly from the overall trend (samples 4370 and 4519), into an equation of the form of eqn. 5.9 with k=2 yields the following empirical subgrain size - stress relationships (Fig. 5.6d):

Anita Bay dunite: $d_s = 0.38 \pm 0.09 * (\sigma + 191 \pm 32)^{-2}$ R=0.93 (5.11a)

Åheim dunite: $d_s = 1.75 \pm 0.34 * (\sigma + 392 \pm 55)^{-2}$ R=0.94 (5.11b)

Note that for both dunites the calculated values of K and σ_0' are distinctly different.

Variations in σ_0' might reflect either a flow law dependency (Edward et al. 1982) or, more specifically, a grain size dependency. De Bresser (1991) derived an extended version of the Twiss (1986) dislocation density piezometer, and introduced a grain size dependence of the stress constant arising from strain incompatibility problems at grain boundaries producing local geometrically necessary dislocations (e.g. Ashby and Verrall 1978). For a material with a given grain size the grain-size dependent stress constant limits the dislocation density at flow stresses approaching zero. A similar factor can be envisaged for a subgrain size piezometer, i.e., a stress constant could put an upper limit to the subgrain spacing at low values of the flow stress.

Variations in K may be even more difficult to explain, but can be expected to lie in the field of thermally activated terms that define the rate-controlling processes for dislocation motion between and in subgrain boundaries (Edward et al. 1982). This remains to be established, however, by experimentation specifically designed to cover a large temperature interval.

5.6 Grain size and subgrain size in stress-relaxation experiments

Stress relaxation tests

The termination of a deformation event and the consequent "freezing-in", under natural conditions, of the steady-state microstructures is likely to involve transients in strain-rate, stress, temperature and pressure (White 1979a, Knipe 1989). The effects of such transients on material properties form an essential part in the extrapolation of experimental data to natural conditions. This is particularly evident for piezometry on natural rocks, because post-tectonic annealing and grain growth may reset recrystallized grain sizes and subgrain sizes such that they do no longer represent the steady-state deformation conditions. Annealing recrystallization and stress-relaxation tests can be used to investigate and quantify transient effects on microstructural and rheological parameters (e.g., Rutter et al. 1978).

Annealing recrystallization experiments are designed to study the evolution of the deformation microstructures when steady-state deformation responsible for their development is followed by stress-relaxation of the specimen during which no further strain is imposed on the specimen. Temperatures are kept high during annealing. At the onset of annealing, the balance between grain size reduction processes and grain growth processes that existed during steady-state deformation is suddenly disturbed in favour of grain growth and as a consequence, the grains will grow reducing their internally- and surface-stored strain energies. It is clear, however, that a sudden stress-release in a typical annealing recrystallization experiment cannot be a good approximation of an end-member type of a geological deformation as stresses will probably decay in natural deformation via a waning stage rather than terminate abruptly.

Stress-relaxation tests are similar to annealing tests with the exception that a transient strain-rate and stress is imposed on the specimen until it is relaxed. Stress relaxation tests are designed such that the elastic strain in the specimen is converted into plastic strain during stress- and strain-rate-decay. In the ideal case, the total length of the specimen is held constant. In practise, however, testing machine designs rarely permit the specimen length to be held truly constant. Instead, it is necessary in most cases that the total length of the specimen plus part of the testing equipment is kept constant rather than the length of the specimen. It follows that elastic rebounds of parts of the testing device must be dissipated through permanent deformation in the sample. This is illustrated in the equation below which relates the decay in strain-rate during the relaxation to the decay

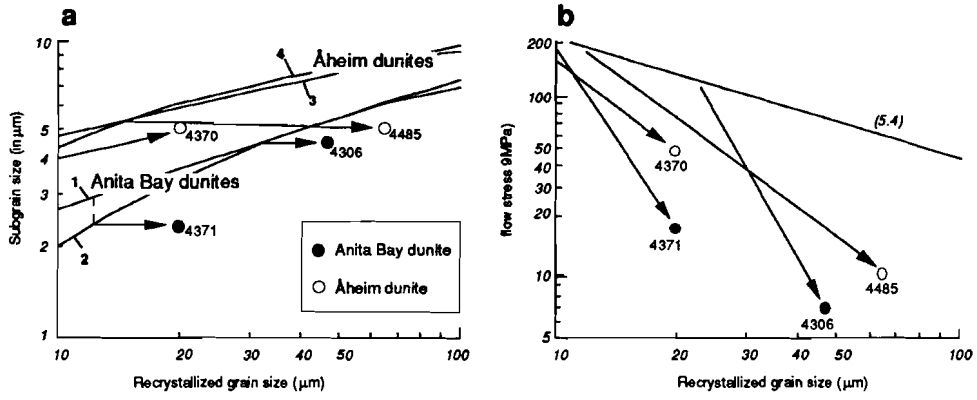

Fig. 5.10: (a) Microstructure equilibrium diagram showing the effect of stress relaxation and annealing on the stability of recrystallized grain size and subgrain size. Curve 1 and 3: Dg (eqn. 5.4) = ds (eqn. 5.6), for Anita Bay dunite and Åheim dunite, respectively, curve 2 and 4: Dg (eqn. 5.4) = ds (eqn. 5.11) for Anita Bay dunite and Åheim dunite, respectively. Note a marked shift of the data in a positive x-direction towards larger recrystallized grain sizes at approximately constant subgrain size. (b) recrystallized grain size in stress relaxation experiments showing deviation of the recrystallized grain size from the established piezometric relationships (eqn. 5.4).

in flow stress:

$$\dot{\varepsilon} = \frac{-(k_s + k_m l_m)d\sigma_a}{dt} \tag{5.12}$$

where $\dot{\varepsilon}$ is the strain-rate, k_m and k_s the compliances of the sample and the machine between the controlled points respectively, and l_m is chosen so that $k_m l_m$ together with k_s relates the specimen elastic strain to the applied load (Rutter et al. 1978). This relationship illustrates how the deformation machine properties can be used to study transient decays in stress, strain-rate etc.

Such relaxation tests may thus represent a much better approximation to the terminal stages of a natural deformation than static annealing. Stress relaxation data have been frequently used to study the rheological properties of the investigated material (e.g. Chopra and Paterson 1981) but may also contain valuable information on recovery processes, such as annealing recrystallization and grain growth at laboratory time-scales. As mentioned before, the processes and mechanisms operating during stress-relaxation could also apply to natural conditions at depth. The relaxation tests may therefore provide information on recovery rates at decreasing stress and strain-rate during the "freezing-in" stage of a natural or experimental deformation event. In order to place constraints on the

relative stability, during the terminal stages of deformation, of the deformation microstructures and of grain- and subgrain-sizes in particular, recrystallized grain sizes and subgrain sizes in one annealed and four relaxed specimen are evaluated below. Additional consequences of stress-relaxation experiments on the microstructural properties of a polycrystalline material are discussed in Chapter 6.

Recrystallized grain size and subgrain size during stress relaxation

Fig. 5.10a shows the effects of stress relaxation and annealing on the microstructure in the specimen, illustrated in recrystallized grain size - subgrain size space. The basis for such plots are outlined in more detail in the next Chapter. Four reference curves are shown which represent microstructural equilibrium between recrystallized grain and subgrain size. Two of these reference curves represent Anita Bay dunite data (curves 1,2) the other two represent Åheim dunite data (curves 3,4). The curves have been calculated by combining the recrystallized grain size piezometer (eqn. 5.4) and the subgrain piezometers (eqns. 5.6 and eqns. 5.11) for Anita Bay and Åheim dunites. The reference curves thus represent combinations of recrystallized grain size and subgrain size in *equilibrium* during steady-state for any stress in the range investigated.

Both annealing and stress relaxation following steady state creep can be seen to cause a considerable shift from the equilibrium point on the pertinent reference curve towards larger recrystallized grain sizes at more or less stable subgrain spacings. Therefore, the effect of stress relaxation and annealing recrystallization is to re-equilibrate the recrystallized grain size upon changes of the flow stress, but to maintain the subgrain dimensions set at steady state flow. A major implication for palaeopiezometric studies is that olivine subgrain sizes could have a much better memory for the (maximum) steady-state flow stress than the recrystallized grain size. This observation in olivine aggregates is at variance with what is generally inferred from observations on natural quartz rocks (e.g. Knipe 1989, his Fig. 11). Annealing experiments on olivine, however, show that provided enough time is allowed, subgrain spacings will also reset (Ricoult 1979), but at much slower rates than recrystallized grain sizes. One may expect, therefore, that only prolonged annealing and complete migration recrystallization will obliterate subgrain dimensions previously set at the steady-state flow stress.

Grain growth kinetics

The stress-relaxed and annealed samples show recrystallized domains with microstructures characterized by largely unstrained grains and straight grain boundaries. These

sample	initial grain size (μm) (1)	measured recrystallized grain size (μm)	T (°C)	time of anneal or relaxation (s)	velocity grain boundary migration (μm/s)
Annealing experiment					
6147	11.6	16	1200	1908	1.15E-03
Relaxation experiments					
4485	13.4	65	1300	10188	2.53E-03
4371	7.7	20	1200	5580	1.10E-03
4306	27.9	47	1300	4968	1.92E-03
4370	12.4	20	1200	6984	0.54E-03

1: Calculated from eqn. 5.4

Table 5.3: Grain growth calculations for the relaxed specimen.

microstructures clearly suggest considerable grain growth. However, the amount of grain growth at low stresses during stress relaxation failed to balance the decreasing stresses because the grain size data do not plot on the piezometric relationship (eqn. 5.4) extrapolated to low flow stresses (Fig. 5.10b). It follows that grain growth ceased at some stage during relaxation, and that the average grain size reached a fixed value which does no longer reflect ambient stress-values. Table 5.3 summarizes the grain growth- or grain-boundary migration rates during stress relaxation and annealing of the "wet" dunites, calculated under the assumption that, prior to annealing or relaxation, the recrystallized grain size remained in equilibrium with the steady-state flow stress according to piezometric equation 5.4. It is clear that grain boundary migration velocities are similar during annealing and relaxation, provided that the temperature and final stress values prior to relaxation are similar, and that during stress-relaxation they are too low to keep the grain growth in equilibrium with ambient decaying stresses.

It is noted, that the estimated grain boundary velocity rates in "wet" Anita Bay and Åheim dunites (0.54 - 2.53 $*10^{-03}$ μm/s at 1200-1300°C) are somewhat faster than those calculated by Toriumi (1982) for dry olivine (0.07 - 1.67 $*10^{-03}$ μm/s at 1240-1500°C). It is concluded, therefore, that grain boundary migration rates in "wet" olivine are higher than those in "dry" olivine (see also Karato 1989). The notion that grain growth is a prominent feature in stress-relaxation experiments discourages the use of olivine recrystallized grain size piezometers in natural systems. Instead, aside the uncertainties involved in extrapolation of laboratory data to natural conditions, subgrain-size piezometers appear to be less sensitive to stress relaxation and are likely to yield better estimates of ambient flow stresses during steady-state deformation in nature.

CHAPTER 6

Rheological significance of shear localization in the Ronda peridotite.

6.1 Introduction

The mechanical behaviour of the lithosphere depends primarily on the depth-dependent physical and chemical environment (e.g. Kuznir and Park 1984, Ranalli and Murphy 1987, Carter and Tsenn 1987). This physical and chemical environment at depth may be extremely heterogeneous as indicated by significant strain localization within ductile shear zones that occurs in upper and middle crustal rock units (e.g. White 1979b, White et al. 1980, Ord and Christie 1984, Rutter and Brodie 1988). Structural studies in peridotite massifs and mantle xenoliths provide information on the degree of shear localization in the upper mantle, and on the significance of shear localization to the bulk mechanical properties of the lithosphere (Rutter and Brodie 1988, Handy 1989, Drury et al. 1991). The latter aspect forms an important objective of this study, which motivates an analysis of the mechanical properties of the zones of localized deformation recognized in the fragment of the W Mediterranean upper mantle now represented by the Ronda peridotite (Chapter 3).

The principal tool used below will be palaeopiezometry, a technique which has been applied as early as 1970 by Raleigh and Kirby. The present study will employ the newly obtained "hydrous" olivine recrystallized grain size and subgrain size palaeopiezometers derived in the previous chapter. The palaeostress estimates obtained from the two

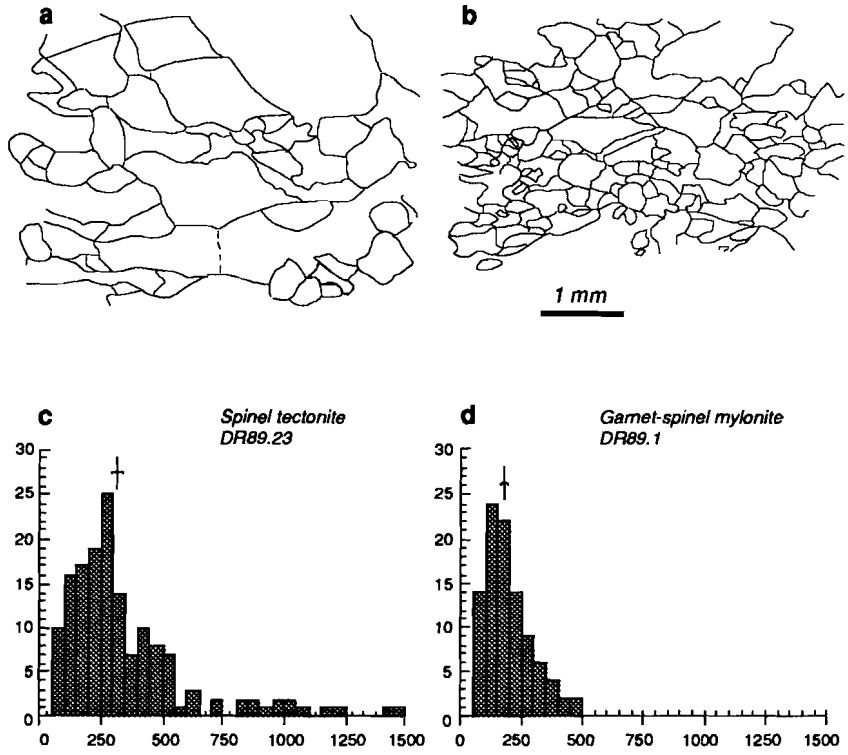

Fig. 6.1: (a) Line-drawing of spinel tectonite microstructure. (b) as (a), for a garnet-spinel mylonite, note increased recrystallized fraction relative to [a]. (c) Typical frequency histogram of maximum grain diameters measured from line-drawings of a spinel tectonite. Note the tail towards large grain diameters, ascribed to the contribution of large palaeoblasts. (d) As (c), for a garnet-spinel mylonite. Note the smaller tail towards large grain diameters presumably due to pervasive recrystallization.

piezometers will be evaluated against each other to place some constraints on the mechanical *evolution* of the zones of localized deformation identified in the Ronda massif.

6.2 Sample selection and microstructure quantification

Setting and microstructural aspects of selected samples

For the purpose of a palaeostress analysis, recrystallized grain sizes and subgrain sizes have been measured in 14 deformed peridotites. Their structural position, microstructures and

olivine lattice preferred orientation (LPO) patterns have been described in Chapter 3, their ambient P-T conditions in Chapter 4. Below I summarize essential microstructural information of the samples studied, and proceed with the results of the palaeopiezometric analysis.

The accuracy of palaeostress studies partly depends on careful sample selection and on a consistent application of experimental techniques to obtain the microstructural parameters. Therefore, I will first focus in some detail on the structural and microstructural aspects of the selected samples. The sample localities are shown in App. A2

In order to minimize obliteration of microstructural properties, relatively fresh specimen have been selected with the lowest possible degree of late-stage serpentinization. Three spinel tectonites have been chosen to study any effects of a variable intensity of the tectonite foliation. Sample DR89.23 shows a low intensity of the foliation, whilst sample DR89.65 shows the most intense foliation development. The average recrystallized fraction in the spinel tectonites is estimated to be less than 30% (Fig. 6.1a). Olivine LPO patterns are of the type [100]{0kl}, with an increasing predominance of [100](010) with increasing intensity of the foliation. All samples contain amphibole as small grains at the edges of the pyroxenes, suggesting that the tectonites developed under hydrous conditions.

All three garnet-spinel mylonites selected for this study are from the 500 m wide mylonite zone in the NW periphery of the massif. They show no obvious structural or microstructural variations, and are almost entirely recrystallized (Fig. 6.1b). Olivine LPO patterns are of the type [100](010) with well defined point maxima distributions for all the crystallographic axes. Hydrous conditions during their development are inferred from the frequent occurrence of small amphibole grains replacing pyroxene grain boundaries. Both spinel tectonites and garnet-spinel mylonites deformed at relative low temperatures in the range 850-900°C (Chapter 4).

As outlined in Chapter 3 and 4, the granular peridotites of the Ronda massif are inferred to result from pervasive high-temperature annealing of a deformed protolith. In order to test this inferred origin, four granular peridotite samples have been included in this palaeostress study. The samples have been selected principally on the basis of the lowest possible degree of serpentinization. Some relict deformation structures such as spinel trails could be recognized in the outcrop yielding sample DR89.88. All other granular peridotites selected are typical coarse-grained granular peridotites in the sense that annealing recrystallization and grain growth has removed all remnants of the earlier deformation (see also Chapter 3). No evidence for magmatic processes such as described in Chapter 3 have been detected in the outcrops from which the samples were taken.

Finally, four plagioclase tectonites have been selected, two of them from the early S-vergent tectonites (DR89.42, DR91.31) and two from the late-stage N/E-vergent tectonites (DR89.79, DR91.29). Three samples have been collected along the road section Ronda - San Pedro de Alcàntara in the eastern part of the Ronda massif, and are not shown on the map of App. A2. The reason for this choice of samples localities is the extensive serpentinization of the plagioclase peridotites from the western part of the massif such that the microstructural details required for this palaeostress analysis have been mostly obliterated. All plagioclase tectonite samples show a considerable recrystallized fraction (~20-30%). Olivine LPO patterns are of the type [100]{0kl} (Chapter 3). Amphiboles replacing pyroxene at grain boundaries suggest hydrous conditions during their development.

Measurement techniques

The techniques used to quantify the microstructures in the experimentally (Chapter 5) and naturally deformed peridotites (this chapter) are essentially the same. One exception, however, had to be made due to the different fractions of recrystallization. Recrystallization in the experimentally deformed samples is restricted to grain boundary areas and triple junction contacts (see. Fig. 5.3), and the recrystallized fraction is low (<20%). This is mainly due to the limited strains that can be achieved in a gas-medium deformation apparatus. As a consequence, the distinction between olivine neoblasts and palaeoblast was always obvious and the neoblast size could be accurately determined. The recrystallized fraction in the natural peridotite samples mostly exceeds 20% and may be close to 100% for the garnet-spinel mylonites, presumably reflecting the larger strains accomplished during deformation. As a result, the distribution of neoblasts is more homogeneous and not spatially related to palaeoblast grain boundaries or triple junctions. The distinction between intensely strained palaeoblasts and newly recrystallized neoblasts is therefore not always clear, yet needs to be accurately assessed before applying recrystallized grain size palaeopiezometry.

The olivine neoblast grain size in the naturally deformed samples has therefore been determined following the procedure outlined below, which differs slightly from the procedure followed in the previous chapter. For each sample, detailed line-drawings of the microstructure have been prepared from colour photographs taken at six different flat stage orientations with respect to the polarizing directions of the optical microscope. The grain diameter of *all* grains, i.e. neoblasts and the larger palaeoblasts, have been measured from the line-drawings and plotted in a frequency histogram such as shown in Fig. 6.1c+d. For all the samples analyzed the shape of the frequency curve appeared to be positively

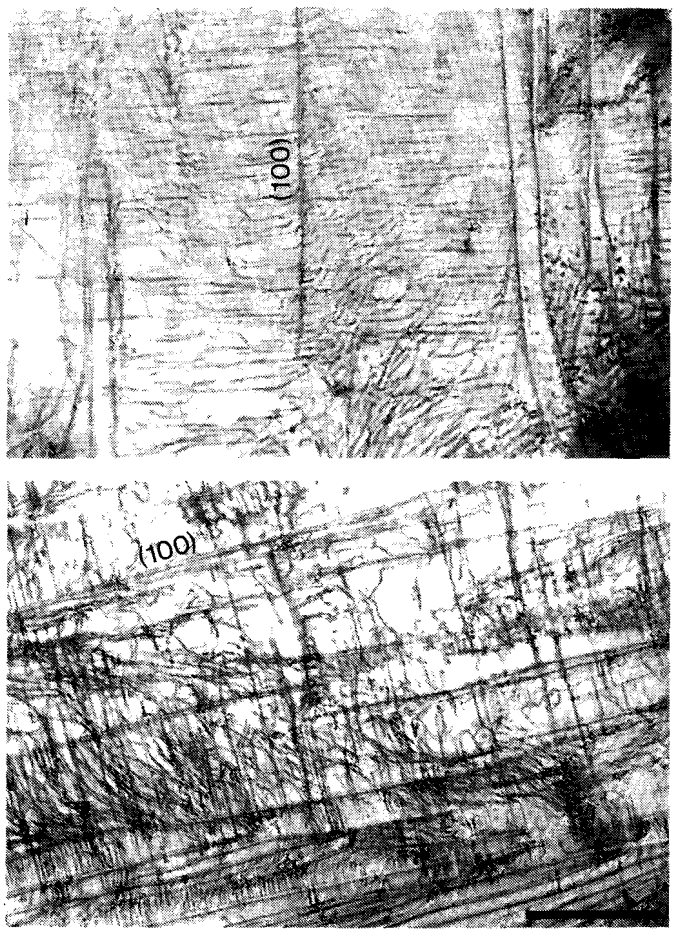

Fig. 6.2: Photomicrographs of a naturally deformed peridotite (DR89.79) showing decorated olivine (100) subgrain wall and dislocations. The trace of olivine (100) is indicated. Scale bar for both photographs 3 μm.

skewed, i.e., showed a long tail from the geometrical mean (median) towards large grain sizes. This tail towards large grain sizes is attributed to the contribution of the palaeoblasts to the measured grain population. The geometrical mean of the frequency histograms has therefore been taken to calculate the average neoblast grain diameter. As a correction factor of 1.2 is commonly used in the determination of grain size dimensions (e.g. Karato et al. 1982, 1986), obtained values have been multiplied with this factor to obtain average neoblast recrystallized grain sizes. The above procedure may introduce analytical errors in the palaeostress estimates, but these errors can be expected to be small compared to many other uncertainties discussed below.

The olivine (100) subgrain wall spacings have been measured following the procedures

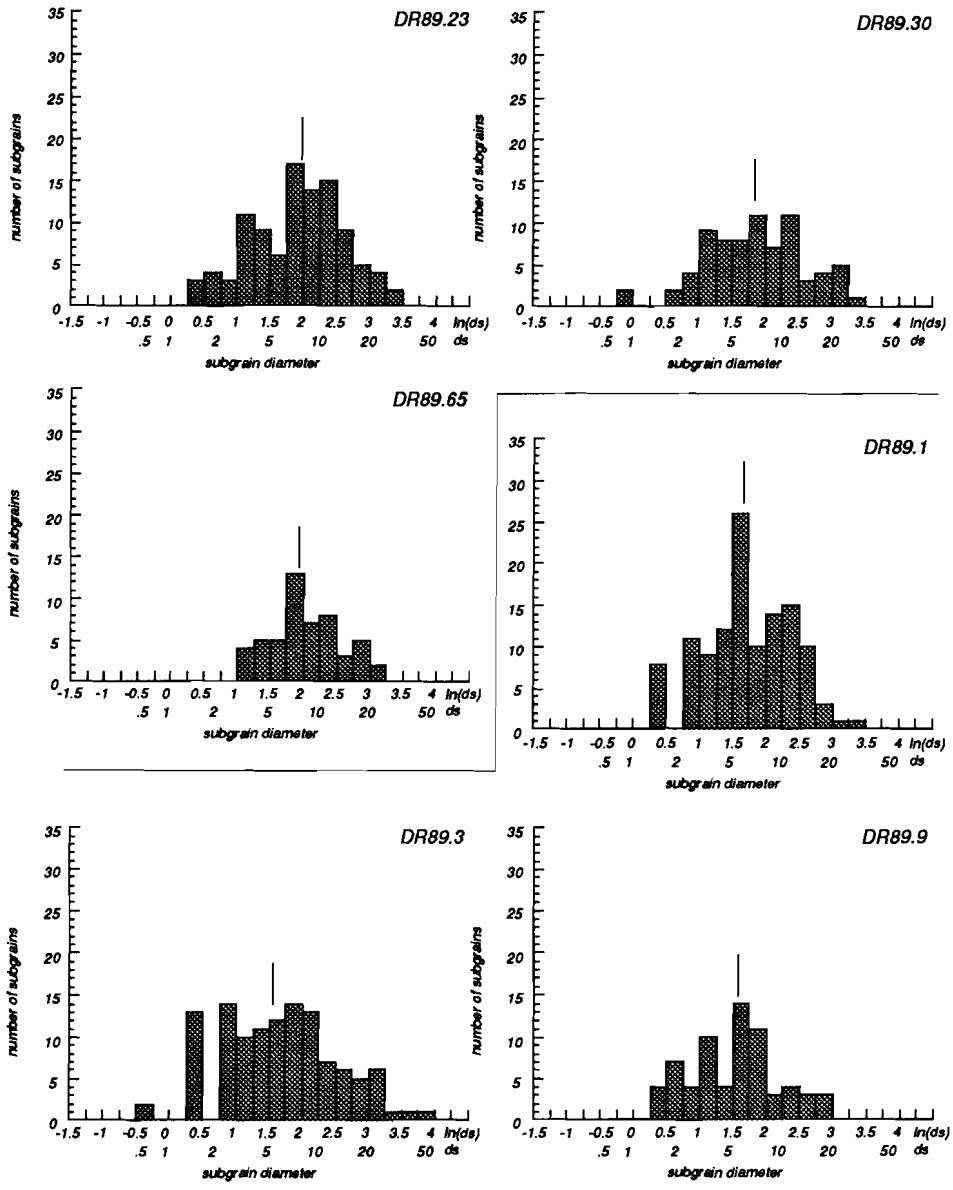

Fig. 6.3: Frequency histograms of olivine (100) subgrain wall spacings (ds) in (a) spinel tectonites and garnet-spinel mylonites, (b) granular peridotites, and (c) plagioclase tectonites. Note in sample DR89.3 the resolution towards small spacings (~1 μm) has probably been reached, which could have induced errors in the determination of the median subgrain diameter.

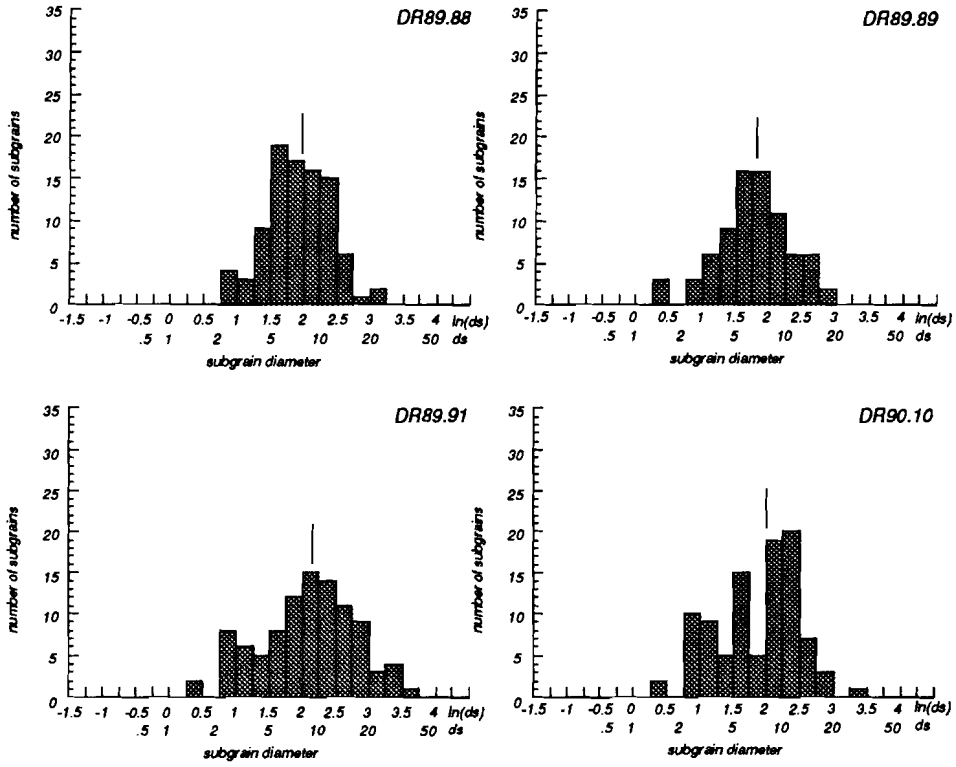

Fig. 6.3 (continued) b.

outlined in the preceding chapter, i.e., on decorated specimen (Kohlstedt et al. 1976). The decoration time, however, was increased to 30 min. at 900°C. Due to late stage serpentinization affecting all samples, only a small fraction of the recrystallized grains has preserved their dislocation substructure. Subgrain characteristics are therefore confined to the olivine palaeoblasts whose average size is listed in Table 6.1. Fig. 6.2 shows some decorated subgrains and dislocations in one of the natural peridotites studied here (DR89.79). The olivine (100) subgrain spacings measured in the Ronda peridotite samples concur with the subgrain data from experimentally deformed Anita Bay and Åheim dunites (Chapter 5) and naturally deformed mantle xenoliths from Eastern China (Jin and Green 1989) in that subgrain spacings show a lognormal distribution (shown graphically in Fig. 6. 3). This supports application of the subgrain size piezometers derived in the previous Chapter, as these are calibrated for the median values of log-normal distributed subgrain populations.

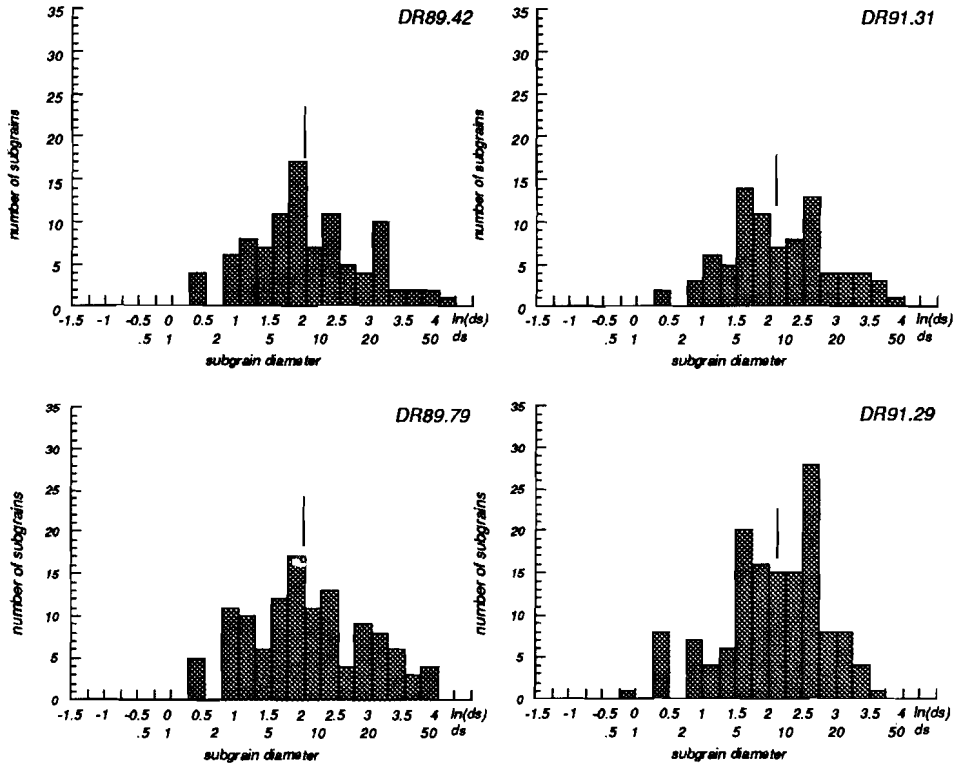

Fig. 6.3 (continued) c.

6.3 Results

The results of the grain size and subgrain size measurements as outlined above are listed in Table 6.1. The mean subgrain spacing is shown as well to allow application of previously published subgrain size piezometers if desired. The following recrystallized grain size and subgrain size characteristics seem critical for the mechanical history of the deformational structures in which they occur.

1: The smallest average olivine (100) spacings were obtained in spinel tectonites and garnet-spinel mylonites with the smallest recrystallized grain sizes. This suggests that both microstructural properties were controlled by the differential flow stress during deformation. The granular peridotites and plagioclase peridotites do not show such a distinct correlation between recrystallized grain size and subgrain size data.

samples	Recrystallized grain size			Subgrain size							
	Dg (μm)	calculated error	N	ds (mean, in μm)	2σ	ds (median, in μm)	2σ	skewness	Kurtosis	N	D* (μm)
Spinel tectonites											
DR89.23	375	23	121	8.55	5.96	7.04	2.03	-0.17	-0.56	102	872
DR89.30	247	23	154	8.38	6.37	6.31	2.11	-0.09	-0.23	75	1037
DR89.65	277	18	100	8.77	5.06	6.78	1.71	0.30	-0.72	52	709
Garnet-spinel mylonites											
DR89.1	208	10	97	6.92	4.86	5.39	1.96	-0.02	-0.54	120	343
DR89.3	171	7	138	7.59	7.61	4.61	2.36	0.21	-0.46	110	318
DR89.9	180	6	121	5.71	4.16	4.85	1.92	0.22	-0.42	116	240
granular peridotites											
DR89.88	3180	---	25	7.53	4.06	6.82	1.66	0.06	-0.30	92	---
DR89.89	3580	---	32	6.62	3.54	6.06	1.73	-0.28	-0.02	78	---
DR89.91	4220	---	27	10.21	7.32	8.47	2.08	-0.21	-0.53	98	---
DR90.10	3740	---	21	7.69	4.56	7.58	1.90	-0.33	-0.76	96	---
plagioclase tectonites											
DR89.42	1173	72	58	11.15	10.76	7.14	2.31	0.25	-0.45	97	872
DR91.31	609	46	63	11.44	9.58	8.20	2.12	0.16	-0.37	85	654
DR89.79	---	---	---	11.43	10.65	7.14	2.39	0.16	-0.75	119	1200
DR91.29	380	19	115	10.16	6.71	8.20	2.10	0.16	0.02	141	960

Key: Dg = recrystallized grain size, Ds = subgrain size, D* = palaeoblast size, N = number of measurements

Table 6.1: Recrystallized grain size and subgrain size data of analyzed samples. N denotes number of measurements.

samples	Recrystallized grain size (1) (MPa)	range	(2) (MPa)	range	Subgrain size (3) (MPa)	range	(4) (MPa)	range	(5) (MPa)	range	(6) (MPa)	range	(7) (MPa)	range
Spinel tectonites														
DR89.23	16	11-25	14	8-27	47	19-193	93	20-∞	41	10-72	108	54-158	183	52-966
DR89.30	17	12-27	15	9-28	57	22-245	120	23-∞	54	22-86	136	80-188	188	54-1001
DR89.65	20	14-32	18	10-35	50	20-209	101	21-∞	46	14-77	117	63-168	176	51-924
Garnet-spinel mylonites														
DR89.1	25	17-40	23	13-47	74	28-346	176	31-∞	75	40-107	179	121-233	250	69-1400
DR89.3	29	19-46	27	15-56	96	34-484	254	40-∞	96	61-130	225	165-281	218	61-1191
DR89.9	28	19-44	26	14-54	88	32-433	225	36-∞	89	54-123	210	151-265	334	88-1962
granular peridotites														
DR89.88	3	<10	2	<10	50	20-207	100	21-∞	45	13-76	116	61-167	221	62-1207
DR89.89	3	<10	2	<10	61	24-267	135	25-∞	59	26-91	146	91-199	267	73-1514
DR89.91	3	<10	2	<10	34	15-129	60	14-∞	21	0-50	64	12-112	140	42-708
DR90.10	3	<10	2	<10	42	17-164	78	17-∞	33	2-63	89	37-139	214	60-1164
plagioclase tectonites														
DR89.42	7	5-10	5	3-9	46	19-187	90	19-∞	40	8-70	104	50-155	123	37-606
DR91.31	11	8-17	9	6-17	36	15-138	65	15-∞	24	0-54	71	19-120	118	36-580
DR89.79	16	11-24	14	8-27	46	19-187	90	19-∞	40	8-70	104	50-155	118	36-581
DR91.29	16	11-24	14	8-27	32	14-119	55	13-∞	24	0-54	71	19-120	141	42-714

1: Recrystallized grain size piezometer, eqn. 5.4 this thesis, 2: recrystallized grain size piezometer, Karato et al. 1980,
3: Subgrain size piezometer, Anita Bay dunites, eqn. 5.6a this thesis , 4: subgrain size piezometer, Åheim dunite, eqn. 5.6b this thesis,
5: Subgrain size piezometer, Anita Bay dunites, eqn. 5.11a this thesis, 6: subgrain size piezometer, Åheim dunite, eqn. 5.11b this thesis
7: Subgrain size piezometer, Karato et al. 1980.

Table 6.2: Calculated palaeostresses based on the microstructural data in Table 6.1

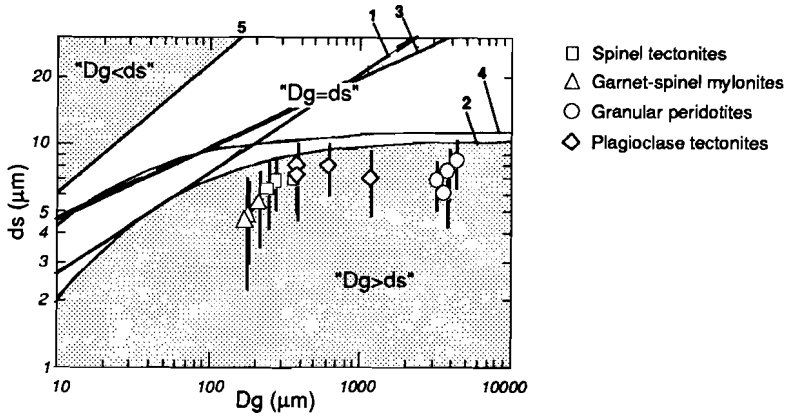

Fig. 6.4 Microstructure equilibrium diagram for the deformational structures in the Ronda peridotite. Note the systematic discrepancy between the size of subgrains and recrystallized grains. Key to the reference curves: 1 and 3: Dg (eqn. 5.4 this thesis) = ds (eqn. 5.6 this thesis) for Anita Bay dunite and Åheim dunite, respectively. 2 and 4: Dg (eqn. 5.4 this thesis) = ds (eqn. 5.11 this thesis) for Anita Bay dunite and Åheim dunite, respectively. 5: Dg = ds (data of Karato et al. 1980)

2: The spinel tectonites do not show any clear correlation between recrystallized grain size or subgrain size and the *intensity* of the foliation. This suggests that the intensity of the foliation in the tectonite domain correlates with the fraction of recrystallized material rather than stress variations across the spinel tectonite domain.

3: The granular peridotites show grain sizes in the range 3-4 mm, i.e. one order of magnitude larger than the spinel tectonites and garnet-spinel mylonites. Some grains, however, have preserved subgrain spacings in the range 6.06-8.47 μm, i.e., subgrain spacings in the range of those measured in the spinel tectonites (Table 6.1). It is noted again that the granular peridotites are inferred to result from extensive high temperature annealing of earlier spinel tectonites. The observed subgrain spacings in the granular peridotites, of the same dimensions as those in the spinel tectonites, are consistent with this interpretation.

4: The plagioclase tectonites have preserved recrystallized grain sizes in the range 1173 to 380 μm. The early "top to the north" plagioclase tectonites show the larger grain sizes. The subgrain spacings, however, show no significant differences between the two types of plagioclase tectonites.

The above grain size and subgrain size data will be checked for internal consistency below employing microstructural equilibrium diagrams. The palaeostress estimates based on the measured grain sizes and subgrain sizes are listed in Table 6.2

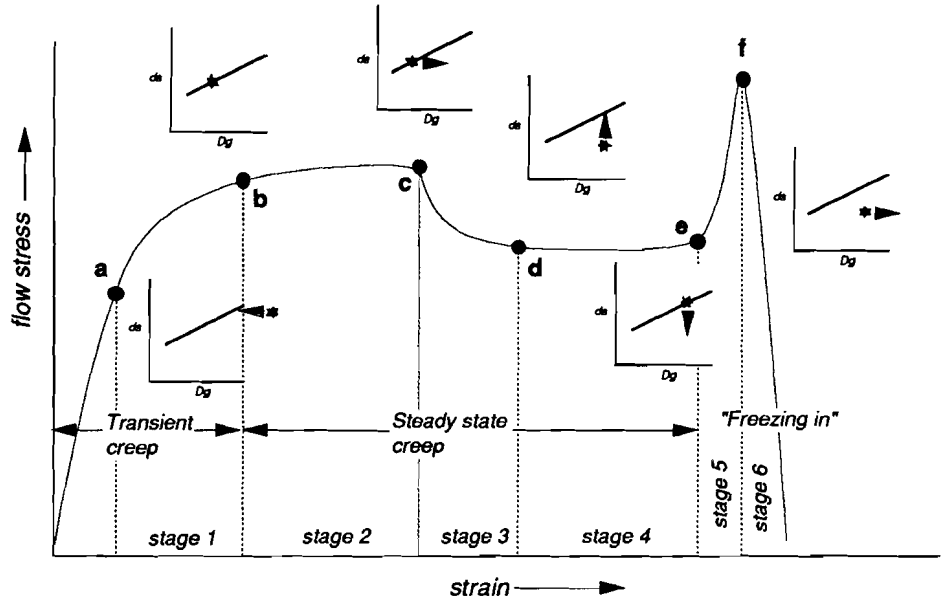

Fig. 6.5 Stress-strain curve of a typical hypothetical deformation cycle with the microstructural response to changing deformation conditions illustrated in equilibrium diagrams. For further explanation see text.

Microstructure equilibrium diagrams

It is generally assumed that flow stresses derived from recrystallized grain size and subgrain size piezometers yield consistent results if both grains and subgrains formed during one and the same syn-tectonic deformation event. If the flow stresses from both piezometers are inconsistent, however, more than one stress or temperature pulse may be inferred (e.g. Ord and Christie 1984, Knipe 1989) and the *mechanical history* of a deformed rock may be addressed. Any (in)consistency between recrystallized grain size data and subgrain size data in palaeostress analyses is conveniently obtained from microstructural equilibrium diagrams such as shown in Fig. 6.4. Reference curves in equilibrium diagrams represent arrays of recrystallized grain size and subgrain size values developed in a dynamically stable microstructure for a certain stress range. They are obtained by combining internally consistent recrystallized grain size and subgrain size piezometers such as those presented in the previous chapter or the data of Karato et al. (1980). Equilibrium diagrams have first been employed by Nicolas (1978), other examples of the use of equilibrium diagrams can be found in Toriumi (1979), Norton (1982), Ord and Christie (1984) and Matsumoto and

Toriumi (1989).

The grain size and subgrain size data from the studied samples are plotted in the equilibrium diagram of Fig. 6.4. Five reference curves have been drawn, obtained by combining the recrystallized grain size and subgrain size piezometers for Anita Bay dunites and Åheim dunites (Chapter 5) and dynamically recrystallized olivine single crystals (Karato et al. 1980). It is immediately obvious that the subgrain sizes and recrystallized grain sizes were not formed during the same recrystallization event because, in all cases, they would be expected to plot in the area enclosed by the reference curves. Instead, the subgrain size in all cases is found to be to smaller than expected for dynamic equilibrium with the recrystallized grain size. Below I will investigate possible explanations for this apparent discrepancy for the different deformational structures, using previously obtained data such as *deformation history* (Chapter 3), the ambient *temperature conditions* allied to their development (Chapter 4) and the *stability of the microstructures* under investigation (Chapter 5).

6.4 Discussion

A hypothetical deformation cycle

Fig. 6.5 shows a hypothetical multistage deformation cycle as envisaged for a tectonic event in the Earth's upper mantle, illustrated in stress-strain space. This cycle comprises six different stages: (a) transient creep, (b) steady-state creep, (c) a syn-tectonic stress relaxation, (d) renewed steady-state creep, (e) a "low temperature - high stress" event during uplift, and (f) post-tectonic stress relaxation. For each stage in this hypothetical multistage deformation event it will be investigated whether microstructural equilibrium can be achieved and, if not, what characteristic microstructural discrepancies will develop.

Consider deformation during transient creep prior to steady-state flow (stage 1; Fig. 6.5). Equilibration of subgrain sizes upon flow stress is inferred to be much faster than equilibration of recrystallized grain size (e.g. Knipe 1989), i.e., at much lower strains. Thus at point A, the subgrain size may have equilibrated with ambient flow stress values whilst the recrystallized grain size has not yet reached a dynamically stable value. The point defined by the current values of recrystallized grain size and subgrain size at A plots below the reference curve in the equilibrium diagram, and will tend to shift in a negative x-direction towards the reference curve. It follows that during stage 1 there will be

microstructural disequilibrium arising from the *insufficient strain* to achieve microstructural equilibrium.

During stage 2, steady-state flow is achieved and microstructural equilibrium exists between subgrain size and recrystallized grain size.

Point C on the stress-strain curve marks the onset of strain softening, hence strain localization, that may occur during high strain deformation as demonstrated experimentally by White et al. (1985). In mechanical terms, strain softening can be expressed as a stress decrease at constant strain-rate or a strain-rate increase at constant stress or, more likely, a combination of both. Stress gradients, possibly reflected by changing values of the recrystallized grain size and subgrain size, can be attributed to either preserved localized stress gradients developed during propagation of the shear zone, or to stress-relaxation towards regional values after strain localization (White et. al. 1980). Strain-rate step experiments of Ross et al. (1980) and Chopra and Paterson (1981, 1984) have shown that a strain-rate step is accompanied by a significant stress drop, but also that the recrystallized grain size rather rapidly re-equilibrates upon the newly achieved lower flow stress, whilst the subgrain size previously equilibrated at higher flow stress values may remain unchanged. Similar observations have been made on rocksalt (Friedman et al. 1981, Carter et al. 1982). As a consequence, the point in the equilibrium diagram defining the current values of recrystallized grain size and subgrain size at any stage between C and D plots below the reference curve, as it shifts in a positive x-direction due to syn-tectonic *stress relaxation.*

At stage 4, renewed steady-state flow has been achieved. Only complete recrystallization during this stage, involving grain boundary migration to completely obliterate any microstructural relicts in equilibrium with previously existing stress conditions, may reset the subgrain spacing to new values in equilibrium with the newly achieved flow stress in the newly recrystallized grains. A dynamically stable subgrain size equilibrated upon the new flow stress will be achieved only in the newly recrystallized grains. From D onwards, the point in the equilibrium diagram defined by the current values of recrystallized grain size and subgrain size will thus shift towards the reference curve in a positive y-direction as a function of the amount of *recrystallization* during stage 4.

Most natural shear zones will probably develop through a history of the type illustrated by stages 1-4, irrespective of the magnitudes of flow stress, strain-rate, or ambient P-T conditions during deformation. Instead, stage 5 represents a stage of late high stress - low strain deformation during "freezing in" of the microstructures inferred by Nicolas (1978) to occur in most mantle peridotites during slow uplift. The microstructural effects of such late-stage deformation may be particularly relevant for rocks previously developed at high

temperatures and low stresses. Uplift may induce some post-tectonic deformation during which the subgrain size equilibrates with the current stress whilst, due to the low strains and temperatures, the recrystallized grain size remains equilibrated with the previous steady-state flow stress. A stage of minor high-stress, low-temperature deformation during *uplift* of the deformed rocks may thus cause a shift of the point representing the current values of recrystallized grain size and subgrain size at E from the reference curve in the negative y-direction depending on the *strain achieved during post-tectonic uplift*. The subgrain size in such cases will not reflect the dominant creep history of the deformed rock.

Finally, the stress is relaxed after deformation during stage 6. The stress relaxation and annealing experiments reported in Chapter 5 suggest that rapid grain growth may occur during stress relaxation or annealing, unless the rate at which microstructural preservation processes can take place is high enough. Two critical factors in the preservation are the rate of stress drop at the end of the deformation event and the temperature history which postdates the deformation (Knipe 1989). Thus, the recrystallized grain size may no longer be representative of the dominant steady-state flow stress whereas the subgrain size remains equilibrated to the maximum stress achieved either during steady-state flow (stage 2 or 4) or during post-tectonic uplift of the deformed rocks (stage 5). A major difference between the microstructures envisaged to develop during stage 3 and stage 6 lies in the olivine neoblast microstructure, i.e., intensely deformed during stage 3, and largely undeformed during the stress relaxation experiments (Chapter 5). Extensive grain growth during *final stress relaxation* would cause a shift of the point, defined by the current values of recrystallized grain size and subgrain size at F, in the positive x-direction depending on grain growth during stress relaxation.

Due to the inferred stability of the olivine subgrain size to maximum flow stress and the relative sensitivity of the olivine recrystallized grain size to stress relaxation, most data from natural peridotites in equilibrium diagrams are expected to fall either on or below the reference curve. Data plotting below the reference curve may indicate: (i) low strains achieved during deformation, (ii) syn-tectonic stress relaxation during strain softening, (iii) high stress-low temperature deformation during post-tectonic uplift, or (iv) post-tectonic stress relaxation or annealing. Below, I will consider these options for the microstructures sampled in the Ronda peridotite.

Spinel tectonites and garnet-spinel mylonites

The structures and microstructures of the spinel tectonites and, in particular, the garnet-spinel mylonites indicate that considerable strain has been achieved (cf. Fig. 3.2e). Low strain, therefore, cannot be held responsible for the observed discrepancy between

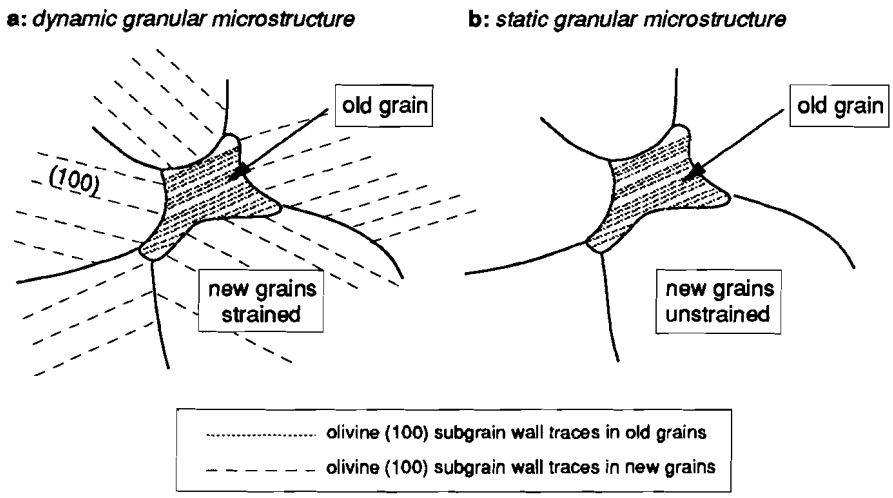

Fig. 6.6. Synoptic diagrams showing possible microstructural difference between granular peridotites with (a) a low stress-high temperature deformational origin and (b) granular peridotites originating from static annealing recrystallization and grain growth. Note that such microstructures can only be recognized in thin section if all grains have olivine [100] oriented in the plane of sectioning.

recrystallized grain size and the subgrain size preserved in the palaeoblasts in the spinel tectonites and garnet-spinel mylonites. In addition, the mylonite microstructure with abundant undulatory extinction and curved and serrated grain boundaries suggests that extensive grain growth due to post-tectonic stress relaxation and annealing recrystallization can be ruled out. Of the remaining two options, i.e., post-tectonic high stress-low temperature deformation and syn-tectonic stress relaxation, the latter is preferred for the following reasons:

1: The transition from spinel tectonites (homogeneous at km-scale) to garnet-spinel mylonites (homogeneous at 100 m scale; see also Fig. 3.3) involves significant strain localization possibly accompanied by syn-tectonic stress relaxation.

2: The recrystallized grain size found in the spinel tectonites and garnet-spinel mylonites suggests flow stresses below 30 MPa which, considering the low ambient deformation temperatures (~840-900°C: Chapter 4), appear too low to accommodate the high strain deformation. The higher flow stresses indicated by the subgrains (74-254 MPa) are probably more realistic for low-T deformation in the upper mantle.

3: There is no significant uplift associated with these deformational structures. Instead, the development of the spinel tectonites and garnet-spinel mylonites is inferred to be related to progressive metamorphism from Ariégite subfacies conditions towards the garnet - spinel peridotite transition.

It is therefore suggested that, in at least the garnet-spinel mylonites, the discrepancy between recrystallized grain size and subgrain size could be due to syn-tectonic stress relaxation, where high stresses allied to the initiation of the garnet-spinel mylonites is recorded by the subgrain spacing in the olivine palaeoblast of both spinel tectonites and garnet-spinel mylonites (74-334 MPa), whilst newly achieved lower stresses prevailing during steady-state flow in the mylonite zones (25-29 MPa) are recorded by the sizes of the neoblasts. Processes involved in the inferred strain softening in the garnet-spinel mylonites are discussed below. The development of an anastomosing mylonitic shear zone system in spinel tectonites could induce stress relaxation *of the spinel tectonites*, leading to significant growth of the newly recrystallized grains in the spinel tectonites to equilibrate upon the background stresses (16-20 MPa) at the scale of the whole domain. A similar process was demonstrated experimentally on a magnesium alloy by White et al. (1985).

Granular peridotites

The large discrepancy between the average grain sizes and subgrain sizes in the granular peridotites appears inconsistent with an origin from high temperature - low stress flow. A much lower average subgrain spacing would be expected in such a case, although some disequilibrium with the grain size may be expected from a contribution of preserved subgrain characteristics in non-annealed grains of the deformed protolith. Instead, as illustrated in Fig. 6.6, the observed major discrepancy is better explained by extensive annealing recrystallization and grain growth where only the non-annealed grains show a subgrain configuration inherited from the deformed protolith. Note that the microstructural differences between grains as illustrated in Fig. 6.6 can only be observed in thin-section if all grains are oriented such that the decorated subgrains can be observed in all the grains, i.e. when olivine [100] lies in the plane of observation. The present data suggest that even a regional event of thermally driven annealing recrystallization and grain growth cannot completely re-equilibrate a pre-existing subgrain configuration until the total rock volume is swept by migrating grain boundaries. This observation is at variance with high-temperature annealing experiments on natural dunites in the temperature range 1100-1700°C (Ricoult 1979) showing significant subgrain growth due to extensive annealing recrystallization. It is emphasized that the palaeostress estimates derived here from the grain sizes and subgrain sizes in the granular peridotites bear no physical meaning to the ambient conditions during annealing.

a: *Low stress / High temperature*

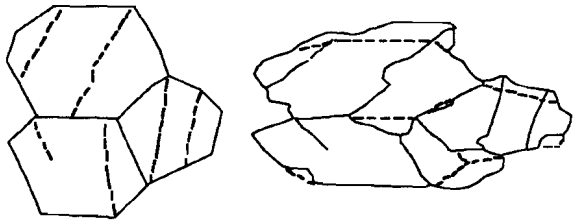

recrystallisation by rotation and extensive migration

b: *High Stress / Low temperature*

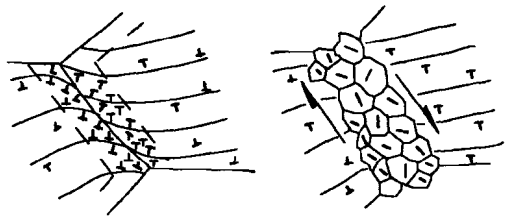

local recrystallisation at old grain boundaries

Fig. 6.7 Schematic diagrams illustrating the recrystallization mechanisms at low stress - high temperature (a) and (b) high stress - low temperature, after Drury et al. 1991. In the latter, the recrystallized grains define a band which potentially is both structurally and geometrically soft as compared to the old grains.

Plagioclase tectonites

The following characteristics of the plagioclase tectonites may place some constraints to the rheological significance of the observed discrepancy between recrystallized grain size and subgrain size:

1: Calculated shear strains (γ>5) for some N/E-vergent tectonites suggest that the observed discrepancies cannot be due to low strains achieved during flow.

2: The N/E-vergent plagioclase tectonites are associated with emplacement of the Ronda peridotite in the crust (Chapter 3). Therefore, the reason for the low subgrain spacings as compared with the recrystallized grain size in both types of plagioclase tectonites could well be a final high stress - low temperature stage associated with emplacement.

3: The S-vergent plagioclase tectonite microstructures occasionally show relatively strain-free polygonal neoblasts (see also Obata 1980), suggesting that some post-tectonic annealing has occurred at temperatures high enough to facilitate post-tectonic annealing recrystallization and grain boundary migration.

It follows that neither the recrystallized grain sizes nor subgrain sizes can be expected to reflect ambient flow stresses during steady-state flow. Instead, the palaeostress estimates based on the subgrain sizes (24-141 MPa) probably indicate an upper bound to the ambient flow stresses, whilst the estimates based on recrystallized grain sizes (5-16 MPa)

place a lower bound.

6.5 Strain softening processes in garnet-spinel mylonites

Four main classes exist of possible strain-related softening mechanisms which may operate in natural rocks (White et al. 1980, Poirier 1980, Schmid 1982): (i) thermal softening induced by strain heating, (ii) structural softening induced by strain-dependent microstructural changes, (iii) geometric softening induced by a change in LPO patterns, and (iv) reaction softening induced by phase transitions during deformation.

It seems unlikely that strain softening in the garnet-spinel mylonites is accompanied by thermal- or reaction-softening processes. First, the progressive development of spinel tectonites to garnet-spinel mylonites is allied to progressive cooling (Chapter 4) which would counteract, if not overrule, possible thermal softening processes. Second, there is no evidence for volumetrically significant changes in mineral compositions allied with possible infiltration of hydrous fluids or melts associated with the transition from spinel tectonites to garnet-spinel mylonites. In addition, the spinel tectonites and garnet-spinel mylonites show essentially similar olivine LPO patterns (see Fig. 3.4) interpreted to have developed during crystal-plastic flow accommodated by the olivine [100]{0kl} slip systems, with a strong predominance of the [100](010) slip system in the garnet-spinel mylonites. It seems unlikely, therefore, that this slight change in slip system will cause any significant geometrical softening. The only feasible softening mechanism that remains is structural softening.

Drury et al. (1991) describe how structural softening may arise from a change in recrystallization mechanism as shown in Fig. 6.7a. At low stresses and higher temperatures, recrystallization occurs uniformly on the grain scale by subgrain rotation throughout the old grains and by extensive migration of old and new grain boundaries. The recrystallization mechanisms operating at high stresses and lower temperatures are poorly constrained but probably involve the development of new grains near old grain boundaries by a combination of local grain boundary bulging, subgrain rotation and subgrain growth (e.g. Ross et al. 1980, Zeuch and Green 1984). For a critical amount of strain, the recrystallized grains start to define a continuous network at the micro-scale which is, potentially, both structurally and geometrically soft as compared with the old grain microstructure (Fig. 6.7b). This type of localization mechanism is held responsible for the development of shear zones and the associated strain softening in experimentally

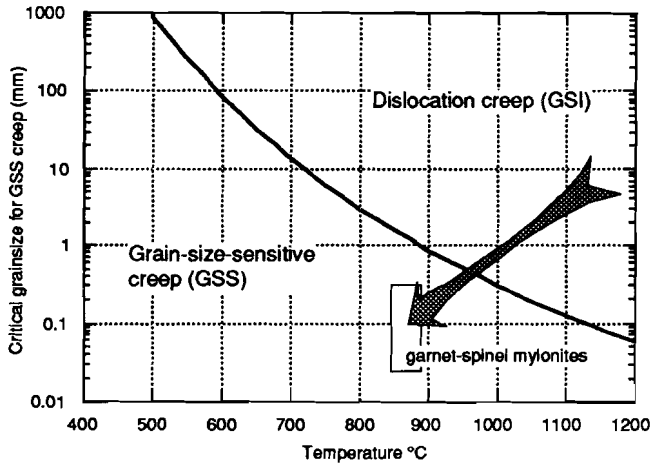

Fig. 6.8 Graph showing critical grain size for grain-size-sensitive (GSS) creep as a function of temperature in "wet" olivine. Wet flow laws from Karato et al. (1986) and stress - recrystallized grain size relationship presented in this thesis (eqn. 5.4). Inferred trajectory for the progressive development of spinel tectonites and garnet-spinel mylonites is shown.

deformed magnesium alloys (White et al. 1985), feldspar aggregates (Tullis and Yund 1985) and possibly dunites (Post 1977, Zeuch 1982). Thus, significant softening could be initiated in the garnet-spinel mylonites as soon as the volume fraction of recrystallized grains reached certain values at which these grains started to form a connected network carrying the bulk strength of the material. Differential stresses of the order of 25 MPa, however, seem still rather low for low T - high strain deformation by dominant dislocation creep mechanisms.

Grain-size reduction caused by dynamic recrystallization may lead to a change of deformation mechanism from dislocation creep, hereafter referred to as grain size insensitive (GSI) creep, to grain size sensitive (GSS) creep (White 1976, White and Knipe 1978, Rutter and Brodie 1988, Handy 1989, Drury et al. 1991). Rutter and Brodie (1988) have shown that experimental flow laws for "wet" fine-grained olivine aggregates (Karato et al. 1986) predict an important role of GSS creep at low temperatures (600-900°C) in the upper mantle. For the ambient conditions associated with the garnet-spinel mylonites (840-880°C; Chapter 4), the onset of GSS creep may occur in peridotites with grain sizes smaller than 1 mm (Fig. 6.8). The occurrence of a strong olivine LPO in the garnet-spinel mylonites, however, may indicate that dislocation creep remained important. On the other hand, once a strong LPO patterns has developed it remains to be established to what extend GSS-creep processes may obliterate any strong pre-existing lattice fabric.

A major effect of GSS-creep operating in ductile shear zones is to reduce their viscosity such that significant strain softening can be expected (Rutter and Brodie 1988). The reason for this lies in a change of the viscous creep parameters from GSI-creep dominated to GSS-creep dominated ductile flow. For hydrous dunites, a change in creep exponent from n=

3.67 for GSI-creep to n= 1.4 for GSS creep is envisaged (Handy 1989). Any network of mylonitic upper mantle shear zones could thus lead to a dramatic reduction by several orders of magnitude in the strength of the upper mantle underneath orogenic regions (Rutter and Brodie 1988, Handy 1989, Drury et al. 1991, Vissers et al. 1991).

In the light of a possible contribution of GSS-creep to the flow processes in the garnet-spinel mylonites, it is therefore concluded that the obtained palaeostresses of the order of 25 MPa represent a significant reduction of the strength of the upper mantle subsequent to the initiation of the garnet-spinel mylonites. This may imply that the rheology of the W Mediterranean mantle at depths around the transition zone from garnet to spinel peridotite became much weaker than expected on the basis of dislocation creep mechanisms alone.

CHAPTER 7

Uplift and emplacement of the Ronda peridotite.*

7.1 Introduction

The structural, pressure-temperature and rheological data documented from the western Ronda massif can be used to test previous and current working hypotheses for the tectonic setting and modes of emplacement of the W Mediterranean peridotites. In this final chapter I will focus on the tectonic implications of these data for the geodynamical evolution of the W Mediterranean region and the Betic-Rif orogen. I will first summarize existing uplift and emplacement models for the W Mediterranean peridotites and the various working hypotheses for the evolution of the W Mediterranean lithosphere. These are then evaluated against the structural, thermal and rheological characteristics of the Ronda peridotite, taking into account the general features of the Internal Betics and W Mediterranean region as a whole. It is concluded that the data from the Ronda peridotite are consistent with uplift and emplacement of the peridotites as the result of extensional collapse of a collisional mountain chain, driven by detachment at depth of gravitationally unstable cold lithosphere.

* Parts of this Chapter have been submitted to Geology as: Van der Wal, D., and Vissers, R.L.M. A tectonic scenario for uplift and emplacement of the Ronda peridotite, SW Spain.

7.2 Existing uplift and emplacement models

Diapiric models

The earlier uplift and emplacement models proposed for the W Mediterranean peridotites involved diapiric uprise of the mantle rocks. Dickey (1970) was the first to carry out a combined field- and geochemical study of the Ronda peridotite. He studied the mafic layers in the peridotite and suggested that, despite substantial sub-solidus changes in their mineralogy, some of these layers still retained their magmatic mineralogies. On the basis of these observations he suggested that the mafic layers formed as partial fusion products of the peridotite in an ascending mantle diapir.

Loomis (1972a) studied the crustal "aureole" immediately NW of the Ronda massif. On the basis of the high-temperature petrogenesis of the metamorphic assemblages within the aureole rocks, the different metamorphic and structural histories of the aureole rocks and the peridotite, the abundant occurrence of mafic layers in the mantle rocks and the steeply dipping foliations in the rocks of the aureole, he suggested that the Ronda peridotite intruded the crust as a hot diapir driving radial extension in the crust, and that the massif in its present-day position still roots in the upper mantle (Loomis 1972b, 1975).

A significant refinement of the above diapir models was made by Obata (1980) who carried out the first combined petrological and *thermal* study of the Ronda peridotite. He concluded that the preservation of all peridotite metamorphic facies within a coherent peridotite body reflected a degree of recrystallization and deformation much higher than previously thought, and that this deformation and recrystallization occurred in essentially *the solid state,* hence, posterior to diapiric intrusion. On the basis of the mineralogical and thermal data, Obata (1980) proposed that the zonation of the Ronda peridotite resulted from syn-tectonic recrystallization of a dynamically cooling, hot solid mass, driven by an unspecified mechanism into the crust. This dynamic cooling during emplacement involved early crystallization of the LT-HP garnet-bearing peridotites in the outer parts of the body, continued recrystallization through the spinel-peridotite facies of the more interior parts, ending in final crystallization of plagioclase-peridotites in the core of the complex. Around the same time, Lundeen (1978) demonstrated that the Ronda peridotite forms an allochtonous thrust sheet instead of a mantle diapir rooting in the present-day upper mantle, and since general agreement exists on solid-state emplacement of the peridotite into the crust.

Extrusion on transform faults

Darot (1973, 1974) carried out a pioneering structural and kinematic study of the Ronda peridotite. Tubia and Cuevas (1986, 1987) performed a similar structural and kinematic study of the Ojén peridotite east of the Ronda massif (see Fig. 3.1). Their interpretation of the geometry and kinematics as regards peridotite uplift and emplacement can be summarized as follows. A phase of possibly diapiric flow at high temperature - low stress conditions has been preserved in the plagioclase lherzolites of the central parts of the massif. The structures allied to this phase are overprinted by mylonitic spinel peridotites at the upper and lower contacts of the massif. These mylonites deformed at low temperature - high stress conditions and show a remarkable structural and kinematic continuity with the surrounding crustal metamorphic units. The oldest deformation would correspond to mantle flow beneath a continental rift undergoing strike-parallel motion, whereas later mylonitic deformation could be ascribed to thrusting of the still hot mantle slab over continental crust (see also Vauchez and Nicolas 1991). The entire process is envisaged to be of Alpine age (Tubia and Cuevas 1986).

Uplift and emplacement in the predominantly solid state

Kornprobst (1969, 1974) interpreted the Beni Bousera peridotite in Morocco as a pre-Alpine slice reworked in Alpine thrusts. In his model, uplift of the Beni Bousera peridotite by a diapiric mechanism brought the peridotites close to the base of the crust. On the basis of a structural and petrological study indicating strong similarities in metamorphic conditions across the contact with the granulite-facies crustal rocks, it was inferred that further uplift occurred in the solid state. More recent structural and petrological studies of the Beni Bousera peridotite and adjacent crustal rocks (Reuber et al. 1982, Saddiqi et al. 1988) complement these earlier studies, and the uplift path is currently inferred to comprise a Mesozoic extensional stage, followed by a compressional stage possibly reflected by the garnet peridotites. Final emplacement is thought to have occurred by peridotite unroofing during Neogene extensional tectonics (Michard et al. 1991). Below I show that the Ronda data point to a tectonic scenario essentially consistent with this interpretation.

7.3 Working hypotheses for the geodynamics of the Alboran region

Four classes of working hypotheses have been put forward to explain the geometry and kinematics of the Betic-Rif orogenic belt: (1) *oroclinal bending* (Carey 1958, Didon 1969, Tubia and Cuevas 1987), (2) dextral *strike-parallel motion,* in a rift setting, between the African and Eurasian plates (e.g., Osete et al. 1988, Vauchez and Nicolas 1991), (3) *indentation* of the "Alboran microplate" between the margins of Afica and Iberia (Andrieux et al. 1971, Leblanc and Olivier 1984, Bouillin et al. 1986) and (4) post-orogenic (Doblas and Oyarzun 1989) or syn-orogenic (Platt and Vissers 1989) *extensional collapse* of an overthickenend collisional ridge in the Alboran region. Except for oroclinal bending, all these working models can be tested with the present structural, thermal and rheological data of the Ronda peridotite. Oroclinal bending, however, has currently been rejected on the basis of palaeomagnetic results from the Betic-Rif chain, revealing opposite senses of up to 60° rotation of Mesozoic limestone sequences across the Alboran Sea, i.e., dominantly clockwise rotations in S Spain and dominantly anti-clockwise rotations in N Morocco (Osete et al. 1988, Platzman 1992).

A scenario for uplift and emplacement of the W Mediterranean peridotites in a rift undergoing strike-parallel motion as proposed by Vauchez and Nicolas (1991), and inspired by the Ojén results (Tubia and Cuevas 1987) possesses two major problems. One lies in the *relative age relations* between the structural and metamorphic domains, the other in the *thermal history* of the peridotites. The models predict that the high-temperature - low stress assemblages possibly related to asthenospheric flow, i.e., the plagioclase tectonites, should be overprinted by low-temperature - high-stress assemblages (spinel mylonites in the NW Ojén massif, garnet-spinel mylonites in the NW Ronda massif, cf. Tubia and Cuevas 1987, their Fig. 10). The opposite is observed in the Ronda peridotite (Chapter 3). Moreover, the strike-parallel motion hypothesis is inconsistent with the thermal history of the Ronda peridotite: although it does predict progressive cooling with emplacement into the crust (Tubia and Cuevas 1986), it does not account for the peak temperatures at Seiland subfacies conditions recorded in the Ronda peridotite (Chapter 4, this thesis). Note that all structural features documented from the Ojén peridotite such as increasing degree of strain localization, reversal in shear sense and the kinematic data for the structures related to crustal emplacement (Tubia and Cuevas 1986, 1987) are also found *within the plagioclase peridotites* from Ronda (Chapter 3, this thesis). Therefore, the structural data obtained from the Ojén massif (Tubia and Cuevas 1986, 1987) are extremely valuable but may apply only to the *later stages of uplift and emplacement* of the peridotites rather than representing *a more complete record* of this history. This is already

suggested by the limited metamorphic facies in the Ojén massif dominated by plagioclase peridotites and limited spinel peridotites but no documented garnet peridotites. In addition to these considerations, the recent palaeomagnetic data impose another problem to the uplift and emplacement models proposed by Tubia and Cuevas (1986, 1987) and Vauchez and Nicolas (1991). Tubia and Cuevas (1987, p. 59) state that "kinematic criteria of shear sense from Betic-Rifean peridotites demonstrate the oroclinal origin of the Arc of Gibraltar". Their interpretation of the Betic-Rif chain strongly relies on the present-day orientations of structural features such as stretching lineations (e.g. Tubia and Cuevas 1987, their Fig. 10). The recently documented palaeomagnetic evidence for rotations of the order of 60° in limestones only few kilometres N and NW of the Ronda peridotite (Platzman and Lowrie 1992) casts doubts to any extrapolation of kinematic data from the peridotites, in view of hitherto undocumented but quite possible rigid-body rotations of the peridotite bodies themselves. Clearly, interpretations of kinematic data for the purpose of tectonic reconstructions of the region as a whole must take such rotations into account. In addition, possible rigid-body rotations may have occurred *within* the peridotites, as structures developed prior to the plagioclase tectonites may have undergone rigid-body rotations during development of a network of plagioclase-tectonite shear zones.

An *indenting microplate* origin of the Betic-Rif chain is currently rejected because such models do not account for the clearly non-rigid, non-plate character of the Alboran lithosphere with its ubiquitous evidence for pervasive faulting in a region of high heat flow. This is consistent with the palaeostress estimates for the various structures in the Ronda massif (Chapter 6) suggesting that the mantle rocks underneath the Alboran domain were mechanically weak during a considerable part of their uplift history.

Post-tectonic emplacement of the peridotites, during major Neogene extension, in *"mantle core complexes"* as proposed by Doblas and Oyarzun (1989) presumes that the peridotites in the Betic Zone form deep-rooted bodies with steeply oriented walls. Among all current models, the one proposed by Doblas and Oyarzun (1989) most notoriously fails to explain any of the internal structural and metamorphic features observed in the Ronda- and other W Mediterranean peridotites. Their hypothesis is further contradicted by the numerous field- and geophysical data indicating that the peridotites are allochtonous thrusted bodies (Lundeen 1978, Tubia and Cuevas 1987, Chapter 3 this thesis, Torné et al. 1992). Tubia (1990) confronted the core-complex hypothesis with structural and kinematic data from the Ojén massif, but in view of the above-mentioned uncertainties surrounding extrapolation of the peridotite kinematic data, the argument may be limited to the structural data demonstrating the allochtonous nature of the peridotites which, in

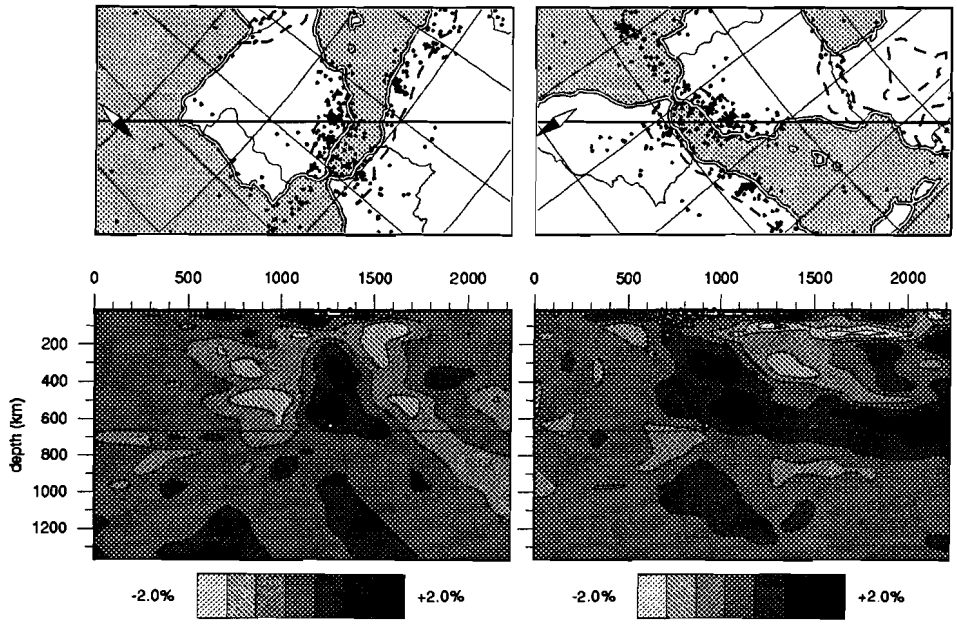

Fig. 7.1: Tomographic image of the deep mantle structure underneath the Betic-Rifean orogen. From Blanco and Spakman, in press.

any case, is inconsistent with the proposed core complex hypothesis.

Syn-orogenic extensional collapse of overthickened lithosphere (Platt and Vissers 1989) driven by some detachment process at deep lithospheric levels seems consistent with the internal features of the Ronda peridotite. Such a hypothesis may account for the early development of low temperature - high pressure assemblages during underthrusting related to convergence between Africa and Iberia, followed by late-stage development of low-pressure assemblages (plagioclase tectonites) during extensional collapse of the thickened lithosphere. The hypothesis is also consistent with the palaeomagnetic data (Platzman 1992) and does not a priori contradict any of the kinematic, thermal and rheological data observed in the peridotites. Instead, the assumption involved in this hypothesis concerning a thermal anomaly in the upper mantle driving orogenic collapse (see also Van Bemmelen 1969, Loomis 1975, Torres Roldán 1979) may clearly be consistent with the observed stage of annealing recrystallization at high thermal gradients documented in Chapters 3 and 4. Below I will elaborate on this hypothesis and investigate if and how the main features of the Ronda peridotite and its emplacement in the Betic crust may be consistent with continental collision, followed by detachment of gravitationally unstable cold lithosphere driving extension in the Betic-Alboran crust and emplacement of the W Mediterranean peridotites.

7.4 General features of the Betic-Rif orogen

Any tectonic model integrating the structural and thermal evolution of the Ronda peridotite must account not only for the features recorded in the peridotites but also for the main features of the crustal geology in the Alboran region and for the geodynamics of the region as a whole. These are as follows: the Alboran basin is underlain by thin (13-20 km) continental crust (Banda et al. 1983), shows distinct gravity highs (Bonini et al. 1973), ubiquitous Neogene vulcanism (Torres Roldán et al. 1986), high heat flow values (Albert-Beltrán 1979), and has subsided 2-4 km since the Middle Miocene (Mulder and Parry 1977). Onshore in S Spain, there is clear evidence for extensional tectonic exhumation of previously developed high-pressure metamorphics (Platt et al. 1983). Extension and subsidence occurred coeval with outwardly directed thrusting in the surrounding chains of the Subbetic and Prebetic domains to the N and NW, and the Rif and Tell to the SW and S. However, Africa and Europe converged slowly during this period (Dewey et al. 1989), so *extension must have been driven within the Alboran system* itself. These observations led Platt and Vissers (1989) to suggest detachment of the underlying lithospheric root developed during Late Cretaceous to Early Tertiary collision, and convective upwelling of asthenospheric mantle to high structural levels in the Late Oligocene.

Recent seismic tomography of the W Mediterranean (Blanco and Spakman, in press) shows a clear positive velocity anomaly (hence a negative temperature anomaly) in the depth range 200-600 km underneath the Alboran region (Fig. 7.1), providing clear support for a geologically recent detachment process in the region. In addition, the elongate shape of the anomaly shows a NE-SW trend consistent with an interpretation in terms of a detached subducted slab (Blanco and Spakman, in press).

Below I combine the above pieces of information with the structural, kinematic, thermal and rheological data from the Ronda peridotite to arrive at a tectonic scenario for the uplift and emplacement of the W Mediterranean peridotites.

7.5 A tectonic scenario

The early uplift of diamond-bearing peridotites, from depths of around 150 km into the spinel peridotite stability field, is difficult to constrain because the Ronda peridotite has

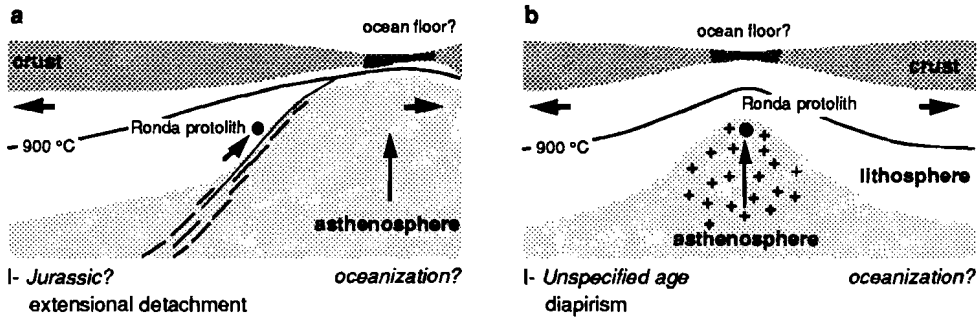

Fig. 7.2: Tectonic scenario for the Alboran Sea and surrounding chains: early uplift accommodated by (a) low angle detachment or (b) diapirism. Arrows denote movement sense of the different tectonic units.

only preserved relict assemblages but no structures whatsoever related to this stage. However, it seems straightforward to ascribe this uplift to the Jurassic phase of extension and breakup (stage I, Fig. 7.2) well-known from the western and central Mediterranean (Dercourt et al. 1986). A much older age of this uplift event, however, cannot be ruled out. Low-angle detachment faults penetrating the lithospheric mantle (stage I, Fig. 7.2a) to accommodate opening of an oceanic basin (Lemoine et al. 1987, Vissers et al. 1991) could provide a mechanism for rapid uplift of diamond-bearing peridotites towards Ariégite subfacies conditions, followed by complete re-equilibration. Diapiric uplift, however, can equally well explain such uplift (stage I, Fig. 7.2b). Any further inference on this early uplift event requires additional geological data, hence portions of upper mantle less affected by later deformations and less overprinted by later metamorphic and magmatic processes. In view of the structural and metamorphic data reported from the W Mediterranean peridotites there seems limited scope that much of this information has been preserved.

To be consistent with the Late Mesozoic to early Tertiary HP-LT metamorphism documented in the crustal rocks of the Betic Zone (Torres Roldán 1979, Goffé et al. 1989, De Jong 1991), extension and uplift at high-temperature conditions probably ceased during the Early Cretaceous. The mineral chemistry data from the Ronda peridotite indicate a stage of significant cooling by some 250°C, allied with increasingly localized deformation and development of spinel-tectonites and garnet-spinel mylonites. The metamorphic assemblages indicate a progressive change of the ambient conditions from the Ariégite-subfacies towards the garnet-peridotite facies (Chapter 3, 4). It is evident that such cooling at possibly increasing pressures requires the presence of relatively cold material close to the rocks now exposed in the Ronda massif. As a first approximation, such

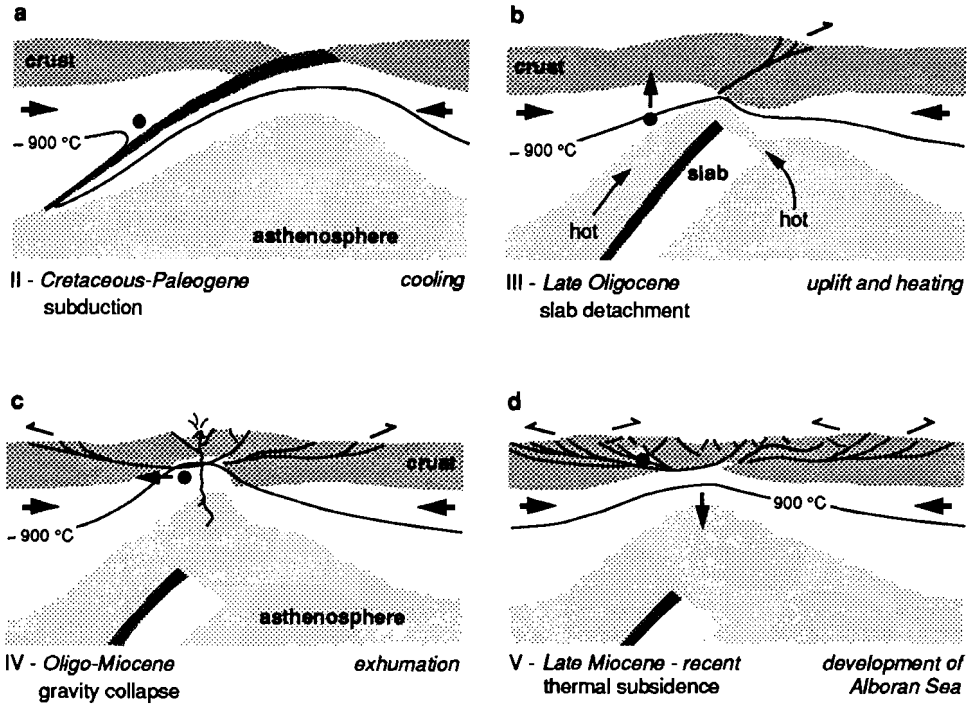

Fig. 7.3a-d: Tectonic scenario for the Alboran Sea and surrounding chains: subduction followed by slab detachment. See text for explanation.

relatively cold material may have had temperatures about twice the pertinent temperature decrease (i.e., 500°C) *below* the ambient conditions at the onset of cooling. This implies temperatures for such cold material of the order of 600°C. An obvious mechanism to account for this temperature decrease is subduction of cool oceanic lithosphere, as possibly even lower temperatures are inferred to exist in the hanging-wall mantle wedge above the upper (~100 km) parts of subduction zones (e.g., Van den Beukel and Wortel 1988 and refs. therein). The spinel-tectonites and garnet-spinel mylonites are therefore interpreted to reflect ductile deformation, at temperatures decreasing to about 850°C, in the hanging wall of a major structural discontinuity accommodating large-scale underthrusting of cool material such as a subducting portion of oceanic lithosphere (Fig. 7.3a, stage II). Unfortunately, the present interpretation of the early cooling towards the garnet peridotite field cannot be substantiated by absolute dating of the garnet-bearing peridotites (see, e.g., Kornprobst 1974). The occurrence of minor amounts of pargasite,

however, may indicate partial hydration at least consistent with fluid ingress released from an underlying subducting slab. In addition, the later infiltration of melts with a boninitic signature "behind" the annealing recrystallization front (Remaïdi et al. 1991) seems also consistent with subduction, provided that "a mechanism capable of raising the shallow upper mantle temperature to > 1100°C must be identified" (Crawford et al. 1989, p. 33). Such a mechanism is proposed below. Additional detailed geochemical studies, however, are needed to firmly substantiate this interpretation.

Detachment of the gravitationally unstable slab during continental collision probably induced convective counterflow of hot asthenospheric mantle, progressively replacing cool lithosphere in the depth range 75-200 km (Fig. 7.3b, stage III). Such an ascent of asthenospheric mantle provides both a driving mechanism for uplift and a heat source for the development of the granular peridotites by thermally driven annealing recrystallization of the upper mantle rocks in the subduction zone hanging wall, the subordinate melting in these granular rocks and the possible generation of a boninitic magma, the progressive development of LP facies series in several of the crustal sequences adjacent to the peridotites (e.g. the Casares unit; Loomis 1972a, Hollerbach 1985) as well as elsewhere in the Betic Zone (Westra 1969), and the scattered mafic, intermediate and silicic vulcanism which occurred in the Neogene (Torres Roldán et al. 1986). The radiometric ages obtained from the felsic dikes transecting the Ronda peridotite (Priem et al, 1979), the LP metamorphic rocks (Zeck et al, 1992), the major extensional detachment (Monié et al., 1991) between the Nevado-Filabride and Alpujarride rocks (Platt and Vissers, 1989), the Neogene vulcanism (Torres Roldán et al. 1986) and the sudden development of partly fault-bounded, Neogene intra-montaneous basins with an early Neogene continental record all suggest that the detachment process occurred sometime during the Late Oligocene.

Detachment may have occurred at essentially the slab-hanging wall contact (Blanco and Spakman, in press; Fig. 7.3b, stage III). It is noted in this context that the differential stresses inferred from the garnet-spinel mylonite microstructures (~25 MPa; Chapter 6) lie within the inferred range of average stresses along the slab segment between the trench and the volcanic line (projected down to the subduction zone). These shear stresses are in the range 10-40 MPa, corresponding to differential stresses of ~20-80 MPa (Van den Beukel and Wortel 1988). It is possible that the detachment process was accommodated by the presence of mechanically weak, low-temperature garnet-spinel mylonite zones, possibly much wider than those exposed in the Ronda massif. However, the detachment process implies that such zones will either sink with the detached slab into the deeper mantle or, if some relics of these rocks remain connected with the hanging wall, will

become overprinted by intense annealing during juxtaposition with upwelling hot asthenosphere.

The ascent of asthenospheric mantle in response to a detachment process most probably contributed to the uplift of the peridotites from the spinel-garnet transition zone through the Seiland facies into the plagioclase stability field, however, part of this peridotite uplift may have been accommodated by tectonic denudation in the Betic Alboran crust at an earlier stage, not necessarily in response to the detachment process, as follows. The total magnitude of depressurization of the Ronda peridotite *prior* to the "hot" stage is about equal to that documented for the Nevado-Filabride rocks by Bakker et al. (1989). Radiometric ages assigned to the early high-pressure metamorphic and late "hot" stages in the Nevado-Filabrides (de Jong 1991) indicate a time span for uplift of around 50 Ma. The Nevado-Filabride pressure-temperature path shows distinct cooling during the earlier part of the uplift trajectory towards a low-greenschistfacies stage dated at 30 Ma, *prior* to late heating. It is therefore conceivable that an unspecified earlier part of the peridotite uplift, from the garnet-spinel transition zone to lower pressures, was accommodated by tectonic denudation in the upper parts of the Betic-Alboran crust or by erosion or both.

Uplift of the thickened lithospheric column in response to detachment of the subducting slab would enhance the gravitational potential energy of the system, driving ductile collapse, tectonic denudation (see also England and Houseman 1986) and radially outward thrusting in the external zones of the system (Platt and Vissers 1989). Once uplifted to depths of around 30 km, it is proposed that fragments of the upper mantle, now represented by the western Alboran peridotites, became exhumed along low-pressure, plagioclase-bearing tectonite shear zones, i.e. major upper mantle extensional faults accommodating tectonic denudation (Fig. 7.3c, stage IV). The transition from early plagioclase-tectonite shear zones developed at the scale of the entire plagioclase-peridotite domain to km-scale localized plagioclase tectonites with reversed shear senses (Tubia and Cuevas 1987, Chapter 3, this thesis) may represent a change of bulk imposed deformation inherent to progressive outward translation of the peridotites from the extension-dominated internal part of the system towards the shortening-dominated outer parts (Fig.7.3c, stage IV). During concomitant cooling, the ductile plagioclase-tectonite shear zones gradually evolved into cataclastic fault zones bringing the Ronda peridotite in its present position amidst tectonic slices of crustal origin. Gradual cooling of the anomalously hot upper mantle in the Alboran region during the later Miocene accounts for subsidence in the central part of the system now occupied by the Alboran sea (Fig. 7.3d, stage V).

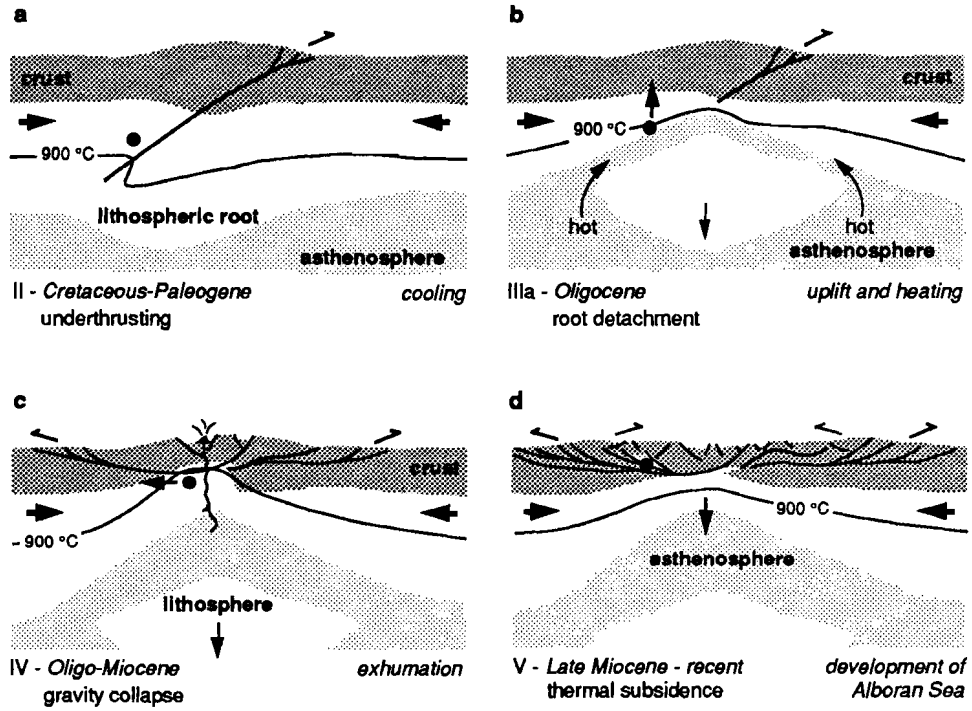

Fig. 7.4a-d: Tectonic scenario for the Alboran Sea and surrounding chains: underthrusting followed by detachment of a lithospheric root. See text for explanation.

The tectonic process as outlined above accounts for the major features observed in the Ronda peridotite, however, some aspects of the process are difficult to test with the present dataset. This concerns in particular the nature and amount of subducted lithosphere as follows. Palaeogeographic reconstructions of the W Mediterranean (Dercourt et al. 1986) as well as the extremely limited occurrence of oceanic rocks in the Betic crust impose questions as to the nature of the Jurassic oceanic domain in the region. Geochemical studies (Bodinier et al. 1987) suggest that the mafic rocks of the Betic Zone probably represent a transitional type of oceanic crust strongly dismembered during the Alpine orogeny, and that a full oceanic stage of Jurassic extension was only reached in the more easterly parts of the Neotethys. Such a transitional character and the inferred small dimensions of oceanic lithosphere in the Western Mediterranean may impose difficulties on descriptions of the entire process in terms of a plate-like ocean-continent convergence. Following Houseman et al. (1981) and England and Houseman (1989), Platt and Vissers (1989) and Platt and England (in press) suggest that the Alpine orogeny in the Alboran

region may possibly be described as largely intracontinental deformation involving relatively homogeneous lithosphere thickening, followed by convective removal of the thickened, gravitationally unstable lower lithosphere. Such detachment of the lithospheric root would enhance the gravitational potential energy of the system driving late orogenic extension. Particularly with regard to the *thermal* consequences of detachment of lower lithosphere, the main implications of this alternative description are probably similar to those of a slab detachment process as outline above. It is felt that the Ronda data provide a poor basis to discriminate between the two alternatives, except that the inferred homogeneous thickening of the lithosphere at the earlier stages of convergence should at least allow for heterogeneities in the deformation at a length-scale sufficient to account for the observed early-stage cooling of the mantle rocks, i.e., for sufficiently large-scale underthrusting of relatively cold lithosphere. A tectonic scenario analogous to the one outlined above but describing the process in terms of homogeneous thickening followed by convective removal is illustrated in Fig. 7.4a-d.

Conclusions

The present tectonic interpretation of the structural, thermal and rheological data of the Ronda peridotite differs from previous and current diapirism and strike-slip rift models, principally because it assigns the Ronda body to the lithosphere rather than to ascending hot asthenospheric mantle. Moreover, in contrast to the diapirism models, the present scenario possesses the advantage of explaining the entire peridotite emplacement in terms of a physical mechanism intrinsic to the geodynamic regime of the Mediterranean area, i.e. continental break-up possibly leading to uplift of diamond-bearing peridotites, followed by closure of a presumably small oceanic domain during collision-related large-scale underthrusting (subduction) and eventually, detachment of gravitationally unstable cold lithosphere. This scenario can be tested by further seismological, geological and geochemical studies, as well as by thermal and thermo-mechanical modelling.

References

Albert-Beltrán, J.F. 1979. El mapa español de flujos calorificos. Intento de correlación entre anomalias geotérmicas y estructura cortical. Bol. Geol. y Minero 90: 36-48.

Andrieux, J., Fontbote, J.M., and Mattauer, M. 1971. Sur un modèle explicatif de L'Arc de Gibraltar. Eath Plan. Sci. Lett. 12: 191-198.

Ashby, M.F., and Verrall, R.A. 1978. Micromechanisms of flow and fracture, and their relevance to the rheology of the upper mantle. Phil. Trans. R. Soc. London 288: 59-95.

Avé Lallemant, H.G. 1967. Structural and petrofabric analysis of an Alpine-type peridotite: the lherzolite of the French Pyrenees. Leidse Geol. Mededel. 42: 1-57.

Avé Lallemant, H.G., and Carter, N.L. 1970. Syntectonic recrystallization of olivine and modes of flow in the upper mantle. Geol. Soc. Am. Bull. 81: 2203-2220.

Avé Lallemant, H.G., Mercier, J-C.C., Carter, N.L., and Ross, J.V. 1980. Rheology of the upper mantle: inferences from peridotite xenoliths. Tectonophysics 70: 85-113.

Bakker, H.E., De Jong, K., Helmers, H., and Biermann, C. 1989. The geodynamic evolution of the internal zone of the Betic Cordilleras (south-East Spain): a model based on structural analysis and geothermobarometry. J. Metamorph. Geol. 7: 359-381.

Banda, E., Udias, A., Mueller, S., Mezcua, J., Boloix, M., Qallart, J., and Aparicio, A. 1983. Crustal structure beneath Spain from deep seismic sounding experiments. Phys. Earth Plan. Int. 31: 277-280.

Bertrand, Ph., and Mercier, J-C. C. 1985. The mutual solubility of coexisting ortho- and clinopyroxene: towards and absolute geothermometer for the natural system? Earth Plan. Sci. Lett. 76: 109-122.

Biot, M.A. 1961. Theory of folding of stratified viscoclastic media and its implications in tectonics and orogenesis. Geol. Soc. Am. Bull. 72: 1595-1620.

Blacic, J.D. 1972. The effect of water on the experimental deformation of olivine. Geophys. Monogr. Am. Geophys. Union 16: 109-115.

Blanco, M.J., and Spakman, W. 1993. The P-wave velocity structure of the mantle below the Iberian Peninsula: evidence for subducted lithophere below southern Spain. Tectonophysics, in press.

Bodinier, J.L., Morten, L., Puga, E. and Diaz de Federico, A. 1987. Geochemistry of metabasites from the Nevado-Filabride complex, Betic Cordilleras, Spain: relicts of a dismembered ophiolitic sequence. Lithos 20: 235-245.

Bonatti, E., Ottonello, G., and Hamlyn P.R. 1981. Peridotites from the island of Zabargad (St. John's), Red Sea: Petrology and Geochemistry. J. Geophys. Res. 21: 599-631.

Bonini, W.E., Loomis, T.P., and Robertson, J.D. 1973. Gravity anomalies, ultramafic intrusions and the tectonics of the region around the Strait of Gibraltar. J. Geophys. Res. 78: 1372-1382.

Bouchez, J.L., and Duval, P. 1982. The fabric of polycrystalline ice deformed in simple shear: experiments in torsion, natural deformation and geometrical interpretation. Textures and Microstructures 5 (3): 171-190.

Bouchez, J.L., Lister, G.S., and Nicolas, A. 1983. Fabric asymmetry and shear sense in movement zones. Geol. Rundschau 72: 401-419.

Boudier, F. 1976. Le massif lherzolitique de Lanzo (Alpes Piemontaises). Etude structurale et petrologique (in French). Thesis, University of Nantes, 163 pp.

Boudier, F. 1978. Structure and Petrology of the Lanzo peridotite masssif (Piedmont Alps).

Geol. Soc. Am. Bull. 89: 1574-1591.

Bouillin, J.P., Durand-Delgas, M., and Olivier, P. 1986. Betic-Rifean and Tyrrhenian arcs: distinctive features, genesis and development stages. In: The orogin of arcs, ed. Wezel, F.D. Elsevier, Amsterdam, p. 281-304.

Boullier, A.M., and Nicolas, A. 1975. Classification of textures and fabrics of peridotite xenoliths from South Afrika kimberlites. Phys. Chem. Earth 9: 97-105.

Boyd, F.R. 1973. A pyroxene geotherm. Geochim. Cosmochim. Acta 37:2533-2546.

Boyd, F.R., and Nixon, P.H. 1975. Origins of the ultramafic nodules from some kimberlites of northern Lesotho and the Monastery mine, South Africa. Phys. Chem. Earth 9: 431-454.

Brady, J.B., and McCallister, R.H. 1983. Diffusion data for clinopyroxenes from homogenization and self-difusion experiments. Am. Mineral. 68: 95-105.

Brey, G.P., Köhler, T., and Nickel, K.G. 1990. Geothermobarometry in four-phase lherzolites I. Experimental results from 10 to 60 Kb. J. Petrol. 31: 1313-1352.

Brey, G.P., and Köhler, T. 1990. Geothermobarometry in four-phase lherzolites II. New thermobarometers, and practical assessment of existing thermobarometers. J. Petrol. 31:1353-1378.

Buiskool Toxopeus, J.M.A. 1976. Petrofabrics, microtextures and dislocation substructures of olivine in a peridotite mylonite (Alpe Arami, Switzerland). Leidse Geol. Mededel. 51: 1-36.

Burg, J.P. 1986. Quartz shape fabric variations and c-axis fabrics in a ribbon mylonite: argument for an oscillating foliation. J. Struct. Geol. 8: 123-132.

Burg, J.P., Wilson, C.J.L., and Mitchell, J.C. 1986. Dynamic recrystallization and fabric development during the simple shear of ice. J. Struct. Geol. 8: 857-870.

Bussod, G.Y., and Christie, J.M. 1991. Textural development and melt topology in spinel lherzolite experimentally deformed at hypersolidus conditions. J. Petrol., special Lherzolite issue: p. 17-39.

Carey, S.W. 1958. A tectonic approach to continental drift. In: Continental drift, a symposition, ed. Carey, S.W., University of Tasmania, Hobart p. 177-355.

Caroll Webb, S.A., and Wood, B.J. 1986. Spinel-pyroxene-garnet relationships and their dependence on Cr/Al ratio. Contrib. Mineral. Petrol. 92: 471-480.

Carswell, D.A. 1986. The metamorphic evolution of Mg-Cr type Norwegian garnet peridotites. Lithos 19: 279-297.

Carswell, D.A., and Gibb, F.G.F. 1987. Evaluation of mineral thermometers and barometers applicable to garnet lherzolite assemblages. Contrib. Mineral. Petrol. 95: 499-511.

Carter, N.L., and Avé Lallemant, H.G. 1970. High temperature flow of dunite and peridotite. Geol. Soc. Am. Bull. 81: 2181-2202.

Carter, N.L., and Tsenn, M.C. 1987. Flow properties of continental lithosphere. Tectonophysics 136: 27-63.

Carter, N.L., Hansen, F.D., and Senseny, P.E. 1982. Stress magnitudes in natural rock salt. J. Geophys. Res. 87: 9289-9300.

Chiesa, S., Cortesogno, L., Forcella, F., Galli, M., Messiga, B., Pasquare, G., Pedemonte, G.M., Piccardo, G.B., and Rossi, P.M. 1975. Assetto strutturale ed interpretazione geodinamica del Gruppo di Voltri (in Italian). Boll. Soc. Geol. Italiana 94: 555-581.

Chopra, P.N., and Paterson, M.S. 1981. The experimental deformation of dunite. Tectono-physics 78: 453-473.

Chopra, P.N., and Paterson, M.S. 1984. The role of water in the deformation of dunite. J. Geophys. Res. 89: 7861-7876.

Clark, W.A.V., and Hosking, P.L. 1986. Statistical methods for geographers. John Wiley and Sons, 518 pp.

Coisy, P., and Nicolas, A. 1978. Regional structure and geodynamics of the upper mantle beneath the Massif Central. Nature 274: 429-432.

Collée, A.L.G. 1963. A fabric study of lherzolites with special reference to ultrabasic nodular inclusions in the lavas of Auvergne, France. Leidse Geol. Mededel. 28: 1-102.

Conquéré, F. 1978. Pétrologie des complexes ultramafiques de lherzolite à spinelle de L'Ariége (France) (in French). Unpubl. thesis, Univ. Paris VI., France.

Crawford, A.J., Falloon, T.J., and Green, D.H. 1989. Classification, petrogenesis and tectonic setting of boninites. In: Boninites, Crawford, A.J. (ed.), p. 1-49. Unwin Hyman 465 pp. ISBN 0-04-445003-6m

Darot, M. 1973. Methodes d'analyse structurale et cinematique. Application a l'etude du massif ultrabasique de la Sierra Bermeja (in French). Unpubl. thesis, Univ. of Nantes, France.

Darot, M. 1974. Cinématique de L'extrusion, à partir du manteau, des péridotites de la Sierra Bermeja (Serrania de Ronda, Espagne) (in French). C.R. Acad. Sc. Paris, Serie D, 278: 1673-1676.

Davies, G.R., Nixon, P.H., Pearson, D.G., and Obata, M. 1992. Graphitised diamonds from the Ronda peridotite massif, S. Spain. Manuscript in prep.

De Bresser, J.H.P. 1989. Calcite c-axis textures along the Gavarnie thrust zone, central Pyrenees. Geol. Mijnb. 68: 367-375.

De Bresser, J.H.P. 1991. Intracrystalline deformation of calcite. Geologica Ultraiectina 79, Publ. Thesis University of Utrecht. 191 pp.

De Roever, W.P. 1957. Sind die Alpinotypen Peridotitmassen vielleicht tektonisch verfrachtete Bruchstücke der Peridotitschale? (in German). Geol. Rundschau 46: 137-146.

De Jong, K. 1991. Tectono-metamorphic studies and radiometric dating in the Betic Cordilleras (SE Spain) - with implications for the dynamics of extension and compression in the western Meditarranean area. Thesis Free University Amsterdam, 204 p.

Dell'Angelo, L.N. and Tullis, J. 1989. Fabric development in experimentally sheared quartzites. Tectonophysics 169: 1-21.

Den Tex, E. 1969. Origin of ultramafic rocks, their tectonic setting and history: a contribution to the discussion of the paper "The origin of ultramafic and ultrabasic rocks" by P.J. Wyllie. Tectonophysics 7: 457-488.

DePaor, D.G., and Means, W.D. 1984. Mohr circles of the first and second kind and their use to represent tensor operations. J. Struct. Geol. 6: 693-701.

Derby, B. 1990. Dynamic recrystallization and grain size. In: Deformation processes in minerals, ceramics and rocks, eds. D.J. Barber and P.G. Meredith, p. 354-364. Mineralogical society of Great Britain and Ireland, Unwin Hyman, London.

Derby, B., and Ashby, M.F. 1987. On dynamic recrystallization. Scripta Metall. 21: 879-884.

Dercourt, J., Zonenshain, L.P. et al. 1986. Geological evolution of the Tethys belt from the Atlantic belt to the Pamirs since the Lias. Tectonophysics 123, p. 241-315.

Dewey, J.F., Helman, M.L., Turco, E., Hutton, D.H.W., and Knott, S.D. 1989. Kinematics of the western Mediterranean, in Coward, M.P.,

Dietrich, D., and Park, R.G., eds., Alpine tectonics. Geol. Soc. London Sp. Publ. 4: 265-283.

Dickey, J.S. Jr. 1970. Partial fusion products in Alpine-type peridotites: Serrania de Ronda and other examples: Min. Soc. Am. Spec. publ. 3: 33-49.

Didon, J. 1969. Étude géologique du Campo de Gibraltar (Espagne Méridonale) (in French), PhD. thesis, Université de Paris. 539 pp.

Doblas, M., and Oyarzun, R. 1989. "Mantle core complexes" and Neogene extensional detachement tectonics in the western Betic Cordilleras, Spain: an alternative model for the emplacement of the Ronda peridotite. Earth Plan. Sci. Lett. 93: 76-84.

Dodson, M.H. 1973. Closure temperature in cooling geochronological and petrological systems. Contrib. Mineral. Petrol. 40: 259-274.

Dodson, M.H. 1976. Theory of Cooling ages. In: Lectures in Isotope Geology, eds. E. Jäger and C.J. Hunziker. p. 194-202. Springer Verlag ISBN 3-540-09158-0.

Downes, H. 1987. Relationships between geochemistry and textural type in spinel lherzolites, Massif Central and Languedoc, France. In: Mantle Xenoliths (ed. P. Nixon) p. 125-134. Wiley and Sons Ltd.

Drury, M.R. 1992. Theoretical relationships between recrystallized grain-size and deformation conditions. Abstract volume IGC, Kyoto, Japan p. 156.

Drury, M.R., and Urai, J.L. 1990. Deformation-related recrystallization processes. Tectono-physics 172: 235-253.

Drury, M.R., Hoogerduijn Strating, E.H., and Vissers, R.L.M. 1990. Shear zone structures and microstructures in mantle peridotites from the Voltri Massif, Ligurian Alps, NW Italy, Geol. Mijnb. 69: 3-17.

Drury, M.R., Vissers, R.L.M., Van der Wal, D., and Hoogerduijn Strating, E.H. 1991. Shear localization in upper mantle peridotites. PAGEOPH. 137: 439-460.

Durham, W.B., Goetze, C., and Blake, B. 1977. Plastic flow of oriented single crystals of olivine 2. Observations and interpretations of the dislocation structures. J. Geophys. Res. 82: 5755-5770.

Edward, G.H., Etheridge, M.A., and Hobbs, B.E. 1982. On the stress dependence of subgrain size. Textures and Micro-structures 5: 127-152.

Egeler, C.G., and Simon, O.J. 1969. Sur la tectonique de la Zône Bétique (Cordillères Bétiques, Espagne). Verh. K. Ned. Akad. Wet. Afd. Natuurk. Reeks (1), 25: 1-90.

Ellis, D.J., and Green, G.H. 1979. An experimental study of the effect of Ca upon garnet-clinopyroxene Fe-Mg exchange equilibria. Contrib. Mineral. Petrol. 71: 13-22.

Elphick, S.C., Graham, C.M., and Dennis, P.F. 1988. An ion microprobe study of anhydrous oxygen diffusion in Anorthite: a comparison with hydrothermal data and some geological implications. Contrib. Mineral. Petrol. 100: 490-495.

England, P.C., and Houseman, G.A. 1986. The mechanics of the Tibetan plateau. R. Soc. London Phil. Trans. ser. A 326: 301-320.

England, P.C., and Thompson, A.B. 1984. Pressure-temperature-time paths of regional metamorphism, part I: heat transfer during the evolution of regions of thickened continental crust. J. Petrol. 25: 894-928.

England, P.C., and Houseman, G.A. 1989. Extension during continental collision with application to the Tibetan plateau. J. Geophys. Res. 94: 17561-17579.

Finnerty, A.A., and Boyd, F.R. 1984. Evaluation of thermobarometers for garnet

peridotites. Geochim. Cosmochim. Acta 48: 15-27.

Finnerty, A.A., and Boyd, F.R. 1987. Thermobarometry for garnet peridotites: basis for the determination of thermal and compositional structure of the upper mantle. In: Mantle Xenoliths (ed. P. Nixon) p. 381-402. Wiley and Sons Ltd.

Freer, R. 1981. Diffusion in silicate minerals and glasses: a data digest and guide to the literature. Contrib. Mineral. Petrol. 76: 440-454.

Freer, R., Carpenter, M.A., Long, J.V.P., and Reed, S.J.B. 1982. "Null result" diffusion experiments with diopside: implications for pyroxene equilibria. Earth Plan. Sci. Lett. 58: 285: 292.

Frey, F.A., and Green, D.H. 1974. The mineralogy, geochemistry and origin of lherzolite inclusions in Victorian basanites. Geochim. Cosmochim. Acta 38: 1023-1059.

Frey, F.A., Stockman, H.W., and Suen, C.J. 1985. The Ronda high temperature peridotite: Geochemistry and petrogenesis. Geochim. Cosmochim. Acta 49: 2469-2491.

Friedman, M., Dula, W.F., Gangi, A.F., and Gazonas, G.A. 1981. Subgrain size vs. stress in experimentally deformed synthetic rocksalt (abstract). EOS Trans. Am. Geophys. Un. 62: 397.

Gasparik, T. 1984. Two-pyroxene thermobarometry with new experimental data in the system CaO-MgO-Al2O3-SiO2. Contrib. Mineral. Petrol. 87: 87-97.

Goetze, C., and Evans, B. 1979. Stress and temperature in the bending litosphere as constrained by experimental rock mechanics. Geophys. J.R. Astron. Soc. 59: 463-487.

Goffé, B., Michard, A., Garcia-Duenas, V., Gonzalez Lodeiro, F., Monie, P., Campos, P., Galindo Zaldivar, F., Jabaloy, A., Martinez, J.M., and Simancas, J.F., 1989. First evidence of high-pressure, low-temperature metamorphism in the Alpujarride nappes, Betic Cordilleras (SE Spain). Eur. J. Mineral. 1: 139-142.

Graham, C.M., and Elphick, S.C. 1991. Some experimental constraints on the role of Hydrogen in Oxygen and Hydrogen diffusion and Al-Si interdiffusion in silicates. In: Diffusion, atomic ordering and mass transport, ed. J. Ganguly. Adv. in Phys. Geochemistry 8: 248-285 - selected topics in Geochemistry. Springer Verlag.

Green, H.W. 1967. Quartz: extreme preferred orientation produced by annealing. Science 157: 1444-1447.

Green, H.W., and Radcliffe, S.V. 1972. Deformation processes in the upper mantle. Geophys. Monogr., Am. Geophys. Union 16: 139-156.

Green II, H.W., and Gueguen, Y. 1974. Origin of kimberlite pipes by diapyric upwelling in the upper mantle. Nature 249: 617-619.

Green II, H.W., and Burnley, P.C. 1988. Pyroxene-spinel symplectites: Origin by decomposition of garnet confirmed (abstract). EOS Trans. Am. Geophys. Soc. 69: 1514.

Green II, H.W., and Borch, R.S. 1990. High pressure and temperature deformation experiments in a liquid cofining medium. In: The brittle-ductile transition in rocks. Geophys. Monogr., Am. Geophys. Un. 56: 195-200.

Griggs, D.T. 1967. Hydrolitic weakening of quartz and other silicates. Geophys. J. 14: 19-32.

Gueguen, Y., and Darot, M. 1980. Microstructures and stresses in naturally deformed peridotites. Rock Mech. suppl. 9: 159-172.

Handy, M.R. 1989. Deformation regimes and the rheological evolution of fault zones in the lithosphere: the effects of pressure, temperature, grainsize and time. Tectono-physics 163:

119-152.

Hanks, T.C., and Raleigh, C.B. 1980. The conference on magnitude of deviatoric stresses in the earth's crust and uppermost mantle. J. Geophys. Res. B 85: 6083-6085.

Harley, S.L. 1984. An experimental study of the partitioning of Fe and Mg between garnet and orthopyroxene. Contrib. Mineral. Petrol. 86: 359-373.

Hess, H.H. 1938. A Primary peridotite magma. Am J. Sci. 235: 321-344.

Hitchings, R.S., Paterson, M.S., and Bidmead, J. 1989. Effects of iron and magnetite additions in olivine-pyroxene rheology. Phys. Earth. Plan. Int. 55: 277-291.

Hobbs, B.E. 1968. Recrystallization of single crystals of quartz. Tectonophysics 6: 353-401.

Hobbs, B.E., Means, W.D., and Williams, P.F. 1976. An outline of structural geology. John Wiley and sons. 571 pp.

Hollerbach, R. 1985. Kontaktverhältnisse Alpinotyper Peridotitemassen, Petrologische, Geochemische und Mineralfaziele Untersuchungen in der Casares-Einheit am Ronda peridotite, Südspanien (in German). Thesis, University of Würzburg, Germany 190 p.

Holt, D.L. 1970. Dislocation cell formation in metals. J. Appl. Phys. 41: 3197-3201.

Hoogerduijn Strating, E.H., Piccardo, G.B., Rampone, E., Scambelluri, M., Vissers, R.L.M., Drury, M.R. and van der Wal, D. 1990. The structure and petrology of the Erro-Tobbio peridotite, Voltri massif, Ligurian Alps - A two-day excursion with emphasis on processes in the upper mantle, Ofioliti 15: 19-184.

Hoogerduijn Strating, E.H. 1991. The evolution of the Piemonte-Ligurian ocean. Geologica Ultraiectina 74. Publ. Thesis, University of Utrecht. 127 pp.

Houseman, G.A., McKenzie, D.P., and Molnar, P. 1981. Convective instability of a thickened boundary layer and its relevance for the thermal evolution of continental convergent belts. J. Geophys. Res. 86: 6115-6132.

Ingrin, J., Doukhan, N., and Doukhan, J-C. 1991. High-temperature deformation of diopside single crystals 2: Transmission electron microscopy investigation of the defect microstructures. J. Geophys. Res. B 96: 14287-297.

Jackson, E.D. 1968. The character of the lower crust and upper mantle beneath the Hawaiian islands. Proc. 23rd Int. Geol. congres, Prague. p. 135-150.

Jamtveit, B., Carswell, D.A., and Mearns, E.W. 1991. Chronology of the high-pressure metamorphism of Norwegian garnet peridotites/pyroxenites. J. Metamorphic Geol. 9: 125-139.

Jenkins, D.M. 1983. Stability and composition relations of calcic amphiboles in ultramafic rocks. Contrib. Mineral. Petrol. 83: 375-384.

Jessell, M.W. 1986. Grain boundary migration and fabric development in experimentally deformed Octachloropropane. J. Struct. Geol. 8: 527-542.

Jin, Z-M., and Green II, H.W. 1989. Microstructures of olivine and stresses in the upper mantle beneath eastern China. Tectonophysics 169: 23-50.

Karato, S. 1987. Scanning electron microscope observation of dislocations in olivine. Phys. Chem. Minerals 14: 245-248.

Karato, S. 1988. The role of recrystallization in the preferred orientation of olivine. Phys. Earth Planet. Int. 51: 107-122.

Karato, S. 1989. Grain growth kinetics in olivine aggregates. Tectonophysics 168: 255-273.

Karato, S., Paterson, M.S., and FitzGerald, J.D. 1986. Rheology of synthetic olivine aggregates: influence of grain size and water. J. Geophys. Res. 91: 8151-8176.

Karato, S., Toriumi, M., and Fujii, T. 1980. Dynamic recrystallization of olivine single crystals during high-temperature creep. Geophys. Res. Lett. 7: 649-652.

Karato, S., Toriumi, M., and Fujii, T. 1982. Dynamic recrystallization and high-temperature rheology of olivine. In: High pressure research in Geophysics, ed. S. Akimoto and M.H. Manghnani, Adv. Earth Planet. Sci. 12: 171-189.

Kelemen, P.B. 1990. Reaction between ultramafic rock and fractionating basaltic magma I. Phase relations, the origin of calc-alkaline magma series, and the formation of discordant dunite. J. Petrol. 31: 51-98.

Kennedy, C.S., and Kennedy, G.C. 1976. The equilibrium boundary between graphite and diamond. J. Geophys. Res. 81: 2467-2470.

Kingery, W.D., Bowen, H.K., and Uhlmann, D.R. 1976. Introduction to Ceramics. Wiley series on the Science and Technology of materials. John Wiley & Sons 1032 pp.

Kirby, S.H. 1985. Rock mechanics observations pertinent to the rheology of the continental lithosphere and the localisation of strain along shear zones. Tectonophysics 119: 1-27.

Knipe, R.J. 1989. Deformation mechanisms - recognition from natural tectonites. J. Struct. Geol. 11: 127-146.

Kohlstedt, D.L., and Goetze, C. 1974. Low-stress High temperature creep in olivine single crystals. J. Geophys. Res. 79: 2045-2051.

Kohlstedt, D.L., Goetze, C., Durham, W.B., and VanderSande, J. 1976. New technique for decorating dislocations in olivine. Science 191: 1045-1046.

Kornprobst, J. 1969. Le masif ultrabasique des Beni Bouchera (Rif Interne, Maroc): étude des péridotites de haute température et de haute pression et des pyroxénites, à grenat ou sans grenat qui leur sont associées (in French). Contrib. Mineral. Petrol. 23: 283-322.

Kornprobst, J. 1974. Contribution a l'étude pétrographique et structurale de la zone interne du rif (in French). Notes et Mém. Serv. géol. Maroc 251, 256 p.

Kornprobst, J., Piboule, M., Roden, M., and Tabit, A. 1990. Corundum-bearing Garnet clinopyroxenites at Beni Bousera (Morocco): Original plagioclase-rich Gabbros recrystallized at depth within the mantle? J. Petrol. 31: 717-745.

Kramer, M.J., and Seifert, K.E. 1991. Strain enhanced diffusion in Feldspars. In: Diffusion, atomic ordering and mass transport, ed. J. Ganguly. Adv. in Phys. Geochemistry 8: 286-303 - selected topics in Geochemistry. Springer Verlag.

Kretz, R. 1982. Transsfer and exchange equilibria in a portion of the pyroxene quadrilateral as deduced from natural and experimental data. Geochim. Cosmochim. Acta 46: 411-421.

Kuznir, N.J., and Park, R.G. 1984. The strength of intraplate lithosphere. Phys. Earth Plan. Int. 36: 224-235.

Lacroix, A. 1917. Les péridotites des Pyrénées et les autres roches intrusives non feldspatiques qui les accompagnent (in French). Cr. Acad. Sci. Paris 165:381-387.

Lambeck, K. 1980. Estimates of stress differences in the crust from isostatic considerations. J. Geophys. Res. B 85: 6397-6402.

Law, R.D. 1990. Crystallographic fabrics: a selective review of their applications to research in structural geology. In: Deformation mechanisms, rheology and tectonics,

eds. R.J. Knipe and E.H. Rutter. Spec. Publ. Geol. Soc. London 54: 335-352.

Law, R.D., Knipe, R.J., and Dayan, H. 1984. Strain path partitioning within thrust sheets: microstructural and petrofabric evidence from the Moine thrust zone at Loch Eriboll, NW Scotland. J. Struct. Geol. 6: 477-498.

Leblanc, D., and Olivier, P. 1984. Role of strike-slip fualts in the Betic Rifean orogeny. Tectonophysics 101: 344-355.

Lee, H.Y., and Ganguly, J. 1988. Fe-Mg fractionation between garnet and orthopyroxene: experimental data and applications. Geol. Soc. Amer. Abstr. Progr. 16: 572-573.

Lemoine, M., Tricart, P., and Boillot, G. 1987. Ultramafic and gabbroic ocean floor of the Ligurian Tethys (Alps, Corsica, Apennines): in search of a genetic model. Geology 15: 622-625.

Lindsley, D.H. 1983. Pyroxene thermometry. Am. Mineral. 68: 477-493.

Lister, G.S., and Snoke, A.W. 1984. S-C mylonites. J. Struct. Geol. 6: 617-638.

Lister, G.S., and Williams, P.F. 1979. Fabric development in shear zones: theoretical controls and observed phenomena. J. Struct. Geol. 1: 283-298.

Loomis, T.P. 1972a. Contact metamorphism of pelitic rock by the Ronda ultramafic intrusion, southern Spain. Geol. Soc. Am. Bull. 83: 2449-2474.

Loomis, T.P. 1972b. Diapiric emplacement of the Ronda high temperature ultramafic intrusion, southern Spain. Geol. Soc. Am. Bull. 83: 2475-2496.

Loomis, T.P. 1975. Tertiairy mantle diapirism, orogeny and plate tectonics east of the Strait of Gibraltar. Am. J. Sci. 275: 1-30.

Lundeen (Thompson), M. 1978. Emplacement of the Ronda peridotite, Sierra Bermeja, Spain. Geol. Soc. Am. Bull. 89: 172-180.

Matsumoto, K., and Toriumi, M. 1989. Mechanical states of the upper mantle under the island arc as inferred from the microstructures of peridotite xenoliths. In: Rheology of solids and of the Earth. Eds. S. Karato and M. Toriumi. p. 374-392. Oxford University Press.

McDonough, W.F., and Frey, F.A. 1989. Rare Earth elements in upper mantle rocks. In: Geochemistry and Mineralogy of Rare Earth elements. Reviews in Mineralogy 21: 99-145.

Means, W.D. 1982. An unfamiliar Mohr circle construction for finite strain. Tectonophysics 89: T1-T6.

Means, W.D. 1983. Application of the Mohr-circle construction to problems of inhomogeneous deformation. J. Struct. Geol. 5: 279-286.

Means, W.D. 1990. Kinematics, stress, deformation and material behaviour. J. Struct. geol. 12: 953-971.

Menzies, M.A., and Dupuy, C. 1991. Orogenic Massifs: Protolith, processes and provenance. J. Petrol. special volume orogenic lherzolites and mantle processes: p. 1-16.

Mercier, J-C. C. 1980. Single-pyroxene thermobarometry. Tectonophysics 70: 1-37.

Mercier, J-C. C. 1985. Olivine and Pyroxenes. In: Preferred orientation in deformed metals and rocks: an introduction to modern texture analysis, ed. H.R. Wenk. p. 407-430.

Mercier, J-C. C., and Nicolas, A. 1975. Textures and Fabrics of upper-mantle peridotites as illustrated by xenoliths from basalts. J. Petrol. 16: 454-487.

Mercier, J-C. C., Anderson, D.A., and Carter, N.C. 1977. Stress in the Lithosphere: inferences from steady state flow of rocks.

PAGEOPH. 115: 199-226.

Michard, A., Goffé, B., Chalouan, A., and Saddiqi, O. 1991. Les corrélations entre les Chaînes bético-rifaines et les Alpes et leurs conséquences (in French). Bull. Soc. géol. France 162: 1151-1160.

Möckel, J.R. 1969. The structural petrology of the garnet-peridotite of Alpe Arami (Ticino, Switserland). Leidse Geol. Mededel. 42: 61-130.

Monié, P., Galindo Zaldivar, J., Gonzalez Lodeiro, F., Goffé, B., and Jabaloy, A. 1991. $^{40}Ar/^{39}Ar$ geochronology of Alpine tectonism in the Betic Cordilleras (Spain). J. Geol. Soc. London 148: 289-297.

Mukhopadhyay, B. 1991. Garnet breakdown in some deep seated garnetiferous xenoliths from the central Sierra Nevada: petrologic and tectonic implications. Lithos 27: 59-78.

Mulder, C.J., and Parry, G.R. 1977. Late Tertiairy evolution of the Alboran Sea at the eastern entrance of the Straits of Gibraltar, in Biju-Duval, B., and Montadert, L., eds., The structural history of the Mediterranean basins, Paris, Editions Technip., p. 401- 410.

Nakada, M., 1983. Rheological structure of the Earth's mantle derived from glacial rebound in Laurentide. J. Phys. Earth 31: 349-386.

Nicolas, A. 1978. Stress estimates from structural studies in some mantle peridotites. Phil. Trans. R. Soc. London A. 288: 49-57.

Nicolas, A. 1984. Lherzolites of the western Alps, a structural review. In: Kimberlites, II: the mantle and crust-mantle relationships (ed. J. Kornprobst), Elsevier, Amsterdam.

Nicolas, A. 1986. Structure and petrology of peridotites: clues to their geodynamic environment. Rev. Geophys. 24: 875-895.

Nicolas, A., and Boudier, F. 1975. Kinematic interpretation of folds in Alpine-type peridotites. Tectonophysics 25: 233-260.

Nicolas, A., and Poirier, J-P. 1976. Crystalline plasticity and solid state flow in metamorphic rocks. John Wiley and Sons, 445 pp.

Nicolas, A., Bouchez, J-L., Boudier, F., and Mercier, J-C.C. 1971. Textures, structures and fabrics due to solid-state flow in some European lherzolites. Tectonophysics 12: 55-86.

Nicolas, A., Boudier, F., and Montigny, R. 1987. Structure of Zabargad Island and early rifting of the Red. Sea. J. Geophys. Res. 92: 461-474.

Nicolas, A., Ceuleneer, G., Boudier, F., and Misseri, M. 1988. Structural mapping in the Oman ophiolites: Mantle diapirism along an oceanic ridge. Tectonophysics 151: 27-56.

Niida, K. 1984. Petrology of the Horoman ultramafic rocks in the Hidaka metamorphic belt, Hokkaido, Japan. Journ. Fac. Sci., Hokkaido Univ. Ser. IV 21: 197-250.

Norell, G.T., and Harper, G.D. 1988. Detachment faulting and a magmatic extension at mid-ocean ridges: The Josephine ophiolite as an example. Geology 16: 827-830.

Norton, M.G. 1982. The kinematic and micro-structural development of some shear zones. Thesis, Imperial college of Science and Technology, Univ. of London.

O'Hara, M.J. 1967. Mineral facies in ultramafic rocks. In P.J. Wyllie ed., Ultramafic and related rocks. J. Wiley and Sons Inc. New York: p. 7-17.

O'Neill, H.St. C. 1982. The transition between spinel lherzolite and garnet lherzolite and its use as a geobarometer. Contrib. Mineral. Petrol. 77: 185-194.

Obata, M, Suen, J., and Dickey Jr., J.S. 1977. The origin of mafic layers in the Ronda high-temperature peridotite intrusion, S. Spain: an evidence of partial fusion and fractional crystallization in the upper mantle. Coll. Int.

du C.N.R.S. 272: 257-268.

Obata, M. 1980. The Ronda peridotie: Garnet-, Spinel-, and Plagioclase-Lherzolite facies and the P-T trajectories of a high-temperature mantle intrusion. J. Petrol. 21: 533-572.

Ord, A., and Christie, J.M. 1984. Flow stresses from microstructures in mylonitic quartzites of the Moine Thrust zone, Assynt area, Scotland. J. Struct. Geol. 6: 639-654.

Osete, M.L., Freeman, R., and Vegas, R. 1988. Preliminary paleomagnetic results from the Subbetic Zone (Betic Cordilleras, southern Spain): kinematic and structural implications. Phys. Earth Plan. Int. 52: 283-300.

Oxburgh, E.R., and Turcotte, D.L. 1974. Thermal gradients and regional metamorphism in overthrust terrains with special reference to the eastern Alps. Schw. Mineral. Petrol. Mitt. 54: 641-662.

Passchier, C.W. 1986. Mylonites in the continental crust and their role as seismic reflectors. Geol. Mijnb. 65: 167-176.

Passchier, C.W. 1987. Efficient use of the velocity gradients tensor in flow modelling. Tectonophysics 136: 159-163.

Passchier, C.W. 1988a. The use of Mohr circles to describe on-coaxial progressive deformation. Tectonophysics 149: 323-338.

Passchier, C.W. 1988b. Analysis of deformation paths in shear zones. Geol. Rundschau 77: 309-318.

Passchier, C.W., and Simpson, C. 1986. Porphyroclast systems as kinematic indicators. J. Struct. Geol. 8: 831-843.

Paterson, M.S. 1970. A high temperature high pressure apparatus for rock deformation. Int. J. Rock Mech. Min. Sci. 7: 517-526.

Pearson, D.G., Davies, G.R., Nixon, P.H., and Milledge, H.J. 1989. Graphitized diamonds from a peridotite massif in Morocco and implications for anomalous diamond occurrences. Nature 338: 60-62.

Pearson, D.G., Davies, G.R., and Nixon, P.H. Geochemical constraints on the petrogenesis of diamond facies pyroxenites from the Beni Bousera peridotite massif, N Morocco. Submitted J. Petrol.

Phakey, P., Dollinger, G., and Christie, J. 1972. Transmission Electron Microscopy of experimentally deformed olivine crystals. Geophys. Monogr., Am. Geophys. Union 16: 117-138.

Piccardo, G.B., Cortesogno, L., Messiga, B., Galli, M., and Pedemonte, G.M. 1977. Excursion to the metamorphic ophiolites of the Gruppo di Voltri, Rend. Soc. Italia Min. Petr. 33: 453-472.

Pickering, F.B. 1976. The basis of quantitative metallography. Metals and metallurgy trust for the Institute of metallurgical technicians. London, 38 pp.

Pike, J.E.N., and Schwartzman, E.C. 1977. Classification of textures in ultramafic xenoliths. J. Geol. 85: 49-61.

Platt, J.P., and Behrmann, J.H. 1986. Structures and fabrics in a crustal-scale shear zone, Betic Cordillera, SE Spain. J. Struct. Geol. 8: 15-34.

Platt, J.P., and Vissers, R.L.M. 1980. Extensional structural in anisotropic rocks. J. Struct. Geol. 2: 397-410.

Platt, J.P., and Vissers, R.L.M. 1989. Extensiona collapse of thickened continental lithosphere: a working hypothesis for the Alboran Sea and Gibraltar arc. Geology 17: 540-543.

Platt, J.P., and England, P.C. Convective removal of lithosphere beneath mountain belts: thermal and mechanical consequences. Am. J. Sci. (in press).

Platt, J.P., van den Eeckhout, B., Janzen, E.,

Kohnert, G., Simon, O.J., and Weijermars, R. 1983. The structure and tectonic evolution of the Aguilón fold-nappe, Sierra Alhamilla, Betic cordilleras, SE Spain. J. Struct. Geol. 5: 519- 538.

Platzman, E.S., and Lowrie, W. 1992. Paleomagnetic evidence for rotation of hte Iberian Peninsula and the external Betic Cordillera, Southern Spain. Earth Plan. Sci. Lett. 108: 45-60.

Platzman, E.S. 1992. Paleomagnetic rotations and the kinematics of the Gibraltar arc. Geology 20: 311-314.

Poirier, J-P. 1980. Shear locaization and shear instability in materials in the ductile field. J. Struct. Geol. 2: 135-142.

Poirier, J-P. 1985. Creep of crystals. Cambridge University Press. 260 pp.

Poirier, J-P., and Guillopé, M. 1979. Deformation induced recrystallization of minerals. Bull. Mineral. 102: 67-74.

Post, R.L. 1977. High-temperature creep of Mt. Burnet dunite. Tectonophysics 42: 75-110.

Priem, H.N.A.K., Hebeda, E.H., Boelrijk, N.A.I.M., Verdurmen, Th.E.A., and Oen, I.S. 1979. Isotopic dating of the emplacement of the ultramafic masses in the Serrania de Ronda, Southern Spain. Contrib. Mineral. Petrol. 70: 103-109.

Quick, J.E. 1981. The origin and significance of large, tabular dunite bodies in the Trinity peridotite, Northern California. Contrib. Mineral. Petrol. 78: 413-422.

Raleigh, C.B., and Kirby, S.H. 1970. Creep in the upper mantle. Mineral. Soc. Amer. Spec. Pap. 3: 113-121.

Ramberg, H. 1960. Relationships between length of arc and thickness of ptygmatically folded veins. Am. J. Sci. 258: 36-46.

Ramsay, J.G. 1967. Folding and fracturing of rocks. McGraw-Hill, New York. 568 pp.

Ramsay, J.G., and Graham, R.H. 1970. Strain variation in shear belts. Can. J. Earth Sci. 7: 786-813.

Ramsay, J.G., and Huber, M.I. 1987. The techniques of modern structural geology, Vol. 2: Folds and Fractures. Academic Press, 700 pp.

Ranalli , G. 1984. Grain size distribution and flow stress in tectonites. J. Struct. Geol. 6: 443-447.

Ranalli, G., and Murphy, D.C. 1987. Rheological stratification of the lithosphere. Tectonophysics 132: 281-295.

Reisberg, L.C., and Zindler, A. 1986/87. Extreme isotopic variations in the upper mantle: evidence from Ronda. Earth Plan. Sci. Lett. 81: 29-45.

Reisberg, L.C., Allègre, C.J., and Luck, J-M. 1991. The Re-Os systematics of the Ronda ultramafic comples of southern Spain. Earth Plan. Sci. lett. 105: 196-213.

Remaïdi, M., Gervilla, F., Bodinier, J-L., Leblanc, M., and Torres-Ruiz, J. 1991. Harzburgite, dunite and pyroxenite association in the Ronda ultramafic bodies - Geochemical evidence - reaction processes in sub-continental mantle. In: Meeting of the working group of IGCP project no. 256 "Ophiolite genesis and the evolution of oceanic lithosphere", Abstracts and field trips guide p. 15-18. Puga, E., Díaz de Federico, A., Torres-Roldán, R.L., Molina-Palma, J.F., Nieto, J.M., and Tendero-Segovia, J.A., eds., ISBN: 84-600-7773-X.

Reuber, I., Michard, A., Chalovan, A., Juteau, T., and Jermoumi, B. 1982. Structure and emplacement of the Alpine-type peridotites from Beni Bousera, Rif, Morocco, a polyphase tectonic interpretation. Tectonophysics 82: 231-251.

Ribe, N.M., and Yu, Y. 1991. A theory for plastic deformation and textural evolution of olivine polycrystals. J. Geophys. Res. 96 B: 8325-8335.

Ricoult, D. 1979. Experimental annealing of a natural dunite. Bull. Mineral. 102: 86-91.

Riegger, O.K., and Van Vlack, L.H. 1960. Dihedral angle measurement. Trans. Metall. Soc. Aime 218: 933-935.

Ross, J.V., Avé Lallemant, H.G., and Carter, N.L. 1980. Stress dependence of recrystallized grain and subgrain size in olivine. Tectonophysics 70: 39-61.

Rutter, E.H., and Brodie, K.H. 1988. The role of tectonic grain size reduction in the rheological stratification of the lithosphere. Geol. Rundschau 77: 295-308.

Rutter, E.H., Atkinson, B.K., and Mainprice, D.H. 1978. On the use of the stress relaxation testing method in studies of the mechanical behaviour of geological materials. Geophys. J. R. Astr. Soc. 55: 155-170.

Sachtleben, T., and Seck, H.A. 1981. Chemical control al Al-solubility in orthopyroxene and its implications to pyroxene geothermometry. Contrib. Mineral. Petrol. 78: 157-165.

Saddiqi, O. 1988. Tectonique de la remontée du manteau: les péridotites des Beni Bousera et leur envoloppe métamorphique, Rif interne, Maroc (in French), thesis Univ. Strasbourg, France.

Saddiqi, O., Reuber, I., and Michard, A. 1988. Sur de tectonique de dénudation du manteau infracontinental dans les Beni Bousera, Rif septentrional, Maroc (in French). C.R. Acad. Sci. Paris 307: (II) 657-662.

Sander, B. 1950. Einführung in die Gefügekunde der Geologischen Körper, Part II: Die Korngefüge (in German). Springer Verlag, Wien und Innsbruck, 399 pp.

Sautter, V., and Fabriès, J. 1990. Cooling kinetics of garnet websterites from the Freychinède orogenic lherzolite masif, French Pyrenees. Contrib. Mineral. Petrol. 105: 533-549.

Sautter, V., and Harte, B. 1988. Diffusion gradients in an Eclogite xenolith from the Roberts Victor kimberlite Pipe: 1. Mechanism and evolution of garnet exsolution in Al2O3-rich clinopyroxene. J. Petrol. 29: 1325-1352.

Sautter, V., Jaoul, O., and Abel, F. 1988. Aluminium diffusion in diopside using the $^{27}Al(p,\gamma)^{28}Si$ nuclear reaction: preliminary results. Earth Plan. Sci. Lett. 89: 109-114.

Schmid, E. 1928. Zn-normal stress law. In: Proc. Int. Congr. on applied mechanics, Delft, the Netherlands.

Schmid, S.M. 1982. Microfabric studies as indicators of deformation mechanisms and flow laws operative in mountain building. In: Mountain Building Processes (ed. Hsu, K.J.) p. 95-110. Acad. Press. London.

Schmid, S.M., Panozzo, R., and Bauer, S. 1987. Simple shear experiments on calcite rocks: rheology and microfabric. J. Struct. Geol. 9: 747-778.

Schubert, W. 1977. Reaktionen im alpinotypen Peridotitmassiv von Ronda (Spanien) und seinen partiellen Schmelzprodukten (in German). Contrib. Mineral. Petrol. 62: 205-220.

Schubert, W. 1982. Comments on 'The Ronda peridotite: Garnet-, Spinel-, and Plagioclase-Lherzolite Facies and the P-T trajectories of a High-Temperature mantle intrusion by M. Obata (J. Petrol. 21: 533-72, 1980). J. Petrol. 23: 293-295.

Simpson, C., and Schmid, S.M. 1983. An evaluation of criteria to deduce the sense of movement in sheared rocks. Bull. Geol. Soc. Am. 94: 1281-1288.

Smith, D. 1977. The origin and interpretation

of spinel-pyroxene clusters in peridotite. J. Geol. 85: 476-482.

Smith, D., and Barron, B.R. 1991. Pyroxene-garnet equilibration during cooling in the mantle. Am. Mineral. 76: 1950-1963.

Solomon, S.C., Richardson, R.M., and Bergman, E.A. 1980. Tectonic stress: models and magnitudes. J. Geophys. Res. 85 B: 6086-6092.

Spear, F.S. 1989. Petrologic determination of Metamorphic Pressure-Temperature-Time paths. In: Metamorphic Pressure-Temperate-Time paths, Short course in Geology nr. 7, Am. Geophys. Union.

Steinmann, G. 1906. Geologische beobachtungen in den Alpen, II. Die Schardt'sche Überfaltungstheorie und die geologische Bedeutung der Tiefseeabsätze und der ophiolitischen Massengesteine. Ber. Naturforsch. Ges. freiberg, Breisgau 16: 1-49.

Suen, C.J., and Frey, F.A. 1987. Origins of the mafic and ultramafic rocks in the Ronda peridotite. Earth planet. Sci. Lett. 85: 183-202.

Tabit, A., Kornprobst, J., Li, J.P., and Woodland, A.B. 1990. Origin and evolution of the massif at Beni Bousera, Morocco: petrological evidence. In: Intern. workshop on orogenic lherzolites and mantle processes (Abstract), Blackwell, p. 19.

Takahashi, E., and Kushiro, I. 1983. Melting of a dry peridotite at hih pressures and basalt magma genesis. Am. Mineral. 68: 859-879.

Takahashi, N. 1992. Evidence for melt segregation towards fractures in the Horoman mantle peridotite complex. Nature 359: 52-55.

Takazawa, E., Frey, F.A., Shimizu, N., Obata, M., and Bodinier, J.L. 1992. Geochemical evidence for melt migration and reaction in the upper mantle. Nature 359: 55-58.

Takeuchi, S., and Argon, A.S. 1976. Steady state creep of single-phase crystalline matter at high temperature. J. Mat. Sci 11: 1542-1566.

Taylor, G.I. 1938. Plastic strain in metals. J. Inst. Metals 632: 307-324.

Thompson, I.B. 1992. Water in the Earth's upper mantle. Nature 358: 295-301.

Toriumi, M. 1979. Relation between dislocation density and subgrain size in naturally deformed olivine in peridotites. Contrib. Mineral. Petrol. 68: 181-186.

Toriumi, M. 1982. Grain boundary migration in olivine at atmospheric pressure. Phys. Earth. Planet. Inter. 30: 26-35.

Torné, M., Banda, E., García-Dueñas, V., and Balanya, J.C. 1992. Mantle-lithosphere bodies in the Alboran crustal domain (Ronda peridotites, Betic-Rif orogenic belt). Earth Plan. Sci. Lett. 110: 163-171.

Torres Roldán, R.L. 1979. The tectonic subdivision of the Betic zone (Betic Cordilleras, southern Spain): its significance and one possible geotectonic scenario for the westernmost Alpine belt. Am. J. Sci. 279: 19-51.

Torres Roldán, R.L. 1981. Plurifacial metamorphic evolution of the Sierra Bermeja peridotite aureole (Southern Spain). Est. Geol. 37: 115-133.

Torres Roldán, R.L., Poli, G., and Peccerillo, A. 1986. An early Miocene are-tholeiitic magmatic dike event from the Alboran sea - evidence for precollisional subduction and back-arc crustal extension in the westernmost mediterraenean. Geol. Rundschau 75: 219-234.

Truesdell, C. 1954. The kinematics of vorticity. Indiana University Press, Bloomington, Ind.

Tubia, J.M. 1990. Comment on "Mantle core complexes and Neogene extensional detach-

ment tectonics in the western Betic Cordilleras, Spain: an alternative model for the emplacement of the Ronda peridotie" by Migual Doblas and Roberto Oyarzun. Earth Plan. Sci. Lett. 96: 499-500.

Tubia, J.M., and Cuevas, J. 1986. High temperature emplacement of the Los Reales peridotite nappe (Betic Cordillera, Spain). J. Struct. Geol. 8: 473-482.

Tubia, J.M., and Cuevas, J. 1987. Structures et cinématique liées à la mise en place des péridotites de Ronda (Cordillères Bétiques, Espagne) (in French). Geodyn. Acta 1: 59-69.

Tullis, J., and Yund, R.A. 1985. Dynamic recrystallization of Feldspar: a mechanism for ductile shear zone formation. Geology 13: 283-241.

Tullis, T.E., and Horowitz, F. 1980. The strength of dry olivine. Eos Trans. Am. Geophys. Un. 61: 375-376.

Twiss, R.J. 1977. Theory and applicability of a recrystallized grain size palaeopiezometry. PAGEOPH. 115: 227-244.

Twiss, R.J. 1986. Variable sensitivity piezometric equations for dislocation density and subgrain diameter and their relevance to olivine and quartz. In: Mineral and rock deformation: laboratory studies - The Paterson Volume. Geophys. Monogr. Am. Geophys. Un. 36: 247-261.

Urai, J.L., Means, W.D., and Lister, G.S. 1986. Dynamic recrystallization of minerals. Mineral and Rock deformation: Laboratory Studies - The Paterson Volume. Geophys. Monogr. Am. Geophys. Un. 36: 161-199.

Van Bemmelen, R.W. 1969. Origin of the western Mediterranean sea. Geol. Mijnbouw 26: 13-52.

Van den Beukel, J., and Wortel, R. 1988. Thermo-mechanical modelling of arc-trench regions. Tectonophysics 154: 177-193.

Vauchez, A., and Nicolas, A. 1991. Mountian building: strike-parallel motion and mantle anisotropy. Tectonophysics 185: 183-201.

Vissers, R.L.M., Drury, M.R., Hoogerduijn Strating, E.H., and van der Wal, D. 1991. Shear zones in the upper mantle - a case study in an Alpine lherzolite massif. Geology 19: 990-993.

Vissers, R.L.M. 1989. Asymmetic quartz c-axis fabrics and flow vorticity: a study using rotated garnets. J. Struct. Geol.11: 231-244.

Waff, H.S., and Bulau, J.R. 1979. Equilibrium fluid distribution in an ultramafic partial melt under hydrostatic stress conditions. J. Geophys. Res. 84: 6109-6114.

Waff, H.S., and Bulau, J.R. 1982. Experimentally determination of near-equilibrium textures in partially molten silicates at high pressures, in High Pressure research in Geophysics, eds. S. Akimoto and M.H. Manghani. Adv. Earth Planet. Sci. 12: 229-236 Center for academic publications, Tokyo.

Wallace, M.E., and Green, D.H. 1991. An experimental determination of primary carbonatite magma composition. Nature 335: 343-346.

Wells, P.R.A. 1977. Pyroxene thermometry in simple and complex systems. Contrib. Mineral. Petrol. 62: 129-139.

Wenk, H-R., and Christie, J.M. 1991. Comments on the interpretation of deformation textures in rocks. J. Struct Geol. 13: 1091-1110.

Wenk, H-R., Bennett, K., Canova, G.R., and Molinari, A. 1991. Modelling plastic deformation of peridotite with the self-consistent theory. J. Geophys. Res. 96 B: 8337-8349.

Westerhof, A.B. 1977. On the contact relations of high-temperature peridotites in the Serrania de Ronda, Southern Spain. Tectonophysics 39: 579-591.

Westra, G. 1969. Petrogenesisof a composite metamorphic facies series in an intricate fault zone in the south-eastern Sierra Cabrera, SE Spain. Thesis University of Amsterdam, 166 pp.

White, S.H. 1976. The effects of strain on the microstructures, fabrics, and deformation mechanisms in quartzites. Phil. Trans. R. Soc. London. 283A: 69-86.

White, S.H. 1979a. Difficulties associated with palaeostress estimates. Bull Mineral. 102: 210-215.

White, S.H. 1979b. Grain and subgrain size variations across a mylonite zone. Contrib. Mineral. Petrol. 70: 193-202.

White, S.H., and Knipe, R.J. 1978. Transformation- and reaction-enhanced ductility in rocks. J. Geol. Soc. London. 135: 513-516.

White, S.H., Burrows, S.E., Carreras, J., Shaw, N.D., and Humphreys, F.J. 1980. On mylonites in ductile shear zones. J. Struct. Geol. 2: 175-187.

White, S.H., Drury, M.R., Ion, S.E., and Humphreys, F.J. 1985. Large strain deformation studies using polycrystalline magnesium as a rock analogue. Part I: grain size paleopiezometry in mylonite zones. Phys. Earth Plan. Int. 40: 201-207.

White, S.H., Evans, D., and Zhong, D-L. 1982. Fault rocks of the Moine Thrust Zone: Microstructures and textures of selected mylonites. Textures and Microstructures 5: 33-61.

Witt-Eikschen, G., and Seck, H.A. 1991. Solubility of Ca and Al in orthopyroxene from spinel peridotite: an improved version of an empirical geothermometer. Contrib. Mineral. Petrol. 106: 431-439.

Wood, B.J., and Banno, S. 1973. Garnet-orthopyroxene and orthopyroxene-clinopyroxene relationships in simple and complex systems. Contrib. Mineral. Petrol. 42: 109-124.

Young, C.M., and Sherby, O.D. 1973. Subgrain formation and subgrain-boundary strengthening in iron-based materials, J. Iron and Steel Inst. 211: 640-647.

Zeck, H.P., Monié, P., Villa, I.M., and Hansen, B.T. 1992. Very high rates of cooling and uplift in the Alpine belt of the Betic Cordilleras, southern Spain. Geology 20: 79-82.

Zeuch, D.H. 1982. On the inter-relationships between grain size sensitive creep and dynamic recrystallization of olivine. Tectonophysics 93: 151-168.

Zeuch, D.H., and Green II, H.W. 1984. Experimental deformation of a synthetic dunite at high temperature and pressure. I. Mechanical behaviour, optical microstructure and deformation mechanism. Tectonophysics 110: 233-262.

Zindler, A., Staudigel, H., Hart, S.R., Endres, R., and Goldstein, S. 1983. Nd and Sr isotopic study of a mafic layer from Ronda ultramafic complex. Nature 304: 226-230.

Appendix

A1: Stability and composition relations in ultramafic rocks, calibrated for the Ronda peridotite.

A major objective of this thesis is the assessment of ambient conditions prevailing during deformation in the upper mantle. Shown in App. A1 are phase relations in the system CaO-Mgo-Al2O3-SiO2-Na2O-H2O in a petrogenetic P-T diagram for ultramafic systems (lherzolites and pyroxenites). For feasible continental and oceanic geotherms, five peridotite metamorphic facies field can be distinguished. These are, in order of decreasing pressure conditions:

1: The diamond-peridotite stability field (DMD), characterized by the stability of diamonds.
2: The garnet-peridotite stability field (GRT), defined by the stability of garnet, both in the host lherzolites and in enclosed pyroxenite layers.
3: The spinel-peridotite stability field (SPL), defined by stability of spinel in lherzolite and harzburgite.
4: The plagioclase-peridotite stability field (PLAG) , defined by the stability of plagioclase in lherzolite, harzburgite or pyroxenite.
5: The chlorite-peridotite stability field (CHT), defined by the stability of chlorite.

The spinel-peridotite stability field can be further subdivided in two fields: the Ariégite subfacies of the spinel-peridotite facies (AR) and Seiland subfacies of the spinel-peridotite facies (SE) (O'Hara 1967). The Ariégite subfacies is defined by the occurrence of garnet pyroxenite layers in spinel lherzolites or harzburgites. Garnet pyroxenites are no longer stable in the lower-pressure Seiland subfacies characterized by spinel pyroxenites. Although the term "Ariégite" has historically been assigned to high-Cr spinel pyroxenites from the Pyrenean lherzolites (LaCroix 1917), the O'Hara (1967) classification is frequently applied to the Ronda peridotite.

The different facies fields in PT space are strongly dependent on the rock and mineral chemistry (e.g. O'Neill 1982). For each particular peridotite massif or xenolith suite, a facies diagram can be constructed which incorporates their chemical signature. Fig. A1 shows a calibrated facies diagram for the Ronda peridotite, compiled on the basis of the following references: (1): Jenkins 1983, (2): O'Neill 1981 and Caroll Webb and Wood 1986, (3): Obata et al. 1977, (4): Kennedy and Kennedy 1976. The peridotite solidi for dry systems (5), and H2O (0.3%) and CO2 (0.5-2.5%) saturated systems (6) and (7) are from Takahashi and Kushiro (1983) and Wallace and Green (1991), respectively.

The position of the transition from spinel peridotite to garnet peridotite has been corrected for the Cr-content of spinel following Caroll Webb and Wood (1986). For the appropriate composition of spinel in the spinel tectonites and garnet-spinel mylonites (Cr/(Cr+Al) = 0.12, see Table 4.2), this correction corresponds to a shift of about 300 MPa towards higher pressures. This shift is largely compensated by a negative "FeO" correction following O'Neill 1982. This latter correction corresponds to a shift of ~200 MPa towards lower pressures for olivine compositions of Fo90. The transition from spinel pyroxenite to olivine gabbro roughly coincides with the transition from spinel-lherzolites to plagioclase-lherzolites and is not shown in the diagram.

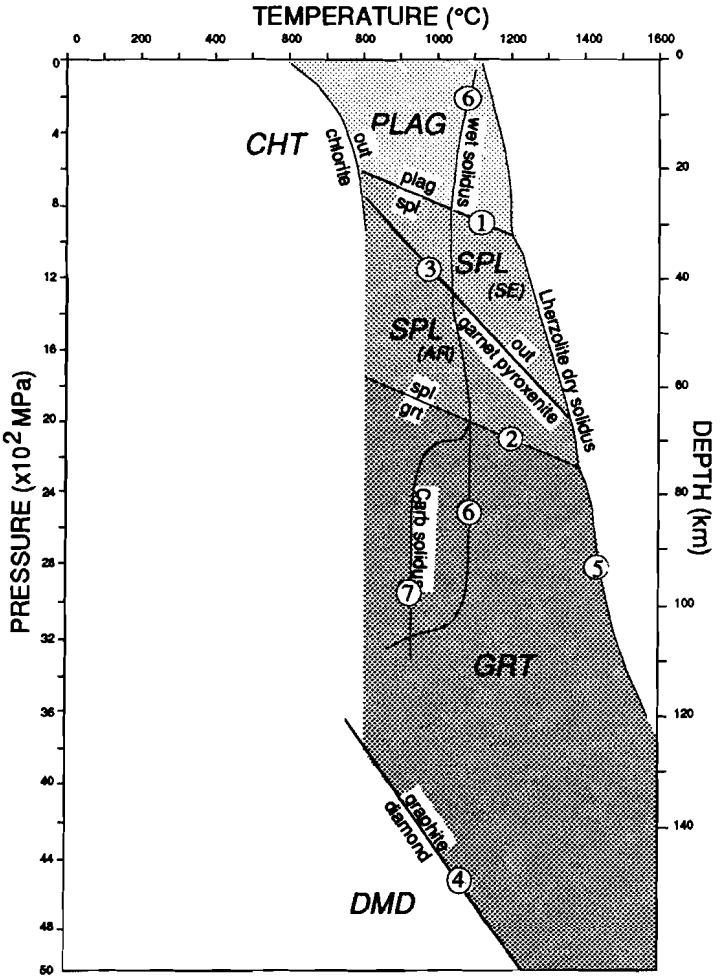

Fig. A1: Petrogenetic grid calibrated for the Ronda peridotite

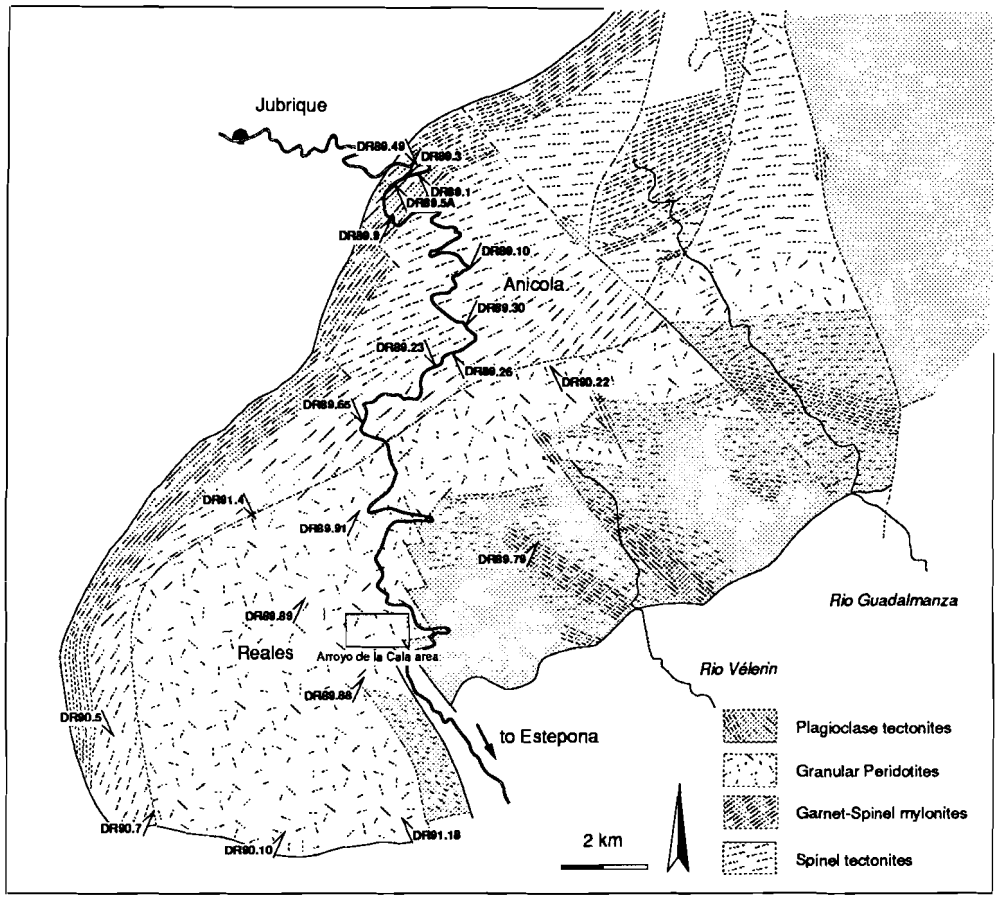

Appendix (continued)

A2: Sample location map

at last page: ▷▷

A3: Tectonic map of the western Ronda massif.

Curriculum Vitae

09-03-1966	geboren te Oranjewoud
1978-1984	Atheneum B, Nassau College, Heerenveen
27-02-1989	Doctoraal examen Geologie, Universiteit Utrecht, Hoofdvak Structurele Geologie, bijvak Petrologie
1989-1993	Assistent in Opleiding, vakgroep Geologie, Universiteit Utrecht

The research presented in this thesis was conducted at:

Institute of Earth Sciences
University of Utrecht
P.O.Box 80.021, 3508 TA Utrecht
The Netherlands

Research School of Earth Sciences
Australian National University
GPO Box 4, Canberra ACT 2601
Australia

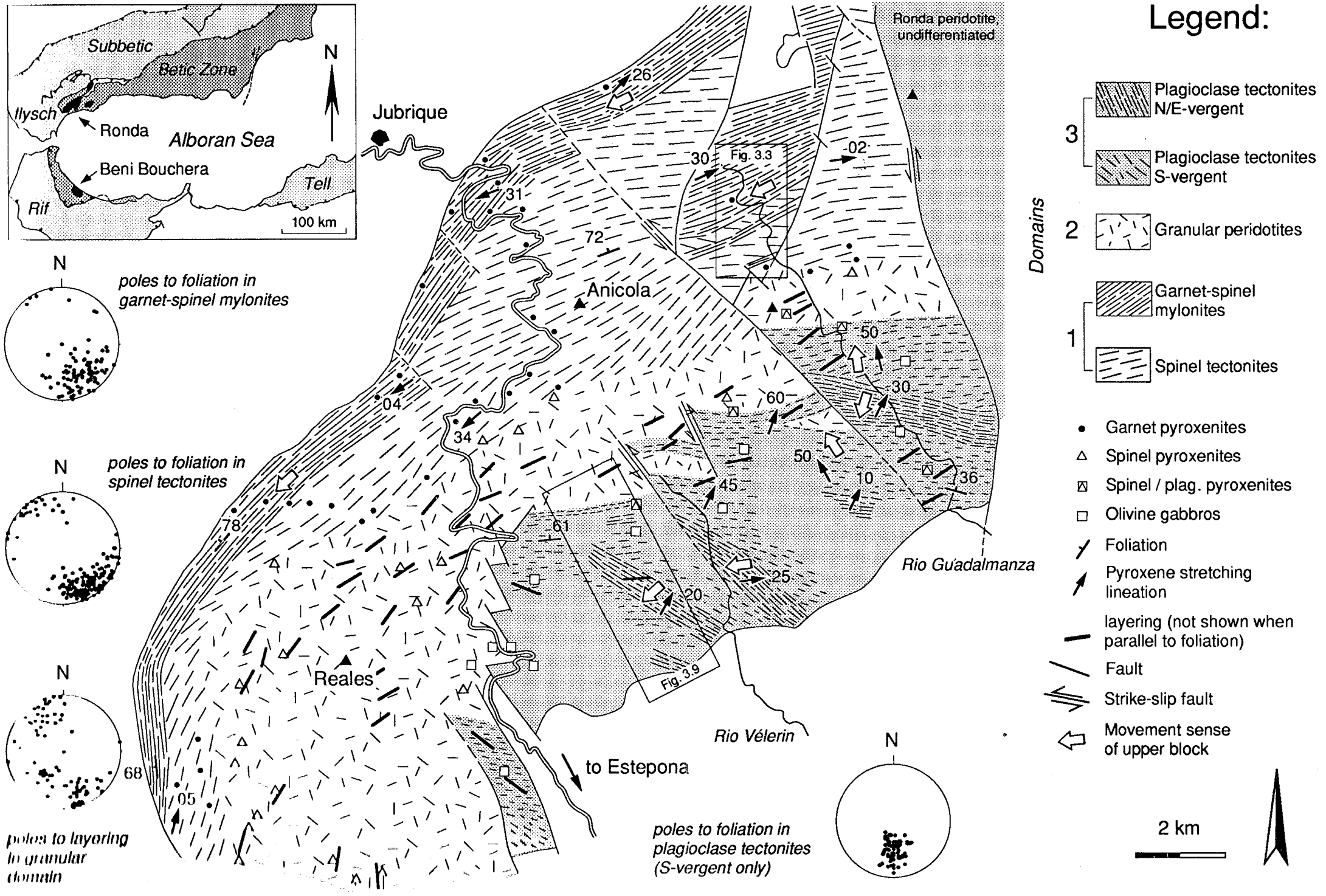
Subbetic
Betic Zone
Ilysch
Ronda
Alboran Sea
Beni Bouchera
Tell
Rif
100 km
N
Jubrique
Ronda peridotite, undifferentiated
Fig. 3.3
Anicola
Reales
Rio Guadalmanza
Rio Vélerin
to Estepona
Fig. 3.9
poles to foliation in garnet-spinel mylonites
poles to foliation in spinel tectonites
poles to layering in granular domain
poles to foliation in plagioclase tectonites (S-vergent only)
Legend:
Domains
3
Plagioclase tectonites N/E-vergent
Plagioclase tectonites S-vergent
2
Granular peridotites
1
Garnet-spinel mylonites
Spinel tectonites
Garnet pyroxenites
Spinel pyroxenites
Spinel / plag. pyroxenites
Olivine gabbros
Foliation
Pyroxene stretching lineation
layering (not shown when parallel to foliation)
Fault
Strike-slip fault
Movement sense of upper block
2 km